UTILIZATION OF MODERNIZED GLOBAL NAVIGATION SATELLITE SYSTEMS FOR AIRCRAFT-BASED NAVIGATION INTEGRITY

A DISSERTATION
SUBMITTED TO THE DEPARTMENT OF
AERONAUTICS AND ASTRONAUTICS
AND THE COMMITTEE ON GRADUATE STUDIES OF
STANFORD UNIVERSITY
IN PARTIAL FULFILLMENT OF THE REQUIREMENTS
FOR THE DEGREE OF
DOCTOR OF PHILOSOPHY

Alexandru Ene

March 2009

I certify that I have read this dissertation and that, in my opinion, it is fully adequate in scope and quality as a dissertation for the degree of Doctor of Philosophy.

(J. David Powell) Principal Adviser

I certify that I have read this dissertation and that, in my opinion, it is fully adequate in scope and quality as a dissertation for the degree of Doctor of Philosophy.

(Per K. Enge) Co-Adviser

I certify that I have read this dissertation and that, in my opinion, it is fully adequate in scope and quality as a dissertation for the degree of Doctor of Philosophy.

(Todd F. Walter)

Approved for the University Committee on Graduate Studies.

To Maria,

Because of you I am here today!

Abstract

An increased number of Global Navigation Satellite System (GNSS) space vehicles, broadcasting at multiple civilian frequencies, are expected to become operational over the next decade. Consequently, each user will be able to independently conduct an integrity check for their estimated position. This research explores Receiver Autonomous Integrity Monitoring (RAIM) as an alternate way to bring airplanes within 200 ft (60 m) of the ground even in poor visibility conditions, and at terrain-constrained airports.

A major role played by ground equipment in traditional aviation is that of providing assistance to aircraft in maintaining the desired trajectory during both terminal and en-route phases of flight. Ground navigational aids owned by the Federal Aviation Administration (FAA) involve large costs which scale with the total number of airports and the overall air traffic capacity. These operational costs can be reduced by equipping airplanes with GNSS-enabled instrumentation. The integrity requirement of having at most one failure to bound the user position errors over 10 million approaches is the most stringent operational constraint and the required error bounds are the tightest in the vertical direction. Therefore, the primary focus of this work is to maximize the performance of a RAIM algorithm from a vertical integrity standpoint for aviation precision approaches.

This dissertation investigates the use of a Multiple Hypothesis Solution Separation (MHSS) RAIM algorithm as an Aircraft-Based Augmentation System (ABAS) which can efficiently take advantage of the capabilities of future multiple-constellation GNSS in order to provide an error protection level for the user. The current research

adds a Fault Detection and Elimination (FDE) method well-adapted to the MHSS RAIM. It also builds the capability of handling multiple simultaneous faults, a well-defined comprehensive threat model, and Vertical Protection Level (VPL) prediction capabilities into the integrity algorithm. The total number of available satellites, and the bias and variance of ranging errors under conditions assumed to be nominal were identified as the key parameters that affect the overall performance, and their influence was measured quantitatively.

Computer-simulated measurements, as well as independently recorded dual-frequency Global Positioning System (GPS) flight data were used to test the performance of the developed RAIM techniques, both under assumed nominal conditions and in the presence of intentionally injected measurement faults. Current results indicate that VPLs in the 10–20 m range are achievable. These protection levels would enable Localizer Performance with Vertical guidance (LPV) approaches down to a 200' minimum height at all runway ends worldwide without the need for a Satellite or Ground-Based Augmentation System (SBAS or GBAS).

Acknowledgements

I would like to express my gratitude to Prof. J. David Powell, my principal dissertation adviser, for his guidance and mentoring. We started interacting when I selected him to serve on my PhD qualifying examinations committee and later, in 2005, he became my thesis adviser and started guiding my steps in transitioning from an Aerospace Engineer to an Aerospace PhD. I am a first generation PhD and to me Dave Powell was a true research father who was there for me when my natural family could no longer offer any assistance in my academic endeavours.

Next, I would like to thank Prof. Per Enge, my co-adviser, for allowing me the opportunity to pursue my research in the Stanford GPS Lab. He was the teacher who introduced me to control engineering in my first quarter at Stanford. Then, in the winter of 2003, he taught the class which introduced me to the Global Positioning System (GPS) and became my Aeronautics and Astronautics (AA) Masters Adviser. I took three classes with Per in my first year and then became a research student in his lab. He served as a continuous source of inspiration for me as I gradually transitioned from taking courses to pursuing research projects. Over the years, I have known Per as a dedicated teacher, an inspirational research advisor, and one of the keenest insiders of GPS I ever met.

For getting where I am today, at the end of a long and arduous task that forced me to dig deep at every step in order to accomplish it, I am equally indebted to Dr. Todd Walter, the GPS and WAAS Lab Director. I appreciate the fact that he was always available for discussion and also to offer me understanding and guidance whenever some sort of research crisis was in place. Whenever some seemingly

insurmountable obstacle lay in my path, things seemed once again doable after each meeting I had with him, whether we discussed something related to my computer algorithms or getting my results ready for the next conference and being able to understand myself what was their practical significance.

I would like to extend my thanks to Prof. Stephen Rock, another one of my control engineering qualifying exam and PhD oral defense committee members. I always appreciated Steve's patience in helping students improve their presentation skills, whether presenting at a research group meeting or in front of the AA department industry affiliates.

Completing my doctoral committee, which played the major role in guiding my steps through the many years of graduate school, my gratitude goes to Prof. Bernard Roth from Mechanical Engineering, who graciously agreed to serve as the committee chair. I first met Bernie in a design thinking workshop in which he taught me the difference between trying something and actually doing it, and also that all important things in this world always happen for very good reasons. To him I owe learning how to think better on my own feet and to become more confident in myself while pursuing a certain goal.

I wish to add my thanks to Dr. Juan Blanch who acted as the research mentor for my thesis research project and contributed to my understanding of RAIM algorithms through many helpful discussions, and to Dr. Dennis Akos and Dr. Samuel Pullen who advised me on GPS multifrequency and ionosphere-related projects earlier on in my graduate career. In addition, I would like to mention the inspiration I received from Prof. Robert Cannon, who, in addition to completing the AA quals committee for my guidance, navigation and controls major, always served as an example to his students of how one can have a most enjoyable life while helping build top notch research programs.

Although their names are many and their influences in my life have been varied, I would like to thank all those people who mentored me at Stanford as they let me set

high goals, they even let me set impossible goals for myself, but never expected me to do impossible things and were always realistic about evaluating my performance.

Finally, I want to thank my colleagues, current and former students of our lab who served to me as mentors, role models and friends. They were a family with whom I could identify while discovering the unknown path laying in front me in my quest for an academic degree. And here I would like to add all those in the Aero/Astro Department at Stanford, past and present faculty, staff and fellow students.

To this already numerous gang I wish to add all those who contributed towards my well-being at Stanford, friends who supported me along the way, as well as the student groups in which I have been involved over the years, with a special mention to the Graduate Student Council. There are just too many people to be mentioned here by name, who interacted with me and shaped my life at Stanford over the past 7 years.

As the custom goes, I would like to thank my family next to whom I grew up. Above all, I would like to pay a special tribute to my grandparents, Dumitru and Maria, who raised me for several years as their own child. Being able to cherish their love is one thing that always gave me strength even after they were no longer with me — the efforts that I put into this thesis go to honor their memory. I am also forever indebted to my best friend Maria, for always supporting me during the hard times of my PhD candidacy. She is the one who would come to bring me food when I did not leave the lab for multiple days in a row.

With this dissertation, I am nearing the end of an endeavor and a great learning experience. But the greatest thing I see in this entire process is that I am still standing here today, not at the end of a road, but at a point where my education at Stanford helped open new horizons in front of me. My greatest learning experience actually begins here, today. I am now filled with more curiosity and more thirst for new knowledge than I was when I started. I am looking forward to take what I learned here at Stanford and apply it to inventing new and better ways of improving the life

of humans and to further the sharing of knowledge. My thanks go to all those around me over the years, for being with me along the way in the past and in the future alike.

Lastly, I would like to acknowledge the logistical support of the FAA Program Office, through the Cooperative Research and Development Agreement grant #08-G-007. I hope that my humble contribution will help the Federal Aviation Administration, the sponsor of this entire work, move a step closer with their effort in planning for the proposed Next Generation Air Transportation System in the United States.

All views expressed in this dissertation belong to its author alone and do not necessarily represent the position of any other organization or person.

Table of Contents

List of Tables

List of Figures

List of Acronyms

AA	Aeronautics and Astronautics
ABAS	Aircraft-Based Augmentation System
AFB	Air Force Base
AL	Alert Limit
ARAIM	Absolute Receiver Autonomous Integrity Monitoring
ARINC	Aeronautical Radio, Inc.
ARNS	Aeronautical Radio Navigation Services
BFS	Breadth-First Search
C/A code	Coarse Acquisition code
CAASD	Center for Advanced Aviation System Development
CDMA	Code Division Multiple Access
CFIT	Controlled Flight Into Terrain
CNAV Data	civil navigation data (on the GPS L2C and L5 signals)
CS	Galileo Commercial Service
DGPS	Differential GPS

DH	Decision Height
DME	Distance Measuring Equipment
DoD	Department of Defense
DOP	Dilution of Precision
EGNOS	European Geostationary Navigation Overlay Service
ENU	East-North-Up Earth-centered coordinate system
ESA	European Space Agency
EU	European Union
FAA	Federal Aviation Administration
FAF	Final Approach Fix
FDE	Fault Detection and Elimination
FDMA	Frequency Division Multiple Access
GAGAN	GPS Aided GEO Augmented Navigation
GBAS	Ground-Based Augmentation System
GEAS	GNSS Evolutionary Architecture Study
GEOs	Geostationary Earth Orbit satellites
GIC	GNSS Integrity Channel
GIOVE	Galileo In- Orbit Validation Elements
GLONASS	GLObal NAvigation Satellite System
GLR	Generalized Likelihood Ratio

GLS	GPS/GNSS Landing System
GNSS	Global Navigation Satellite System
GPS	Global Positioning System
GRAS	Ground-Based Regional Augmentation System
GSS	Galileo Sensor Station
HAL	Horizontal Alert Limit
HDOP	Horizontal Dilution of Precision
HMI	Hazardous Misleading Information
HPL	Horizontal Protection Level
ICAO	International Civil Aviation Organization
ICD	Interface Control Document
iid	identically-distributed random variables
ILS	Instrument Landing System
INS	Inertial Navigation Systems
IRNSS	Indian Regional Navigational Satellite System
IS	Interface Specification
ITR	International Telecommunications Rules
L1	Link-1
L2	Link-2
L2C	L2 Civil Signal

L5	Link-5
LAAS	Local Area Augmentation System
LNAV	Lateral Navigation
LOS	line of sight
LPV	Localizer Performance with Vertical guidance
LS	Least Squares
MAAST	Matlab Algorithm Availability Simulation Tool
MASPS	Minimum Aviation System Performanace Standards
MCS	Master Control Station
MEO	Medium-Earth Orbit
MHSS	Multiple Hypothesis Solution Separation
MOPS	Minimum Operational Performanace Standards
MSAS	Multi-functional Satellite Augmentation System
NANU	Notice Advisory to Navstar Users
NAS	National Airspace System
NAV Data	navigation data (on the GPS L1 signal)
navaids	navigation aids
NextGen	Next Generation Air Transportation System
NGA	National Geospatial-Intelligence Agency
NSTB	National Satellite Test Bed

OC	Operations Center
OCX	Operational Control Segment
OS	Galileo Open Service
OWAS	Optimally Weighted Average Solution
P code	P(Y) semi-encrypted Precision code
PAN	Performance ANalysis (reports for the GPS constellation)
$\mathcal{P}HMI$	Probability of Hazardous Misleading Information (also PHMI)
PL	Protection Level
PLL	Phase Lock Loop
PRN	Pseudo-Random Noise
PRS	Galileo Public Regulated Service
PS	Performance Standard
QZSS	Quasi-Zenith Satellite System
RAIM	Receiver Autonomous Integrity Monitoring
RF	Radio Frequency
RFI	radio frequency interference
rms	root-mean-square
RNP	Required Navigation Performance
RNSS	Radio Navigation Satellite System
RRAIM	Relative Receiver Autonomous Integrity Monitoring

rss	root-square-sum
RT	Real-Time
RTCA	Radio Technical Commission for Aeronautics
RVR	Runway Visual Range
SA	Selective Availability
SBAS	Satellite-Based Augmentation System
SCAT-I	Special Category I
SIS	Signal-In-Space
SISA	Signal-In-Space Accuracy
SISMA	Signal-in-Space Monitoring Accuracy
SoL	Safety of Life
SPS	Standard Positioning Service
SS	Solution Separation
SSE	Sum of Square Errors
SV	Space Vehicle
T_{GD}	Satellite differential group delay
TDMA	Time Division Multiple Access
TEC	Total Electron Content
Tech Center	William J. Hughes Technical Center
TTA	Time-to-Alert

URA	User Range Accuracy
URE	User Range Error
US	United States
USA	United States of America
USSR	Union of Soviet Socialist Republics
VAL	Vertical Alert Limit
VDOP	Vertical Dilution of Precision
VNAV	Vertical Navigation
VOR	Very High Frequency (VHF) Omni-directional Range
VPL	Vertical Protection Level
WAAS	Wide Area Augmentation System
WADGPS	Wide-Area Differential GPS
WLS	Weighted Least-Squares
WSSE	Weighted Sum of Square Errors
ZAOD	Zero Age-Of-Data

Part I.

Initial Remarks

1. Introduction

Initially proposed for satisfying an operational need of the United States (US) military, the advent of the Navstar Global Positioning System (GPS) has also revolutionized the field of navigation for civilian applications over the past two decades. Satellite-based positioning immediately generated a transformation in the way the concept of navigation was perceived in relation to air, marine and terrestrial transportation systems. Along with this looming change, the topic of satellite navigation safety gained in importance relative to these multiple applications. While the position of most vehicles using Global Navigation Satellite System (GNSS) guidance for navigation is constrained to a 2 - dimensional surface, i.e. Earth's surface, the movement of airplanes can take place along any of the three spatial directions. Navigation safety is consequently hardest to achieve for the case of unconstrained three-dimensional movement, and at the same time civil aviation is one of the domains where safety is the paramount issue.

1.1. Problem Statement

Vertical errors are critical during aviation precision approaches, and they are also generally greater than horizontal errors for satellite-based positioning, because of the inherent geometry between the receiver and the ranging sources. Therefore, a significant portion of the work presently done to address satellite navigation safety has gone into tackling the harder problem of providing vertical guidance to airplanes. Given the fact that the constraints on the navigation errors are tighter in the vertical

direction, once a general solution is devised to address the related safety issues, the same approach will also be available to provide a solution for simplified versions of the problem as particular cases. Less stringent versions of the navigation error bounding problem problem would be the task of bounding errors in the horizontal direction, or that of providing navigation integrity for vehicles whose motion is constrained along one of the spatial dimensions, unlike the motion of aerial vehicles.

As unaugmented GPS is currently not certified as a sole-means of navigation for aviation precision approaches [82], expensive ground and space equipment has been commissioned for augmenting the satellite positioning signals. However, in anticipation of the modernization of GPS and additional multi-frequency GNSS constellations proposed by other nations, the utilization of Aircraft-Based Augmentation Systems (ABAS) for aviation approaches has become a highly significant area for exploratory study. With Receiver Autonomous Integrity Monitoring (RAIM) aboard the aircraft, a more efficient solution to provide airplane navigation safety can be foreseen, by redistributing the workload more efficiently between the user, space and ground segments of the navigation system. Thus, the declared goal of this thesis is to determine and optimize the performance of an unaided multi-frequency GNSS constellation from a vertical integrity standpoint for aviation precision approaches. The achievement of this goal means going a step beyond the capabilities of those current GPS augmentation systems which rely on the ground monitoring of satellite signals. These existing systems perform measurement fault detection by comparing the the position solution based on satellite signals to the true position based on corrections provided by ground stations. In contrast, ABAS does fault detection by making a statistical comparison of one satellite signal to signals from the other satellites in view.

1.2. Outline of Thesis Contributions

The fundamental goal of the research in this thesis was to investigate new ideas for navigation system architectures that could provide integrity support for vertically-guided civil aviation operations. This work was also completed in support of the Federal Aviation Administration (FAA) GNSS Evolutionary Architecture Study (GEAS) workgroup. The panel members were drawn from across US government agencies, industry, and academia, and their efforts focused on validating new system architectural concepts and making a recommendation about the future capabilities that GPS should implement for a better support of civil aviation over the National Airspace (NAS). Within this context, the main purpose of the research documented in this dissertation is to demonstrate that a high level of navigation integrity can be provided with multiple frequency GNSS signals and a minimum of 30 satellites in optimized orbits, whether they belong to a single or multiple constellation GNSS.

It should be mentioned here that the applicability of this work is not limited to only aviation applications. The provided general framework is flexible enough to be particularized to both airplane vertical and lateral guidance, as well as to marine, road and rail transportation integrity needs. Rather than confining the potential uses of the current work, the framework of civil aviation vertically-guided approaches serves as the testbed for developing the integrity algorithms of the future. In contrast with surface ground and water transportation, the motions of an air vehicle are unconstrained in any of the three spatial dimensions. The safety requirements are the most stringent for vertical guidance of civil airplanes, providing the toughest possible operation conditions for developing integrity algorithms.

The contributions described in this doctoral thesis were made in the following areas:

1.2.1. RAIM algorithm development {Chapter 3}

— Developed a well-defined comprehensive threat model and improved the Multiple Hypothesis Solution Separation (MHSS) RAIM algorithm to handle multiple simultaneous range measurement faults in a flexible manner, in order to take advantage of the increased number of ranging sources expected with future multiple GNSS constellations;

— Proposed an original Fault Detection and Exclusion (FDE) method well adapted to the probabilistic approach of MHSS RAIM, and completed the algorithm with additional Vertical Protection Level (VPL) prediction capabilities;

— Demonstrated that the integrity calculation for these algorithms allows for a straightforward mathematical proof that the computed protection levels meet the Probability of Hazardous Misleading Information (PHMI) requirements.

1.2.2. Determination of parameter space over which desired RAIM performance is achievable {Chapter 4}

— Conducted an analysis of the simulated performance of RAIM with unaided GPS for users worldwide;

— The performance capabilities of future GNSS under multiple possible scenarios were assessed in terms of the overall number of operational satellites and constellations;

— Parametric studies were conducted in order to identify on which external factors is the VPL the most sensitive, and for which assumptions performance is not significantly affected over a large range of possible values.

These studies identified the parameter space width over which the results with the current MHSS RAIM algorithm are applicable and the assumptions that need to be met.

1.2.3. Validation of the pseudorange error model {Chapter 5}

— Calibrated the model for nominal ranging errors across different signal frequencies;

— Developed realistic models of the actual ranging errors based on dual frequency ground station and flight test data available from the FAA Tech Center. The focus was on finding the most realistic values to consider for the two components of the user range error model: the error variance and the mean (assumed to be non-zero);

— Searched for the most appropriate way to model error standard deviation (assuming approximately Gaussian errors) and maximum biases such that the VPL results are realistic and not overly conservative. If both parameters prove to have a significant impact on the VPL values, future augmentation systems will want to consider broadcasting both the error sigma and maximum biases in order to improve the worst-case navigation performance [96];

— The statistics of realized errors in the available data sets exhibited a near-Gaussian behavior, with a slightly higher amount of probability located in the tails of the distribution and small nominal levels of bias at the centimeter level.

1.2.4. Verification of the MHSS algorithm with real data {Chapter 6}

— Validated the MHSS algorithm with independently-recorded flight test data;

— Conducted testing under a variety of scenarios that include both nominal measurement data and a wide range of inserted satellite failures;

— Verified the ability of the developed RAIM method to detect and eliminate faulty measurements as they propagate and increase over time.

1.3. Roadmap of the Thesis

The thesis will be structured into four distinct logical units. Parts II and III will contain the main chapters, which document the above research contributions. This core of the dissertation will be surrounded by an introduction (Part I) and a conclusion (Part IV). Each part will be consisting of two chapters.

At the outset, a significant amount of background information and also an overview of the previous work need to be provided in order to place this body of research fully into context. Therefore, the upcoming Chapter 2 will be dedicated to providing a general level of information on GNSS and the efforts that have been currently made to adapt satellite navigation to the rigors of civil air transport. An overview of the prior art is provided in Section 2.4. It is followed by an in-depth review of earlier RAIM algorithms in the first half of Chapter 3, as the development of the MHSS algorithm unfolds and its connections with previous methods are outlined.

Further on, the four contributions will be organized in separate chapters, with additional context-specific information as is relevant to each part of this work. Two main focus areas in demonstrating the capabilities of a Receiver Autonomous Integrity Monitor will emerge. The theoretical development and software simulation phase will be described in Part II, comprised of chapters 3 and 4, while the data calibration

and post-processing validation with recorded in-flight measurements will constitute the subject of Part III, comprised of chapters 5 and 6. A set of closing remarks will follow, outlining the findings of this thesis and providing a glimpse into a possible future, in which RAIM is one of the essential elements of a safer air navigation system.

2. Background on GNSS and Airplane Navigation

During the last 30 years, the Navstar Global Positioning System (GPS) has revolutionized the field of navigation. GPS provides navigation services to hundreds of millions users on the ground, at sea, in the air, and even for space applications. Many of these applications are Safety of Life (SoL) operations. For example, GPS is used to guide vessels docking in harbors or navigating within narrow waterways. GPS also provides location and guidance to terrestrial emergency services while they conduct their critical missions. In particular, the application of GPS to civil aviation, both worldwide and especially in the USA, has been viewed as an excellent opportunity to both lower operating costs and increase flight safety, in particular for the most demanding phases of flight — take-off, aircraft approach and landing.

The first part of this introductory chapter will review the modality in which GNSS is utilized for navigation in general (Section 2.1). Next, a closer look will be taken at how satellite measurements are used for civil aviation guidance (Section 2.2). This topic will make the main object of the current thesis and more particularly the problem of the safety of an autonomous aircraft in the presence of navigation signals from multiple GPS-like constellations. Section 2.3 will focus on providing a motivation for the present endeavor and a description of previous research in the same direction. Additionally, specific background information will continue to be provided in the subsequent chapters to accompany the presentation of an original solution proposed by this dissertation for the airplane navigation integrity problem.

2.1. Background on GPS / GNSS

This expository section will open with the definition of the broader notion of global navigation (2.1.1). That will be followed in 2.1.2 by a description of GPS and the current plans of modernizing the system in order to better serve its applications in the civilian community. Next, 2.1.3 will add descriptions of the other constellations that together with GPS form the Global Navigation Satellite System (GNSS). Eventually, 2.1.4 will go into a deeper level of detail by providing a more technical background about the types of measurements that are currently based on the civil GPS signals and a description of the errors affecting them. That will prepare the ground for Section 2.2, which addresses the problems that the aviation user faces in relying on GNSS for the guidance of its aircraft.

2.1.1. Global navigation

> **Navigation** is the process of reading, and controlling the movement of a craft or vehicle from one place to another. All navigational techniques involve locating the navigator's position compared to known locations or patterns.
>
> Wikipedia, *http://en.wikipedia.org/wiki/Navigation*

Navigation is the process used by mankind since the oldest times in order to explore the surrounding environment and to be able to travel between spatial locations. This exploration process pushed boundaries farther and farther over time until travel and transportation expanded across the entire plant which we inhabit. The first documented circumnavigation of the Earth was realized by F. Magellan between 1519–1522 AD. With it the broader concept of *global navigation* was born. Thus, it can be said that the field of global navigation is at least five centuries old, though many historians might argue that global navigators roamed the oceans much earlier, with the vikings sailing across the North Atlantic, the Phoenicians circumnavigating Africa

and Polynesian tribes traveling across the Pacific. While the origins of navigation remain an open topic to this day, this thesis will focus on modern techniques for global navigation, and more precisely on satellite navigation for airborne vehicles.

A more explicit definition of navigation, which will be employed for the purposes of this dissertation will involve the ability of a navigator, or vehicle pilot, to position themselves on a map, and subsequently perform a path planning process between different locations on the given map. While many of the early seafarers were sailing into uncharted territories, the field of recording geographical features and the distance span between them to aid with navigation reckoning is as old as navigation itself. Although some of the contemporaneous navigators still sometimes fail to reach their desired destination due to imperfections in the maps which they are using, cartography is today a very exact science and offers most vehicle pilots an abundance of information to assist them with both route planning and reaching their final goal.

The part of the navigation process that makes the direct object of research for this thesis and for the present-day field of navigation in general is *positioning*. The ability to determine their exact location at any point in time relative to a reference map is quintessential for any navigator, and a *sine qua non* requirement for any route planning process. While such techniques as dead reckoning or celestial navigation have been perfected over the centuries in order to determine a vehicle's relative or absolute position with higher and higher precision, the technological advances of the 20^{th} century brought the new techniques of electronic and radio navigation into common use by pilots of land, sea and air vehicles. Satellite navigation is one of the newest forms of radio navigation, bringing along multiple advantages over previously existing techniques. It can provide information to users at any location on and off the ground that have a direct line of sight (LOS) to several of the Space Vehicles (SVs) circling the planet in Medium-Earth Orbit (MEO). While it is the first truly global man-made navigation system, positioning based on satellite signals offers the potential for determining the location of the navigator with a high precision, and also its state of motion and attitude relative to the Earth.

We are therefore assisting to the advent of a navigation system that, by itself, could provide pilots with the ability to perform both positioning and route planning, without the need to resort to any additional methods or outside information besides a high fidelity map of the Earth. At the same time, satellite positioning offers the opportunity of transitioning from visual to fully automated navigation everywhere around the globe based on a single navigation system. Therefore it opens the doors to superior safety standards for many navigation applications in visibility-impaired conditions which were previously hazardous or even impossible to handle for human navigators. Satellite navigation is not the only system that can provide such high performance standards, but it has the advantage of unifying many of the advantages of the previously existing systems and in certain cases it can offer improved performance in terms of precise positioning and safety risks.

2.1.2. The Global Positioning System (GPS), current state and modernization plans

GPS is a passive satellite-based ranging system, in that the time interval necessary for a radio frequency (RF) signal to travel from a spacecraft to the user provides the basis for position estimation. A user can employ an electronic device to independently receive signals from four or more satellites and determine its distance to each of the spacecraft based on the broadcast information about the SV locations. Therewith, a GPS / GNSS *receiver* can form a (generally overdetermined) system of equations, allowing it to solve for the three spatial components of its antenna location and the deviation of the user clock from *GPS time*. An algorithm for estimating a position solution based on satellite range measurements will be described in Chapter 3.

The GPS was developed by and is currently operated by the United States (US) military, and a comprehensive description of the system was made available from the Secretary of Defense Office at the Pentagon, as the Standard Positioning Service (SPS) Performance Standard (PS) document [93]. A summary overview of

Source: http://www.kowoma.de/en/gps/control_segment.htm

Figure 2.1.: Worldwide distribution of the GPS ground monitoring segment stations.

the system will be given here as well, as a general information background for the current thesis. GPS in its entirety is divided among the following three segments:

Space segment: The GPS nominally consists of 24 SVs, which are distributed on six equally-spaced orbital planes at 60° apart in longitude and an inclination of 55° with respect to Earth's equator. Each spacecraft revolves on an approximately circular orbit with a radius of 26,560 km and a period of about 12 hours, ensuring that its ground tracks repeat exactly twice each sidereal day.

Control segment: There are eleven ground monitoring stations across the globe — five GPS control stations plus six National Geospatial-Intelligence Agency (NGA) stations, as illustrated in Figure 2.1. Data collected by these stations is used to determine the satellite ephemeris and clock offsets for each of the SVs, and monitor the health of the spacecraft. Subsequently, the Operations Center (OC) will upload navigation messages using the Master Control Station (MCS) at the Schriever Air Force Base (AFB), Colorado.

User segment: The user segment includes US military applications on one hand and a diversified variety of civilian applications on the other hand. Since part of the

information broadcast by GPS is encrypted and intended for US military use only, any information about GPS and its applications described in this dissertation will only rely on the publicly available positioning signals and system documentation.

The US Department of Defense (DoD) GPS Wing regularly maintains 24–32 active birds on orbit to enhance the system availability, however newer SVs are placed as spares next to older ones nearing the end of their operational cycle. From a measurement geometry standpoint, an optimal distribution of the satellites in orbit would have the SVs equally spaced across the sky. Thus, currently, users cannot take full advantage of the higher number of operational satellites, since they are distributed around the original 24 nominal slots, which is the only guaranteed number of signal sources that any SoL user equipment can assume.

The transmitted information normally accessible to the civil user comprises of two different signals called Link-1 (L1) and Link-2 (L2). All of the satellites broadcast over the same civilian bandwidth, with center frequencies at 1575.42 MHz and respectively 1227.6 MHz. The signals are composed of an L-band carrier wave, modulated with a PRN code and a navigation data stream. The L1 signal is modulated by both a 1.023 MHz rate Coarse-Acquisition (C/A) code and a 10.23 MHz clock rate precision P(Y) code. For the most commonly-used civilian GPS signal, each cycle of the L1 carrier frequency is about 0.19 m long and each C/A code chip is equivalent to approximately 293 m. These are the features of the GPS signals that civilian receivers employ in their measurements. The C/A code is openly available for civil users, while the P(Y) code is partially encrypted to prevent unauthorized users. The L2 signal is currently modulated only by the P(Y) code, except for the block IIR-M satellites launched since September 26, 2005, which broadcast a civil code on L2 that is not yet fully-operational.

A unique PseudoRandom Noise (PRN) sequence of codes is assigned to each satellite, based on which users can distinguish between the different ranging signals. This system of simultaneously sharing multiple channels of information at the same

frequency is called Code Division Multiple Access (CDMA). For a given SV, the code pseudorange is based on measuring the offset between the received PRN code and a locally-generated replica of the code produced by the receiver itself. The navigation data provides information for calculating the position of the spacecraft location on orbit.

The future of civil satellite navigation is going to involve multiple frequency transmissions. This would allow SoL applications to become more robust against potential radio frequency interference (RFI), whether it is intentional or unintentional, and it would also offer more signal redundancy given the very low amount of signal power at the user receiver at present. In the next decade, GPS is expected to see the addition of a civil signal at L2 (L2C) plus a third civil frequency for both redundancy and improved the overall performance. The L2C signal will allow an upgrade of the navigation (NAV) data to a revised format called civilian navigation (CNAV) data. It will also add a codeless sequence broadcast as part of a Time Division Multiple Access (TDMA) scheme, which is intended to benefit applications that require longer integration times of the transmitted C/A code. The completely new Link-5 (L5) signal centered at 1176.45 MHz will benefit from an increase in the emitted power and also a higher code chipping rate, equivalent to that of the current P code, that will allow higher precision positioning. The first GPS SV broadcasting the L5 signal is part of the block IIF series of spacecraft, and is scheduled to launch at the earliest towards the end of 2009.

A complete description of the current and future signal structures, as well as ways to recover the information contained in these signals are publicly available through the GPS User Interface Specification (IS) documents [2, 3]. A large amount of literature has additionally been published on the topic of GPS modernization in the past decade, mirroring the amount of excitement in the world of civilian satellite navigation with the upcoming improvements in the system. Receiver design for the multiple-frequency scheme has also started more than a decade in advance of the planned initial operational capability of the new signals [4].

2.1.3. Galileo and other planned GNSS constellations

With the turn of the new millennium, the Global Navigation Satellite Systems (GNSS) are also experiencing a new era of expansion of modernization. In the last decades of the 20^{th} century, there have been only two navigation constellations or satellite systems in existence, those operated by the governments of the United States of America (USA) and the Union of Soviet Socialist Republics (USSR). These original systems were not built for seamlessly working together, but in order to compete with each other as part of the space race during the Cold War of the 1970s and 1980s. Their primary purpose was to serve military operations, and each spacecraft transmitted a single civil signal in only one frequency band.

In recent years, the significance and value of global satellite navigation has been recognized by more and more governments around the world. In particular, the European Union (EU) is developing their own system, called Galileo and envisioned as an equivalent of GPS. China was also involved in the incipient stages of Galileo planning and development, but later decided to begin development of its own regional and global positioning systems. Other governments followed suit, if not in putting up their own full-fledged navigation constellations, then at least in building space equipment to augment the existing GPS or deploying ground infrastructure to assist GNSS meet the stringent requirements of Safety of Life (SoL) applications. A far from all-inclusive list includes the country members of the European Space Agency (ESA), Australia, Japan, India, and even Nigeria.

At full development, the whole family of GNSS is projected to consist of more than 100 satellites by 2020. Moreover, these modern SVs will be capable of transmitting multiple civil signals in multiple frequency bands. Another major difference in the approach of most governments involved is an unprecedented opening for exchange of information and interoperation between the multiple systems being commissioned. This new environment had the effect of fueling the hope of seeing a global effort come to fruition: multiple countries working together for serving and ensuring the safety of the entire world population. A more complete overview of the modernized GPS

system and additional GNSS constellations is presented in [43], while a summary of this information will be provided below.

The US GPS was already described in the previous section and it is to date the most widely-used form of GNSS around the world. In the meantime, the jurisdiction over the ex-Soviet Global Navigation Satellite System (GloNaSS) has passed in the 1990s to the newly created political entity called the Russian Federation. The constellation initially fell into disrepair, due to the change of its managing authority, however it has seen a revitalization over the past decade — the Russian Federation is planning a modernization phase and it renewed its commitment to provide a free public service. Under a 2007 Presidential Decree, the country has decided to repopulate the constellation up to the nominal level of 24 SVs by 2010 using the second generation Uragan-M satellites, and is also in the process of deploying third generation Uragan-K satellites to extend the constellation to 30 active spacecraft, in an attempt to achieve the same level of performance as GPS.

On a second level of its efforts, Russia has initiated talks with other countries to participate in its GNSS program. Among these are discussions within a GPS-GLONASS Interoperability and Compatibility Working Group on the compatibility of signals with the GPS services, including plans to switch some of the transmission capabilities from the old Frequency Division Multiple Access (FDMA) plan to the CDMA method in order to facilitate common integration in the user receiver technologies. For the time being, the old GloNaSS constellation design includes 24 SV slots (including 3 active spares) in 3 orbital planes, at an altitude of 19,100 km, with an inclination of 64.8°, and with a nominal period of approximately 11 h 15 min. Only 18 of those slots hold active satellites at present, and their civilian broadcast signals can be located in the L1 band between 1598 and 1609.4 MHz, which is further divided into 21 sub-bands with center frequencies spaced at 0.5625 MHz apart. A second set of higher precision encrypted military GloNaSS signals is known to exist in the L2

band between 1242.9 and 1251.7 MHz, divided into 21 sub-bands with center frequencies spaced at 0.4375 MHz apart, but no further information is publicly available at this time about those signals.

The last update of the public Interface Control Document (ICD) has been made in 2002 [89], and it does not provide details on the proposed frequency plan for the future GloNaSS CDMA transmissions, which will be designed for compatibility with the other GNSS. Currently, the Russian GNSS is used by a small minority of the current civil user applications. However, due to the existing political environment and the uncertainty related to the future of this system, many SoL applications choose not to rely on GloNaSS signals at present. In what concerns government and private entities outside the Russian Federation, this decision is unlikely to change unless strong guarantees will exist on the continuous operation and public availability of the navigation signals transmitted by the Russian system.

In addition to its existing four Geostationary Earth Orbit satellites (GEOs) put in space between 2000 and 2007, on April 14, 2007 China launched its first and so far only MEO positioning satellite, called Compass-M1. The older spacecraft in GEO orbits are part of an active satellite-based regional ranging system, called Beidou-1, relying on bidirectional transmissions between a user, the GEOs and an MCS. That system is however set to evolve into a true GNSS called Compass (Beidou-2) with a projected number of 30 additional SVs broadcasting unidirectional ranging signals at multiple civil frequencies. The shift in direction from a two-way ranging technique to one-way pseudoranging falls into the trend demonstrated also by the Russian GloNaSS; that is, of aligning existing satellite systems to similar standards to those imposed worldwide by GPS.

The Compass-M1 satellite is currently broadcasting at the following frequencies: E1 and E2 in the L1-band, centered at 1561.10 and 1589.74 MHz respectively, E5b around 1207.14 MHz situated midway in between the GPS L2 and L5 signal frequencies, and E6 around 1268.52 MHz situated in between the GPS L1 and L2 signal frequencies. These frequency bands are in fact identical with those in an early signal

scheme proposed for the EU GNSS, a program with which China has actively cooperated in the first half of this decade. Besides a limited amount of information revealed publicly, the Chinese government maintains a significant amount of secrecy about its future plans in the realm of GNSS. As a consequence, there currently exists a high level of uncertainty about the current developmental stages and about the future of this system as a global navigation resource. Future communication is expected about a guaranteed Performance Standard and a detailed description of the Compass user interface. For fairness reasons, it could be said that some amount of uncertainty exists about the 3^{rd} generation of modernized GPS satellites (GPS III), which is yet to enter its final development phase. Nonetheless, the full interface specifications have already been published for the future modernized GPS signals in the L1, L2 and L5 bands.

Political and economic considerations have always played a major role in governmental decisions to develop and deploy major systems, such as a GNSS constellation. The EU system, called Galileo after the famous renaissance astronomer, makes no exception from that rule. However, the Galileo planning and development managed to successfully survive two global economic crises and a failed attempt at commissioning a GNSS constellation based on private investments, as a proposed system that would pay for itself in direct user fees over time. The discussion and negotiations stages in an attempt to secure funding for this system surely went on for an entire decade, however these efforts were markedly more open and transparent to the public than in the case of the other three GNSS constellations mentioned so far.

The Galileo Project Office and the European GNSS Supervisory Authority were never under the sole authority of a single government or entity. Thus, the general feeling is that the information was made publicly available as soon as the details had been finalized, and this was also the case because the EU and ESA had a higher obligation to communicate openly with the governments of all the countries participating in the program. For the technical aspect, the Galileo program first released an IS document in 2006 and has deployed its first two testbed satellites

as part of the Galileo In–Orbit Validation Elements (GIOVE) operations segment. The GIOVE-A and GIOVE-B spacecraft were launched respectively on December 28, 2005 and April 27, 2008. These will be followed by satellites able to broadcast the final signal structure devised for the Galileo system, which are expected in the 2010 timeframe, while an operational constellation of 27 SVs plus 3 active spares is expected to be fully deployed sometime in the next decade. In summary, the future Galileo constellation will consist of 30 spacecraft, each with design lifetime of 12 years, revolving around the Earth at an orbital altitude of 23,222 km, corresponding to an orbit radius of 29,600 km. They will be evenly distributed in three orbital planes at 56° of inclination with respect to the Earth's equator.

Signal	Carrier Frequency (MHz)
E1	1575.420
E1b	1589.740
E1c	1561.100
E5	1191.795
E5a	1176.450
E5b	1207.140
E6	1278.750

Table 2.1.: Carrier frequency for each of the Galileo signals.

Adopting a different position from the other governments developing nationally-controlled GNSS constellations, the EU has held the stance that Galileo is a neutral technology, available to all countries, with no military-controlled segment and lacking the ability to only deny their opponents the use of highly accurate GNSS. A fully detailed description of the Galileo User Interface for its Open Service that will be freely available to the public is given in [31]. Some of the main characteristics of the system described in this ICD will be summarized below. Table 2.1 displays the center frequencies for the planned signals. These signals will be emitted in the allocated Radio Navigation Satellite System (RNSS) bands in accordance with the International

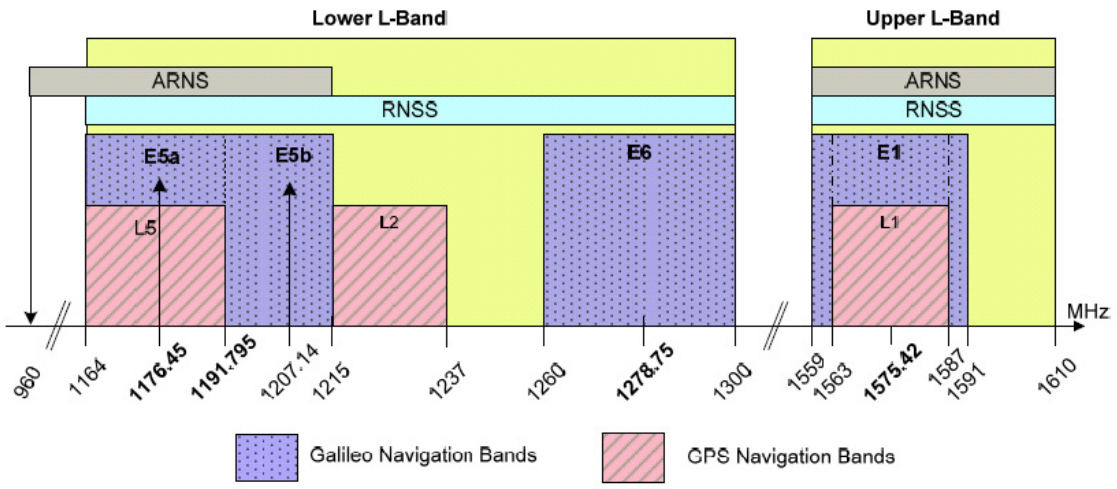

Figure 2.2.: Galileo and modernized GPS frequency plans (from [31]).

Telecommunications Rules (ITR). Moreover, openly available signals will be broadcast in the E1 and E5 frequency bands that are specially reserved for aviation under the Aeronautical Radio Navigation Services (ARNS). These bands also correspond to the GPS L1 band (or Upper L-band) and the future GPS L5 band (in the Lower L-band), as depicted in Figure 2.2. This devised signal structure makes it easier to design dual-frequency receivers that will combine both Galileo and GPS signals for civil aviation purposes, with a large enough separation between the two carrier frequencies that will allow for an effective elimination of ionosphere propagation effects.

Each of the different navigation signals either belong to one type of service or are shared between the freely available Galileo Open Service (OS) and SoL Services, or the more restricted Public Regulated Service (PRS) and Commercial Service (CS). As detailed in [38, 37, 59], some Galileo navigation signals are composed of a data and a dataless component, while others only contain one data channel. In all, a total of 6 navigation signals are to be transmitted by the Galileo system in 3 frequency bands, divided into 10 signal channels or components:

- 4 signal channels (OS/SoL/CS) in the frequency range 1164–1215 MHz (E5a–E5b);
- 3 signal channels (CS/PRS) in the frequency range 1260–1300 MHz (E6);

- 3 signal channels (OS/SoL/CS/PRS) in the frequency range 1559–1591 MHz (E2-L1-E1).

The continually shown openness for international cooperation and the system's compatibility and interoperability with the existing GPS are essential conditions that will allow SoL applications to adopt the European system as a second GNSS constellation for the provision of positioning information. The current thesis will investigate the combination of the GPS L1 and L5 signals with the Galileo E1 and E5 signals, as a basic dual-frequency, dual-constellation system.

2.1.4. GPS measurements and error sources

This section will provide a brief technical overview of how GPS measurements are being utilized at present by civilian users. A complete overview of the fundamentals of GPS which lay at the basis of the research in this dissertation is also available in more detail in [61]. When additional GPS signals or GNSS constellations become operational, the information which they provide will be processed in a similar manner, by extension of the current methods to the new signals.

The GPS observation equations for the code pseudorange and respectively the carrier range at each frequency bandwidth are:

$$\rho = r + b - B + I_\rho + T + \nu_\rho \tag{2.1}$$

$$\phi = r + b - B - I_\phi + T + N \cdot \lambda + \nu_\phi \tag{2.2}$$

where the above symbols represent specific quantities to each satellite LOS to a single user, and a set of two such equations corresponds to each single-frequency signal. The literals above represent the notation employed throughout this dissertation and have the following signification:

ρ is the code pseudorange measurement at each frequency

ϕ is the carrier phase measurement at each frequency

r	is the true range, or distance between the satellite and the user
b	is the receiver bias, or clock offset from GPS time
B	is the satellite clock bias, or offset from GPS time
I	is the ionospheric delay, measured from the code (positive) or at the carrier (negative)
T	is the tropospheric delay
ν	represents the receiver thermal noise and multipath delay, as measured at either the code or the carrier
$N \cdot \lambda$	is the integer cycle ambiguity specific to the carrier wave measurements

An overview of how position is determined starting with the above range measurements, and more specifics on how range measurement errors are modeled in this thesis will be provided as appropriate in the following chapters 3 and 5. The GPS ranging measurement error sources, as presented in [61, Ch. 5], are illustrated in Figure 2.3 and described below:

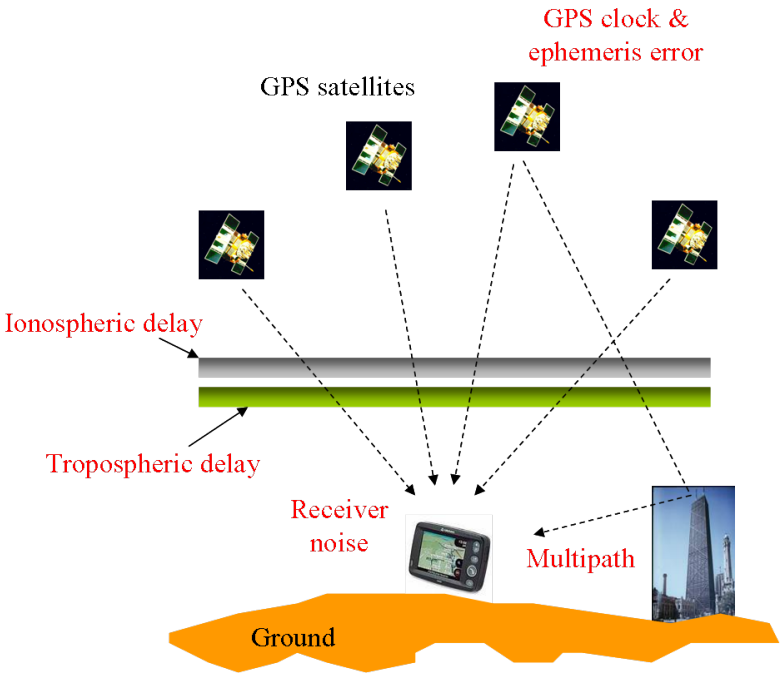

Figure 2.3.: GNSS range measurement errors.

Satellite Clock Error: This represents the difference between the actual GPS time and that of the clock onboard the broadcasting spacecraft, which accumulates small drifts over time and which is periodically reset / corrected during data uploads from the MCS. Before May 2000, there used to be two error sources: the real residual clock and the Selective Availability (SA) intentional clock dithering. The SA was deactivated in 2000, following a US Presidential Decision, and in September 2007 the DoD decided that this capability will not be implemented on future SVs, effectively making the disabling of the SA permanent.

Satellite Ephemeris Error: This represents the difference between the real satellite in-orbit position and the spatial position predicted by the most recently broadcast ephemeris model. Currently, the satellite clock and ephemeris error terms, have a combined 1-sigma value (σ_{URA}) of less than 1 m, and their value has been continually decreasing as the GPS evolved over time [57].

Ionospheric Delay: The Earth's ionosphere is a refractive medium affecting the propagation of GPS signals. The code phase is delayed and the carrier phase is advanced, mostly by equal amounts [19]. The time delay is proportional to the Total Electron Content (TEC) in the ionosphere, and the electron density is a function of time and location. The nominal ionospheric zenith delay typically varies at mid-latitudes from about 1–3 m at night to 5–15 m in the mid-afternoon, while magnetic storm events generally triggered by solar activity can increase the amount of the vertical delay to over 50 m [24]. This delay can be mitigated by using multiple frequency GNSS signals as it will be explained in Chapter 5.

Tropospheric Delay: This delay is caused by the signal traveling through the lower atmosphere, and its magnitude depends on the broadcasting satellite elevation, local temperature, barometric pressure, and humidity. The cumulative amount of this error is on the order of 2.5–25 m. After users correct this error based on a known model [85, sect. 2.1.4.10.3], the residual value of tropo errors can be reduced to 1 m or less.

Receiver Clock Error: This represents clock deviations caused by the imperfect oscillator used in the receiver, which is almost always designed as a low-cost component. The error is common to all pseudorange measurements and it can generally be eliminated as a fourth unknown coordinate during the user position estimation.

Integer Ambiguity: The carrier wave observations also suffer from an ambiguity error [60, sect. 4.1.2], because the distance between a satellite and the receiver is represented by an unknown number of integer wavelengths or cycles in addition to the fraction of cycle measured by the receiver Phase Lock Loop (PLL).

Multipath Effect: This effect describes the phenomenon of a positioning signal reaching the user antenna via two or more propagation paths, usually due to reflection and diffraction of the radio waves off obstacles lying in the user proximity. Multipath errors can be reduced by using careful siting, a narrow correlator receiver, antenna gain pattern shaping, or a software calibration algorithm [61, sect. 10.7]. Approximate theoretical models have been devised for the aviation user [85, 87], taking into account antenna patterns and attempting to average multipath phenomena over a variety of settings [64]. The future GNSS would have a better performance in multipath mitigation, through different phasing of the reflections of the different frequencies.

Receiver Noise: This type of error comes largely from the thermal noise in the receiver front end, which can be approximated as white Gaussian noise. In general, the receiver noise error is on the order of magnitude of 1 m for code measurements and 1 mm for carrier measurements. In this thesis, a single model will be used for describing both the multipath and receiver noise errors.

A large portion of the total GPS range measurement error is common to all users or very highly correlated over relatively short distances ranging from ten to a few hundred kilometers. The only errors that are user location specific, other than the user clock bias, are the receiver noise and multipath and, infrequently, ionospheric disturbances can be highly localized in affecting only certain users. An immediate

application of this property was that of providing differential corrections to high-fidelity positioning and navigation applications.

The concept of Differential GPS (DGPS) relies on placing a receiver at a surveyed location, which is sometimes called a ground station, and using its measurements to compute error corrections by differencing between the estimate based on satellite signals and the known position of this receiver. Furthermore, these differential corrections will be broadcast almost in real-time (RT) to the users in the vicinity of the ground station. The closer these users are to the ground station, the closer will be the differential correction estimate to the actual user errors. Given the usually high spatial and temporal correlation of GPS errors, this procedure has proven very useful in removing most of the above-mentioned ranging errors, thus improving the user positioning accuracy. Residual positioning errors after the differential correction prove to be significantly lower than those in unaided GPS, as documented in [60, sect. 4.1.2] and [43, Ch. 8].

This improvement in performance comes, however, at a cost. The number of ground stations that need to be installed and maintained is directly proportional to the desired coverage area. In the USA, the Wide-Area Differential GPS (WADGPS) and pseudolite systems to assist with airplane landings were precursor concepts to the present-day GPS augmentations systems. Higher positioning accuracy is by itself not sufficient for supporting SoL applications. When human lives are potentially at risk, a user or system would also need a bound on the inaccuracy of its measurements. Nominally, the GPS OC does monitor the end-to-end performance of the navigation system; however it does not have the means to provide timely alarms to the users in the event of a SV or control ground segment failure.

2.2. Case Study: Providing Vertical Guidance to Civil Users

This section will start by introducing the official requirements for a system to meet the safety and other performance considerations necessary for its certification and subsequent utilization in aviation applications (2.2.1). It will then review the systems that are presently in place or upcoming in the immediate future for aiding the GNSS signals, such that their users will be able to derive the necessary performance levels to meet aviation and other Safety-of-Life standards (2.2.2). A brief discussion on the remaining challenges for the civilian use of future GNSS will sum up the topic.

2.2.1. Aviation navigation requirements

The US Federal Aviation Administration (FAA) is making constant efforts to go a step farther than the GPS OC to service users in high need of safety assurances, with a specific focus on civil aviation users. Therefore it is appropriate that the needs of aviators will constitute the primary concern of the current research, while the concepts developed over the course of this dissertation can be subsequently applied to other categories of users as well. The objective of the FAA in using GPS is to provide enhanced services and reduce infrastructure cost for aircraft navigation. For that purpose, the Required Navigation Performance (RNP), among other requirements, must meet four different metrics. These parameters are defined in [85, 87] as follows:

Accuracy is the measure of the deviation of the navigation position estimate from the true position under nominal fault-free conditions. It is typically specified as a 95% (or 1.96 σ) bound on the position error. The fault-free mode, also called the H_0 hypothesis, represents an operating condition of a given subsystem for which all functions are performed in a normal manner.

Integrity is a measure of the trust that can be placed in the correctness of the information supplied by a navigation system in its entirety. It includes the ability of

the system to provide timely warnings (alerts) to users when the system should not be used for the intended operation. *Integrity risk* is the probability of an undetected navigation system error or failure that results in Hazardously Misleading Information (HMI) being passed to the aircraft pilot. The navigation system must be able to provide error bounds in real time under all conditions.

Continuity is the ability of the total system (comprising all elements necessary to maintain aircraft position within the defined airspace) to perform its function without interruption during the intended operation. It represents the probability that the specified system performance will be maintained for the duration of a phase of operation.

More specifically, continuity is the ability to provide the navigation function over the entire course of a flight operation, presuming that the system was available at the beginning of that phase of operation and was predicted to remain available throughout the operation. It is measured as the likelihood that the navigation signal-in-space (SIS) supports both the accuracy and integrity requirements for the duration of the intended operation. *Continuity risk* is the probability that a procedure will be interrupted by a loss of services, or that a detected but unscheduled navigation function interruption occurs after an approach has been initiated.

Availability is an indication of the ability of the system to provide usable service within the specified coverage area with the required accuracy, integrity and continuity. Signal availability is the percentage of time that navigational signals transmitted from external sources are available for use. Availability is a function of both the physical characteristics of the environment and the technical capabilities of the transmitter facilities.

Strictly for RNP purposes, availability is the ability of the navigation system to provide each user with the required function and performance at the initiation of their intended operation. Its corresponding metric is the probability that the

navigation and fault detection functions are operational and that the signal accuracy, integrity, and continuity of function requirements are met. Short-term system availability is the probability that the aircraft can conduct the approach at the destination given that the service at the destination was predicted to be available at dispatch. Long-term service availability is the probability that the SIS from the service provider will be available for any aircraft intending to conduct the approach.

The availability and continuity of service metrics are interdependent and both are measured against meeting the integrity standard prior and during the execution of an aviation approach. For vertical guidance in particular, the system is available when the Vertical Protection Level (VPL), the estimated vertical error bound, is less then the specified Vertical Alert Limit (VAL). Similarly, for lateral guidance both requirements are satisfied when the Horizontal Protection Level (HPL), an estimated horizontal error bound, is less than the Horizontal Alert Limit (HAL) throughout the given operation. In general, the Alert Limit (AL) for a given parameter measurement, is defined as the error tolerance not to be exceeded without issuing an alert. Conversely, when the computed error bound exceeds the alert threshold, the integrity requirement mandates that an indication is provided to other aircraft systems or an annunciation is issued to the pilot in order to identify that an operating parameter of a navigation system is out of tolerance. Failure to do so constitutes a hazardous condition, which should not occur more frequently than a strict probability specification.

In the context of air navigation safety, misleading information is defined to be any data that is output to other equipment or displayed to the pilot, and which has an error larger than the alert limit (AL), without any annunciation of the error (e.g. flag) within the time-to-alert (TTA) for the applicable phase of flight. For equipment that is unaware of the navigation mode, such that implicitly the AL is also not known, the HMI is defined relative to the current Protection Level (PL).

Finally, the navigation mode refers to the aircraft phase of flight, encompassing the following modes: oceanic / remote, en route, approach, departure and terminal.

<table>
<tr><th rowspan="3">Aircraft Phase of Flight</th><th colspan="2">Accuracy</th><th colspan="3">Integrity</th><th colspan="2" rowspan="2">Maximum Probabilities of Failure</th></tr>
<tr><th colspan="2">(2σ or 95%)</th><th colspan="2">Alert Limits (4-6σ)</th><th rowspan="2">Time To Alert</th></tr>
<tr><th>Vertical</th><th>Horizontal</th><th>Vertical</th><th>Horizontal</th><th>Integrity</th><th>Continuity</th></tr>
<tr><td>NPA, Initial Approach, Departure</td><td>N/A</td><td>0.22 - 0.74 km</td><td>N/A</td><td>1.85 - 3.7 km</td><td>10 - 15 s</td><td>10^{-7}/hr</td><td>10^{-4}/hr</td></tr>
<tr><td>LNAV / VNAV</td><td rowspan="5">20 m</td><td>220 m</td><td rowspan="2">50 m</td><td>556 m</td><td rowspan="3">10 s</td><td rowspan="6">1-2 x 10^{-7} / 150 s</td><td rowspan="6">4-8 x 10^{-6} / 15 s</td></tr>
<tr><td>LPV</td><td rowspan="6">16 m</td><td rowspan="6">40 m</td></tr>
<tr><td>APV I</td><td>35 m</td></tr>
<tr><td>APV II</td><td>8 m</td><td>20 m</td><td rowspan="3">6 s</td></tr>
<tr><td>LPV-200</td><td rowspan="2">4 m</td><td>35 m</td></tr>
<tr><td>Precision Approach CAT I</td><td>10 m</td></tr>
<tr><td>Precision Approach CAT II/III</td><td>< 2.9 m</td><td>< 6.9 m</td><td>5.3 m</td><td>< 17 m</td><td>< 2 s</td><td>< 10^{-9} /150 s</td><td>< 4x10^{-6} /15s</td></tr>
</table>

Table 2.2.: FAA and ICAO requirements for landing of civil aircraft [41].

As part of the same specific phase of flight, the approaches are divided into types that are generally differentiated by the specific operational requirements applying to each category (see Table 2.2). Additionally, for each approach there are separate requirements regarding the overall visibility and the runway visual range (RVR) as determined at or before passing the Final Approach Fix (FAF) point, which is considered to be the initiation point for the respective approach. Depending on the height of the FAF point, each approach type has a corresponding Decision Height (DH). The particular type of approach that will be used throughout this dissertation in order to evaluate the performance of the vertical guidance algorithms proposed in the following chapters is the LPV 200 approach [18, 49]. In addition to the above mentioned

navigation requirements, its corresponding parameters are a 200 ft (60 m) DH, and either a visibility of 0.75 nmi or an RVR not less than 0.5 nmi. If the required visual reference to continue the approach has not been established by the time the airplane reaches an altitude equivalent to the DH, and no additional instrument-based landing system is available for further guidance, a missed approach procedure must be immediately initiated.

2.2.2. GNSS augmentation systems

By applying differential corrections to measurements made with a satellite navigation system like the current GPS, only the performance in terms of accuracy can be directly improved among the aviation requirements enumerated above. As integrity means also bounding the inaccuracy, the ability to bound SIS measurement errors is planned to be implemented in modernized GPS, as well as in additional GNSS constellations. However, in the case of GPS, this capability is not expected to be operational for at least the next two decades, and it is unclear when Galileo will achieve this functional ability. Until that time, aviators who would like to navigate with the aid of GNSS require additional infrastructure to compile and broadcast integrity information. As a consequence, through diligent engineering work over the last decade of the 20^{th} century, in the current decade it was possible to commission into operation systems formed of ground monitoring stations and/or GEOs that augment the existing GPS and provide both differential corrections and integrity information for safety-critical GPS uses. In a need to strike an optimal balance between short differential baselines for more precise corrections, a large area of geographical coverage and prompt alert times, both local area Ground-Based Augmentation Systems (GBAS) and Space-Based Augmentation Systems (SBAS) were devised.

GBAS include the world's first certified GPS Landing System (GLS) — Special Category I (SCAT-I) in Norway, the Ground-Based Regional Augmentation System (GRAS) under development in Australia and the Local Area Augmentation System (LAAS) in the USA which has successfully completed a prototype testing phase just

over a year ago. These systems generally rely on installing monitoring stations at each airport or for a smaller area on the order of 100 km^2.

For geographic surfaces of the size of entire continents, where there is a need for the information to travel within seconds from measuring stations over the entire area to a central processing station and then to the user, the augmentation systems will include a GEO satellite that has the role of relaying an additional data signal to all users. Such currently operational systems are the Wide Area Augmentation System (WAAS) over North America, the European Geostationary Navigation Overlay Service (EGNOS) over Europe, and the Multifunctional Satellite Augmentation System (MSAS) over Japan. Additionally, India is in the process of commissioning its own GPS Aided GEO Augmented Navigation (GAGAN) system. Some governments in Asia are currently going one step farther, such is the case of Japan's upcoming Quasi-Zenith Satellite System (QZSS), proposed for further enhancing GPS over the far East and Australia. This system is planned to evolve beyond the level of a SBAS into an actual regional navigation system, much like the neighboring China's Beidou system and India's Indian Regional Navigational Satellite System (IRNSS), which are anticipated to come into operation over the next 5 years.

The aforementioned augmentation systems were designed to operate based on measurements with the currently existing GNSS constellation (i.e. using mainly GPS), however their design is sufficiently flexible to include the capability of processing ranging measurements from any of the upcoming GNSS. Yet, the still-standing challenge is that of extending SBAS coverage to support truly global navigation operations seamlessly, while still meeting the International Civil Aviation Organization (ICAO) mandated 6 s Time-to-Alert requirement. The purpose of the current dissertation is to find an alternate way to address the above challenge. More specifically, this thesis will discuss a method to provide the same performance of the current-day WAAS in a more efficient way, with regards to the allocation of resources and integrity responsibility between ground and space systems and the users themselves.

2.3. Aircraft-Based Augmentation Systems (ABAS)

The current section will start by providing a motivation for using ABAS in the context of the larger and more complex airspace system in the USA (2.3.1). The current thesis research investigates the provision of information to aircraft systems in order to help obviate Controlled Flight Into Terrain (CFIT), which is the leading cause of aircraft fatalities and can be mitigated with vertical guidance. Additionally, the current research effort seeks ways to provide this vertical guidance without incurring the cost of dedicated equipment at each airport to be served. A discussion will follow in 2.3.2 on the advantages and potential drawbacks of performing integrity monitoring autonomously in the aircraft. This background chapter will then close with a summary of the previous research that enabled the accomplishments presented in this thesis (2.4.1).

2.3.1. Motivation

The FAA is currently involved in a comprehensive plan of restructuring the aviation infrastructure for the US National Air Space (NAS), and of transitioning to a proposed Next Generation Air Transportation System (NextGen). While satellite-based navigation is not the solution to all the problems being addressed, it is an essential part of the FAA vision for the next 25 years. A few of the advantages of using satellite navigation for both civil aviation guidance and commercial air traffic control and scheduling will be enumerated below, after which it will be pointed out where the focus of the research in this thesis fits into this larger picture.

Aviation guidance in the USA at the end of the 20^{th} century relied on radio navigation aids (navaids), such as the Very High Frequency Omni-directional Range (VOR) beacons and Distance Measuring Equipment (DME), and Inertial Navigation Systems (INS) to help aircraft with establishing their en route trajectory. It also relied on the Instrument Landing System (ILS) to assist with landing approaches at airports. Instead of the current system of flying straight line segments between VOR

waypoints, the use of GNSS can assist pilots in flying point-to-point on a continuously-defined curved path. Therefore, satellite navigation can help increase the overall flight-planning efficiency in terms of setting more flexible ways to define optimal flightpath, maximizing the airport traffic capacity, as well as minimizing the path, velocity, and altitude constraints on in-flight airplanes. This renewed efficiency would also translate in significant fuel savings and decreased environmental impact in the form of noise, emissions or any other type of interference. Finally, traffic guidance based solely on ground beacons is quickly reaching capacity in the US, given the difficulty in building new airports safely spaced out from the current air hubs or continually increasing the capacity of existing airports. Implementing NextGen will result in cost savings from the FAA being able to eliminate ground navaids and implicitly the related expenses for installation, maintenance and land leases for this equipment, which are not sustainable in the long run. Since GNSS is not area-limited and does not need to be scaled with the number of users, the transition to satellite-based navigation would therefore allow overcoming the current constraints of both the capacity and timing of commercial flights.

However, one of the key problems that needs to be addressed in implementing an entire aviation system reliant on GPS and GNSS is that of the safety risks potentially introduced by this new technology. Flight safety is a paramount concern, and any potential danger against human lives needs to be appropriately addressed. From an aviation standpoint, integrity monitoring functionality would be ideally integrated into the future GNSS. It seems that the optimal way to do that would be to build the integrity monitoring capability into the ground segment of any GNSS and share the same facilities that already provide its control, monitoring and SIS accuracy functionality. In this manner, ground resources would be most efficiently utilized while the GNSS SVs themselves could be the ones providing integrity information. The Galileo system is in fact projected to combine all these capabilities into its ground sensor network and provide signal accuracy and integrity as part of its SoL services. However, GPS was initially developed with categories of users in mind that are most interested in high availability and positioning accuracy rather than integrity.

While work is in progress to include integrity capabilities in the third generation of modernized GPS III satellites (in the 2030 timeframe), another attractive option is for the aviation community to retain control over its own integrity monitoring systems and keep a separation between the accuracy and integrity functions. The option explored in full depth in this thesis is that of locating most of the integrity functionality in the aircraft cockpit, while stating the additional requirements which need to be fulfilled by the space and ground segments of a GNSS in order to enable each airplane to achieve the desired level of navigation performance. Such an architecture is called in general terms an Aircraft-Based Augmentation System (ABAS).

2.3.2. The Use of RAIM in Conjunction with GNSS

Generally, an ABAS implies the use of Receiver Autonomous Integrity Monitoring (RAIM) algorithms within the cockpit, instead of relying on external signals to provide integrity assurance for the aircraft operations. RAIM works on the principle that measurements from redundant satellites (i.e. beyond the minimum required to estimate the user position) can be employed in order to protect the user against large positioning errors. As long as the likelihood of a multiplicity of the range measurements to be hazardously erroneous is low, a majority of the satellites in view can be trusted to have low levels of error. Thus, a statistical comparison between their corresponding pseudoranges can help identify faults along any of the lines of sight and contribute to decreasing the positioning error by eliminating the outliers. To quantify the above statement, a sufficiently low probability of measurement fault is that for which the chance of a majority of the measurement channels containing a fault is lower than a fraction of the total integrity risk budget as shown in Table 2.2. In particular, for the WAAS-certified LPV 200 approaches, the maximum acceptable value for the integrity risk is 1 part in 10 million (or 5.33 sigma if a normal error distribution is assumed).

The initial step in offering ABAS as an alternative to WAAS-like systems is to replicate the performance of the latter while lowering the requirements on the future ground infrastructure. Therefore, the same integrity risk benchmark will be set for RAIM with unaugmented GNSS as in present-day WAAS. Three different options for architectures that redistribute the integrity responsibility between the space, ground and user segments of the next generation of aviation satellite navigation systems will be presented in more detail in the first section of Chapter 3. A brief overview will be included here only on the differences between the Absolute RAIM (ARAIM) architecture and the current GNSS augmentation systems.

Given the fact that in ABAS the integrity monitor and the user are collocated in the cockpit, the short TTA requirements become less of an issue, as the pilot would be able to monitor the fault status of all satellites in view in real-time. Even assuming a 1 Hz sampling rate for making range measurements, the longest interval between the moment when a fault becomes detectable and the instance when it is displayed to the pilot and can be accounted for by the aircraft control is of 1-2 sec. The RAIM algorithm developed in this thesis will ensure very fast computational times. It will also give aviation users the ability to detect and eliminate potential failures, immediately after the first measurement update in which the presence of the fault affects the performance of the navigation system and the position error bounds by a small threshold. The precision with which navigation Protection Levels (PLs) will be determined in this work will be set to 1 cm for algorithm testing purposes in later chapters. Therefore, the minimum change in the VPL interval caused by a detectable measurement anomaly will also be on the order of centimeters, a full two orders of magnitude below the specified maximum acceptable error bounds known under the name of Alert Limits (AL). The novel approach to fault detection is one of the key improvements brought to RAIM by the research in this thesis, along with the exploration of a comprehensive threat space, including multiple simultaneous faults, constellation failures, and measurement biases. The full framework of the RAIM algorithm will be also described in Chapter 3.

The three parameters that a user will expect to be provided by a combined ground and space constellation monitoring system are the User Range Accuracy (URA) or SIS accuracy, a value of the maximum nominal user range bias and an *a priori* probability of failure for each of the satellites in view, based on the long-term history of occurrence of such incidents in the respective constellation. The effect of these external parameters on the RAIM performance will be explored in Chapter 4 of this dissertation. Provided the ability of ARAIM to generate integrity warnings directly at the user location, the additional TTA requirements on space and ground segments that support this type of ABAS can be relaxed considerably. These additional segments will have the mission to provide updates to the user with a frequency of only once an hour or two, though it is recommended that informational messages be repeated more often without update to enable rapid initialization of the user systems and also an extra level of redundancy. With the much lower data bandwidth that is required in this case, it becomes feasible to broadcast the satellite health and integrity information directly through the GNSS satellites, as opposed to having additional dedicated GEOs and associated transmission channels for this purpose.

An additional constraint that ARAIM places on an external GNSS constellation is an increased robustness in the measurement geometry, in terms of the number and distribution of the ranging beacons across the sky. The results in [26, 99] establish that an average of 6 additional satellites in the GPS constellation would be necessary to ensure a navigation performance equivalent to that of the present-day WAAS, while operating with a GPS constellation that guarantees 24 SVs equally spaced in orbits across the sky. The trade-off for having to maintain an additional 6 GPS satellites in orbit is however not having to maintain additional GEOs and a net reduction in the complexity of the ground monitoring network. Nevertheless, given that the projected availability of new GNSS constellations over the next decade will more than double the overall number of positioning satellites in orbit, an ARAIM-based navigation solution will be the one best suited to take advantage of the multi-constellation setting with signals at additional civil frequencies.

2.4. Previous Work

Before proceeding with the full development of a RAIM algorithm that will enable the ABAS infrastructure outlined above to support civil aviation operations, an overview of the prior art in the field of RAIM will be provided here. A considerable amount of research effort has been dedicated to providing ARAIM capabilities to avionics navigation systems. Additionally, a number of studies have been performed on validating the performance of previously proposed RAIM algorithms through computer simulations, as well as with data from real-life airplane flights. Finally, the modeling of the nominal GPS pseudorange errors has been of interest from the point of view of aviation and non-aviation applications alike.

2.4.1. Overview of existing RAIM methods

Over the past two decades, studies of RAIM techniques have known a considerable development, accompanying the steady improvements in GPS service to civil users of satellite navigation. Pioneers of RAIM, such as R. Grover Brown [13], Young C. Lee [50], Mark A. Sturza [90] and Bradford Parkinson [75] have made significant contributions to these algorithms even before GPS became fully operational in January 1994. A synopsis on classical RAIM algorithms will introduce Section 3.2. Later on in the 1990s, while the civil GPS signals still contained the Selective Availability (SA) degradation until year 2000, a significant group effort took place for defining RAIM standards that would be applicable to civil aviation [51].

At the turn of the millennium, with the announcement of the planned deployment of the European Galileo system, renewed efforts were made to reap the anticipated benefits of having at least two interoperable constellations available for navigation purposes. Given the expected increase in the number of ranging sources for the aviation user, a breakthrough is expected to be made in the use of satellite navigation for precision approaches and other critical operations. Recent developments have already been published in an effort to improve the original Least Squares

(LS) and Solution Separation (SS) RAIM algorithms. Newer flavors of RAIM include NIORAIM [39], the Optimally Weighted Average Solution (OWAS) algorithm [53], Multiple Hypothesis Solution Separation (MHSS) [77] and snapshot and sequential algorithms based on the Generalized Likelihood Ratio (GLR) [68]. A special mention needs to be given as well to Pieter B. Ober for the most comprehensive theoretical treatment of modern RAIM methods to date [70], which, along with the previously referenced work, constitutes the basis for significant further development.

In anticipation of the future launches of dual-frequency GNSS satellites, such as Galileo and GPS III, a series of new developments has taken place in the field of RAIM. Of particular interest were the topics of multi-constellation RAIM and analyzing the impact of multiple simultaneous ranging failures. In the current decade, with the perspective of a modernized GPS constellation and additional GNSS systems being developed by other countries, the focus has shifted towards including satellites from multiple constellations [52]. In addition to that, the current research will also accounting for the higher likelihood of multiple failures by employing multiple hypothesis techniques [25]. The MHSS RAIM algorithm investigated in this dissertation is one of the first algorithms to implement multi-constellation RAIM with the possibility of multiple simultaneous failures across all constellations. To capitalize on the latest opportunities offered by the field of satellite navigation, the goal of the research presented in the following chapters of this thesis is to optimize the performance of an unaided multifrequency GNSS constellation from a vertical integrity standpoint for aviation precision approaches.

2.4.2. RAIM algorithm performance testing and range error model validation

Along with the development of different flavors of RAIM algorithms over the course of the past 20 years, studies have been conducted to demonstrate the performance of the proposed methods relative to the stringent safety requirements of aerial navigation. Among the early pioneers in the field, Brown conducted simulations of

RAIM performance [15], employing different values of the number of satellites in the GPS constellation.

More recent efforts, enabled by the processing capabilities of modern computers, have involved conducting worldwide simulations of RAIM integrity [68], including parallel work performed while the current thesis research was in progress [56]. Other coetaneous efforts with the current research work produce simulations of inertially-aided RAIM fault detection methods for dual constellation Galileo / GPS [35] for a single user at a time. The results presented by these authors, where the used RAIM methods are comparable, are very much in agreement with the conclusions presented in the current thesis. However, no previously published studies systematically simulate the worldwide performance of an incomplete dual constellation. Therefore the work presented here (in Chapter 4) comes to fill an existing gap, by studying under-populated constellations during the initial deployment phase of dual-frequency emitting spacecraft into orbit, as well as several options for each full modernized GPS or Galileo constellation, with up to 30 active spacecraft arranged in geometry-optimized orbits.

In terms of the external parameters influencing the ABAS performance, existing literature illustrates results with sets of typical parameter values [53, 54, 65], which do not capture the entire picture of the dependence of PL values on the multiple parameters. They presented results are for simulations over the US with a number of selected values of the URA and mask angle values, but this earlier research does not explore the entire nominal bias and failure prior threat spaces. After the results obtained as part of the current dissertation research were published [26, 28], independent studies at the MITRE Corporation's Center for Advanced Aviation Systems Development (CAASD) [55] have confirmed the present findings by showing availability figures for the required integrity level which do not differ by any significant amounts. In summary, existing simulation studies have determined the RAIM performance at

isolated points in the parameter space, in agreement with this dissertation. However, they did not also capture the continuous values of the integrity and availability metrics as a function of each parameter.

A small number of the previous research efforts on RAIM algorithms also culminated with a verification of the operational performance for air navigation with real flight test data. The validation of RAIM performance for aviation approaches started in the mid-1990s [62, 76, 11], and continued in order to support the certification of RAIM algorithms used in conjunction with the GPS measurement corrections broadcast by augmentation systems in the US and worldwide [33, 66]. Nevertheless, this thesis represents the first effort at validating an ARAIM algorithm with real time dual-frequency L1-L2 GPS flight data that did not benefit from corrections broadcast by WAAS or another external augmentation system. A subsequent independent analysis by MITRE / CAASD came to confirm the positive results obtained in this work [23].

Finally, in order to complement the performance tests of integrity algorithms, there is a need to initiate validation efforts for the range measurement error models that serve the specific needs of users in the airborne environment. In the post-SA era, studies of past performance of GPS SIS in the vein of the analysis in the PAN Reports [34] were undertaken [91]. However, these approaches were not always forward looking in their characterization of the error. A more general model for the pseudorange errors was proposed by the WAAS MOPS [86, sect. 2.5.9.2] and LAAS MASPS [87], this error model having been derived and validated in the process of establishing the WAAS and LAAS performance standards. Nevertheless, most prior measurements of the errors have been carried out on the ground by the WAAS reference stations and other existing ground monitoring facilities. Studies with flight data were limited to the observations of a particular error type, e.g. multipath or antenna delays [63, 64], and did not cover the comprehensive error model. These previous investigations are confined to L1 civil navigation signal measurements, and no previous efforts were made to characterize the pseudorange errors resulting from the

L2 semicodeless measurements with ground or airborne receivers for aerial navigation applications.

Part II.

MHSS RAIM - Model and Simulation

The first part of the work performed towards the completion of this dissertation involves the development and simulation effort for an advanced RAIM method. The Multiple Hypothesis Solution Separation (MHSS) algorithm introduced in this part is designed to take advantage of the increased number of ranging sources and the improvement in ranging accuracy afforded by dual frequency diversity. These advances are expected over the next decades, with the advent of modernized GNSS constellations. The intent of this initial effort was to provide a proof-of-concept scheme for a RAIM algorithm that is able to achieve the required navigation performance for aviation LPV 200 approaches worldwide, relying solely on unaided GNSS signals.

The overall purpose of this thesis work is to evaluate the performance of an unaided dual-frequency satellite constellation from a vertical integrity standpoint for aviation precision approach. Within that context, the focus in the next two chapters will be on the development of a RAIM algorithm, based on the earlier MHSS prototype in [77]. The current algorithm differs significantly from the classical versions of the Least-Squares (LS) and Solution Separation (SS) RAIM algorithms, both in what concerns the intrinsic statistical approach towards error overbounding, as well as in its approach towards Fault Detection and Elimination (FDE). The devised FDE method emphasizes the achievement of an optimal user performance over directly identifying a particular faulty system component, or any attempts to determine the absolute failure state of the overall navigation system. The probabilistic model also allows the MHSS algorithm to produce a prediction for the Protection Levels (PLs) achievable with a given satellite geometry, a novel capability which was not present in any of the previously published RAIM algorithms. A standardized and comprehensive failure threat model for use with satellite navigation integrity applications has also been proposed and the extent of this threat space, in which the desired navigation performance is achievable, has been determined through the means of parametric computer simulations.

The scope of Chapter 3 is to describe the development process of the MHSS algorithm. It will provide an overview of the underlying assumptions and the description of the threat space. Afterwards, the framework of the proposed RAIM method will emerge from ideas contained in previous RAIM algorithms through a set of original enhancements, which constitute one of the primary contributions of this thesis. The subsequent analysis of the navigation performance of this algorithm in Chapter 4 will culminate with studies on the sensitivity of the obtained results to external parameters, which characterize the space and ground segments of the navigation system. The conclusions of this analysis have already been instrumental to the FAA GPS Evolutionary Architecture Study (GEAS) workgroup [32], whose mission was to make recommendations on the future architecture of satellite navigation systems to support aviation operations within the US National Airspace System (NAS).

3. Algorithm Development

This chapter will describe the original contribution made by this dissertation to MHSS RAIM algorithms, as an incremental development of the MHSS algorithm with respect to an existing method proposed by [77]. The earlier MHSS RAIM algorithm only considered the possibility of a single measurement fault, and without offering a precise definition of a "*satellite failure*". It subsequently optimized its integrity risk allocations based on prior failure probabilities and the knowledge of the real-time measurement vector, but in the process it employed a number of approximations which would not always pass a rigorous analysis to determine the maximum guaranteed Probability of Hazardous Misleading Information ($\mathcal{P}$HMI) [6]. One of these assumptions was that the prior probability of failure for a given satellite is the same as the *a posteriori* probability, after making a measurement of distance between the user and that satellite. In the case in which the user has a relatively good estimate of their position from an earlier measurement, or based on a significant number of redundant range measurements to additional satellites, this gives them the ability to detect the presence of a fault in the current measurement. Accordingly, the posterior probability will grow very close to 1, and the above assumption clearly cannot hold if the given prior is actually much smaller and thus closer to 0. This distinction between *a priori* and *a posteriori* fault probabilities will be further expounded in section 3.3.3. Finally, the earlier version MHSS algorithm did not include FDE capabilities, which will prove to be the essential ingredient in providing the required RAIM performance without relying on ground augmentation.

This thesis will propose an enhanced Multiple Hypothesis RAIM algorithm, originally published in [26], for which both a theoretical proof of concept and a practical verification of the achieved navigation performance are being provided. This is a more rigorous treatment of the subject than the basic requirements of the WAAS MOPS [86], which specify that certified algorithms must pass a simulation test. The trajectory of this research will be different, although there is a rich history in this field of testing algorithms to show that they work satisfactorily only through simulation, and without a rigorous theoretical proof that the $\mathcal{P}$HMI requirement is satisfied for any combination of threats. All algorithms developed in this thesis will be verified mathematically at the outset (Chapter 3), before implementing them in simulation (Chapter 4), and finally validating them against flight test data (Chapter 6). Additionally, the current work will formalize an original failure detection and exclusion method for the MHSS algorithm (section 3.3.2), originally published in [27]. It will also assess the capability of MHSS to predict VPLs without a set of local pseudorange measurements (section 3.3.3), originally developed in [28], such that airplanes en route to a certain airport would have the ability to forecast conditions at the target airport for initiating GNSS-assisted approaches.

The current chapter will start by discussing the type of assumptions that need to be made about GNSS and its associated monitoring systems, which will be relied upon to provide to the user system health information and data about the current nominal performance of the system. Section 3.1 will be divided between discussing the system architecture and establishing a threat model for the potential faults that a user can expect, and also a model for the nominal errors that will be observed. Subsequently, Section 3.2 will provide an overview of the fundamental RAIM algorithms that have been previously proposed for non-precision aircraft operation, and whose method and results will serve as the reference for the subsequent development of the MHSS algorithm. Section 3.3 will contain the theoretical principles of the newly-developed algorithm and its applications to Real-Time (RT) integrity monitoring, Fault Detection and Elimination (FDE) and a prediction tool which can provide a "dispatch" Protection Level (PL) to the user. The mathematical description of

MHSS RAIM will be followed in Section 3.4 by a summary discussing the advantages of MHSS on existing snapshot RAIM methods, and by a validation of the algorithm through simulation in Section 4.1.

3.1. Underlying Assumptions

The current discussion of the MHSS algorithm will start by describing the underlying assumptions made with respect to circumstances independent of the users, which nevertheless affect their ability to precisely estimate the current position and correctly determine the bounds on the errors affecting this estimation process. The existing GPS satellites by themselves do not provide sufficient measurement integrity, nor can they guarantee availability and continuity of service in order to replace the current system of ground-based navigation aids for manned Safety-of-Life (SoL) applications such as aviation, maritime and land transportation [58]. Moreover, there are aspects such as the maximum Time-To-Alert (TTA) for certain operations which make it difficult to attain the required performance worldwide even when relying on additional GNSS augmentation systems.

Consequently, an important objective for future GNSS architectures is to reach a level of service equivalent to that of present-day man-rated radio-navigation aids, such as the ILS, VOR and DME stations in the USA. Of all the federally-mandated navigation performance metrics, the integrity requirement is the most difficult for a system to satisfy, as in most cases once integrity is provided, the 95% accuracy is also attained, while the availability and continuity depend on integrity being achieved in the first place. Therefore, the focus of the current work will be initially on the integrity requirement exclusively, and once this initial goal is reached, it will shift to adding in the other performance metrics as well.

3.1.1. System assumptions

Since the initial commission into operation of GPS until the present times, no system integrity information has been broadcast to civilian users by the GNSS themselves. In the earliest development stages of GPS, the primary requirements-driver was weapon delivery accuracy, and only later did the system evolve up to the point where it had to meet a multiplicity of needs, both civil and military. Though it is publicly unknown whether any integrity information had been broadcast by the currently operating GPS and GLONASS to military users, the disclosed information on the performance of the space segment of GPS has shown that over the years the system performance has exceeded its guaranteed standards and it has also been continually improving in time.

The relevant figures made public in regular program updates by the United States (US) Department of Defense (DoD) GPS Wing on the performance of the constellation are yearly summaries of the root-mean-square (rms) Signal-in-Space (SIS) User Range Error (URE). The SIS URE is defined as the projection onto the user line-of-sight (LOS) of the difference between the true values of a GPS Space Vehicle (SV) position and clock offset from GPS Time, and their values according to the navigation (NAV) data broadcast by the satellite. This SIS URE is monitored by the GPS Master Control Station (MCS), based on well-defined algorithms [22], and the levels of error are subsequently uploaded to the SVs on a daily basis and broadcast to the users [**?**]. The most recently published values show an average SIS URE of 0.92 meters, with lower Zero Age-Of-Data (ZAOD) values averaging 0.22 m after a fresh upload [57, p. 15]. The standard deviation of the SIS error values, assuming they are normally distributed, is called the User Range Accuracy (URA) in the Navstar GPS Interface Specification [2, sec. 6.2.1], and the SIS Accuracy (SISA) when referred to in the Galileo system documents. Maximum anticipated URA values are currently broadcast in the navigation data of the GPS satellites as a discrete URA index, whose precision is scheduled to be refined when upgraded civil

navigation (CNAV) data will become available in conjunction with the modernized L2 Civil (L2C) and L5 signals.

Additionally, the FAA William J. Hughes Technical Center (Tech Center) publishes the running values for every quarter of the 95% and 99.99% positioning accuracies measured at its own monitoring stations and the 1–2 σ overall range error, in the Tables 5-1 and 5-2 of its GPS Standard Positioning Service (SPS) Performance Analysis (PAN) Reports [34]. However, these 1–4 σ numbers alone are insufficient for many civilian SoL applications of GPS. Consequently, civilian authorities have worked to set up augmentation systems to GNSS in order to provide the missing necessary safety information. In what concerns aviation applications, non-augmented GPS could meet navigation requirements for phases of flight other than precision approaches according to the Minimum Aviation System Performance Standards (MASPS) for GPS in RTCA / DO-202 [82].

For civil aviation purposes, GPS / GNSS can be used as a supplemental means, but is not yet certified as a sole-means of navigation until GNSS performance is proven to allow the ability to meet all requirements described in section 2.2.1. For the safety of airport surface operations, more than GPS / GNSS alone would be necessary [84], including additional technological solutions such as ADS-B. Nevertheless, the object of the research in this dissertation will be to focus solely on the airport approach phase of flight. At least for the next 20 years,

> *GPS, as currently planned by the DoD, will not provide integrity warnings that meet FAA requirements for all phases of flight considered herein, nor will it provide the continuously available coverage redundancy necessary to satisfy the coverage requirements of a sole-means system. Since there are no coverage requirements for supplemental use of GPS, DoD planned GPS coverage is adequate for GPS supplementary approval.*
>
> *[RTCA/DO-202]*

However, the utility of GPS for aerial navigation has come a long way over the past two decades, and the outlook for the modernized GPS III another 20 years from now is even more promising. The conceptual details of the planned support for positioning

integrity to be built into the GPS system itself were already made public and they are described in [47]. The future of satellite navigation never looked brighter.

As pointed out in the motivation for this work (Section 1.1), the ability of initiating precision approaches is essential at all airports that are likely to experience reduced visibility conditions due to the weather, which will add to the safety hazard of existing constraints on the approach path due to the geographical relief or man-made obstacles. Currently, integrity information for aviation satellite-guided precision approaches is offered by augmentation systems. While other similar systems are in operation across the globe, WAAS is the SBAS operational in the US, and it is designed to cover the entire National Airspace System (NAS) in terms of satisfying the navigation requirements designed by the US Federal Aviation Administration (FAA) and the International Civil Aviation Organization (ICAO).

One of the goals of the current work is to enable autonomous GNSS integrity monitoring and to increase aviation safety for the Next Generation Air Transportation System (NextGen), while reducing the amount of expensive ground and space equipment necessary for the augmentation of satellite navigation signals. Overall integrity monitoring is responsible for addressing the totality of the threats derived from a GNSS signal fault tree, such as the framework outlined by [58, in Fig. 3]. The FAA GNSS Evolutionary Architecture Study (GEAS) Panel has identified three architectures that would allow the positioning integrity workload to be redistributed more efficiently between the user, space and ground segments of the navigation system [32]. The system setup concepts are called Absolute RAIM (ARAIM), Relative RAIM (RRAIM) and the GNSS Integrity Channel (GIC). In ARAIM, the majority of the integrity burden resides with the users themselves, while the GIC architecture lies at the opposite end of the scale, relying almost entirely on integrity monitoring outside the aircraft. However, the GPS III modernized constellation is unlikely to support an integrity channel during the initial phases of deployment until at least 2033, given the necessary lead time for planning and development phases in order to include new features and technologies in the SVs themselves. Therefore, any GIC architecture

before that time would have to rely on an SBAS-like system being deployed and operational worldwide. Such an enterprise would face significant technical challenges in meeting the required 6-second TTA over a vast geographical area, in addition to the financial challenges for the government agencies in the countries involved. A more even distribution of the system integrity responsibility would be achieved with the inclusion of RAIM capabilities in the user equipment.

With RRAIM, the users would also rely on external information from a combined ground and space monitoring system, however they will only require 30–300 s alert rates. In between updates, each user would coast based on redundant range measurements to the satellites in view by using RAIM techniques. In comparison, ARAIM would only require an information update rate of once every 1–2 hrs. This is the same rate as for the current ephemeris information being broadcast by the GPS satellites, making it much easier to support this operational architecture in future GNSS constellations with only a minimal additional bandwidth. Moreover, the ARAIM concept would only require a minimal amount of ground monitoring [8], without all the additional complexities of an SBAS in charge of also determining integrity parameters for the users.

For the case of multiple operational GNSS constellations in the near future, the satellite geometry will readily exceed the minimum necessary for aviation navigation with ARAIM. Nevertheless, in the presence of GPS alone ARAIM would require an estimate of three additional satellites in an optimized orbital configuration in order to provide the same level of performance as RRAIM worldwide. While the use of ARAIM will be slightly more demanding on the GNSS constellation geometry, it has the ability to significantly reduce the required information latency and bandwidth from the external monitoring systems, thus in turn greatly reducing the variable costs involved with the safety of worldwide operation of aircraft. Specifically, the expenses of installing ground stations and space equipment in addition to the GNSS constellations themselves will be optimized, as these costs are generally proportional with the geographical area covered and the total number of runways being serviced.

To enable the ARAIM concept proposed in this dissertation, either the GNSS Operations Center (OC) or monitoring stations maintained by the civilian authorities would need to compile and maintain the historical probabilities of failure for each satellite and constellation, as well as the URA / SISA values, and make regular updates available to the user base. As such, ARAIM is envisioned by the author of this work as a more robust solution for providing navigation integrity to aviation users, as it relies entirely on mature technologies in terms of the user-side integrity determination, the ground monitoring network and the space segment technology. Throughout the rest of this dissertation, the term of RAIM will refer exclusively to ARAIM.

3.1.2. Satellite failure threat space

The *threat space* is a consistent and complete set of assumptions about the environment in which a RAIM algorithm is applied. A standardized threat space can be regarded as a general test case against which each individual algorithm may be verified. It has to be universal enough such that it can constitute a frame in which to apply the particular set of assumptions of each particular algorithm, and it should include all considered threats. The threat space is in fact the sample space of all failure modes, including the nominal conditions or "no failure" case. The terms *failure* and *fault* will be used interchangeably throughout this dissertation.

A *failure mode* is the outcome of each of the navigation beacons (viz. satellites) being in a "healthy" or "failed" binary state, with a certain probability. *Nominal conditions* contain the modes of behavior normally expected from the satellites, propagation medium, and user receiver within the surrounding environment. Under these conditions, corresponding to a *healthy state*, users achieve their expected level of performance. The *failed state* is an anomalous condition that can threaten the accuracy and integrity of the system when undetected, and the continuity and availability when it is detected. Such failures should be infrequent and short in duration. The threat model places limits on the extent and behaviors of fault modes. Each RAIM method

can be different with respect to its vulnerability to various fault modes. Nonetheless, the threat space needs to be all-inclusive, such that all potential events are taken into account, including events introduced by the algorithm itself.

For the purposes of the RAIM algorithms involved in this work, full dual-frequency GPS and Galileo constellations will be assumed. Therefore, threats due to the conditions in the Earth's ionosphere, such as storms and other perturbation events, will not be considered. Likewise, second order Total Electron Content (TEC) delays and scintillation phenomena will not be investigated here, as they are considered beyond the scope of this dissertation work. The troposphere model will match the one in the WAAS Minimum Operational Performance Standards (MOPS) and is assumed to be bounded by the confidence level provided in [86, sect. 2.5.9.2]. The SV clock and ephemeris errors are assumed to be normally distributed $\mathcal{N}(0, \sigma_{URA})$ under nominal, healthy satellite conditions. In addition to a zero-mean, pure Gaussian component (ε_i), each residual ranging error will also contain biases:

$$\nu_i = \varepsilon_i + b_i + f_i \tag{3.1}$$

Previous literature seems to be much in agreement on a theoretical way to describe the normally-distributed errors at the user. For that reason, the latest model in [53] was considered appropriate, with only minor modifications made at the suggestion of the FAA GEAS Working Group [32]. The residual range error variance for satellite i is described here by:

$$\sigma_i^2 = \sigma_{i,URA}^2 + \sigma_{i,tropo}^2 + \sigma_{i,iono-free}^2 \tag{3.2}$$

Receiver noise and multipath are also bounded by the provided iono-free sigma term. Note that, similar to the way in which they are treated in GBAS and SBAS, receiver failure and excessive multipath terms are not explicitly put into the threat space. However, RAIM offers some protection against such fault modes where no ground augmentation can.

The first bias component (b_i) represents a small level of *nominal bias* present in the measurements, for which a maximum level per satellite will be broadcast to the users. The *failure bias* component (f_i) will be non-zero only in order to define a measurement fault, and its magnitude will be unknown to the user. It represents the instantaneous realized value of an abnormal type of error with an undefined probability distribution.

The *a priori probability* of satellite failure will be discussed as part of the definition of the threat space, while a $\mathcal{P}$HMI analysis needs to be conducted for each RAIM algorithm in terms of the relevant number of failures. The *satellite failure* is defined here as the behavior of a SV ranging signal when its corresponding range error cannot be overbounded with a Gaussian $\mathcal{N}(0, \sigma)$. In practice, faulted measurements occur when the standard ranging error model assumed by the RAIM algorithm fails to describe the actual distribution of the errors. Although, this is not the most precise way to define a fault state of the system, and a user would not be able to make more than a probabilistic determination of the existence of a fault state based on a single snapshot of measurements, the working definition of the failure provided here will prove to be a very practical one. The present approach seems to have a more natural way to describe a failure for a multiple-hypothesis type algorithm, which weighs all possible outcomes in a probabilistic manner in order to determine an expected value of the error bound.

As it will be seen later in this chapter, even methods that employ a much more precise failure definition will eventually fail to make a 100% precise determination about the presence of a measurement failure on a consistent basis. As a result, classical RAIM algorithms have to explicitly compute additional probabilities of a false or missed detection, or of excluding the wrong satellite as faulted, a process which is not always mathematically straightforward. Although it is a good binary discriminator, the customary method of setting a failure threshold for pseudorange error in earlier RAIM schemes, designed to provide only Lateral Navigation (LNAV) approach guidance, does not help detect faults which are not generated by a single

large range error, or which are generated by relatively small fault biases. Multiple medium-sized faults can also conspire to create Hazardous Misleading Information (HMI) events. Attempts to generalize these slope-based RAIM algorithms for handling multiple faults and multiple constellations have been made [54, 5, 40], however a caveat of these approaches is their inability to clearly define a consistent threat model, while their proofs of safety still rely on approximations. Currently, these algorithms do not provide a method to identify systematic errors when they are just below the threshold. Additionally, as the prospective GNSS accuracy improves, the slope-based threshold for failure would decrease, such that more and more events that do not pass as failures today will do so in the future, with an undesired impact on the *a priori* likelihood of failure. Thus, a single threshold will be no longer appropriate for dealing with such fault scenarios and a new definition of a failure should be applicable to each individual range measurement separately.

However, for the case of the MHSS RAIM algorithm developed in this dissertation, it will be demonstrated that a precise determination of whether a measurement error can be classified as nominal or not is not necessary, as long as a probabilistic model exists that takes into account all fault hypotheses. A satellite navigation user will be able to derive the best possible performance in terms of both positioning accuracy and integrity based on this statistical assessment. Thus, the ABAS system can pragmatically fulfill its mission of providing the maximum safety for the aircraft, even absent absolute knowledge of whether a fault exists in the system and what exactly caused that particular fault. In the context of the present dissertation, a measurement fault event does not necessarily imply a discrete component failure of the navigation system, but can be also caused by anomalous signal propagation events, such as ionospheric disturbance events, anomalous tropospheric delays or excessive multipath measured by the receiver. The goal of the MHSS FDE algorithm will be to also identify this type of propagation failures and treat them as events that could cause HMI. However, this will be accomplished without making a specific distinction between discrete and propagation failures. As a matter of fact, the errors which affect the pseudorange measurements will be regarded in a holistic manner, and the

realized values of these errors in the measurements will be used as information that allows potential improvements of the navigation system performance, without regard for the specific nature of the cause of each error. The practicality of detecting failures according to this new approach needs nonetheless some further scrutiny, which will be provided in later chapters as well as in future studies. In MHSS RAIM, as long as a threat can be well-defined and an *a priori* probability for it can be provided, the algorithm can account for it. The underlying probabilistic framework of MHSS is extremely flexible — as long as one can compute the position and error bound in the known presence of each threat, a corresponding PL can be derived.

The total error budget for HMI being passed to the user is strictly limited for the case of aviation precision approaches, such that the maximum allowable integrity fault risk is 10^{-7}/approach. This budget needs to be divided between all the possible failure modes, and the resulting PLs will be very sensitive on the allocation of this integrity budget. Normally, in applying any previous RAIM algorithm, multiple failures are neglected, for modes which are less likely than a certain threshold. The reason why certain improbable failure modes need to be neglected is that the entire threat space is extremely large and impractical to compute. Therefore, it is imperative to limit the computation of the position error only to the most dangerous events from an integrity point-of-view. At the same time, when using MHSS RAIM, one can afford to conservatively assume the worst case scenario (i.e. failure generating HMI) for the remaining threats, as they would have a small enough probabilistic impact on the total error or the total integrity anyway. Ultimately, the MHSS method lends itself to a relatively simple proof of safety, which involves adding up the contributions of each failure included in the threat model fault tree, similar to what is done in the present-day WAAS integrity calculations.

To sum up, this section provided a description of the failure threat space which will be addressed by the algorithms developed in this work. As a first step, an error model for user range errors under nominal conditions has been laid out. Subsequently, a definition was provided for what are considered here to be abnormal

or failure conditions. Finally, it should be noted that the present definition of a failure for integrity purposes represents a departure from the treatment of the same subject in the development phase of previous RAIM algorithms.

3.2. Classical RAIM Algorithms

Theoretical investigation of signal integrity monitoring for civilian SoL applications has started ever since the late 1980s, as GPS, the first of the GNSS constellations, was about to become operational. In time, two types of RAIM methods have been developed: sequential and snapshot algorithms. In addition to providing a safety check for the user by providing measurement integrity, both types of algorithms sought to also to increase the operational availability by employing "best guess" methods to detect possible measurement faults with a high degree of certainty. The idea behind *sequential RAIM* is that of using a history of consecutive measurements which would allow comparing navigation solutions over time in order to detect potential faults as they gradually develop, and as soon as a high confidence identification could be made [67]. However, a drawback of this type of algorithms comes from the fact that in practice there is a short (2–6 sec) time-to-alert (TTA) requirement for all detected integrity faults, while actual GPS measurement errors exhibit a high degree of correlation over longer periods (tens of seconds). Thus, it is not always efficient to design a more complex algorithm to compile measurement sets from multiple instances in time, when this does not offer a clear advantage over processing a single sample of the range measurements and making a speedy decision on the system integrity. The *snapshot RAIM* methods do exactly that, offering the potential for less computationally complex algorithms while only considering the set of measurements from the current instant in time.

In fact, the earliest RAIM methods were snapshot algorithms proposed in the late eighties as the excitement of the first GPS satellites orbiting the Earth encouraged the takeoff of the field of satellite navigation [50, 13, 75, 90]. All of these

pioneering works investigated the use of the Least-Squares (LS) residuals obtained in the normal course of determining a GNSS position estimate, and employed redundant measurements in order to make a statistical determination of the ranging and navigation errors. These LS methods have been found to be mathematically equivalent by R. Grover Brown in 1992 [16], and as such they are commonly referred as the *classical LS RAIM algorithm*. A different flavor of RAIM, which tried to identify potential faults by examining all possible subsets of the available ranging sources, was proposed in the same period [12, 14] and was later developed separately as the *SS algorithm*. The framework of these two classes of methods will be described below in sections 3.2.1 and 3.2.2, as they constitute the foundation of further development in the field of RAIM [25]. The overview of the algorithms will then be followed in 3.2.3 by a discussion of their benefits and limitations, as well as an overview of derived versions of RAIM focusing on either improving fault detection, decreasing the position error or increasing navigation availability.

3.2.1. Least Squares RAIM algorithms

The same Least Squares (LS) algorithm described in [16, 94] was used here for comparison purposes in terms of vertical integrity. An overview of the common LS algorithm is presented below. The LS RAIM algorithm starts with the linearized position difference equation employed in the standard iterative LS position estimation [60, sect. 5.1.1]. Specifically, an enhanced version called the Weighted Least-Squares (WLS) position estimation, which applies different weights for each range measurement, will be used throughout this dissertation. The unknown quantity for which this method is trying to solve is the difference between the current user position guess $\tilde{x}$ and true position $\overline{x}$:

$$x \equiv \tilde{x} - \overline{x} \tag{3.3}$$

The measured quantity is accordingly represented as the difference between pseudo-range $\tilde{\rho}$, based on the user position guess and the satellite position deduced from the

broadcast ephemeris, and the measured pseudorange ρ:

$$y \equiv \tilde{\rho} - \rho \tag{3.4}$$

By linearizing the measurement equations for the n satellites in view around the difference x, the following equation is obtained:

$$y = \mathrm{G} \cdot x + \nu \tag{3.5}$$

Here, y and ν are the $n \times 1$ measurement and noise column vectors, while $\mathbf{G}$ is the "skinny" satellite geometry matrix and the above-defined x is called the *position vector*. The system of equations is thus overdetermined when the number of range measurements is larger than the number of unknown space-time user coordinates. Therefore, an estimate solution for x can be obtained by employing the WLS method:

$$\hat{x} = (\mathrm{G}^{\mathrm{T}} \cdot \mathrm{W} \cdot \mathrm{G})^{-1} \cdot \mathrm{G}^{\mathrm{T}} \cdot \mathrm{W} \cdot y \equiv \mathrm{H} \cdot \mathrm{G}^{\mathrm{T}} \cdot \mathrm{W} \cdot y \tag{3.6}$$

The weighting matrix employed in this process will be the inverse of the error covariance matrix for range measurements along each LOS: $\mathrm{W} \triangleq \Sigma^{-1}$. The matrix $\mathbf{\Sigma}$ is diagonal only if the errors are assumed to be uncorrelated, which is a simplifying assumption that can be made for demonstration purposes when exhibiting the working of a particular RAIM algorithm.

With the additional notation for the pseudoinverse of the geometry matrix $\mathrm{S} \equiv \mathrm{G}^{\dagger}$, and by using $\mathbf{P}$ to denote $\mathrm{P} \equiv \mathrm{G} \cdot \mathrm{S}$, the measurement noise $\nu = y - \mathrm{G} \cdot x$ can be estimated by the same LS method. Instead of consistently denoting the estimate of the noise by $\hat{\nu}$, the alternate customary notation from the literature will be employed:

$$w \equiv (\mathrm{I} - \mathrm{P}) \cdot y = (\mathrm{I} - \mathrm{P}) \cdot \nu \tag{3.7}$$

The Weighted Sum of Square Errors (WSSE) quantity is then calculated as:

$$\mathrm{WSSE} = w^T \cdot \mathrm{W} \cdot w \tag{3.8}$$

This is an observable quantity, while the $\hat{x} - x$ LS error is not known, since it requires perfect knowledge of the absolute user position $\overline{x}$. Assuming the standard deviation of the range measurement error is σ, a value which overbounds the individual values of σ_i as given by equation (3.2) for each satellite, a dimensionless normalized test statistic can be formed for the LS RAIM algorithm [75], as:

$$test\ statistic = \sigma \cdot \sqrt{\frac{\mathrm{WSSE}}{(n-4)}} \tag{3.9}$$

where n is the number of ranging satellites whose signals are being acquired by the user. With σ as a parameter of the algorithm, the more satellite measurements are available to the user and the less the noise in each channel, the smaller the test statistic will become, which is equivalent with a superior performance for the user.

In identifying a measurement fault, in order to make a meaningful comparison, a predetermined threshold is chosen, which will be compared with this test statistic at each snapshot in time. For example, in order to make a decision about the integrity in the vertical direction, according to both [16, 94], a corresponding one-dimensional error slope will be computed for each satellite as:

$$V\mathrm{SLOPE}_i = \frac{|\mathrm{S}_{3,i}| \cdot \sigma_i}{\sqrt{(1 - \mathrm{P}_{i,i})/(n-4)}} \tag{3.10}$$

Here, the worst possible scenario from the user standpoint is assumed for conservatism: instead of being the product of arbitrary errors distributed among all measurement lines of sight (LOS), the entire vertical error represented by the WSSE is concentrated along a single satellite LOS, while the errors along all other LOS are null. This scenario represents the greatest threat in terms of the effect of individual range errors on the overall user position error. The quantity VSLOPE is consequently

chosen as the ratio of the worst possible vertical navigation error to the corresponding test statistic. Hence, not accounting for other measurement noise, the maximum amount of vertical error an user can incur while no integrity flag is being raised occurs when the test statistic is exactly equal to the chosen detection threshold T:

$$\epsilon_{\mathrm{v,max}} = \max_i \left(V\mathrm{SLOPE}_i\right) \cdot T \tag{3.11}$$

A graphical depiction of the relationship between the distribution of vertical errors and the values of the test statistic is provided in [94, Fig. 1], along with the original description of this RAIM algorithm for use in conjunction with WAAS. However, in the version implemented as part of the work for this thesis for algorithm comparison purposes, no failure decisions are made directly by the LS RAIM algorithm. Instead, the Vertical Protection Level (VPL) is set large enough to include the largest position error. Users can thus make the decision themselves, by comparing the VPL with their required Vertical Alert Limit (VAL), if available. Instead of using a decision threshold for fault detection, the adapted LS method presented here uses the VSLOPE value to compute a user Protection Level (PL). This approach is still conservative, since it continues to allow the total Sum of Square Errors (SSE) along any of the LOS as the worst case scenario. In the current implementation however, a test statistic assuming the total error along each possible LOS is used to yield the corresponding ϵ_{v} values. As such, the maximum navigation error interval, a primary ingredient of the VPL, is in fact based on the total error from all satellites occurring in the worst possible mode (i.e. along the LOS most sensitive to error). Subsequently, in addition to the geometry considerations above, a term also assuming a worst case realization of the normally distributed measurement noise errors is added to form the VPL for the user:

$$\mathrm{VPL} = \max_i \left(V\mathrm{SLOPE}_i\right) \cdot T + k\left(\mathrm{I}\right) \cdot \sqrt{\mathrm{H}_{3,3}} \tag{3.12}$$

The $k(\mathrm{I})$ function is based on the Gaussian error function and it computes how many standard deviations away from the mean is the worst case sample with probability $(1 - \mathrm{I})$:

$$k(\mathrm{I}) = \sqrt{2}\,\mathtt{erfc}^{-1}(\mathrm{I}) \tag{3.13}$$

where I is the probability of the user experiencing an integrity fault, alias the *integrity risk*, whose maximum allowed magnitude is the specific $\mathcal{P}$HMI value for the current operation regime. The FAA navigation requirements for LPV 200 approaches set this probability to be 10^{-7}/approach [99, p. 8].

3.2.2. Solution Separation RAIM algorithms

The name Solution Separation (SS) is used here to identify the RAIM algorithm which combines position solutions from different subsets of the satellites in view to compute a Protection Level (PL), particularly the VPL. By hypothetically assuming one or more SVs to be faulty and eliminating them from the position equation, one can obtain a partial position solution based only on the remaining satellites. Among all the partial subsets of satellites, the existence of at least one fault-free subset is thus guaranteed, and consequently the correct position solution will certainly be included in the range of positions that constitutes the VPL interval. Instead of the ϵ_{v} term, the *navigation error* is computed for each satellite subset as the difference between the estimated positions with the partial and all-in-view satellite sets, such that a VPL interval can actually be associated with each partial position solution.

The way in which one can compute the estimated navigation position error for SS-type algorithms will be described below in more detail. It is important that this procedure does not require the actual pseudorange measurements, just the range residual errors. Therefore, the performance of RAIM algorithms can be simulated for a given user pseudorange error model, allowing the computation of a PL based only on knowledge about the relative geometry between the user and the GNSS constellations. A VPL performance comparison between the LS, SS and MHSS algorithms will be provided at the end of this chapter, in Section 3.4. Based on the assumed

SV probability of failure and the average number of satellites in view, a decision will be made on what is the maximum number of simultaneous failures that need to be considered. This approach represents an advantage over the LS algorithm, which only explicitly handles the assumption of one SV failure at a given time. The computational load of the SS algorithm will however increase exponentially with the number of assumed simultaneous failures.

As in the case of LS RAIM, one starts out with the linearized measurement equation for a number n of satellites in view:

$$y = \mathrm{G} \cdot x + \nu \tag{3.14}$$

The linearization took place around the estimate minus actual position deviation vector x, which is five-dimensional for the case of the dual GPS and Galileo constellation: East, North, Up (ENU) spatial directions and one time coordinate for each constellation. A simplifying assumption could be made by considering a fixed, known Galileo-GPS clock bias, but the choice was made not to use that assumption for any of the algorithms and results presented in here, in order to maintain generality. The simulation studies in Chapter 4 will estimate the magnitude of the impact of this assumption. The other terms above are the $n \times 1$ measurement vector y containing the differences between the expected ranging values and the raw pseudorange measurements to each of the n satellites, the $n \times 5$ geometry or observation matrix $\mathbf{G}$, and the n-dimensional measurement error ν. For the algorithm simulation purposes, the error along each satellite LOS is taken to be zero-mean Gaussian noise with the σ_i^2 variance defined earlier in equation (3.2).

The Weighted LS solution for x is given by:

$$\hat{x} = (\mathrm{G}^{\mathrm{T}} \cdot \mathrm{W} \cdot \mathrm{G})^{-1} \cdot \mathrm{G}^{\mathrm{T}} \cdot \mathrm{W} \cdot y \equiv \mathrm{S} \cdot y \tag{3.15}$$

where $\mathbf{S}$ is called the weighted pseudoinverse of $\mathbf{G}$ and the weighting matrix $\mathbf{W}$ is the inverse of the measurement noise covariance matrix $\mathbf{\Sigma}$. For simplification, it

was assumed that the error sources are uncorrelated between all the different LOS. Therefore, $\mathbf{\Sigma}$ is a diagonal $n \times n$ matrix:

$$\Sigma = \begin{bmatrix} \sigma_1 & 0 & \cdots & 0 \\ 0 & \sigma_2 & \cdots & 0 \\ & & \ddots & \\ \vdots & \vdots & \sigma_i & \vdots \\ & & & \ddots \\ 0 & 0 & \cdots & \sigma_n \end{bmatrix} \tag{3.16}$$

The σ_i range error variance was defined earlier in equation (3.2). While the uncorrelation assumption may not be strictly true, it is often a reasonably good and conservative approximation. The equations subsequently derived do not depend on this assumption, which only makes them easier to implement in practice.

At this point, in the case of the LS algorithm, one would estimate the measurement noise:

$$w \equiv (I - G \cdot S) \cdot y \tag{3.17}$$

in order to be able to compute the SSE metric. Instead, the SS RAIM employs the range residuals from estimating the actual position error:

$$\delta x = \hat{x} - x = S \cdot \nu \tag{3.18}$$

for the all-in-view solution. For the partial solutions, $\hat{x}$ and x will be replaced with the corresponding vectors based on a partial set of measurements. Of interest here is only the third element in δx, the vertical component of the navigation error denoted further as x_{v}. To compute the vertical error only, the third line of the weighted pseudoinverse of the geometry matrix can be multiplied by the noise column vector:

$$x_{\mathrm{v}} \equiv \mathrm{S}_{3,i} \cdot \nu \tag{3.19}$$

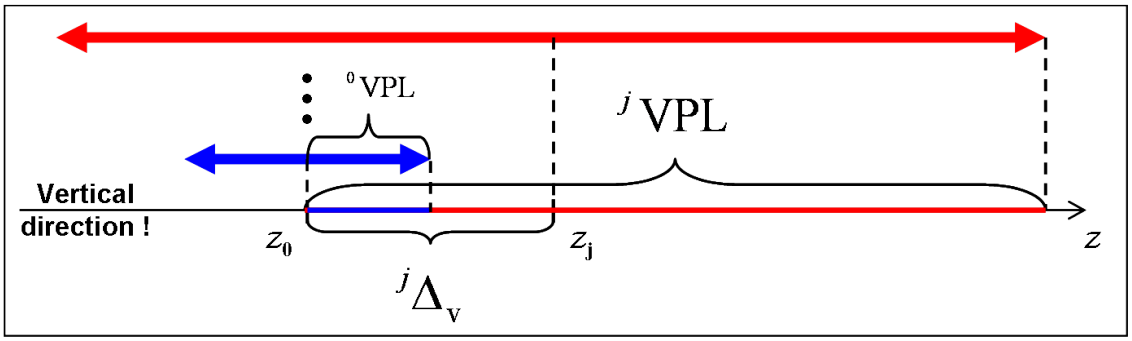

Figure 3.1.: Graphical representation of the Solution Separation partial VPL.

For the ordinary SS algorithm, an assumption on the maximum number of failed satellites is made ahead of time and a partial VPL interval will be computed for each subset position solution:

$$VPL = x_v \pm k(I) \cdot \sigma_v \tag{3.20}$$

where k is the number of standard deviations equivalent to the required vertical integrity confidence interval — e.g. $k(I) \simeq 5.33$ for an integrity risk value of $I = 10^{-7}$, and σ_v, called the *vertical positioning confidence*, is a measure of vertical accuracy derived from the covariance of the position estimate:

$$\sigma_v^2 = [(G^T \cdot W \cdot G)^{-1}]_{3,3} \tag{3.21}$$

Figure 3.1 provides a graphical description of how SS VPLs are determined for the case where all satellites in view are utilized in the position solution (^{0}VPL), as well as the case where a partial subset of the visible SVs is employed (^{j}VPL). The corresponding values of x_v are given by the vertical z-axis coordinates z_0 and z_j. The solution separation distance, $^j\Delta_v$, represents the difference between these two coordinates, which are the vertical position estimates based on the two different subsets of range measurements. Henceforth a single number, as opposed to an error interval, will be used to characterize each partial VPL. Its value will be taken to be half of the error bound, which is symmetric around each partial position solution, plus

the magnitude of the solution separation ${}^{j}\Delta_{\mathrm{v}}$. On the graphical depiction, the blue and red arrows mark the two-sided error bound around the respective all-in-view or partial position estimates, while the VPL interval is an one-sided error bound around the all-in-view position solution z_0 for every partial mode. Finally, the overall VPL for the SS algorithm will be chosen such that it defines an interval around the all-in-view estimated position including all the partial solution error ranges.

3.2.3. Discussion on the evolution of RAIM algorithms

When computing the VPL for both the above algorithms, for each position solution (all-in-view, and subsets of satellites in view in the case of SS), a $5.33\,\sigma$ confidence interval (i.e. a 1-10^{-7} probability) is generated and added on top of the vertical error. In the SS case, the minimum VPL is half of the size of the union of all error intervals corresponding to subsets of satellites in view. Nonetheless, if smooth changes in the position solution are desired for the SS algorithm, the VPL interval can be centered around the all-in-view solution, but it is still necessary to ensure a large enough VPL value is selected, as to include the above union of error intervals.

In the past two decades, new methods were proposed and developed as the disadvantages of the classic slope-based LS RAIM algorithms were pointed out. The classical RAIM algorithms were called overconservative, in that they lack a direct correspondence between the actual measurement noise level and the user protection level [69]; and also there is no direct relation between the acceptable HMI risk and the performance of the integrity monitor [7]. One distinct idea, that could be adapted to both snapshot and sequential algorithms is that of employing the Generalized Likelihood Ratio (GLR) Test [73, 44, 68], which relies on formulating multiple fault hypotheses and selecting the most probable one of them.

During the 1990s the research focus was on using RAIM while also augmenting the GPS based on ground monitoring or on inertial sensors, in order to achieve the necessary performance for aviation approaches. Conversely, during the current decade a different approach to RAIM looks promising, based not just on single-frequency

GPS but on the highly redundant future multiple-constellation GNSS. At present, with the perspective of modernized GPS constellations, several signal frequencies and additional GNSS monitoring systems being developed by multiple countries over the world, the focus has shifted towards including satellites from multiple constellations interchangeably, and also accounting for the higher likelihood of multiple failures by employing multiple hypothesis techniques. Based on the classical way of doing fault removal, which implies comparing an error test statistic to a given threshold, integrity could be lost if a potential fault were either misidentified or if it could not be excluded. A different approach in the algorithm presented in Section 3.3 seeks to eliminate those possibilities by guaranteeing integrity for the computed error bound in all cases, and allowing for separate tests to determine whether continuity and availability requirements are also met.

3.3. Multiple Hypothesis Solution Separation (MHSS) RAIM Algorithm

The plus that the MHSS brings to the pre-existing SS RAIM algorithms is a reduction in conservatism, along with a closer agreement between the noise level affecting each measurement and the overall position error bounds. Instead of examining each pseudorange separately in establishing a VPL, the classical LS and SS algorithms assume the worst possible combined error along all LOS and then proceed to protect the user against that hypothetical case or attempt to eliminate a faulty satellite. Particularly, the SS algorithm considers the maximum position solution separation between any of the evaluated measurement subsets and the all-in-view case as a test statistic, regardless of what the actual likelihood is for a failure to reduce the set of all satellites in view to that particular subset. This approach would be useful in case the aviation navigation requirements would specify the maximum acceptable integrity risk to be zero, viz. the probability for this worst-case scenario to occur and cause HMI to be passed to the user. However, given the current aviation requirements

which set a small but non-negligible limit for the $\mathcal{P}$HMI, the pessimistic approach of the classical RAIM methods can prove impractical in real-life situations.

The civil airplane navigation requirements presented in Chapter 2 specify a maximum probability of integrity loss in order to make possible a potential tradeoff between integrity on one side and the availability and continuity on the other. Given the unavoidable uncertainty in the ranging measurements, if an algorithm artificially assumes the maximum $\mathcal{P}$HMI to be zero or near-zero by always considering only the worst-case scenario, that RAIM algorithm would then be forced to significantly increase its PL outputs and could thus become unable to offer a high availability to the user. Consequently, the most elegant and natural way to address integrity is to analyze every threat probabilistically. This approach is also mathematically more rigorous, as it does not need to make additional assumptions about the size of the threshold corresponding to the maximum allowable magnitude of the position error, worst-case distribution of error between LOS, and the maximum permissible number of simultaneous satellite failures. The MHSS RAIM algorithm weighs fault modes based on their (prior) probability and eliminates the comparison against a given error threshold. As such, it retains the ability to point out which LOS was affected by an anomalous error, by not aggregating all measurements / information into a single test statistic. The algorithm robustness to uncertainties in the knowledge of the prior probabilities, a necessary precondition for employing a different treatment of failure events, will be demonstrated next, in Chapter 4, through comprehensive simulations.

Finally, as it will be detailed in the discussion about the integrity risk allocation tree in section 3.3.1, MHSS only considers faults that could have an impact on the measurement integrity. The ultimate enhancement to the MHSS algorithm will be presented in 3.3.2 as an original method to perform satellite exclusion, and which eliminates the disadvantages of fault isolation methods employed by previous RAIM algorithms. Section 3.3.3 will then present an addition to the MHSS algorithm that simultaneously offers both integrity and continuity information to the user.

3.3.1. Real - Time algorithm

The MHSS algorithm described here is a generalization of the algorithm proposed in [77] for use in conjunction with LAAS. This algorithm was already tested against a CAT III VAL requirement of 5 m and demonstrated to achieve low VPLs. Furthermore, its assumptions are general enough such that it can be used for any RAIM-type integrity computation. In the current work, multiple SV failures were considered in order to address all possible failure modes included in the threat space. The probability of occurrence of each failure mode is taken into account and a search is made for the VPL which most closely makes use of the entire integrity budget available.

In the work for the current dissertation, a *fault tree* has been developed in order to divide up the allowable $\mathcal{P}$HMI of 10^{-7}/approach as *integrity risk allocations* to each of the possible fault modes included in the threat model described earlier in section 3.1.2. A *failure/fault mode* represents a unique way in which specific satellites correspond to the faulty measurements. At the same time, the *order* of a failure specifies how many range measurements contain a fault at the current instant in time. Therefore, given a total number of n visible ranging sources, a failure of the kth order can be represented as n-choose-k different fault modes. The potential failures are ordered in the fault tree from the *no-fault mode* (the 0^{th} order failure) to the highest order (the nth order failure). The satellite failure model relies on assigning each ranging source a binary fault state: nominal or faulted. As such, the total number of satellite fault modes will be $m = 2^n$. In the default or *nominal state*, the corresponding pseudorange error is assumed to be overbounded by a normal distribution with a determined mean (or *bias*) and standard deviation (or *sigma*), according to an error model which will be described more in detail in Chapter 5 (section 5.2.1 on page 153). On the other hand, a satellite in the *failed state* will be associated with range measurement errors that do not fall under the same Gaussian overbound and therefore should be discarded by the user in order to avoid potentially erroneous navigation results.

In applying the MHSS algorithm, higher orders of failure are not considered for the position calculations when their number of SV failures is less likely than an empirical 10% of the total $\mathcal{P}$HMI budget, or 10^{-8}/ approach. The correct fraction of the integrity budget to be allocated to uncomputed failure modes is within an order of magnitude smaller than the overall budget. As an example, based on a binomial fault probability model, for a 10^{-4}/ SV probability of failure and at most 24 satellites in view it is necessary to explicitly consider up to two satellite outages, while for any prior probability larger that $1.7 \cdot 10^{-4}$/ SV three or more failures will be taken into account. The modes belonging to an order of failure whose probability is smaller than this minimum threshold will automatically receive their entire allocated integrity budget, without an actual computation of the position solution or a protection level calculation being performed for any of these degenerate geometries. Therefore, these modes were dubbed *unknown failure modes*, and they generally correspond to orders of failure which were neglected altogether by earlier RAIM algorithms. They nevertheless receive full consideration under MHSS. The uncomputed modes taken as a set will be consolidated as an unknown failure, and its corresponding integrity risk will be accounted for and diminish the total integrity budget. In the MHSS algorithm design, this choice to only estimate the most probable orders of failure was made in order to prevent the computational complexity of the algorithm from increasing exponentially due to the estimation of the most improbable fault modes, which would ultimately not constitute an inadmissible integrity threat to the user.

Besides the cases with none to all measurement being faulty, an additional *a priori* probability will be associated with each possible constellation failure. There are several reasons why including the *constellation failure hypothesis* is an important consideration for a RAIM algorithm. This additional type of fault modes is needed to address the correlation of errors across a whole constellation or a significant portion thereof, which is not already accounted by the model for individual satellite failures. Such cases, in which a majority of the measurements along each LOS "conspire" against the user, require their separately defined fault modes since any RAIM algorithm based on the statistical agreement between redundant measurements will

not be able to identify systemic failures in which a preponderance of the information available to the user is faulty. This last failure type was not considered in the classical RAIM algorithms, as those algorithms make a conservative worst-case scenario assumption for each possible fault, thus making it impossible to provide a PL if a constellation failure is even considered.

Acknowledging that the degree of fault correlation across different constellations is generally much smaller than the correlation between satellite failures within the same constellation also serves in identifying another level of redundancy in GNSS, viewed as a system of systems. Besides having multiple redundant satellites to provide user range measurements, a multiple-constellation system with a single-constellation fall-back mode can be considered to also contain redundant satellite constellations.

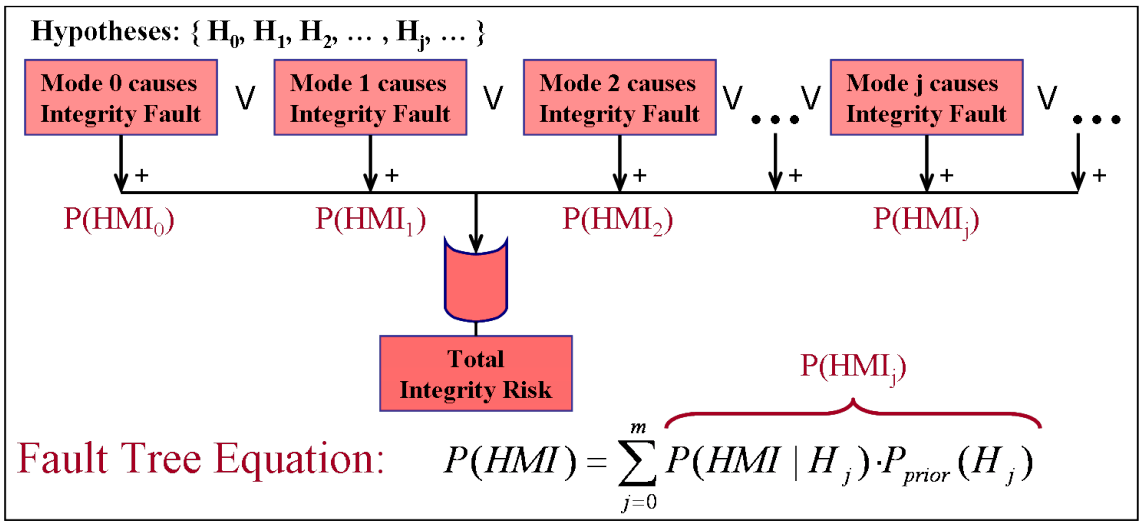

Figure 3.2.: Model of fault tree for the assessment of integrity risk.

The "leaves" of the fault allocation tree mentioned on page 73 represent all individual fault modes. They will constitute the set of different fault hypotheses considered by the RAIM algorithm developed here. The *hypothesis set* will be denoted as $\mathbf{H} = \{H_0, H_1, H_2, \ldots, H_j, \ldots\}$, where H_0 always denotes the *fault-free* state of the system, and the index j will be employed from here on to represent the number of the current fault mode, ranging between 0 and the maximum possible number of faults. When a *partial position solution* is subsequently computed, the result will be based on only those ranges which are unaffected by measurement faults under

the respective hypothesis. With each hypothesis there will be an associated prior probability for that particular fault mode to occur, denoted as $\mathcal{P}\{H_j\}_{prior}$; and under each hypothesis there will exist a separate probability for an integrity fault to occur, denoted as $\mathcal{P}\{\text{HMI} \mid H_j\}$ or ${}^j\mathcal{P}_{\text{HMI}}$ in short form. A stylized graphical depiction of the overall fault tree is depicted in Figure 3.2.

The overall $\mathcal{P}$HMI is the probability that the true user position lies outside the error bound determined by the integrity algorithm. According to [6, 7], the usual interpretation is that this probability is conditioned on the nominal error model and the satellite geometry, but not on the realized values of the pseudorange errors determined by the users from their measurements. Therefore, $\mathcal{P}$HMI can be expressed as the sum of the HMI contributions under each hypothesis, weighed by the corresponding *a priori* probability:

$$\mathcal{P}\text{HMI} = \sum_{all\, j} \mathcal{P}\{\text{HMI} \mid H_j\} \cdot \mathcal{P}\left\{H_j\right\}_{prior} \tag{3.22}$$

In terms of the user safety analysis, the MHSS algorithm chooses the more natural way of backtracking from the FAA and ICAO specifications [49] to both find an adequate overall error bound with the required certainty and to protect the user under all partial geometries. This is in contrast to the case of earlier RAIM algorithms, which started with a given measurement geometry and its associated least-square position solution, and then tried to find an artificial threshold in order to match the resulting test statistic to the integrity requirements. As such, users employing MHSS do not have to venture in additional complex calculations to explicitly determine false alert and missed detection probabilities, as their Protection Level calculations intrinsically satisfy the required level of user integrity. This premise is accomplished by satisfying a partial integrity requirement for the case of each separate fault or *partial mode*:

$${}^j\mathcal{P}_{\text{HMI}} \cdot \mathcal{P}\{H_j\}_{prior} \leq {}^j\mathcal{P}_{alloc} \tag{3.23}$$

In the ensuing discussion on the separate treatment of each partial mode within the MHSS algorithm, the superscript j will be prefixed to each quantity when it particularly refers to the jth hypothesis, and not the general case. In order to satisfy the $\mathcal{P}\text{HMI} \leq \text{I}_{\text{req}}$ integrity requirement at all times, the MHSS algorithm ensures that the terms in equation (3.22) corresponding to each fault mode are at most equal to the integrity allocation for that particular mode. According to section 2.2.1, for the LPV 200 type of approaches, the total allocated vertical integrity budget is:

$$\text{I}_{\text{req}} = \sum_{all\, j}^{m} {}^{j}\mathcal{P}_{alloc} = 10^{-7}/\text{approach} \tag{3.24}$$

A binomial model was adopted for computing the prior probability of failure under each hypothesis, stemming from the duality between the error distribution allowing a Gaussian overbound for nominal measurements and the errors under failure conditions, which are assumed to belong to an undefined probability distribution. If the satellite faults are assumed to be independent from each other,

$$\mathcal{P}\{H_j\}_{prior} = \binom{n}{k} \cdot p^k \cdot p^{n-k} \tag{3.25}$$

Here, p is taken to be the *a priori* probability for a satellite range measurement to contain a fault, assuming that all SVs have equal probabilities of failure at a given moment. As such, the probabilities of all the satellite fault modes are already normalized:

$$\sum_{j=0}^{m} \mathcal{P}\{H_j\}_{prior} = 1 \tag{3.26}$$

Furthermore, ${}^{j}\mathcal{P}_{\text{HMI}}$ is taken to be 1 for the uncomputed modes and it has an equal value for all the other (lower order) modes in which a position estimate and a PL are computed separately. Hence, the ensuing strategy for distributing the integrity budget between the fault modes in the case of the RT MHSS algorithm will be called *equal allocations*. A discussion on a different strategy for optimizing the distribution of the integrity allocations and about when it is appropriate to use

this optimal strategy will follow in section 3.3.3 below. Until then, the maximum integrity risk for each mode will be taken to be constant and will be obtained by splitting the overall budget for integrity faults ($\mathrm{I_m}$) into equal $1/m$ shares for each of the fault modes, where:

$$\mathrm{I_m} = \mathrm{I_{req}} - \mathcal{P}_{unknown} \tag{3.27}$$

This expression represents the remaining integrity risk after accounting for the probability of all modes in which a position solution cannot be computed or whose odds of occurrence are extremely low, as $\mathcal{P}_{unknown}$ is a sum of the prior probabilities of all these unknown failure modes. As a side mention, $\mathcal{P}_{unknown}$ could include additional constellation failure scenarios as well, if after such failure there were an insufficient number of remaining nominal range measurements for computing a user position solution. At this point, given the set of equations 3.23 – 3.27, by substitution of $\mathcal{P}\{\mathrm{HMI} \mid H_j\}$ into (3.22), it will necessarily follow that:

$$\mathcal{P}\mathrm{HMI} \leq \mathrm{I_{req}} \tag{3.28}$$

Once the algorithm established that it can meet the overall integrity requirement, it will determine a value for the Vertical Protection Level for each of the modes being evaluated, which will serve to ensure that:

$${}^{j}\mathcal{P}_{\mathrm{HMI}} \leq \frac{\mathrm{I_m}}{m \cdot \mathcal{P}\{H_j\}_{prior}} \tag{3.29}$$

The VPL value which leads to the above inequality being satisfied under each hypothesis, represented by the subset of remaining nominal measurements, is given by the following expression:

$${}^{j}\mathrm{VPL} = {}^{j}\Delta_{\mathrm{v}} + \sum_{i=1}^{n} \left| {}^{j}\mathrm{S}_{3,i} \cdot B_{max,i} \right| + k\left({}^{j}\mathcal{P}_{\mathrm{HMI}}\right) \cdot {}^{j}\sigma_{\mathrm{v}} \tag{3.30}$$

This equation for the partial subset VPL has strong similarities with equation (3.20) for the classical SS algorithm. The first term, called the *solution separation term*, represents the difference between the vertical coordinates of the partial subset position solution and the overall position solution employed by the user. Given the very small satellite fault probabilities (p), the no-fault mode will generally have a prior probability very close to 1, and thus it will be allocated the large majority of the integrity budget. Hence, its corresponding position solution can be taken to be the reference position estimate for the user.

$$ {}^{j}\Delta_{\mathrm{v}} = {}^{j}x_{\mathrm{v}} - {}^{0}x_{\mathrm{v}} \tag{3.31} $$

As it can be noticed, the magnitude of this term is zero for the fault-free mode, since its purpose is only to align all other partial VPLs around a common position solution, which was taken here to correspond to the all-in-view hypothesis H_0.

The actual error bound for each mode against its own partial subset position solution is then given by the latter two terms in the partial VPL equation (3.30). The second term in that equation, the *bias overbound term*, is an addition to enhance the ability of the algorithm to model range error distributions that contain small to moderate amounts of nominal biases, and as such are not necessarily zero-mean as assumed in the classical RAIM algorithms and the present-day augmentation systems RAIM algorithms [20]. The last term in (3.30), called the *Gaussian overbound term*, only differs from (3.20) in that the probability argument for the inverse complementary error function $k(P)$ corresponds to the partial ${}^{j}\mathcal{P}_{\mathrm{HMI}}$.

It has already been proposed [6, 96, 99] that the next generation of GNSS and SBAS include a nominal bias term in their navigation data (denoted above as $B_{max,i}$ for satellite i), along with the URA values being currently broadcast for civilian users of unaided GPS. Taking the measurement biases explicitly into consideration as in equation (3.30) has been proven to generate the lowest possible user VPL [78]. Moreover, the results obtained with this approach have been previously used as an optimality reference for error overbounding techniques, in cases where the bias term

is unknown and thus the sigma values need to be inflated instead, such as the case of RAIM applications in conjunction with present-day WAAS and LAAS [79, 95, 80]. Therefore, it is expected that future systems will opt for the reduction in complexity along with the superior performance supported by broadcasting maximum level nominal biases instead of overbounding them by a combination of unbiased distributions. Figure 3.3 provides a graphical description on how avionics would be able to implement the MHSS RT algorithm, provided the GPS measurements, the appropriate prior probabilities of failure, as well as URA and nominal bias values.

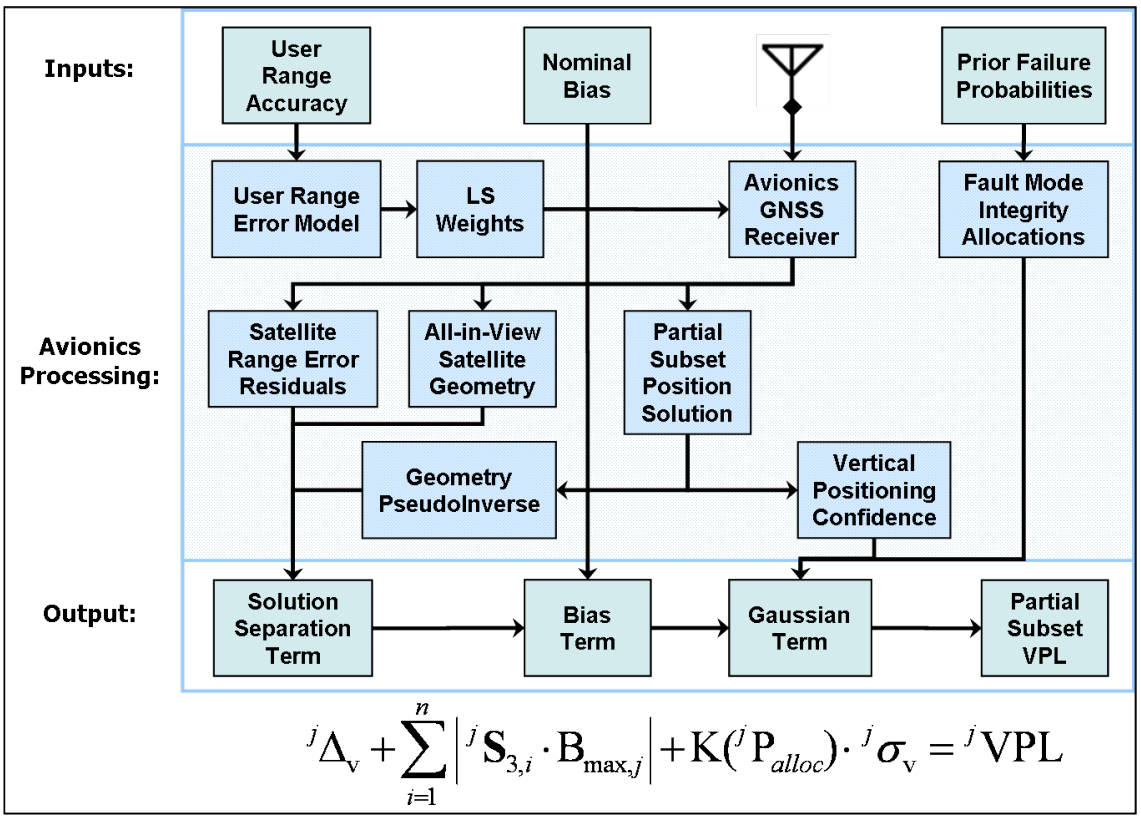

Figure 3.3.: Flow diagram for the implementation of the MHSS Real Time algorithm.

As a final step, once error bounds have been computed for all partial modes, the overall VPL value will be the one which protects every single fault mode against integrity failures with a probability above its specific allocation. Accordingly, the maximum of all partial VPLs will be chosen to meet that condition:

$$\mathrm{VPL} = \max_{j=0}^{m} \left({}^{j}\mathrm{VPL} \right) \tag{3.32}$$

The mathematical proof of safety for using this maximum VPL is at this point straightforward for the MHSS RAIM algorithm and it was derived in full detail in [7]. The advantage of this RAIM method is that it automatically guarantees the desired integrity performance for any satellite geometry for which it is able to produce a finite VPL value, while it does not require the precise identification of any failure mode that is actually present as if the user had absolute knowledge of its current state. However due to the low probabilities of satellite failure that were historically measured, the fault-free mode will receive a prior very close to one and most of the weighting in the algorithm when determining navigation integrity. This leads to a less conservative approach than giving all the weight to a fictitious worst-case scenario. This decrease in the level of conservatism will be quantified through the comparison of algorithm simulation results in Section 3.4.

Overall, the MHSS RAIM algorithm assumes the no-fault hypothesis (i.e. no known satellite failures) for determining a position solution, and then considers all possible, yet undetected failure modes. The integrity risk is computed based on satellite geometry and the partial position solutions, but the prior probabilities of failure are fixed and not updated based on the measurements. These probabilities of failure can be assumed to be lower if the user has the possibility to run a χ^2 check and detect a satellite fault or has access to external information such as integrity flags that may be broadcast by the GNSS satellites or an external monitoring system, e.g. by the WAAS GEOs. The MHSS algorithm can also be applied after excluding such faulty satellites. The principal reason why a user would want to employ satellite elimination is improving its availability for the navigation solution, and this aspect will be demonstrated based on an FDE method proposed in the next section.

3.3.2. Fault Detection and Elimination (FDE) method

While the development of the MHSS RT algorithm above was based on previous work done in the field at the end of the nineties, the following section contains work that is entirely original and constitutes one of the main contributions of this

thesis. The procedure outlined below shows how one or more satellites can be purposefully eliminated before a position solution is computed, in order to achieve a better VPL and eliminate a potential SV failure. Improving the availability for the navigation solution is another reason for employing satellite elimination. The FDE method proposed here is uniquely adapted for the multiple hypothesis probabilistic threat model employed by the current RAIM algorithm. Inspired from artificial intelligence outcome optimization techniques in computer science [88], the MHSS FDE is a Breadth-First Search (BFS) algorithm with a pre-specified maximum search depth for controlling the overall computational time necessary to obtain a solution. The RAIM hypothesis set can be ordered as a searchable tree, which is a common data structure encountered in computer science and graph theory. This *hypothesis search tree* is a distinct construct, not to be confounded with the integrity fault allocation tree previously described on page 73.

Each node of the tree corresponds to one of the hypotheses, with the no-fault hypothesis lying at the root. Every edge of the graph will correspond to one elimination operation, such that, from each parent node, child nodes are derived as the hypotheses which correspond to a satellite being eliminated from the parent's set of healthy satellites. Thus, if the root hypothesis assumes having n good user range measurements, the children of this node will correspond to hypotheses assuming a subset of $(n-1)$ good measurements available to the user, and so forth. The depth level of a node in the tree will correspond to the order of failure defined in 3.3.1. As such, all nodes at depth d will correspond to hypotheses assuming d eliminated satellite failures and a number of $(n-d)$ remaining healthy satellites. Each node at depth d will in turn generate $(n-d)$ child nodes by assuming an additional measurement is faulty and removing it, until there are no measurements left to remove by the time depth n is finally reached. The number of distinct hypotheses at depth d in the graph will be equal to n-choose-d, corresponding to the number of ways in which n range measurements can be partitioned, with d of them being faulty and $(n-d)$ of them being nominal.

The search algorithm will traverse the graph starting with the root, up to a maximum depth d_{max}, established based on the maximum amount of computational time available for the fault detection process. Conceptually, d_{max} corresponds to the maximum number of simultaneous measurement faults considered by the FDE algorithm. At each step in the search process, a VPL value will be determined for the current node, assuming the current hypothesis is the fault-free hypothesis and that all measurements not included in the current healthy subset were never available to the user. The governing principle in determining partial VPL values is that an user cannot be misled by potentially erroneous information that is not even being considered. It is therefore possible to optimize the user performance in this fashion, since all partial VPLs are equivalent from an integrity point-of-view, the integrity being guaranteed by construction of the VPL according to equations (3.30) and (3.32). After the tree has been completely traversed up to depth d_{max} and a partial VPL value has been computed for each evaluated node, the minimum of these VPL values will be selected as the one which offers the best performance to the user by maximizing the navigation availability, according to the following equation:

$$\mathrm{VPL} = \min_{k=1}^{2^n} \left({}^{k}\mathrm{VPL} \right) \tag{3.33}$$

Algorithm 1 Step-by-step description of the MHSS FDE

- `Compute the Real-Time VPL for the given all-in-view configuration as usual;`
- `Also compute VPLs after eliminating up to` d_{max} `satellites for all possible such partial configurations;`
- `Choose the minimum of all these possible VPLs and record the subset that generated this VPL;`
- `If this minimum VPL is smaller than the original all-in-view VPL, then a fault has been recorded on the satellites eliminated from the recorded subset.`

The name FDE was chosen for this method in order to comply with historical nomenclature in the field of RAIM. Actually, the question on whether a SV is failed or not is not as relevant here as is the question on whether eliminating one of the pseudoranges (and implicitly its associated measurement error) from the position equations, can provide a more accurate position with a smaller VPL confidence interval associated to it. The more measurements (viz. satellites) are used by the algorithm, the better will the geometry be and the tighter the confidence bound that can be can ultimately be set. Thus, VPLs based on a partial subset of the satellites in view will be most of the time larger than the all-in-view VPL. Removing a healthy satellite would have the effect of increasing the VPL, and hence detection would not happen since satellite elimination under nominal conditions normally degrades the geometry. Only if a large ranging error actually translates into a significant positioning error for the user, it is beneficial to exclude that satellite from the measurement equations. Therefore, detection and elimination under this algorithm only occur when a SV causing a position error to the user can be removed from the position solution equation without actually increasing the overall integrity risk above the required 10^{-7} threshold.

The nominal error distribution model, consists of zero-mean noise (allowing a Gaussian overbound) and biases in each channel. In theory, a failure is defined based on whether the navigation error distribution can be overbounded by a Gaussian curve or not, but the only information which is available to a snapshot algorithm like the one employed in this work is the instantaneous value of the error and not its probabilistic distribution. In practice, navigation errors can affect the VPL and the measurement confidence level. Small errors might increase the integrity risk without causing the $\mathcal{P}$HMI to exceed the alert level. Therefore, a FDE algorithm only needs to detect those errors that affect the VPL and $\mathcal{P}$HMI. Many existing RAIM algorithms compare their test statistic to a threshold in order to make a "fault / no fault detected" decision. However, one of the caveats of this approach is that a constant failure bias can be just below the chosen threshold and thus go undetected for any length of time. Also, combined effects of errors along multiple LOS can push a particular test

statistic over the threshold in the absence of a hazardous failure on any particular pseudorange measurement. Thus, the single failure assumption does not always hold to make exclusion possible. Lastly, in previous RAIM algorithms a separate analysis is also necessary to determine the probabilities of failed and false detection, and that of failed exclusion every time a detection threshold is employed. In the present algorithm, such additional analysis is not necessary, since it can be shown that one or more satellite exclusions do not affect the confidence level or the integrity that is already guaranteed for the position solution both before and after FDE is employed. The MHSS algorithm only estimates the navigation errors for each partial position solution, but it does not define a threshold for failure, recognizing the probabilistic nature of position measurements.

The reasoning behind the FDE algorithm is that while all satellite subsets are equivalent in terms of guaranteeing integrity for the user with position error bounds equal to their corresponding Protection Level, these subsets are at the same time not equivalent in what concerns range measurement geometry. Assuming that the SVs in GNSS constellations are placed into optimized orbits, in terms of the satellites being evenly distributed across the visible sky, the main remaining factor which determines the satellite geometry is the sheer number of navigation signal beacons. Thus, a measurement set including a higher number of satellite ranges will be favored to provide a lower VPL, all other things equal, since it will yield lower Vertical Dilution of Precision (VDOP) and σ_{v} values. By carefully examining equation (3.30), it can be observed that given a higher value of σ_{v} for a partial subset of the satellites in view, its corresponding VPL could only become lower if one of the other terms were also lower. Since the pseudoinverse matrix $\mathbf{S}$ also depends on geometry and B_{max} is a given system constant, the only term that can make a difference is a substantially smaller noise term ν. Hence, it can be concluded that the FDE method proposed above favors the inclusion of as many ranging sources as possible in the measurement set, as long as their corresponding range errors have small, nominal values. However, when a measurement is affected by an abnormally high level of error compared to all other measurements at the same snapshot in time, its exclusion from the position estimate

will be warranted as long as the reduction in overall measurement noise more than makes up for the resultant deterioration in geometry. The FDE algorithm does not, however, attempt to determine the cause for any anomalous error reading, whether it is due to a system fault, an improbable high level of nominal noise or any other circumstance. Given the limited amount of information that is generally available to the user at any snapshot of time, an absolute determination on the characteristics or even presence of a failure are not normally warranted.

In practice, the optimal solution to the search problem is far more likely to lie at a very shallow depth within the graph, given the very low probability that a higher-order measurement fault occurs, affecting the all-in-view VPL to a degree that would warrant eliminating multiple satellites simultaneously. However, the higher the number n of satellite measurements available initially, the higher becomes the chance of a multiple satellite failure and at the same time the less critical each satellite becomes for the overall measurement geometry. Thus, for the case of multiple constellation GNSS users, it is critical that a RAIM algorithm well-adapted to handling multiple simultaneous faults is employed. In order to demonstrate exactly how this algorithm performs in the context of satellite navigation, simulation results with the proposed FDE method will be provided in Chapter 4 and a real data evaluation of the obtainable VPL values will be presented in Chapter 6.

3.3.3. Prediction algorithm

Both the integrity and availability requirements were addressed by the MHSS RAIM algorithm with FDE capabilities developed over the previous sections. The question remains however on the continuity offered by this algorithm. Continuity is needed to guarantee that once a user made the decision to initiate a vertically-guided approach to an airport, the aircraft operation will not be subsequently put at risk by possible unpredicted errors that can develop over the course of that approach. To respond to this eventuality, an additional capability of the MHSS algorithm will be developed below, which allows setting a conservative bound on the contingency of an

availability loss during the course of an approach. This new capability will allow an aircraft at any point before or during its flight to compute a prediction VPL value for both current and future satellite geometries.

Under the MHSS algorithm, the real-time VPL depends on the range error residuals and is the union of all partial VPL intervals generated under the different failure assumptions included in the defined threat space. Thus, the overall VPL is practically determined by the largest such partial VPL interval, as long as one chooses the fault-free mode position solution as the position estimate and all other VPL intervals are centered around this position, called the all-in-view solution. If a *dispatch* VPL value is needed before the actual range measurements were available, it is possible to conservatively predict this VPL value at a given point in the future. That is achieved here without actually measuring the realized value of the error residuals, based on the fact that the measurement errors are normally distributed around the true position according to a specified error model.

Given a continuity requirement for the navigation solution, an interval can be defined for the measurement errors around each partial solution, such that the continuity requirement is always satisfied. The continuity requirement for the navigation solution considered here is a maximum probability of availability loss of $4 \cdot 10^{-6}$/ approach, in agreement with the GEAS Panel and the FAA specifications [99] (see also section 2.2.1). A corresponding uncertainty interval can be defined for the measurement errors around each partial solution, inside which the loss of service risk is lower than a specified value. The total continuity risk budget above is then split equally between all possible failure modes into continuity allocations, akin to the manner in which allocations were made for the integrity risk. Subsequently, the worst case error residual that still satisfies the corresponding continuity risk allocation is considered for each of the partial position solutions. That is done assuming again a distribution of the ranging errors that can be approximated by a Gaussian curve, and the expected value of the error residual is subsequently generated using a confidence bound approach similar to the way VPL is computed in RT MHSS. In

other words, the statistical worst-case navigation error is considered in computing each partial predicted VPL, before the union of all partial VPLs is taken by the same algorithm as in the case when real-time measurements were available. By this procedure, a conservative worst-case VPL is produced based only on the satellite geometry and the modeled statistics of nominal errors. It is expected that this will be an upper bound on the VPL that the user would determine in real time while performing a precision navigation operation. If the largest error value which would still allow the required continuity level for the operation results in a VPL larger than the required VAL, then there is a chance that the approach will not be able to be performed safely and a warning will be issued to the user.

Especially in aviation applications, it is important to be able to guarantee to the user that the actual VPL will not grow in excess of the required VAL, such that a precision operation will not even be attempted if there is a danger of an availability loss at any point during that operation. In particular, the predictive capability of the MHSS algorithm will be useful in reducing the number of missed approaches when satellite navigation would not be able to guarantee the safety of the user throughout the planned operation. This capability allows civil aviation integrity to be enhanced to a superior level, where the navigation system does not limit itself simply to a 6 sec time-to-alert. On the contrary, the MHSS RAIM algorithm is also able to provide longer term forecasts, such that when the satellite navigation system becomes unreliable a pilot does not need to seek a last-minute solution, but would be warned well ahead of time and would have time to seek an alternative means to land. It must be mentioned that since the FDE algorithm seeks to eliminate those measurements for which a large error in the satellite pseudorange also translates into a large error in the user position, it is not possible to use FDE for minimizing the predicted VPL values in the absence of real-time measurements.

The only term in equation (3.30) which depends on the measured ranging errors, ${}^{j}\Delta_{\mathrm{v}}$, will be replaced in the prediction algorithm with an estimate of the solution

separation as a Gaussian plus a bias component. The principles behind this estimation process are very similar to those for determining the partial mode error bounds. The Gaussian Solution Separation (SS) term is an upper bound based on the allocated continuity for each individual mode, from a total budget of $\mathcal{P}_{\text{Cont}} = 4 \cdot 10^6/approach$. At the recommendation of the FAA GEAS Panel [32], this budget represents half of the total continuity risk allowable by the ICAO aviation requirements [41], the same way in which the integrity budget mentioned earlier was set to half of the total integrity risk specification set by ICAO. The other half of these required risk budgets will apparently not be allotted to the RAIM algorithm itself, but to additional user and system equipment which is employed for aircraft guidance and navigation. The maximum loss of continuity risk permitted for the RAIM algorithm is split likewise equally between all fault modes, except for the all-in-view mode, for which the value of ${}^{j}\Delta_{\text{v}}$ would be 0 anyhow, as mentioned earlier:

$$ {}^{j}\mathcal{P}_{\text{cont}} = \frac{\mathcal{P}_{\text{Cont}}}{m-1} \tag{3.34} $$

Furthermore, as the SS components ${}^{j}x_{\text{v}}$ and ${}^{0}x_{\text{v}}$ from equation (3.31) cannot be estimated directly in the absence of the range measurements, the normal distribution assumption for the error allows a Gaussian model to be developed for their difference, ${}^{j}\Delta_{\text{v}}$. Based on (3.31), the standard deviation for the vertical separation of a partial position solution from the all-in-view reference is described by the equation:

$$ {}^{j}\sigma_{SS}^2 = \left[\left({}^{j}\text{S} - {}^{0}\text{S} \right) \cdot \Sigma \cdot \left({}^{j}\text{S} - {}^{0}\text{S} \right)^{\text{T}} \right]_{3,3} \tag{3.35} $$

An interesting relationship between σ_{SS} and σ_{V}, whose proof was offered in detail in [7], can be shown for the case when the measurement covariance matrix ($\mathbf{\Sigma}$) is diagonal:

$$ {}^{j}\sigma_{SS}^2 = {}^{j}\sigma_{\text{v}}^2 - {}^{0}\sigma_{\text{v}}^2 \tag{3.36} $$

Under the most conservative assumptions, the range biases for the all-in-view measurement set and the current partial subset could conspire to further increase the

separation of the two position solutions. However, unlike in the case of the integrity error model, which needs to represent a normal overbounding density function for the distribution of ranging errors, the continuity error model can represent an average over all possible circumstances for each user geometry. For instance, the expected value of the SS bias term would be zero. Nevertheless, the choice was made to provide here the most general expressions for the predicted value of the solution separation, with the mention that less conservative values can be selected for $\mathbf{\Sigma}$ and b, depending on the degree of conservatism that is desired for the prediction VPL:

$$ {}^{j}\Delta_{SS} = k\left({}^{j}\mathcal{P}_{\text{cont}}\right) \cdot {}^{j}\sigma_{SS} \tag{3.37} $$

$$ {}^{j}B_{SS} = \sum_{i=1}^{n} \left| {}^{j}\text{S} - {}^{0}\text{S} \right|_{3,i} \cdot b_i \tag{3.38} $$

In order to illustrate how different assumptions for the nominal error mean and standard deviation, as well as an independent allocation of the integrity and continuity fault budgets can take place in the process of providing a prediction VPL value, the graphical flowchart in Figure 3.4 has been provided. The vertical position error bound as the integrity term and the solution separation as the continuity term would be computed separately based on Gaussian models. At the end, they would be combined into a VPL value which guarantees both navigation requirements with the required probabilities.

To sum up, by applying the continuity requirement to the assumed nominal error model, "dispatch" VPL values can be computed and broadcast to aviation users before they initiate a critical flight operation, according to the following formula:

$$ {}^{j}\text{VPL} = k\left({}^{j}\mathcal{P}_{\text{HMI}}\right) \cdot {}^{j}\sigma_{\text{v}} + \sum_{i=1}^{n} \left| {}^{j}\text{S}_{3,i} \cdot B_{max,i} \right| + {}^{j}\Delta_{SS} + {}^{j}B_{SS} \tag{3.39} $$

In the case of the RT MHSS algorithm, the proof of safety relies on the assumed probability priors for all fault modes, while the VPL expression contains terms

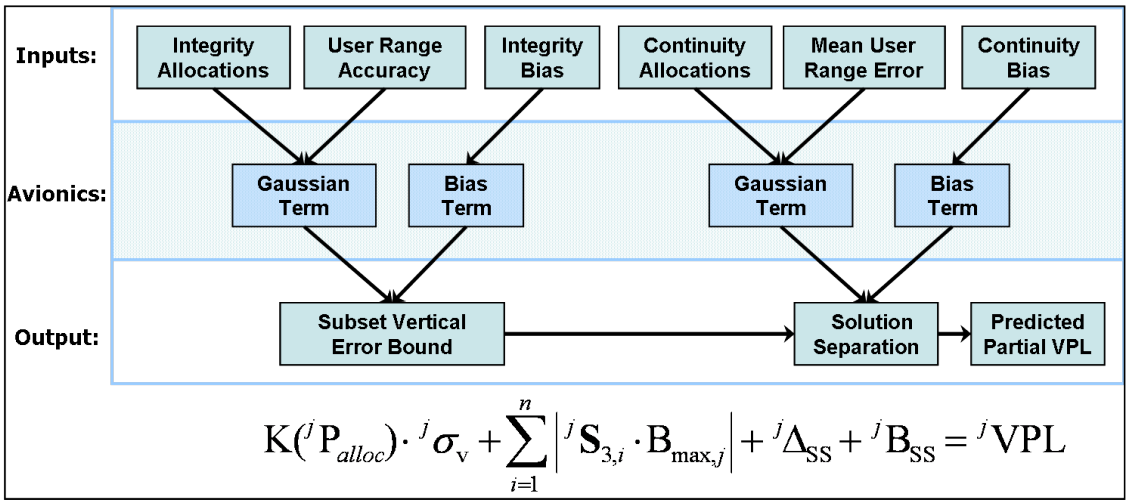

Figure 3.4.: Avionics processing flow diagram for the VPL prediction method.

which directly depend on the measured range errors. Therefore, posterior probabilities $\mathcal{P}\{\text{HMI} \mid H_j, y\}$, which apply to cases when ${}^{j}\mathcal{P}_{\text{HMI}}$ is conditioned on information of the realized ranging errors, cannot be directly employed in determining how the integrity budget should be allocated. Since the RT integrity allocations cannot be conditioned on the measurements, they need to be independent of the VPL. Accordingly, the MHSS RT allocations were fixed before the range measurements were employed in determining the VPL, as they could only depend on the satellite geometry and the failure priors. It can be said that the RT VPL relies on a static allocation of the integrity budget. Nevertheless, as the prediction VPL is no longer dependent on the realized range errors, in the MHSS prediction algorithm the integrity budget can be dynamically redistributed when calculating the VPL, in such a way as to minimize the overall Protection Level value. A slight improvement in performance for the user can be achieved in this way, without sacrificing any of the necessary conservatism in the VPL prediction process.

Given the monotonicity of the terms in the above equation for the prediction subset VPLs (in particular the two Gaussian terms), as functions of the integrity and continuity risk allocations, and the fact that the overall VPL is the maximum of all subset VPLs, it follows that the optimal performance for the user in the prediction mode is obtained when all partial VPLs have equal values. In particular, the method

demonstrated in [77] will be adapted here for optimizing the overall VPL by making all partial protection intervals equal: ${}^{j}\mathrm{VPL} = \mathrm{VPL}_{\mathrm{opt}}$. That original MHSS algorithm only suggests making optimal integrity allocations, but a proof in full detail is also given by Blanch in [9] on how to redistribute both the integrity and continuity budgets across all estimated fault modes in order to minimize the final prediction VPL values. A suggestion is also made by the same author, that an optimization process could also adjust the weights of the WLS position estimation algorithm, as a third variable parameter, in order to minimize the VPL. However, seeking an optimality volume in a three-dimensional space could be very computationally inefficient and as such it would only carry value from a theoretical perspective. Since only a minor advantage is derived from optimizing the continuity risk allocation between the fault modes as well, the more computationally efficient method of only redistributing the integrity budget while maintaining equal continuity allocations is presented below. In terms of practical applications of this RAIM algorithm, it is expected that the simplicity of the method will be an equally important consideration when attempting to achieve a superior navigation performance with the minimal time delay for warning the user on the existence of a potentially hazardous circumstance.

Introducing the notation ${}^{j}D_{\mathrm{v}}$ for the sum of the final three terms of equation (3.39), which are not functions of the partial integrity allocation, the expression for the risk allocations from equation (3.29) can be explicitly developed [77] as follows:

$$\mathrm{I_m} = \frac{1}{2}\sum_{j=0}^{m} \mathcal{P}\{H_j\}_{prior} \left[\mathtt{erfc}\left(\frac{\mathrm{VPL_{opt}} - {}^{j}D_{\mathrm{v}}}{\sqrt{2}\,{}^{j}\sigma_{\mathrm{v}}}\right) + \mathtt{erfc}\left(\frac{\mathrm{VPL_{opt}} + {}^{j}D_{\mathrm{v}}}{\sqrt{2}\,{}^{j}\sigma_{\mathrm{v}}}\right)\right] \quad (3.40)$$

The optimum VPL is the one which causes the allocations of all computed modes to sum up exactly to $\mathrm{I_m}$. The above relationship establishes the value of the integrity allocation terms in the summation as functions of the common VPL for all fault modes. Hence, the equation can be solved numerically through a binary search process for the VPL value that most closely meets the integrity condition, without causing the integrity budget to be exceeded. The binary search requires knowledge of the interval in which the optimal VPL is contained, or at least estimates for an upper

and lower limit to the values of VPL_{opt}. The interval bounds can be either determined analytically, based on the VPL expression in 3.32, or more pragmatically, they can be taken to be [0, 2·VAL], if the value of the VAL is known to the RAIM algorithm. This latter solution can increase the running speed of the MHSS algorithm with no downside to the user, since indifferent of how high VPL values raise above the VAL, they are not of practical interest to a user trying to achieve navigation availability for their scheduled or in-progress mode of operation.

The same allocation optimization process could also be applied to the RT algorithm only if it would always be safe to make the approximation that the *a posteriori* probability of satellite failure given the measurements does not differ significantly from the assumed prior:

$$\mathcal{P}\{H_j \,|\, y\,\}_{posterior} \cong \mathcal{P}\{H_j\}_{prior} \tag{3.41}$$

This approximation could hold, for example, if the *a priori* probability were originally determined based on a sufficiently long period of historical observation, such that the limited amount of additional data a user could collect during an approach procedure would not be enough to substantially update the initial prior. If this were the case, the optimization process could be similarly undertaken in RT through a dynamical allocation of the integrity budget conditioned on the realized values of the range errors, in order to further reduce the VPL values to the levels achieved by [77].

Another interesting idea suggested by [9] is feeding the integrity allocations from the prediction mode back into the RT algorithm. It should be mentioned that using the same allocations (optimized for the prediction algorithm) in the real-time algorithm would yield greater or equal values of the RT VPL compared to the prediction mode, although additional information on the realized range errors is being employed. This is a consequence of the fact that the all-in-view VPL, which does not depend on the actual measurements since its solution separation terms are always zero, will not change its value as long as its integrity allocation does not change. Thus, the maximum VPL of all modes for the RT algorithm using the allocations

optimized in the prediction mode will be at least equal to the all-in-view mode VPL, which in turn is identical with the overall prediction VPL. In many cases, using the allocations derived in the prediction algorithm with the real-time method will yield slightly larger RT VPL values, while using the equal allocation strategy for the RT MHSS will generally yield lower overall VPL values, in the absence of satellite faults.

While the predicted VPL is insensitive to the presence of faulty measurements, the RT VPL is designed to always bound the position error in the presence of failures, with a probability equal to I_{req}. Therefore, it is essential that any aviation user has a way to compute the RT VPL at all times, as an effective measure to protect against temporary unpredicted failures. It is also essential that there exists an external system to the aircraft with the capability to set potentially failed satellites to unhealthy within a reasonable amount of time, such that the periods during which an unflagged failure can affect aviation users are not long enough to significantly affect the assumed failure prior for one or more satellites.

3.4. Comparison with Classical Algorithms and Discussion

After careful consideration, the MHSS method was found to be the most appropriate for combined Galileo-GPS RAIM. Intuitively, this algorithm brings an added advantage, since it does not conservatively assign equal weights to all considered failure modes. More insight is gained by examining the results from the MHSS simulation in Chapter 4. As demonstrated in [25], compared to the previously examined algorithms, a lower VPL will be generated by MHSS for the same geometry and there is a visible improvement in the overall performance. The key results from the algorithm comparison study will be summarized below, starting with a comparison between LS and SS RAIM and subsequently introducing the MHSS results in the benchmarking process.

Initially, the classical LS and SS algorithms introduced earlier in Section 3.2 have been implemented and a test environment has been simulated and validated, in which the performance of RAIM algorithms can be observed against a standard failure threat model, under the assumptions set up by section 3.1.2. For the simulation analysis performed in Part II of this thesis, the MatLab Algorithm Availability Simulation Tool (MAAST) has been used. This software platform was initially developed in [42] and it has been maintained and further enhanced within the GPS Laboratory at Stanford University, including over the course of the current dissertation research work.

The tool allows a computer to initialize a user location grid distributed across a wider geography, ultimately permitting the RAIM results to be averaged over a diversity of receiver-constellation geometries. Since the measurement integrity is the primary concern of this research, the algorithm performance in terms of the computed VPL values is not simply averaged across all users and and across all time points. In order to reflect the additional high availability requirement once a PL has been determined, a value of the VPL closer to the worst-case for each user will be considered. The 99.5% highest VPL across all time steps for each user location on the grid will be used here for subsequent analyses of the results, in order to account for the fact that a high percentage availability needs to be insured at every location over a vast geography that is covered by the ABAS-guaranteed navigation solution. Therefore, when further metrics are used to aggregate performance over multiple users, it needs to be kept in mind that the VPL values chosen for each user are already 99.5% worst-case given the above availability considerations. For example, if subsequently, an average VPL is taken over all users in a geographic region, this will be the average of the 99.5% VPL values for each user.

With these considerations in mind, the significance of the results in Figure 3.5 can now be explained. The data points in this figure represent the 99^{th} percentile statistics among all the users locations considered, where for each user the 99.5% VPL in meters was taken as mentioned earlier. At the same time, three different elevation

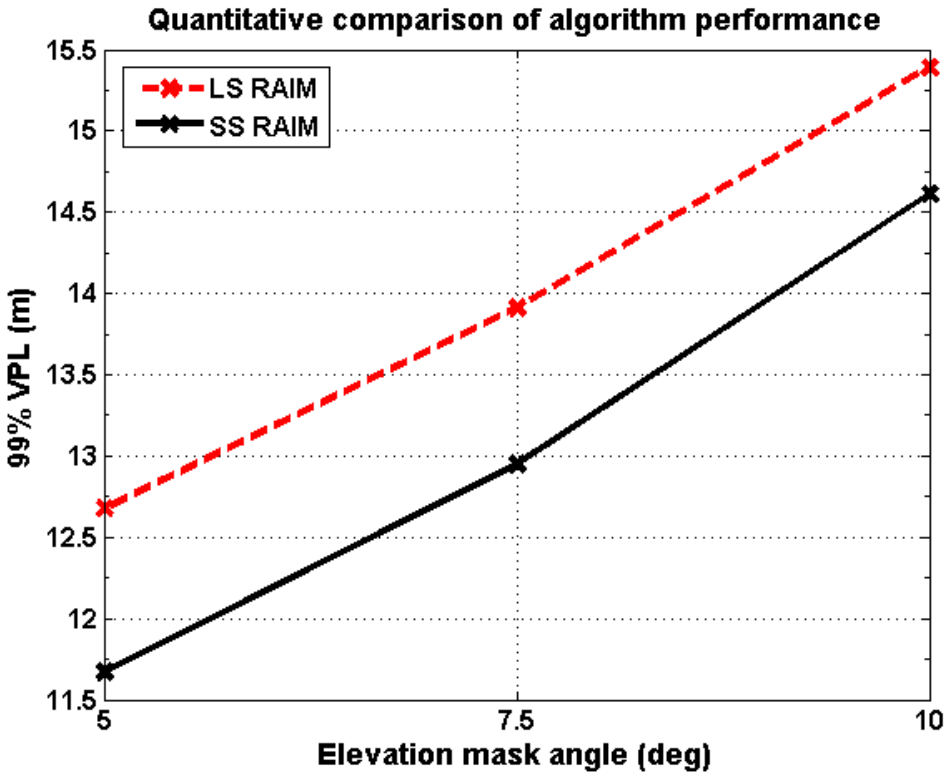

Figure 3.5.: Comparison of LS and SS classical RAIM algorithms. Aggregate simulation results for worldwide simulations with the dual Galileo / GPS constellation. At each location on the user grid, the 99.5% availability VPL is chosen among all time points, then the 99^{th} percentile VPL over all locations is taken. The LS VPL is given by equation (3.12) and the SS VPL by equation (3.20).

mask angle values were considered, for filtering out satellites that are visible too close to the horizon for each user, and whose data is thus prone to larger signal propagation errors. Separate simulations were performed in order to test each of the RAIM algorithms against the same threat model. Each simulation lasts 72 h, with at least 500 time steps and a minimum of 200 users over the entire world. The aggregation of the obtained results was thus necessary in order to bring the data into a form that is visually easy to read and understand.

A first observation is that SS performs better than basic LS RAIM under an identical threat model. There is a good explanation for that. In classical LS RAIM, information is lost in the process of forming the SSE statistic, in the respect that the

total error is summed over all geometrical directions or LOS. In the meantime, the SS algorithm clearly associates each position error with the corresponding LOS, or the geometry of a particular satellite subset, and does not assume that the maximum total error can be generated entirely by a single satellite. A second conclusion that can be drawn based on Figure 3.5 is that if the mask angle is increased in the simulations, less SVs will be in view on the average, causing the satellite geometries to deteriorate and the VPL to increase.

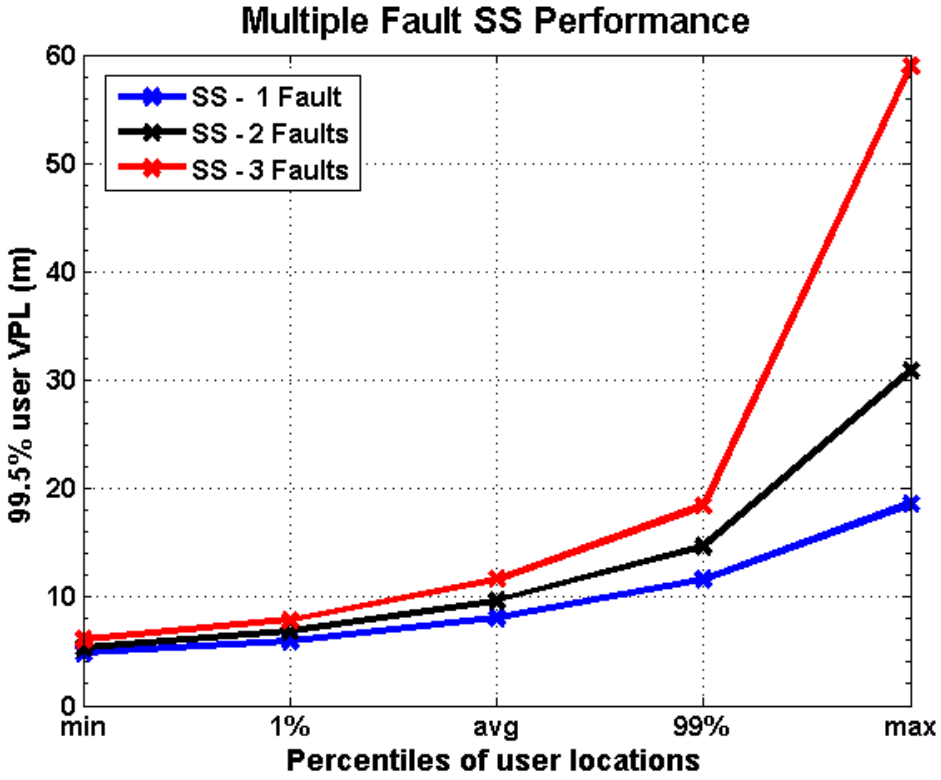

Figure 3.6.: Effect of assumed number of potential failures on SS RAIM performance. Aggregate simulation results for worldwide simulations with the dual Galileo / GPS constellation. At each location on the user grid, the 99.5% availability VPL is chosen among all time points and represented on the vertical axis. The VPL percentile among all the locations on the user grid is mapped against the horizontal axis. The SS VPL is computed according to equation (3.20), while considering a maximum number of either 1, 2, or 3 potential failures.

A topic for further exploration was the way in which multiple satellite failures could affect the performance of ARAIM. While the LS algorithm is designed to detect

at most one fault at each time step, the SS algorithm can consider partial subsets of any size, making it possible to identify multiple simultaneous faults. However, since both algorithms base their VPL on the worst-case assumption, when the SS algorithm was modified to consider subsets with $n-1$, $n-2$ or $n-3$ faulty measurements, its performance became worse and worse with the increase in the assumed number of simultaneous failures. Figure 3.6 displays the statistics for the SS RAIM performance under the various failure assumptions enumerated above and a standard 5° mask angle. As it was expected, single satellite elimination provides better position accuracy than multiple satellite elimination. Although one can discard several large positioning errors by eliminating multiple satellites from the position equation, this operation also leads to a loss of good geometry (e.g. high elevation satellites), thus in fact degrading performance.

If also represented on the plot in Figure 3.6, LS RAIM results would fall in between SS results assuming a single potential fault (SS1) and the results assuming the possibility of two simultaneous faults (SS2). However, this would not be a fair comparison since the implemented version of LS can handle a single measurement failure (viz. deviation of a range measurement from the nominal error model), a condition under which its performance is generally inferior to that of the SS algorithm. Since classical LS RAIM does not apply to cases where more than one failure needs to be considered, it is impossible to make a direct comparison with the results from SS with more than one satellite out. However, it is evident that the premise of multiple failures causes the VPL values to degrade rapidly, especially for the worst-case geometry. This could be a reason why previous work has chosen to ignore multiple failures based on their very small probability of occurrence. Nonetheless, in the case of a dual constellation, the probability of multiple failures is increased. Consequently, a method that can address these issues appropriately needed to be examined.

A corresponding set of results with the MHSS RAIM algorithm in its RT variant is presented in Figure 3.7. All the statistics by percentile of all users and by the different mask angle assumptions are summarized here in a single graph. It can

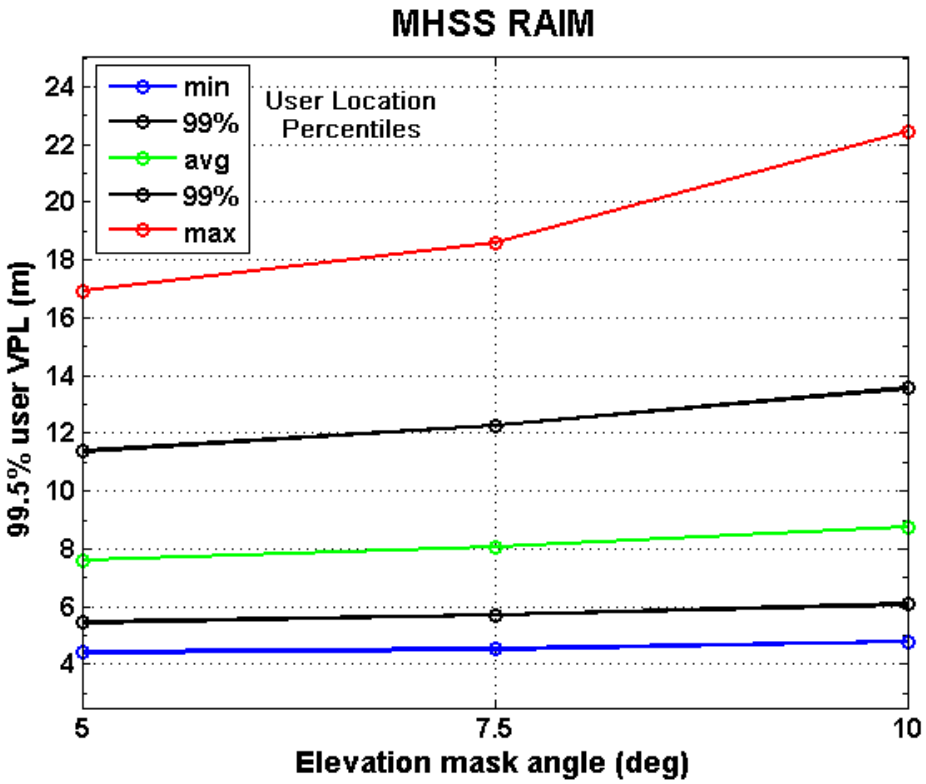

Figure 3.7.: Vertical performance of MHSS RAIM and its dependence on the elevation mask angle. Aggregate simulation results for worldwide simulations with the dual Galileo / GPS constellation. At each location on the user grid, the VPL which gives a 99.5% availability is chosen among all time points and represented on the vertical axis. The different lines on the plot represent different VPL percentiles among all the locations on the user grid. The MHSS Real-Time VPL is computed according to equation (3.32), while considering all potential failure hypotheses.

be seen that the performance of the developed MHSS algorithm, while it considers all failure hypotheses simultaneously, does not degrade with the assumed number of faults; on the contrary, MHSS RAIM is capable of providing an improvement in performance over SS because it weighs the impact of each hypothesis probabilistically and therefore it is not limited by the worst-case hypothesis. The only impact that a higher number of assumed potential failures has on the MHSS performance is that the computational complexity of the VPL computation increases as more partial fault modes need to be evaluated. Although such practical limitations on the run time will never translate in an inferior performance level for the aviation user, certain

measures have been taken to ensure the speed of the algorithm is not an issue. As described in the previous sections, not evaluating all possible fault modes in the position domain and only searching for VPLs in an interval between [0, 2·VAL], are ways to harness the computational complexity of the algorithm. For example, since once the required navigation performance becomes unavailable the aircraft pilot is prohibited from relying on satellite guidance, whether the VPL is barely above the VAL or it becomes orders of magnitude larger is interesting only for theoretical considerations about this RAIM algorithm, while it ads no practical significance from a user standpoint.

For each of the algorithms examined in this work, the most natural way to compute the VPL is to search for a range of position errors which ensures a $\mathcal{P}$HMI at most equal to the given integrity risk. Concurrently, every attempt will be made to minimize the VPL interval centered on the all-in-view position solution. Nonetheless, instead of the all-in-view solution, a different, optimal position solution can be chosen as suggested in [77], on which to center the VPL at each time step. This technique could help achieve a slightly lower protection bound. Nevertheless, for the reasons expressed above related to practical considerations on the computation complexity of the algorithm, the choice was made in this work to use the all-in-view position estimate as the reference point for all PL intervals. A trade-off is being made here, since the process of computing the optimal position is more computationally complex and also it may not always lead to a smooth position solution over time. In consequence, the decision was made to give preference to the smoother all-in-view solution while saving the algorithm some additional computational time. As a future consideration, it will definitely be interesting for more advanced versions of the MHSS algorithm to explore this trade-off between computational complexity and an optimal user position solution. This alternative should especially be considered as potentially frequent satellite outages or eliminations from the position estimation could cause much larger variation in the end-user position solution than the optimization process for a center position to the error bound interval.

Ultimately, a simple comparison of the VPL with the VAL corresponding to the user's needs will be needed for making a decision on whether to proceed with the desired operation. As a matter of fact, this approach is similar to the calculation of integrity risk at the Alert Limit (AL) proposed for Galileo integrity [71], which is a method that has already received careful consideration for use in integrity monitoring in that context. However, under this approach a problem will occur with equipment and human navigators that do not always have to keep track of the AL for the current operation under the current aviation system setup. Thus an ABAS based on a RAIM method like the current MHSS algorithm would be preferable, in that the proposed MHSS RAIM simply minimizes the VPL value under any given conditions, which might prove to be more practical for aviation operational purposes. Intuitively, this newly developed algorithm brings an added advantage over classical algorithms, since it does not conservatively assign equal weights to all considered failure modes. More insight will be gained by further examining the simulation results with MHSS in Chapter 4. Compared to the previously examined algorithms, a lower VPL will be generated for the same geometry and consequently a visible improvement in the overall performance will be demonstrated.

4. Determination of Parameter Space

The present chapter will present performance results obtained with a computer simulation of the Galileo and GPS constellations. Based on these results, a parametric study will be conducted to determine the sensitivity on the assumed values of the external parameters and the maximum operational range of the MHSS algorithm, inside which the LPV 200 aviation requirements can be met with the dual constellation. The first part (4.1.1) of Section 4.1 will contain a description of the initial setup and assumptions of the conducted worldwide simulations of MHSS RAIM performance. Meanwhile, subsection 4.1.2 will focus on presenting worldwide charts of the VPL values and availability coverage that can be provided with a dual-frequency combination of Galileo and GPS, based on the civil signals in the L1 and L5 bands. A discussion describing the avionics inputs required by the integrity algorithm, as well as the necessary performance specifications for future GNSS constellation to support ABAS, will follow in 4.1.3. Subsequently, Section 4.2 will present quantitative summaries across specific sets of simulation configurations. Subsection 4.2.1 will present the dependence of the RT VPL values on the Gaussian standard deviation and maximum nominal bias of the modeled error and on the assumed *a priori* measurement fault probability. The same analysis will then be conducted, this time for the prediction VPL, in 4.2.2. A set of conclusions on the achievable navigation performance in 4.2.3 will serve as a closing argument for the current chapter.

4.1. Simulation Studies of RAIM Performance

After careful consideration against the other algorithms described in Chapter 3, the MHSS method was found to be the most appropriate for aviation guidance with the future multi-constellation GNSS, and in particular for combined Galileo-GPS RAIM. In addition to the already operational GPS, Galileo was chosen as a complementary constellation, since at the time this research was performed it seemed the most likely candidate for the next satellite system to become fully operational worldwide.

4.1.1. Setup for simulations of worldwide MHSS performance

Simulations were performed in order to test the MHSS RAIM algorithm against a comprehensive threat model including multiple simultaneous failures as well as constellation fault modes and an unknown clock bias between the two constellations. According to system specifications, 30 active Galileo satellites and the minimum guaranteed 24 active GPS SVs are assumed to be present in the nominal constellations. Moreover, different elevation mask angles, of 5° for GPS and 10° for Galileo are used, as recommended by the program offices of the two systems, given the differences in the constellations orbital layout.

Since for all practical purposes, once a receiver is able to acquire the different signal formats, the derivation of a position estimate from the range measurements follows the exact same process, no further distinction is made between spacecraft belonging to different constellations. The only exception is made when assessing the possibility of an entire system / constellation fault. A constellation failure probability of 10^{-7} per each approach will be considered only when multiple constellations are present, such that the one constellation failure mode will represent the degraded case with only a single healthy constellation remaining available for navigation. For the individual satellites, a common sigma value is assumed for the GPS URA and the Galileo SISA, as well as for all other Gaussian and bias components of the ranging

error model. Unless otherwise specified, the standard value for σ_{URA} is 1 m, and the maximum nominal bias is considered to be 0 m, while all the other terms of the theoretical error model are uniquely determined as mentioned in section 3.1.2. Not until Section 4.2 of this chapter will the values of the URA, nominal bias, as well as the satellite failure prior probability be considered as variable parameters. At that point, it will be determined what their working ranges are, for which it is possible to achieve the desired RAIM navigation performance.

In terms of the individual satellite failures, it will be assumed that once a satellite failure occurs, it persists for an average of 1 hr before it is removed by the ground control. Given a historical average of 3 failures / year that can affect the users' range measurements by more than 30 m, this translates into a SV failure rate of 10^{-4}/ approach [51, 58]. Multiple independent faults will be considered in the combined Galileo / GPS constellation. The MHSS algorithm can be readily expanded to handle different probabilities and probability models for multiple failures, but the independent fault model was adopted in this work in light of possible satellite clock failures as main threat sources. In the later chapters, a model for correlated satellite failures will be tested as well. Additionally, separate constellation failure modes will be considered for the case where a majority of correlated faults exist across either the GPS or Galileo constellations but not both. Any systemic failures of an entire GNSS constellation have yet to be observed at the present time, after more than 20 years of continuous operation. In the meantime, a constellation failure rate between $10^{-8} - 10^{-7}$/ approach has been conjectured, corresponding to an average of approximately one event every 3–400 years, which is insofar impossible to measure in practice. Hence, the worst possible constellation fault rate which allows meeting the integrity requirements will be assumed, absent the ability to directly estimate a relevant historical value at the current time.

For each simulation setup, a user location grid which covers the entire globe is chosen. At each user location over the world, the 99.5^{th} percentile VPL over the

simulation period has been mapped in order to illustrate the high availability performance of RAIM. The maps are then colored by interpolation between grid points. A geographic average of the 99.5% VPLs is also provided for each plot. The grid step size is generally of 5–15 degrees in latitude and longitude, with finer or coarser spacing depending on the computational complexity involved for computing a VPL at each user location. More specifically, computing a VPL in RT while evaluating at most one potentially undetected satellite fault at each time step requires the least computational load. As the number of simultaneous faults to be considered increases, or additional VPL prediction with optimized allocations and FDE capabilities are added, the computational complexity of the MHSS algorithm will increase accordingly, sometimes exponentially. It should be mentioned here that while performing a simulation for users spread across the globe can require a significant amount of time, the practical application of the MHSS algorithm in aviation will only imply determining the VPL for the current user. Thus, each time MHSS RAIM is employed within the cockpit, regardless of whether additional prediction and fault detection capabilities are employed, the results will be available within fractions of a second, in quasi-RT.

It is important to emphasize the fact that current results reflect the performance on an average day under the given assumptions, without any failures being intentionally introduced over the duration of the simulation under nominal conditions. Unless specifically mentioned, no failures were inserted in the measurements; however, the algorithm always assumes failures could be present and computes position solutions based on partial subsets of the SVs in view, in order to guarantee that a fault-free solution is always included in the VPL. Furthermore, a particular user can only receive information from a subset of the SVs, specifically the ones at an elevation above a predefined mask angle. Thus, it is practical to consider only the satellites in view from the location of each specific user when assessing the prior probabilities of failure for each of the modes.

User Grid	5 deg lat	10 deg long
Constellation Size (optimized orbit spacing)	24 GPS satellites	30 Galileo satellites
Elevation Mask Angle	5 deg (GPS)	10 deg (Galileo)
Period	150 sec/ approach	24 hours total
A Priori Fault Probability	Satellite: 1×10^{-4}/ approach	Constellation: 1×10^{-7}/ approach

Table 4.1.: Summary of simulation parameters.

These standard assumptions employed during the MHSS algorithm simulation were originally presented in [27] and have been summarized here in Table 4.1. Due to the expected 10-day Galileo constellation ground track repeatability, it would be very computationally demanding to run a simulation over the whole period of the Galileo constellation with frequent enough temporal sampling so as not to miss potentially short-lived critical geometry configurations. On the other hand, the orbital periods of each of the Galileo SVs will be approximately 14 hrs, while GPS SVs complete a full orbit in about 12 hrs. To ensure that a full orbit is observed for each of the satellites, the duration of the simulations will be set to 24 hrs, making it possible to achieve sampling frequencies of every 150 sec while running the simulations on a PC computer. The period of 150 s is the specified duration for an airplane approach in the approach integrity requirements [41]. Also, in order to take into account the worst possible alignment of the Galileo and GPS constellations, the three orbital planes of the Galileo constellation are aligned with three of the GPS orbital planes at the beginning of each simulation period. With regard to the celestial motions of the two constellations, it should be mentioned here that there will be a slow relative drift of the orbital planes over time. This means that any features or anomalies observed on the VPL maps will slowly move along constant geographic latitude lines, having the potential to affect any locations at the same latitude. For example, the presence of a weak geometry region, generating higher VPLs somewhere over the Pacific Ocean, will eventually affect continental areas as well, as the anomaly is revolving around the

globe. In the future studies, longer simulation periods with less frequent time steps will also be attempted, such that these artificial features with no real geographical significance will average out along each latitude.

4.1.2. Simulation results

The current section will provide an overview of the different MHSS RAIM performance analyses conducted through simulation. It will then be within the scope of the following section to synthesize these results into several parametric studies and draw more general conclusions related to the applicability of MHSS as part of an ABAS for aviation applications.

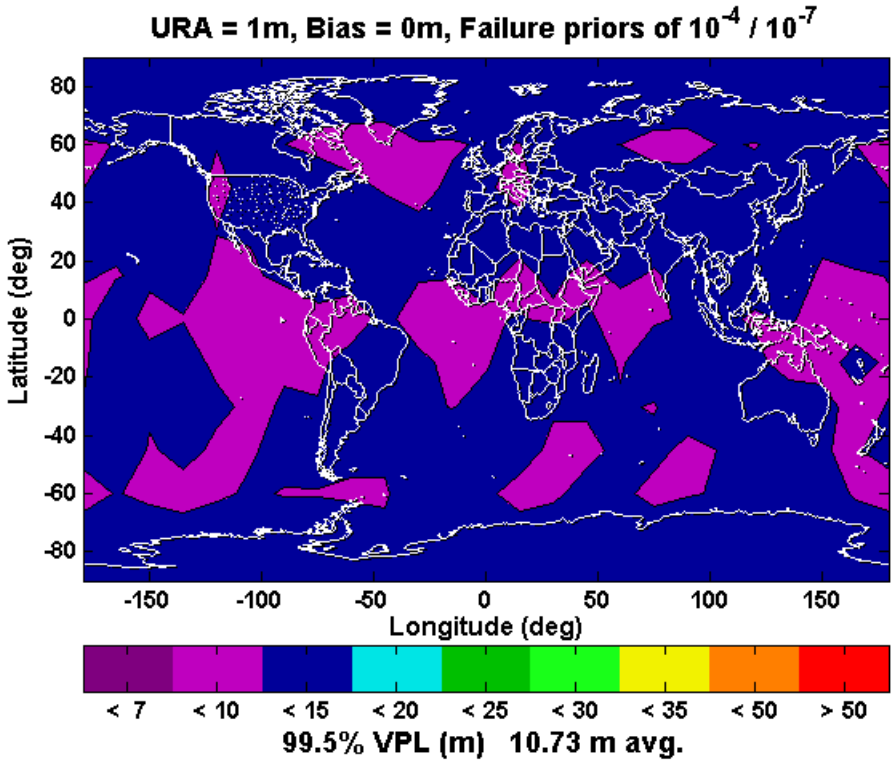

Figure 4.1.: Galileo-GPS dual-constellation baseline results for worldwide performance. At each location on the user grid, the VPL which gives a 99.5% availability is chosen. The average of such 99.5^{th} percentile VPLs over all locations is given beneath the plot.

The first results provided in Figure 4.1 represent a baseline of the MHSS RAIM performance in relation to which subsequent results under a variety of test conditions

will be evaluated. This first simulation makes typical conservative assumptions which, as a rule, will be summarized at the top of each map of the VPL results. In this case, the assumed value for σ_{URA} is 1 m, and the maximum nominal bias is considered to be 0 m, while the *a priori* probability of fault for each independent satellite is 10^{-4}/approach and the prior constellation failure rate is of 10^{-7}/approach. The latitude vs. longitude map is colored based on the 99.5% VPL at each user location, and an interpolation methodology is used for determining the corresponding color in between the grid points. Purple and blue nuances signify a low VPL, indicative of superior RAIM performance, green and yellow signify higher VPL values still in the acceptable performance range, while orange and red colors signify VPL values above the 35 m VAL, which would cause an LPV 200 type of aviation approach to become unavailable. The color scale and the associated VPL values in meters are located beneath each colored map, and the significance of the colors will be the same for all subsequent maps for consistency purposes. Finally, at the very bottom of each plot, an average value of the 99.5% VPL across all user locations will be provided.

Figure 4.2 summarizes the outcome of the MHSS algorithm simulation in the presence of measurement biases. While in the absence of biases VPL values are mostly around 10 m over the entire globe, accounting even for a small to moderate level of nominal bias at the user has a significant effect on the VPL values. Since RAIM PLs need to bound the actual error under any circumstances, an integrity algorithm like MHSS needs to assume that the maximum level of nominal bias can be present in any of the range measurements at any point in time. Under this conservative treatment, Figure 4.2(a) shows how adding in the assumption of a 50 cm level of the maximum bias causes the worldwide average 99.5% VPL to increase by approximately 2.5 m. It is expected that the presence of biases will not only increase the VPL for each user at any point in time, but also increase the overall spread between the minimum and maximum PL values computed by each user. As such, the effect of biases will be more pronounced for high percentile VPLs (viz. closer to the worst-case on record) than for low percentile VPLs. This assumption will be factually tested as part of the parametric studies in Section 4.2. In Figure 4.2(b), it can be seen how a 3.5 m

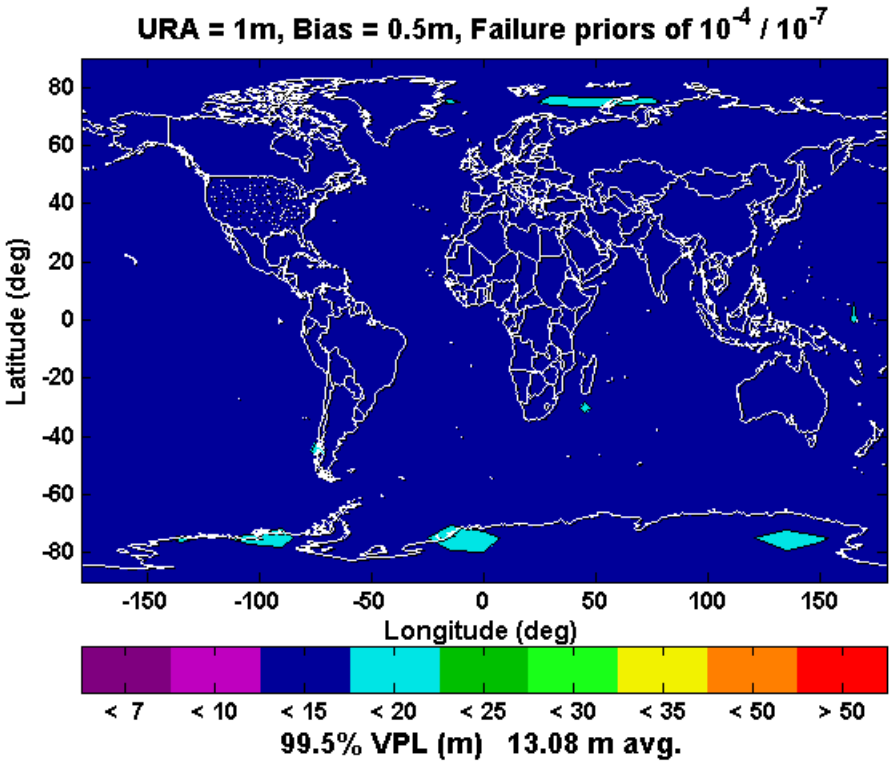

(a) assumed bias magnitude of 0.5 m.

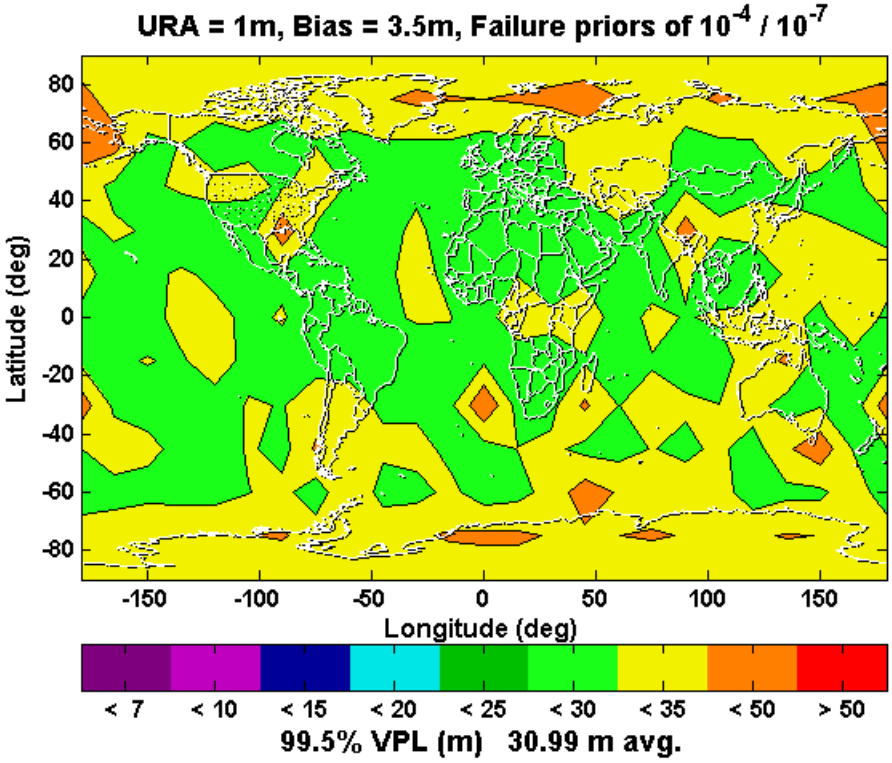

(b) assumed bias magnitude of 3.5 m.

Figure 4.2.: Influence of maximum nominal biases on MHSS RT VPL.

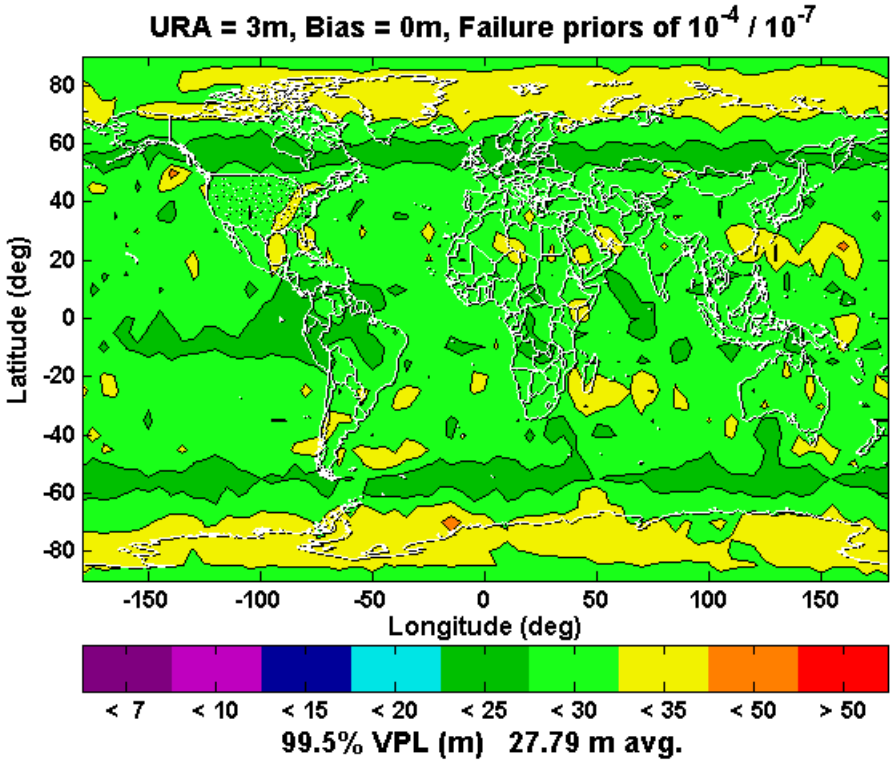

Figure 4.3.: Influence of User Range Accuracy on MHSS RT VPL.

nominal level of bias is sufficient to raise the 99.5^{th} percentile VPL to the vicinity of the 35 m AL.

Another set of prior assertions to which VPL values are sensitive are the additional premises made about the GNSS satellite performance. The Galileo and GPS Signal-in-Space (SIS) performance is generally recorded as the magnitude of the satellite clock and in-orbit position errors, characterized by a ranging accuracy Gaussian standard deviation measure. This metric is known as the SISA value for Galileo and URA value for GPS; therefore the two terms might be used interchangeably in this dissertation to refer to the same quantity. Figure 4.3 displays the recorded VPL values for an increase of the assumed URA value to 3 m, relative to 1 m in Figure 4.1. This value of the URA was more characteristic of the initial phases of GPS operation from 15 years ago, however the nominal URA guaranteed by the GPS system continues to be as high as 6 m to this day. As it can be seen here, a corresponding temporary or permanent deterioration in the GNSS space segment performance would still allow

aviation users to perform LPV 200 approaches at airport runways worldwide, though with a much tighter margin between the 99.5% availability VPL and the AL. The maximum SISA value which would still allow a MHSS RAIM algorithm to meet the 35 m VAL requirement will be determined as part of the study in Section 4.2.

One feature caused by satellite geometry effects for the dual constellation is noticeable on this last VPL map. The different color bands around the equator and at high latitudes close to the poles are caused by the fact that more satellites are visible on the average in these geographical regions. Given that the orbital inclinations are of 65° for Galileo and of 55° for GPS, those angles also represent the maximum latitudes at which users can still have any of the positioning satellites visible directly overhead (viz. in the zenith direction). Users close to the equator will not have any visible satellites at elevations below the zenith minus orbital inclination angles, which corresponds to 25° for Galileo, respectively 35° for GPS. This fact generally guarantees robust measurement geometries, although the lack of ranging sources close to the horizon might cause a slightly higher Horizontal Dilution of Precision (HDOP) for these users. Users at mid-latitudes will be able to observe the full range of satellite elevations (between 0° and 90°), though they will experience a "hole" in coverage in the direction of their closest pole, since the SV ground tracks will never reach beyond the arctic circle. Finally, using a dual Galileo-GPS constellation at high latitudes will cause the "hole" (i.e. area of the visible sky in which navigation satellites will not be observed) to shift across the middle of the sky. Although users in the polar regions will be able to see more satellites on the average than the mid-latitude users, all these satellites will be located closer to the horizon, thus offering an overall poorer measurement geometry, especially so in terms of the vertical positioning precision. With these considerations in mind, the distribution of VPLs by latitude on the simulation maps presented here can be better explained, though finer local variations in positioning performance still remain, due to the fact that the simulation period is shorter than the time needed for the ground tracks of the combined constellation to repeat exactly. It is expected that all the localized features present on these maps

will slowly rotate around the Earth over time, as the orbital planes of the two constellations rotate relative to each other. Taking an average of the computed VPLs for all the users at the same latitude would be a valid illustration of the long-term forecasted performance of the dual GNSS system.

The next dimension which was explored in simulation were the original assumptions related to the historically-based prior probabilities of failure for both individual satellite signals and for entire constellations or positioning systems. While the fault priors for individual signals will be explored later in this chapter, Figure 4.4 illustrates the influence of different constellation failure probability assumptions on the results obtainable with the MHSS RAIM algorithm. Based on these results, it can be concluded that changing this failure rate does not lead to changes as dramatic as the influence of different assumptions for the range error model terms on the VPL results. Nonetheless, it can be observed that varying this probability by four orders of magnitude leads to an increase in the average 99.5^{th} percentile VPL by about 4 m. Moreover, constellation priors lower than 10^{-8} per approach prove to have an insignificant impact on the overall VPL, since the likelihood of a constellation failure becomes practically negligible.

The effects of changes in the constellation failure probability are however no longer linear, as was the case for changing the URA and bias; instead, the VPL tends to increase by larger quantities for every order of magnitude increase in the constellation failure rate. For likelihoods of constellation failure lower than 10^{-8}, no additional visible performance gain is generally observed, since the chance of experiencing a failure is already insignificant enough compared to the integrity threshold. Therefore a further reduction in the prior would make very little difference in the computed VPL results. On the other hand, for a change in the decimal logarithm of the constellation prior probability of failure from -8 to -7, an increase of 19 cm in the average 99.5% VPL has been recorded. From a logarithm of -7 to -6, the increase was of 45 cm, between -6 and -5 of 220 cm, and from -5 to -4 it was 136 cm. Furthermore, above a certain probability of an independent failure of each constellation, it will become

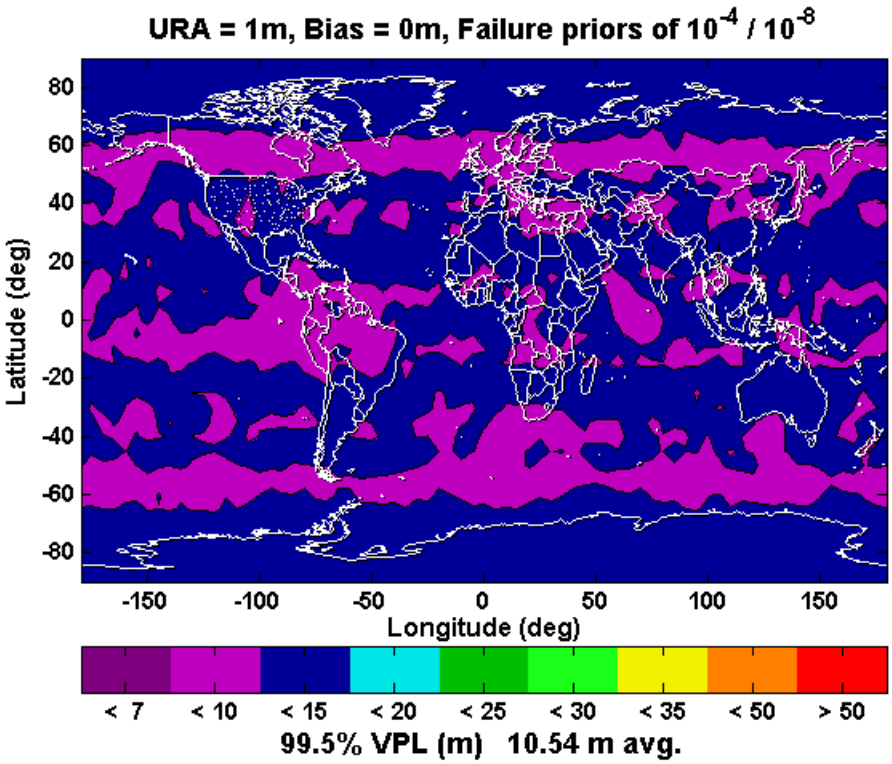

(a) assumed constellation failure rate of 10^{-8}/ approach.

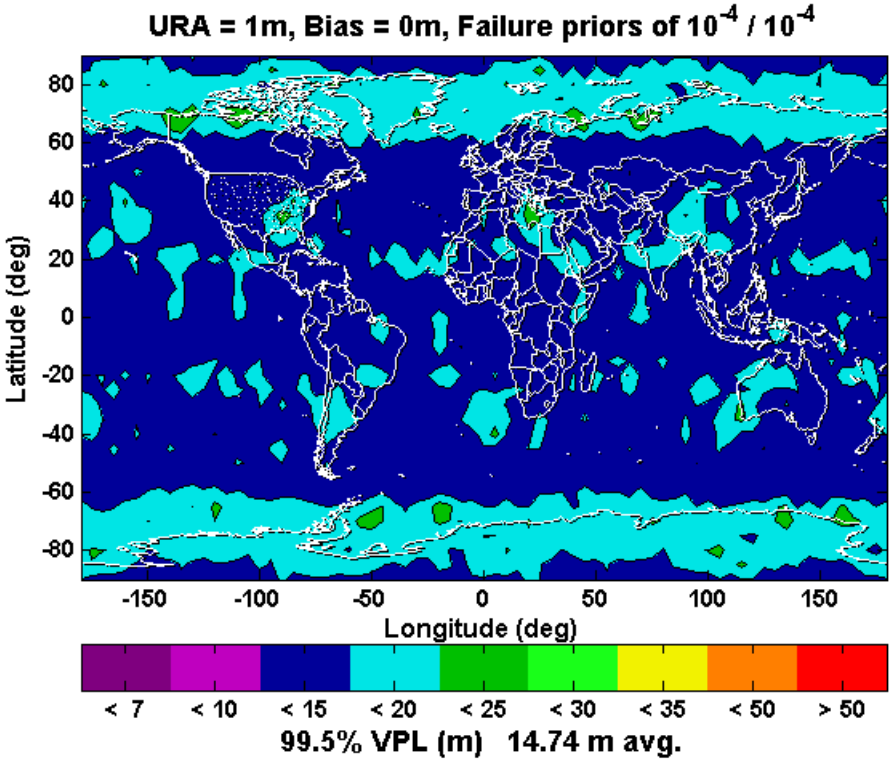

(b) assumed constellation failure rate of 10^{-4}/ approach.

Figure 4.4.: Influence of constellation prior on worldwide MHSS performance.

no longer feasible to rely on a single constellation fall-back mode, as the chance of both constellations failing independently from each other gets sufficiently close to the 10^{-7} integrity risk limit per approach. Fortunately, the current historical experience with the GPS constellation being continuously operational for almost two decades indicates that the actual probability of failure for an entire constellation is much lower than the critical value needed for the safe operation of civil aviation applications with ARAIM. Thus, the overall degradation in performance for the user is comparably much less significant for a decrease in satellite system failure reliability, compared to the potential degradation in performance caused by lower precision in the satellite clock and ephemeris elements or by higher levels of nominal biases.

A few additional questions that have been asked as part of this research about the preconditions needed for satisfying the aviation navigation requirements and about the needed robustness of the GNSS constellation for operating with MHSS RAIM. These questions regard the degree of interoperability required of the future GNSS constellations, the total number of needed satellites on whose signals RAIM needs to rely and the criticality of an unexpected loss of any of these satellites. Attempts to determine the minimal number of active SVs necessary for RAIM robustness have been made by running simulations with both full and partial versions of the combined Galileo-GPS constellation, containing anywhere between 24 and 60 spacecraft in the corresponding MEO orbits. The results of those studies have already been expounded in [26], and are summarized here. Table 4.2 presents a comprehensive set of simulations results covering the dual constellation partial operation modes. These results should be indicative of the level of RAIM performance achievable during the deployment process of modernized GNSS spacecraft in their corresponding orbits. For each simulation, the number of GPS and Galileo satellites included in the combined constellation is given, as well as the overall 99.5^{th} percentile VPL value for the entire world, and the percent of the points on the world map for which a 35 m VAL is available at least 99.5% of the time. When a value is missing from the third column, it means that in over 0.5% of the cases a position solution could not be computed with a probability of HMI of less than 10^{-7}, due to an insufficient level of redundancy among

Number of satellites		99.5% VPL (m)	coverage with 99.5% availability
GPS	Galileo		
30	30	9.32	100%
27	30	9.73	100%
27	27	9.90	100%
27	24	10.53	95.69%
24	30	9.92	100%
24	27	10.08	100%
24	24	10.86	96%
24	18	-	18.15%
24	16	22.59	14.46%
20	20	13.95	78.76%
18	18	-	11.38%
16	24	33.09	1.84%
16	16	-	0.61%
12	12	-	0.00%

Table 4.2.: Study of performance in the degraded operation modes of the dual Galileo / GPS constellation.

range measurement to the SVs in view. The presence of an infinite VPL value makes it also impossible to compute an average VPL for that case. Other approaches have also been employed in answering the question on the minimum number of required active satellites, based on real GPS data in Chapter 6 and based on single constellation GPS simulations in [32], which was supported by the results of this work.

The most frequently asked question regarding the system compatibility between Galileo and GPS is whether they will use the same master clock, their system times being either synchronized or separated by a precisely known bias, or whether users will have to consider a different receiver clock bias for each system, thus raising their total number of unknown position and time coordinates from 4 to 5. The results presented in Figure 4.5 try to address the effect that each of those different options would have on RAIM-based navigation. This map was colored based on results with a simulated Galileo-GPS dual constellation for which all spacecraft clocks are synchronized to a common system time. In the meanwhile, the remainder of the current

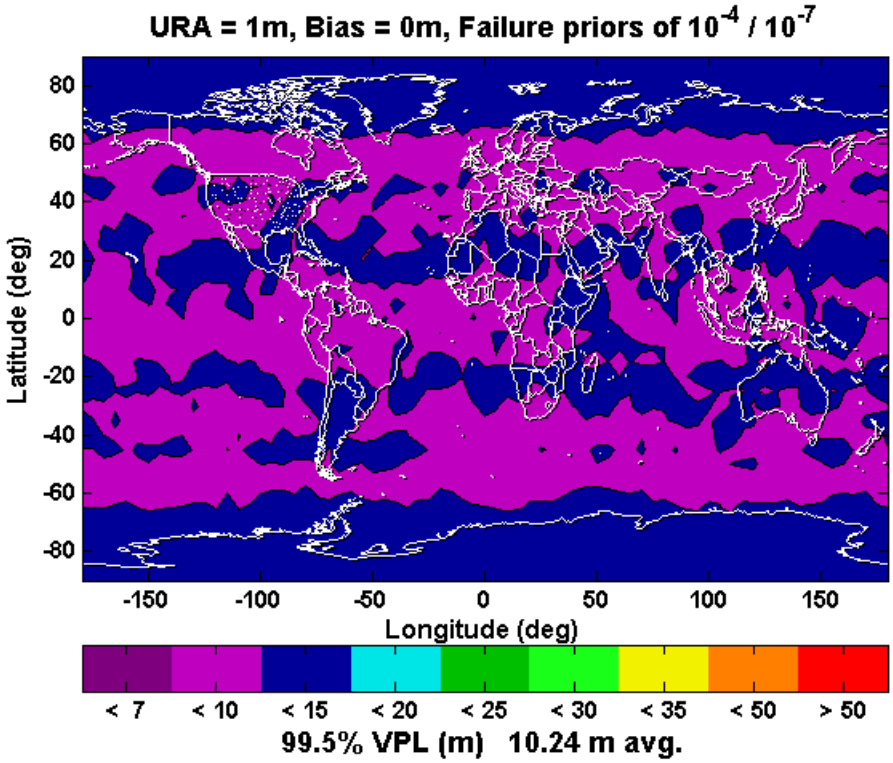

Figure 4.5.: Effect of synchronized GPS and Galileo system times on MHSS RAIM performance.

thesis has assumed a more conservative option to be the default, that of independent system times. Thus, the minimum number of visible satellite required for computing a position solution was raised from 4 to 5, with an additional range measurement being necessary to the determination of the second user clock bias. The corresponding results for this second option were already presented in Figure 4.1.

At this time, it is left to the appropriate decision-making bodies to determine whether it is more efficient to launch and maintain a number of 3 additional satellites in orbit, which would make up for the fact that all users need an additional satellite in view in order to resolve their two clock biases, or to identify a solution for synchronizing the two system times from the ground. In any eventuality, the approximately half-meter difference between the averaged VPLs under the two system set-ups is what users stand to lose from that decision under nominal conditions. Possibly, under poor geometry conditions or other degradations in the mode of operation of the

satellite navigation system, user can experience up to 2–3 m in higher error bounds as a price for precisely determining the clock difference between satellites of the two constellations. It should also be mentioned here that, in the single-constellation fall-back mode under the MHSS algorithm, when the user reverts to using measurements from only one constellation, the algorithm also reverts to needing a minimum of 4 satellites for the basic position estimate. Nevertheless, a RAIM algorithm needs measurements from at least two satellites in addition to the minimum number in order to compute user error bounds, as only the presence of redundant measurements gives it the ability to perform a statistical comparison between different solution subsets.

Having an additional time variable to determine leaves one less range measurement available for integrity monitoring. Effectively, this situation is very similar to the satellite elimination scenario below, except that the eliminated measurement is not the most geometrically critical one, so the deterioration of the VPL is less marked. In practice, when an arbitrary satellite is lost by the receiver during regular operation, it is not generally the most critical one. Therefore, the gain from synchronizing the two system times will be very similar to having an additional three SVs in orbit for the combined constellation (i.e. an additional satellite in view at any given time). All other results presented in this work presume unsynchronized system times since no guarantees were offered so far by the Galileo and GPS program offices that a common clock will be adopted and implemented. It is however in the interest of all users of the dual system to have a single time unknown to determine from the measurements, thus allowing a slight benefit for both the integrity and availability of the position fix.

The results in Figure 4.6 are meant to provide an answer to the third of the above questions, regarding the effect of losing access to measurements of the distance to a given satellite. In this case, the forfeited range measurement is the one that is most critical for the satellite geometry at that given point in time. It can be seen that while the decrease in the average 99.5% VPL is of approximately 3 m worldwide, there will be limited geographical areas where the damage to the satellite geometry

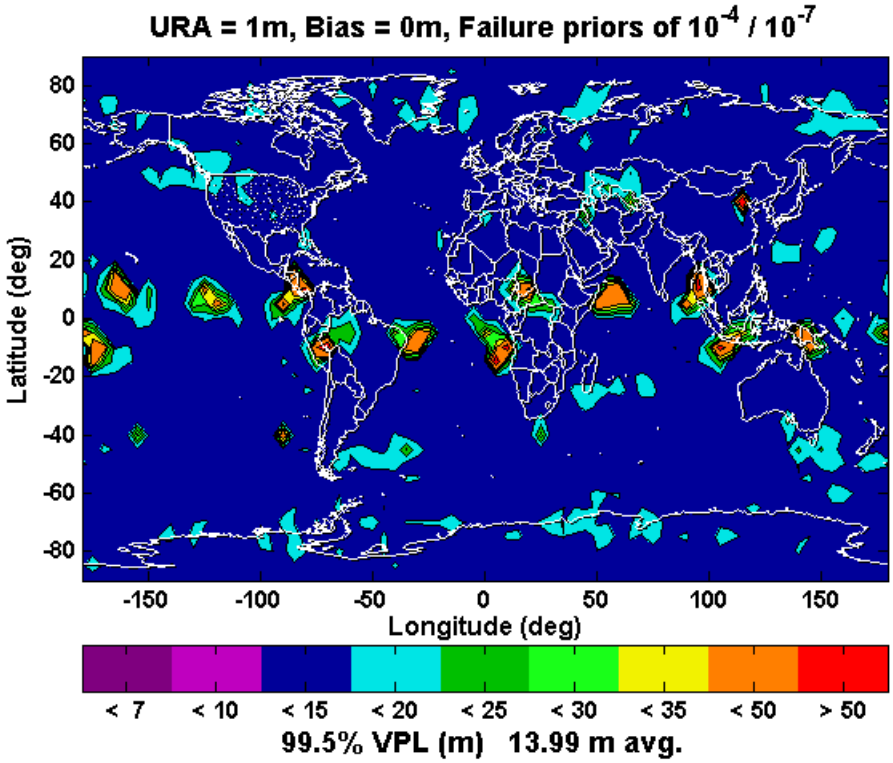

Figure 4.6.: VPL levels after each user loses the signal of the most critical satellite from a measurement geometry perspective.

is significant enough to lead to a loss of availability. This test scenario is however an unrealistic worst-case, in which each user would lose its own most critical satellite. In reality, a single satellite outage would affect users across the world to various degrees, and only a very limited number of these users would be relying on geometries in which the affected satellite is essential for the availability of the intended operation. Equatorial regions in particular are markedly prone to experiencing satellite outages, as those geographical areas can experience the phenomenon of ionospheric scintillation. This effects into a dimming of the satellite signals passing through an area of ionospheric turbulence, thus making them too weak for users along that particular LOS to be able to decode. Addressing this problem is nevertheless beyond the current scope of this thesis research, while the principal focus of the present work is to investigate availability of satellite navigation for civil aviation around populated areas at mid-latitudes, where these abnormal ionospheric phenomena have not been observed.

Since no previous study has been found, which determines how much the VPL deteriorates in the absence of the most critical satellite for stand-alone GPS and Galileo constellations, additional simulations have been performed also for the individual constellations. The VPL degradation upon losing the most critical satellite from a single constellation is much more significant, with an average resulting 99.5^{th} percentile VPL of 20 m for Galileo and 30 m for the unaided GPS. A more serious problem that affects single constellations upon the loss of the critical satellite is the diminishing in availability levels. The availability level is determined by comparing the VPL with the given VAL. In this thesis, the performance of the Galileo-GPS constellation is demonstrated against a 35 m VAL. By 99.5% availability, it is meant that the 99.5^{th} percentile VPL needs to be at most equal to the VAL. While the dual constellation maintains its full level of coverage at 99.5% availability over the entire world in the case of a satellite loss, Galileo availability drops to an availability level as low as 80% after losing the critical satellite. The standalone GPS constellation has the least assumed number of average SVs in view for any user under the current simulation assumptions. More specifically, with an average of 8 visible satellites as opposed to 10 for Galileo, the performance of RAIM with unaided GPS only starts with a 95% availability when operating in the nominal fault-free mode. This availability drops steeply to around 50% when the most critical SV is taken out. Also, the 99.5^{th} percentile GPS-only VPL exceeds the 35 m VAL for the entire surface of the Earth in all cases.

The last set of simulation results is meant to provide insight into what are the roles of the additional FDE and prediction methods, and also what are the essential advantages that they additionally bring to the MHSS RT algorithm. While the previous results presented in this chapter provided or computed the real-time VPL in order to baseline the performance of this newly developed algorithm, it is expected that any practical ABAS applications of MHSS RAIM will have both FDE and prediction as essential capabilities that enhance the flight safety and maximize the performance from a user standpoint.

In figures 4.7–4.9, the effects of FDE can be observed when implemented in conjunction with the MHSS algorithm. First, FDE is run under nominal conditions, when only nominal noise and biases are simulated in the measurements (Fig. 4.7). It can be seen how a small improvement in the VPL of about 25 cm is achieved. The VPL decrease is due to the increased confidence in the computed position solution, and also to the fact that any nominal ranging error, which can potentially cause a small position error, can be discarded from the position solution equation to improve the agreement between position estimates using only the remaining SVs. The proposed MHSS RT algorithm is already designed to be robust, in that it provides both integrity and availability in the presence of small amounts of random noise and moderate biases in the pseudorange measurement under nominal conditions. However, when the navigation error is large enough that the VPL would exceed the VAL, a failure can be declared to reduce that PL. In simulation, large failure biases will be inserted on top of the noise in one or several pseudoranges to test the detection capabilities with the proposed method. The fact that MHSS is working with system-level failure probabilities (not based on the actual measurements) enables the algorithm to be able to generate a VPL interval not only for the full set of satellites in view, but also for any partial set of these SVs. Due to the assumed pseudorange measurement independence, all confidence bounds based on the full set or a subset are equally trustworthy in guaranteeing that at most 10^{-7} integrity risk lies in the tails of the probability distribution. As elimination is done after an exhaustive search in the partial solution space, the uncorrelated measurement information discarded in the process has no detrimental influence on the integrity risk or $\mathcal{P}$HMI, which will not increase above the required limits upon satellite elimination.

In Figure 4.8, it is shown how the RT VPL results would change in the presence of a 10 m fault bias, which is intentionally introduced on one of the range measurements in order to simulate a satellite failure. For every user location on the worldwide latitude / longitude grid and at every time step, the most critical satellite from a geometry or VDOP point-of-view is identified and its ranging error is increased by 10 m.

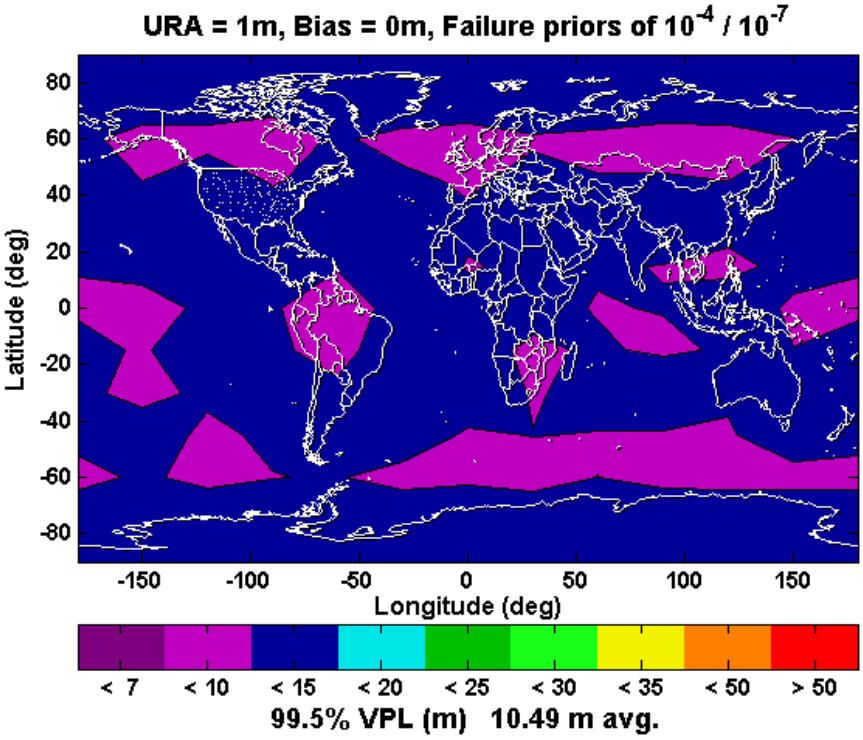

Figure 4.7.: Application of the FDE method under nominal conditions.

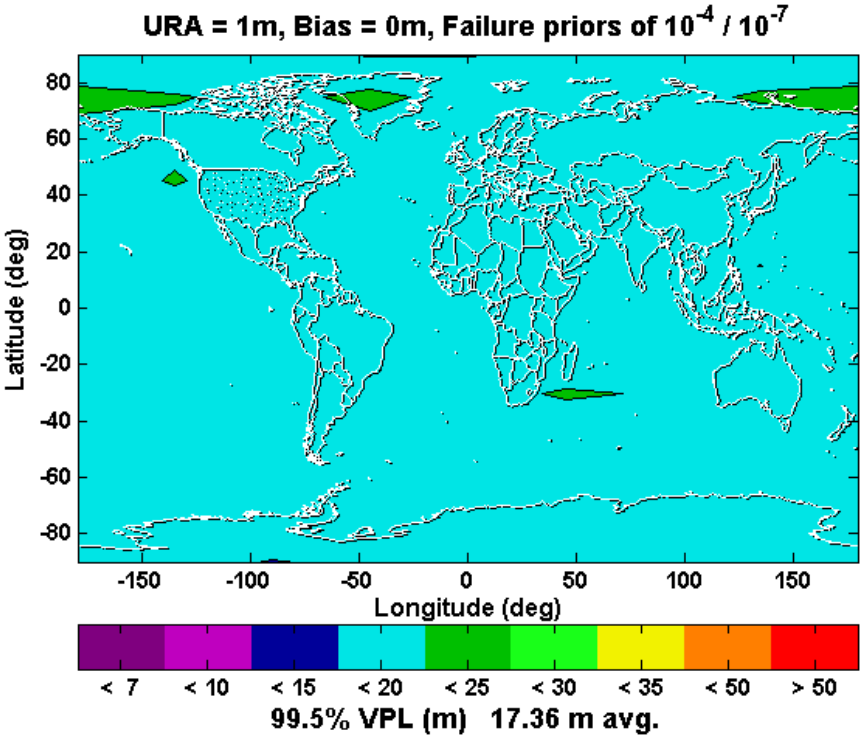

Figure 4.8.: MHSS RT results after the insertion of a 10 m fault bias.

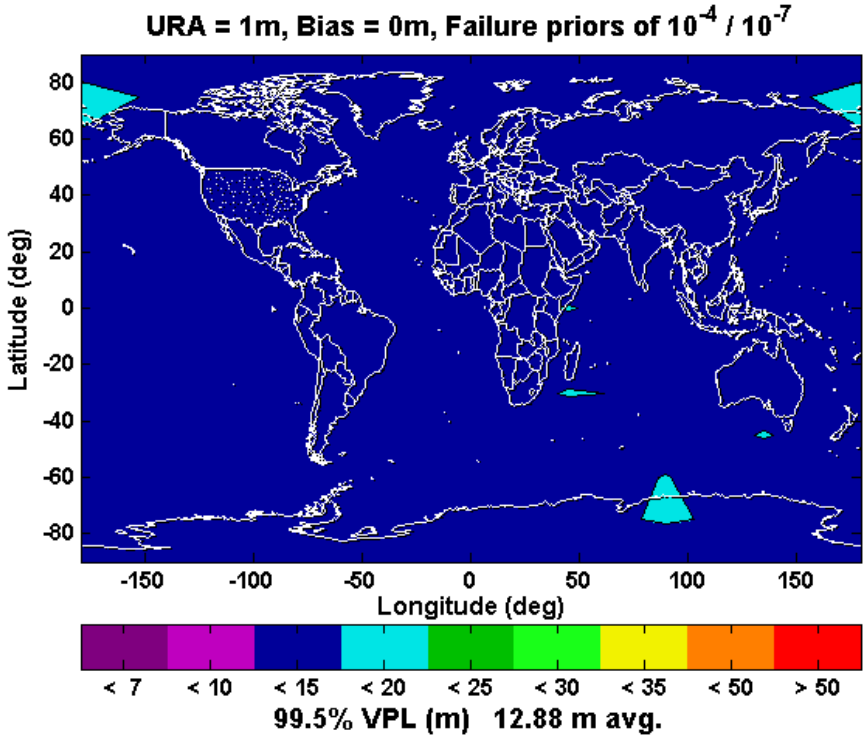

Figure 4.9.: FDE method successfully eliminates the intentionally-inserted 10 m fault.

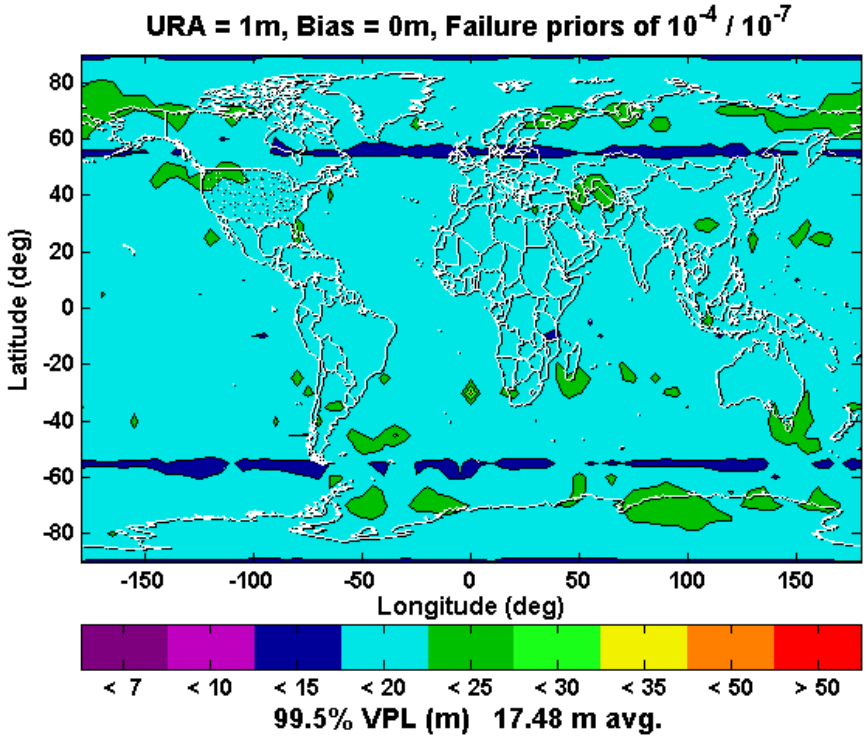

Figure 4.10.: VPL values obtained with the MHSS prediction algorithm.

This procedure ensures that the failure is implemented in the most unfavorable way to each user, on the satellite that is the most needed for having a good measurement geometry. Nevertheless, this 10 m failure bias on one of satellite ranges is still only as severe as the effect of assumed nominal biases of around 1 m on all SVs in view would be. Furthermore, once FDE is run on the measurement set containing the fault, the algorithm consistently identifies the satellite on which a large abnormal bias is applied and eliminates it from the position solution. In general, as long as the failure bias is consistently larger than the nominal measurement errors from the healthy SVs, the fault will unequivocally cause the largest position error when it is included in a measurement subset. On the other hand, if the failed satellite bias were comparable with the level of nominal noise on the remaining healthy satellites, then a different satellite could have been excluded instead, depending on the overall geometry. That is, however, not a cause of concern for the aerial navigation user, because FDE guarantees that the minimum possible VPL will be achieved regardless of the overall geometry conditions and ranging errors for the other satellites. The use of the FDE method in conjunction with MHSS provides the most possible integrity to the user whether the removed satellite was faulty or some combination of SV geometry and signal propagation errors was the culprit for the largest positioning error seen by the user.

From Figure 4.9 it can be seen that, even after the exclusion of the failed satellite, the VPL still depreciates compared to its nominal values in Figure 4.1. This effect is caused by the fact that the removed SV was purposely chosen to be critical to the measurement geometry. Inserting a fault on the most critical satellite for each user at every time step is certainly a very conservative way to determine what is the VPL in the worst-case scenario. For comparison, a more realistic case may be considered, where at every time step a single SV is chosen, whose failure will have the worst possible overall effect on the integrity performance worldwide, though it might not represent the failure of the most critical satellite for each individual user.

In reality, when a satellite fault occurs, it will not affect all the users in the world to the same extent. For some users that particular SV might not have been in view anyway, while for other users a signal from the same satellite is received, but the ranging errors might not have the most critical effect on the final position solution. In conclusion, it is expected that less conservative results will be obtained when the vertical integrity performance is measured against real data. Nevertheless, the FDE algorithm will always bring an added layer of protection to the user against ranging errors that could translate into hazardous positioning errors, whether this happens under nominal or abnormal measurement conditions.

The final simulation results, those employing the MHSS prediction tool, practically show an upper limit for the VPL in the presence of error residuals that are borderline to posing a continuity threat. Since no range measurements are used in producing the predicted VPL values, it must be conservatively assumed that threatening errors can exist along all ranging LOS and not only in a particular channel. The advantage of being able to provide a dispatch VPL to the user is the ability to guarantee integrity to a planned critical operation without the threat of continuity loss. Comparing the predicted VPL (Fig. 4.10) with the case where a failure was simulated (Fig. 4.8), it can be seen that the prediction tool adds a layer of robustness to the MHSS algorithm, such that even 10 m of failure bias on one of the range measurements would not threaten the required continuity for a critical operation to the aircraft user. In practice, the probability of a 10 m erroneous bias in the GNSS measurements is much lower than one. That explains why the real-time VPL, which is an expected value $(1-10^{-7})$ error bound given the measurement residuals, is significantly lower than the dispatch VPL, which is an expected worst-case scenario error bound in the absence of any information on the pseudoranges.

4.1.3. Discussion about the implications of the simulation results

When both the modernized GPS and Galileo constellations are fully operational, it will be possible to implement in practice the RAIM algorithm presented in this thesis. Only GPS User Range Accuracy (URA) and Galileo Signal-in-Space Accuracy (SISA) values are needed by the algorithm, along with a prior probability of failure for each satellite and for the constellations themselves. The value of the SIS Monitoring Accuracy (SISMA) calculated by the Galileo Sensor Stations (GSS) and broadcast by Galileo SVs is not necessary in order to calculate the integrity for the user, but it could be used in order to derive an implied fault probability of a satellite based on a Gaussian treatment.

Simulation results anticipate the possibility of using GNSS signals as the primary means for navigation in civil aviation. However, one feature of the dual Galileo-GPS constellation that can significantly improve RAIM performance would be the interoperability in terms of system clock synchronization. In the present work it was assumed that there are two separate system time unknowns, one for each constellation, such that a minimum of five satellites from the combined constellation is needed in order to solve for the 3D position and the two time variables. The additional satellite would thus not be available for performing RAIM redundancy checks. Due to the orbital geometry, a third of the total number of active SVs is visible to the average user. Hence, the integrity performance of the double constellation considered here is equivalent to that of a combined constellation with three less SVs in orbit, but a single system time which is synchronized across all active satellites. As a possible downside, once the system times are synchronized, a new common mode failure possibility is generated, which does not allow the two constellations to be treated as independent any longer. One of the beauties of the use of two independent systems is that there is no common fault mode. One important thing that was shown by the simulation results above is that the combined constellation is much more robust to satellite failures than any of the two individual constellations operating independently. The key factor

is the increased number of 18 average satellites in view, which leaves enough room for the elimination of one or two faulty SVs without greatly endangering the integrity or availability performance for the user. A separate study of single-constellation RAIM was carried out in Chapter 6, in order to determine the minimum required capabilities of the SVs within the future GPS constellation, such that LPV 200 guidance can be achieved even if a second constellation will not become available to aviators within the USA.

4.2. Parametric Studies

The failure priors, nominal bias and URA were chosen to be the variable parameters for more comprehensive, studies since their values are determined outside RAIM, depending on the particular constellation characteristics. Thus, in the current section, the evolution of the VPL versus each of the parameters under study will be given as a continuous dependence, in order to derive the corresponding amount of sensitivity on each external parameter. In contrast, the earlier simulation results simply assumed a few bounding values for each of the parameters. Since the MHSS RAIM algorithm described in Chapter 3 has the capability of operating in both real-time (RT) and in prediction mode, it was deemed appropriate that separate parametric studies are conducted for the two types of operation. Thus the following subsection is dedicated exclusively to the study of the RT mode, while the corresponding results for the prediction mode will be deferred to 4.2.2.

4.2.1. Real-time parametric studies

Figures 4.11–4.12 summarize the parametric studies for the Real-Time algorithm, showing how the simulation outcome of MHSS depends on the presence of measurement biases, the value of the URA, and satellite prior probabilities of failure. The VPL results under the parametric study were originally published by this author

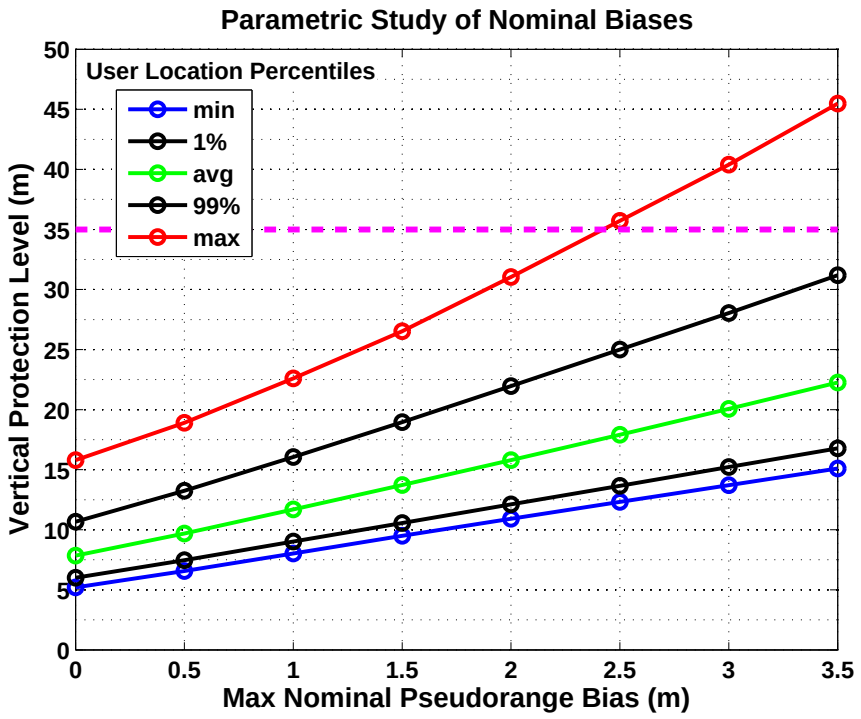

Figure 4.11.: Real-Time VPL dependence on nominal biases. The sigma URA and *a priori* probabilities are maintained constant in the meantime, at their baseline values used to produce Figure 4.1 on page 108.

in [26] and what follows below is a summary of the key points derived in that paper. Figure 4.11 summarizes the outcome of the MHSS algorithm simulations in the presence of measurement biases. This figure can be interpreted as an illustration of what are the minimum alert limits (ALs) for which a corresponding coverage figure between 0–100% could be obtained globally, while ensuring a high 99.5% availability figure for each user. If, for example, the 99% curve is examined, it characterizes the VPL level for which an approximately 99% global coverage is achieved, with a 99.5% availability at each location. While in the absence of biases, 99% coverage VPL values are mostly around 10 m over the entire globe, a 3.5 m bias raises the corresponding protection level to the vicinity of 30 m. Upon a visual estimation, the minimum VPL increases by about 10 m for each additional 3.5 m of bias, while the maximum VPL value changes by 20 m for each additional 2.5 m of bias. What is the most relevant, however, is the evolution of the 99^{th} percentile VPL, which is increased by 20 m by

an additional 3.5 m of bias. Therefore, the presence of biases is an important limiting factor on the VPL values achievable with a Galileo-GPS constellation.

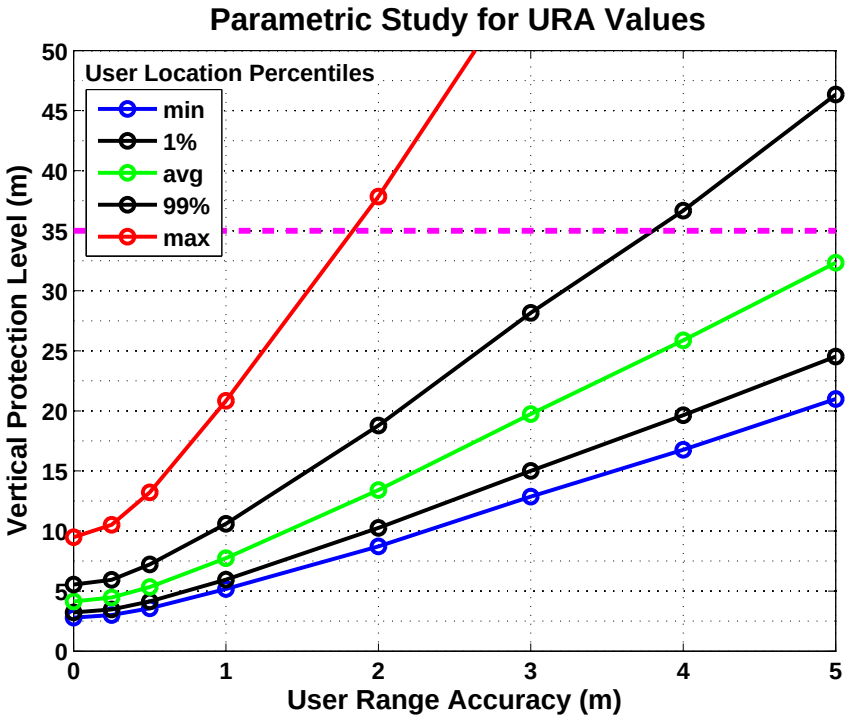

Figure 4.12.: Real-Time VPL dependence on URA. The nominal values for the bias and *a priori* probabilities are employed, as given earlier for the baseline results in Figure 4.1 on page 108.

Another parameter to which the VPL results are very sensitive is the URA value (Fig. 4.12), and implicitly the overall variance of the modeled nominal error. A reality check needs to be made for all values involved with this error model, since a 1 m change in the URA in this case can influence the average 99.5% VPL over the world by about 8 m. This indicates a stronger dependence of the results on the Gaussian error model than the influence of assumed failure priors or nominal biases. The effect of the value of the satellite *a priori* fault probability on the computed VPLs is illustrated in Figure 4.13. It can be noticed how VPL values increase dramatically for failure probabilities of 10^{-2} or higher. This proves that above a certain prior probability enough satellites are likely to fail simultaneously, such that a position solution cannot be computed at all time steps and the 99.5% VPL becomes unavailable (viz. infinite in value). For a prior of 10^{-2}, the likelihood of six simultaneous ranging faults is

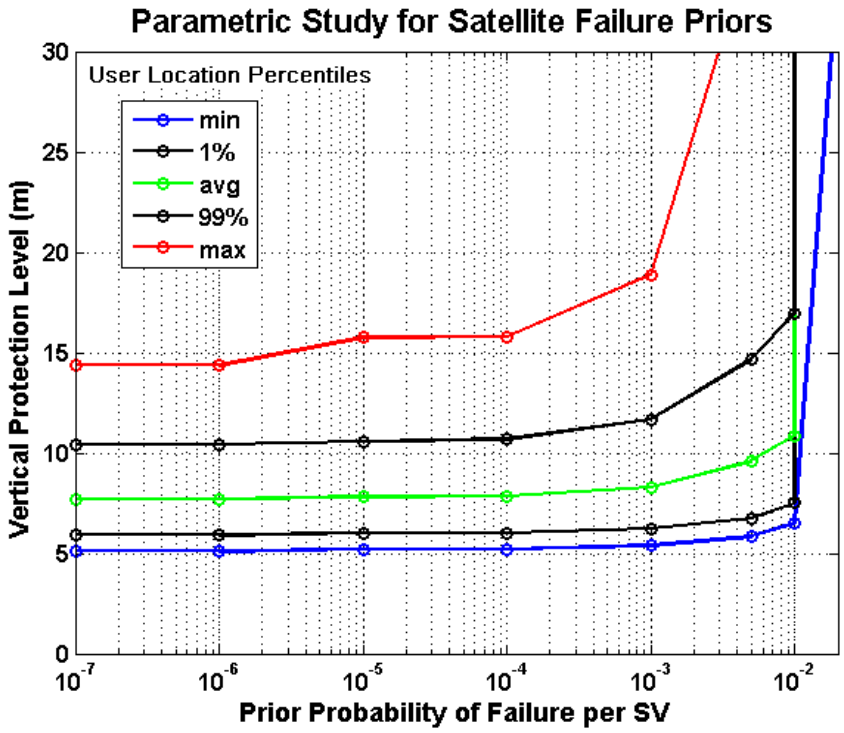

Figure 4.13.: Real-Time VPL dependence on SV prior. The baseline values of 1 m for the URA and 0 m for the nominal bias are considered in conjunction with the variable prior fault probability.

higher than 10^{-8}/ approach. Moreover, the number of probable simultaneous failures grows very rapidly as the satellite prior is increased beyond that value.

Nevertheless, for SV fault priors below $10^{-3}/150\,\mathrm{s}$ (i.e. at most three failures are likely to occur with a probability greater than 10^{-8} per approach), the average VPL is quite insensitive to the chosen failure priors. What changes significantly with the value of the prior, however, are the tails of the VPL distributions, making the worst case more extreme, as critical satellites for the geometry are more likely to fail. It might look surprising at first sight that the average VPL is quite insensitive to the chosen failure priors for such a wide range of fault probabilities. One way to explain this result is by the fact that multiple failures are much less likely than single failures and are always weighted accordingly. Adding more possible failure modes into consideration does not change the probability distribution of the position solution significantly. Therefore, the limits of the VPL interval, outside of which the

realized positioning error is less likely than 10^{-7} to lie, do not change considerably. What changes with the failure probabilities, however, are the tails of the distributions, making the worst case more extreme, as critical satellites for the geometry are more likely to fail.

The parameters on which the VPL results are very sensitive are the nominal measurement error standard deviation (e.g. the satellites' URA / SISA) and bias values. A 1 m change in the URA or the bias can influence the average 99.5% VPL over the world by about 5–7 m. This indicates a stronger dependence of the results on the Gaussian error model than the influence of assumed failure priors. In conclusion, the presence of biases and the system-specified variance for the clock and ephemeris errors are all important limiting factors on the VPL values achievable with a Galileo-GPS constellation. The average VPL is not very sensitive to the chosen satellite and constellation failure priors, and it increases approximately linearly with the value of range errors and noise variance.

4.2.2. Prediction Mode Parametric Studies

This section summarizes parametric studies, showing how the outcome of the MHSS prediction algorithm simulation depends in turn on the presence and size of nominal measurement biases (viz. the mean value of range measurement noise) and the value of the URA (or the standard deviation of the Gaussian measurement noise in general). The results of studies on the dependence of the VPL values on the measurement error under nominal conditions and the satellite failure priors are presented in figures 4.14 and 4.15. These two parametric study results were originally published and presented in full detail in [28]. A 1 m change in the URA or the nominal bias can influence the average 99.5% predicted VPL over the world by about 5–10 m. In the absence of satellite clock and ephemeris errors, which are characterized by the SISA for Galileo and the URA for GPS, VPL values would be under 5 m, due to the other terms in the error model (excluding biases). However, a 3 m URA is sufficient

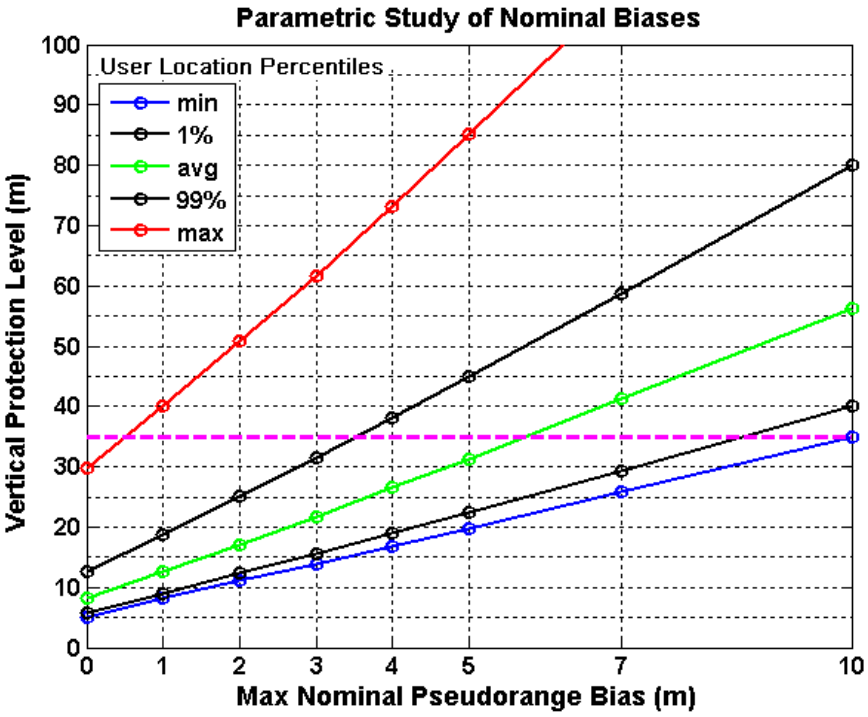

Figure 4.14.: Prediction VPL dependence on nominal biases. The URA is chosen to be 1 m here, and the satellite and constellation failure probabilities are fixed at 10^{-4} and 10^{-7}/approach, respectively.

to increase the 99.5% VPL values close to the assumed Vertical Alert Limit (VAL), represented by a horizontal dashed line on these plots.

There is certainly a significant overall performance difference between the two types of VPLs and this can be seen by comparing figures 4.14–4.15 to the previous figures 4.11 and 4.12. The VAL which needs to be satisfied for LPV 200' civil aviation approaches is 35 m for both real-time and prediction. Nevertheless, the conservatism built into the prediction algorithm should not substantially reduce the ability to dispatch a flight. It can be seen that although the same quasi-linear relationship exists between the size of the VPL and the amount of URA and bias in the measurements, less pseudorange inaccuracies can be tolerated before the alert limit is exceeded in the case of predicted VPLs. In terms of the modernized GNSS constellations, one can confidently assume that these systems will provide higher precision pseudorange measurements, thus lowering the nominal error term that is determined by both the

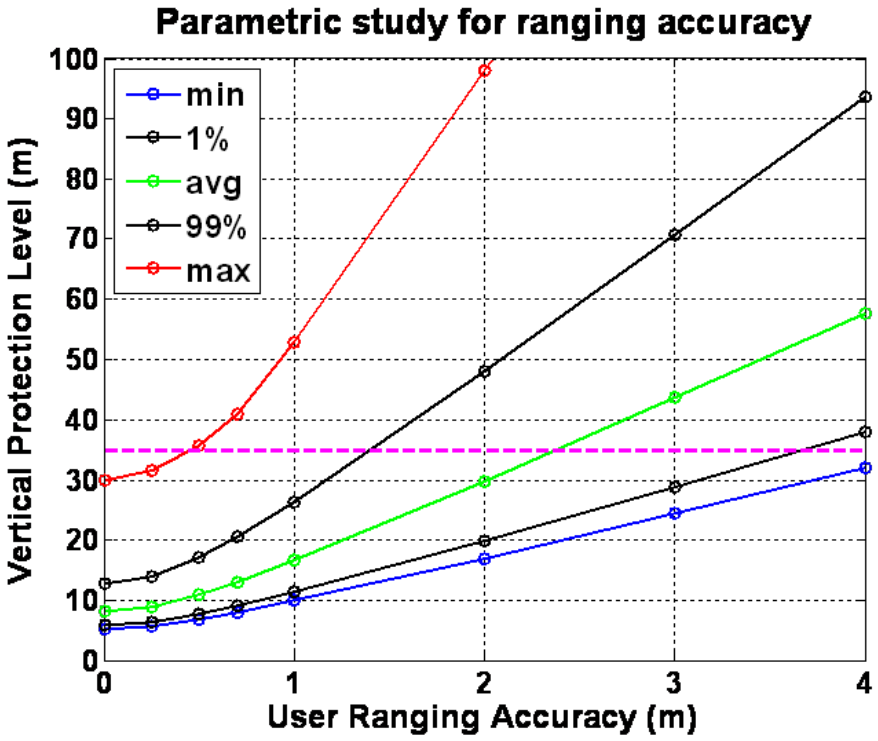

Figure 4.15.: Prediction VPL dependence on URA. The nominal bias is zero, and the satellite and constellation failure probabilities are fixed at 10^{-4} and 10^{-7}/ approach, respectively.

URA and bias values. Even with today's GPS signals, the measurement errors are most of the time lower than the nominal errors in the conservative model used here, so it is expected that the current simulation results will prove to be conservative when the MHSS algorithm will be validated with real data.

4.2.3. Conclusions from the parametric studies

The fact that the VPL was found to be quite insensitive to the chosen failure prior, and the conservative value used for this prior gives confidence that the current MHSS is a viable algorithm. The algorithm is tolerant to multiple simultaneous failures, and it makes it easy to account for a comprehensive threat space. Nonetheless, single or partial constellations do not seem to satisfy the precision approach requirements for availability, when 24 satellites or less are operational in the overall constellation. The prior probability of constellation failure plays a decisive role in

determining the availability figure for the degraded operation modes. With the use of RAIM, an unaided Galileo-GPS constellation can provide nominal VPLs of under 20 m, assuming a conservative threat space, and a URA of 1 m. As the magnitude of the measurement biases or range error variance is increased, the VPL values will degrade in a linear manner. Even in the presence of biases of up to 3.5 m on each LOS, the unaided performance of RAIM was found to be appropriate in order to meet the 35 m VAL requirement for LPV 200' aviation approaches, which is equivalent to the current performance available to WAAS users.

Part III.

Real Data Analysis

The second part of the work performed towards the completion of this dissertation involved the use of flight data for the purposes of verification and testing of the MHSS FDE algorithm. The intent of this effort was to complete the earlier investigation on what VPL values could be achieved with RAIM under realistic flight test conditions. The focus in the next two chapters will be on understanding what are the differences, if any, between the assumptions previously made while testing the performance of the MHSS algorithm in simulation under different scenarios, and the factors that influence the performance of unaided RAIM when actual GPS measurement data is being used.

The measurement sets used as part of this effort were taken in September 2006 during airport flight inspections at the Memphis, TN airport in the USA. The aircraft used was a Boeing 727, property of the United States FAA. The original purpose of the data collection effort was the testing of a LAAS prototype setup, as described in [33, sect. 10.4]. Data was collected with for both an Ashtech Z-Extreme and a NovAtel OEM4 receiver onboard the aircraft, as well as another NovAtel OEM4 receiver located on top of a hangar on the ground, used as reference. The purpose of analyzing the three distinct flight inspection data sets from Sept. 19–20, 2006 was not to compare the performance of the two airborne receivers, as in different circumstances or under a more comprehensive evaluation, each of the receivers could have performed differently. In order to avoid endorsing or criticizing the devices manufactured by one company or the other, the choice has been made to generically identify these receivers as Receiver 1 and Receiver 2 in the description of the data processing results. RINEX-format raw measurement files were provided through the Tech Center FTP site, as well as the processing results for the single-frequency *"truth"* differential GPS position solution, using available Wide Area Augmentation System (WAAS) corrections. The truth files were generated using the Waypoint GrafNav software, according to T. McHugh from the FAA Tech Center, who kindly made this data available to researchers at the MITRE corporation, Stanford University and Illinois Institute of Technology. The "truth" position estimate was used as reliable

measurement of the airplane trajectory during the test, and also as a reference against which independent in-house processing results of the same data were compared.

The overall purpose of this thesis work is to evaluate the performance of an unaided dual-frequency satellite constellation from a vertical integrity standpoint for aviation precision approach. Part III will summarize the steps taken in the unaided processing of the in-flight GPS measurements and obtaining a dual-frequency position solution. The main body of the ensuing discussion in Chapter 5 will be dedicated to understanding how the assumptions made about the size of the satellite ranging errors under nominal conditions compare to the observed errors. The accuracy of error modeling can be a determining factor on whether the RAIM algorithm produces protection levels that are realistic. When new GNSS signals become available in the future, additional studies will be able to use the method described here in conjunction with additional flight data sets in order to validate the error model. Subsequently, Chapter 6 describes how the VPL value will be determined at each point in time during the recorded flight, in the same way integrity monitoring results would be obtained in real time. By comparing the dual-frequency position solution to the "truth" reference, a relatively precise estimate of the Vertical Positioning Error (VPE) can be determined in order to assess how the error values compare with the protection level, guaranteed by the MHSS algorithm to bound the error with a probability of $(1 - 10^{-7})$.

5. Validation of the Range Error Model

Once an integrity algorithm has been designed (Chapter 3) and a range of assumed values for the external factors which affect RAIM performance have been tested in simulation, their operational domain has been determined through parametric studies (Chapter 4). The model for the residual range errors is the key piece left to be studied, before a conclusion can be drawn on the performance of MHSS RAIM. This chapter will describe how the actual distribution of the errors was studied. In order to do so, sets of real measurement data need to be processed in an identical way to that in which GNSS signals would be used inside the cockpit in order to determine both the aircraft position and the integrity error bounds associated with it. The method of processing dual-frequency GNSS signals in a way in which the ionospheric propagation error is eliminated will be described in Section 5.1. The next section will discuss the existing error model based on both theory and observations of the GPS L1 signal. Afterwards, Section 5.2 will discuss how these same errors are measured based on the flight inspection data, and then it will demonstrate what needs to be done in order to generalize the existing error model based on the new information. Finally, after a way to calibrate the error model has been described, Section 5.3 will briefly discuss the applicability of this method to new GNSS frequencies, taking the future GPS L5 and L2C signals as an example. A summary of the current results and the factors identified to influence the error level in RT measurements will then be discussed in Section 5.4, and conclusions will be drawn on how the developed error calibration method will be applicable to future GNSS signals.

5.1. Dual Frequency Positioning

5.1.1. L1 - L2 data processing method

The available GPS observation data includes the raw code and carrier pseudoranges for each of the two existing broadcast signals, in the L1 and L2 frequency bands. The greatest challenge during this process is that four different values of the distance between each satellite and the receiving user antenna (i.e. *user range measurements*) are available at every point in time, and these four measurements do not always agree closely. While the carrier ranges are affected by a relatively lower root-mean-square (rms) overall level of noise, they are also affected by an integer ambiguity in terms of the exact number of carrier cycles (i.e. wavelengths) included in the distance measurement. It is therefore advantageous to smooth the code pseudorange with the available carrier range measurements before using the ranging data to determine a position solution for the user.

However, the smoothing process can only take place over sections of the data in which the receiver is able to maintain a constant value of the aforementioned integer ambiguity. While that is the case, the receiver is said to be *tracking* the carrier, and in situations where the value of the integer ambiguity changes due to a data dropout or for any other cause, the receiver is said to have lost lock of the signal. When the latter happens a large jump in the value of the carrier range can occur upon the resuming of the signal tracking, such that the smoothing filter will have to be reset in order not to bias the code pseudorange measurements unaffected by a similar jump in value. It is thus essential for a positioning algorithm to point out those instances when the carrier observations are affected by errors stemming from the limited ability of the receiver to track the satellite signal at each of the two frequencies. These tracking errors, called *cycle slips*, can at times prove orders of magnitude larger than any other errors affecting the propagation of the satellite signals. Only the carrier measurements can be affected by the uncertainty in estimating the exact number of integer cycles included in the measured range at each frequency, and sudden changes in the integer

estimate can affect the two frequencies identically or in different amounts. A basic cycle slip detection algorithm designed to meet the needs of processing the current data sets will be described in section 5.1.2. The detection process was implemented for each of the carrier measurements at L1 and L2, such that the large biases caused by the slips can be later eliminated from all quantities which are derived from the carrier ranges.

As it proves out, aside from errors caused by the integer ambiguity, the largest source of disagreement between corresponding measurements at the L1 and L2 frequencies is the amount by which the Earth's ionosphere affects the propagation of each signal. The ionospheric effect amounts to an increase (delay) in the code pseudorange and an equal decrease (advance) in the carrier range. Section 5.1.3 will describe a procedure to remove the ionosphere propagation error by combining the range measurements at each of the L1 and L2 signals to yield an ionosphere-free range measurement. Subsequently, the resulting carrier ranges will be used for smoothing the corresponding iono-free code observations, as it will be described in section 5.1.4. Finally, section 5.1.5 will describe the process of transforming the resulting smoothed iono-free pseudoranges for each satellite into an estimate for the location of the user.

5.1.2. Description of the cycle slip detector

None of the four types of measurements mentioned above can be used as an absolute reference for the other three, given that they could each be affected by errors with significantly different magnitudes. Therefore, the most effective way to build cycle slip detection into the process is by comparing each carrier measurement with previously available historical values of itself. It is expected that normal range measurements exhibit a smooth continuous variation in time, due to the relative motion between the ranging source (in this case a GPS satellite) and the user receiver. Therefore, it will be assumed that the speed at which these range measurements vary should be practically constant over a short period of time and roughly equivalent to the dominating term in the relative velocity, which is the speed of the satellite motion

relative to a reference point on the Earth surface. Generally, this speed is considerably greater than any reasonable velocity of the user itself with respect to the ground, and it can be determined to be approximately 7200 knots based on knowledge of the satellite in-orbit dynamics.

The applicable navigation requirements for civil aviation receivers specify that the relevant dynamics during normal aircraft maneuvers do not exceed ground accelerations of 0.58 g (horizontal) and 0.5 g (vertical) at speeds of up to 800 kt, and maximum total jerks of 0.25 g/s. Here, g is the standard gravitational acceleration with a value of $9.8\,\mathrm{m/s^2}$. The same RTCA specifications document [86, sect. 2.1.2.5] also defines abnormal maneuvers as those cases in which the above values for the accelerations are exceeded, up to maximum accelerations of 2 g (horizontal) and 1.5 g (vertical), a maximum jerk of 0.74 g/s, while the maximum ground speed remains 800 kt. The slip detection algorithm presented here relies entirely on the apparent relative velocity and acceleration between the GNSS user and each satellite used as a ranging source, as deduced from the range measurements. Therefore, the acceleration limits specified by the operational requirements will constitute the cycle slip detection threshold of the receiver algorithm. Assuming the worst-possible alignment between the SV and airplane acceleration vectors, only the largest possible acceleration of the airplane along any spatial direction will be taken into consideration. The nominal acceleration of in-orbit satellites, by and large under the sole influence of the Earth's gravitational field, is equivalent to 0.06 g at the altitude of the GPS satellites' Medium-Earth Orbits (MEO). Given the above consideration, it can be concluded that a cycle slip detector needs to distinguish between artificial changes in the measured range due to imperfect RF wave tracking and the real dynamics of the aircraft-satellite system that produce maximal accelerations below $6.25\,\mathrm{m/s^2}$ during normal maneuvers and up to $20.16\,\mathrm{m/s^2}$ under abnormal operation circumstances.

The data analyzed in this work was recorded during airport flight inspection measurements [33]. Therefore, it is not expected that the airplane had to undergo any emergency maneuvers during the collection process. For reference, the trajectory of

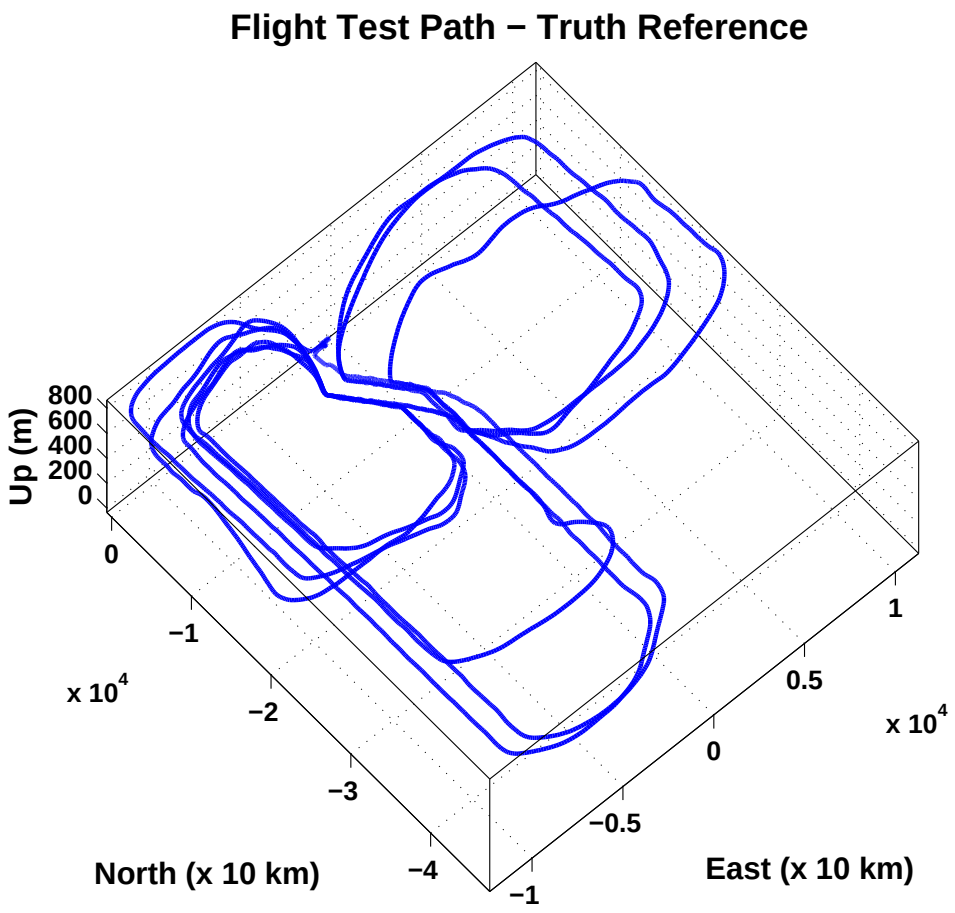

Figure 5.1.: Trajectory of the Memphis airport inspection flight on Sept. 19, 2006 in ENU coordinates.

aircraft motion relative to the ground for one of the flight tests used to collect data is provided in Figure 5.1. This flight took place at the Memphis airport between 17:35 and 19:55 UT on the 19th of September, 2006. The maximum flight altitude was less than 1000 m, as the test aircraft did a succession of takeoffs and landings. Rough estimations based on the available data confirm that nominal relative accelerations along the receiver–satellite line of sight (LOS) did not exceed $8\,\mathrm{m/s^2}$. For the purpose of cycle slip detection in the carrier range measurements, it was determined empirically that setting a threshold of $10\,\mathrm{m/s^2}$ could effectively help distinguish between natural satellite-user relative motion and errors introduced by sudden jumps in the

value of the integer ambiguity estimate at the receiver. Since there was a difference of a couple of orders of magnitude present between range variations caused by cycle slips as opposed to the natural motion of the positioning signal emitter and receiver, the use of an approximate threshold proves an effective method of detecting so-called cycle slips. Employing thresholds anywhere between $10\,\mathrm{m/s^2}$ and $25\,\mathrm{m/s^2}$ ended up yielding identical cycle slip results.

The detailed description of the cycle slip detection procedure for the purposes of flight inspection data processing is given below. Initially, the carrier range measurements are differentiated between each successive pair of 5 Hz measurements for the same satellite, in order to obtain the velocity and acceleration of the carrier range variation. The algorithm then checks the acceleration against the given threshold, while also comparing the slope of the range measurements with its previously observed values along the same LOS. A severe slip can extend across multiple recorded samples, while the receiver attempts to track the carrier frequency based on the wrong estimate of the integer number of cycles. Therefore, while an unusually steep range variation might signify the beginning or the end of the slip, all measurement samples with an out-of-range apparent relative velocity will be flagged as cycle slips. Likewise, when a cycle slip ends, although a high acceleration may be recorded once again, a nominal value of the velocity will cause this sample not to be flagged, indicating that the receiver returned to the normal continuous tracking of the positioning signal. The model for the types of cycle slips detected by this algorithm is depicted in Figure 5.2. The green data points represent nominal range measurements taken while the receiver is correctly tracking the signal, while the red points are samples affected by a cycle slip. It should be noted that, based on the real time observations available from the data sets, this model is a little bit more complex than a simple step bias "jump" between two intervals of continuous tracking. The cycle slips in this model represent a series of consecutive such "jumps" in the same direction, which cause an anomalously high acceleration in the range measurements. Consequently, the choice was made for the slip detector to not necessarily flag all points with an abnormally high range acceleration, but only those points for which the range slope also has abnormally

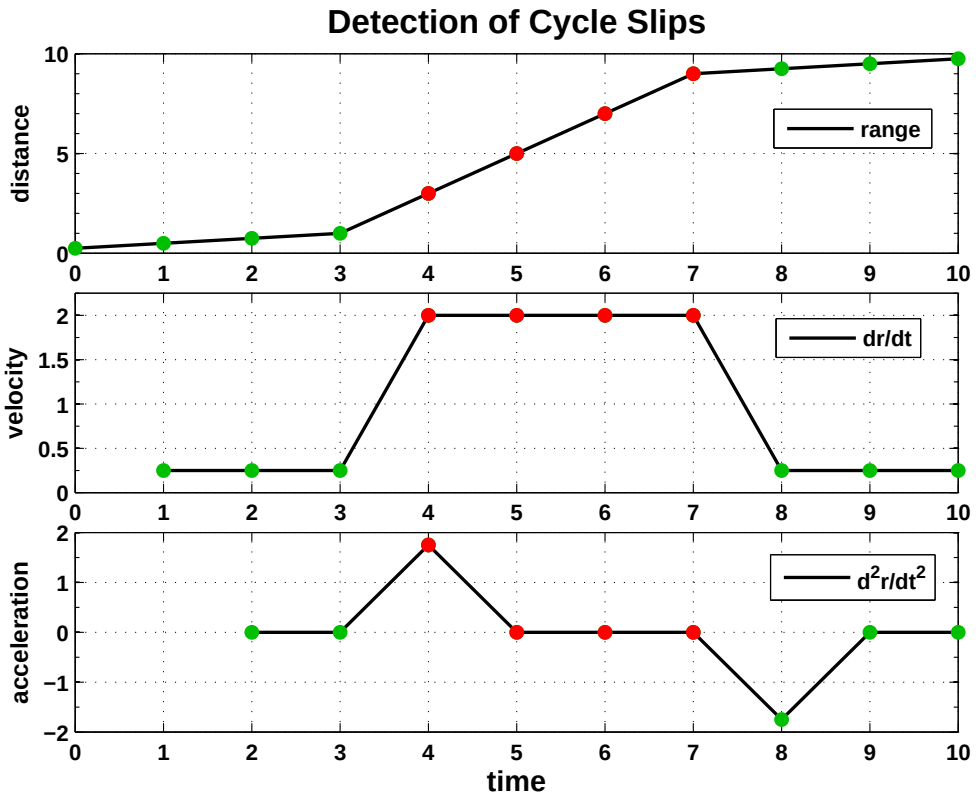

Figure 5.2.: Cycle slip threat model.

high values, as it can be seen in the middle plot. A high range acceleration only marks the beginning of the cycle slip (at t = 4), followed by a series of anomalously fast variations of the carrier range value (times 5 through 7), while the next high acceleration in the opposite direction actually marks the return to normal tracking (at t = 8) and will no longer be flagged as a slip. The procedure outlined here is one of the basic ways to search for cycle slips in the data, while implementing more complex algorithms [92, 48, 74, 72] currently employed by GNSS receiver manufacturers for high performance is beyond the scope of the current work.

Other slip detection methods chose different, usually more sophisticated approaches. For example, when a concern exists about either the space vehicle (SV) or user clocks experiencing sudden jumps, processing the difference between the L2 and L1 measurements might be the best option. This technique, would eliminate the clock errors by subtraction, while the ionospheric delays introduced in the process would typically be much slower in their variation, allowing the tradeoff between a fast and a

slow-varying error. However, in the case of the relatively short-duration data analyzed here, there was a greater concern that the differencing process would also eliminate cycle slips that are characterized by equal magnitude biases at each frequency, such that when the need arised to later perform carrier smoothing at each frequency, and not with the combined iono-free measurements, the earlier mentioned identical cycle slips would escape undetected and cause uncharacteristically large measurement errors for the user. Several options, such as comparing code and carrier measurements in the same frequency or examining the difference between the carrier measurements at different frequencies, have been attempted in processing these particular data sets, however they yielded unsatisfactory results due to the particularities of the given data.

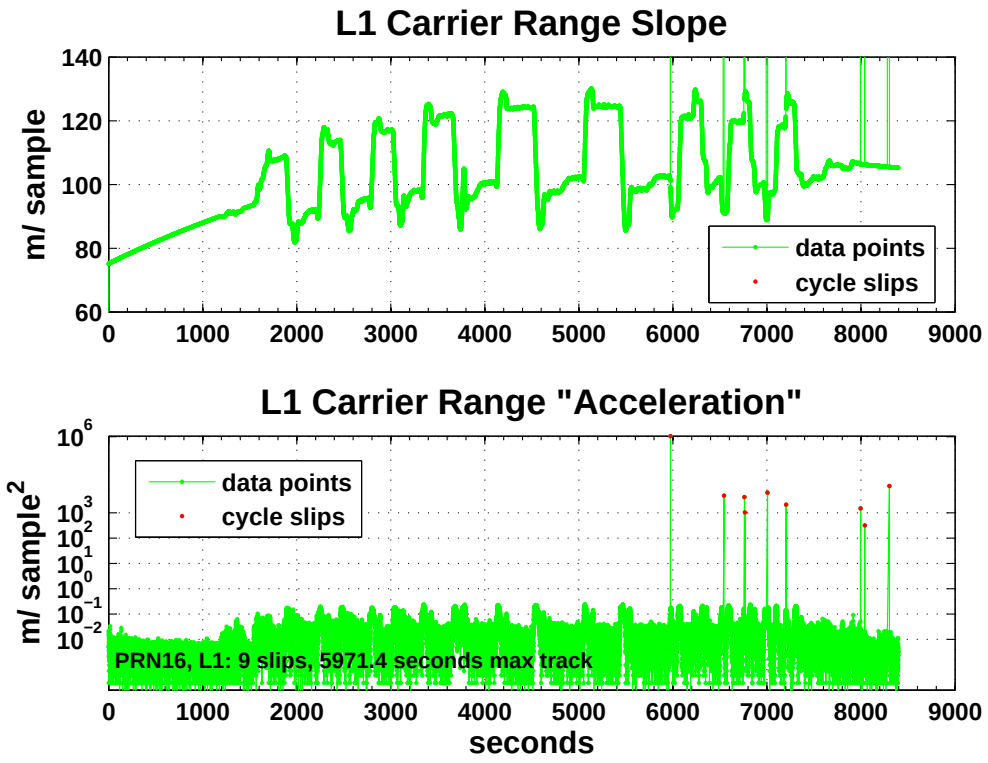

Figure 5.3.: Detection of cycle slips based on 1^{st} and 2^{nd} order differentiation of carrier range measurements.

Sample output of the cycle slip detection algorithm is shown in Figure 5.3 for PRN 16 observed with Receiver 2 on Sept. 19, 2006. The top plot illustrates the

variation in the carrier range between each pair of successive measurements, while the bottom logarithmic plot shows the difference between successive samples on the top plot — i.e. the apparent instantaneous acceleration of the relative motion between the user receiver and the GPS SV. In particular, each data set might contain several data dropouts. That means that consecutive samples are farther apart than a single sampling period, however the instantaneous velocity and acceleration will still be determined in the same manner, by dividing the difference in the range measurements in between consecutive samples by the actual time interval between the same measurements.

After a computer algorithm verifies signal tracking and automatically flags cycle slips, there is also the opportunity for the visual inspection of the results and manual flagging of rarer but more complex cycle slips, such as those formed by a succession of two slips in opposite directions. Given the limited size of the data sets, manual verification during post-processing is an option in order to validate the accuracy of the results. This is an important step in the process, since each carrier slip can introduce an arbitrary bias in the measurement for the entire next segment of continuous tracking. Once all slips have been accurately identified, these biases can be removed, and the different carrier tracking segments can be aligned relative to each other. However, an unambiguous value of the range measurement will subsequently remain available only from the code pseudorange.

5.1.3. Removal of ionospheric propagation errors

While the GPS Radio Frequency (RF) signals travel from the satellite to the user, the free electrons present in the ionosphere layer surrounding the Earth will affect the propagation of these electromagnetic waves as it will be detailed in section 5.3.1. An important property of the ionospheric effect is that the amount by which the velocity of the signals changes, relative to the light speed in vacuum, during the passage through the ionosphere is directly proportional to both the density of the free electrons, called Total Electron Content (TEC), and the inverse of the square of

the radio wave frequency. When range measurements are available at more than one frequency, this property allows an analytical solution for determining the magnitude of the ionospheric delay and its removal from the code pseudorange, as it was shown in [45]. From the L1 and L2 measurements, a value of the pseudorange corrected for the ionospheric delay can be obtained according to the following equation:

$$\rho_{\mathrm{IF}} = \frac{\gamma\rho_{\mathrm{L1}} - \rho_{\mathrm{L2}}}{\gamma - 1} \tag{5.1}$$

where γ is a coefficient dependent on the center frequencies of the L1 and L2 bands: $\gamma = (f_{L1}/f_{L2})^2$, and ρ_{L1} and ρ_{L2} represent the values of the two smoothed pseudoranges. According to [61, p. 166], the delay estimation process based on the L1 and L2 measurements trades the potentially large ionospheric propagation error for a smaller residual noise, with an rms value only 2–3 larger than that of raw single-frequency code measurements. Alternately, the amount by which the ionospheric propagation delays each signal can be calculated; for example, the iono delay at L1 will be computed according to the following formula:

$$I_{\mathrm{L1}} = \frac{\rho_{\mathrm{L2}} - \rho_{\mathrm{L1}}}{\gamma - 1} \tag{5.2}$$

For the carrier measurements, a similar iono-free combination can be formed, however it may contain large biases due to cycle slips in any of the two frequencies. The corresponding value of the carrier ionospheric error at each frequency can however be corrected up to a fixed bias term during post-processing, by removing the mean from each segment of continuous tracking in between a pair of cycle slips and subsequently aligning all the different tracks. Alternately, during carrier smoothing, the following processing step, only those values of the iono-free carrier range at times when no cycle slips have occurred will be used.

5.1.4. The carrier smoothing process

Carrier smoothing is the process of combining the code and carrier measurements to obtain a range value with less noise than the original pseudorange based on the coarse acquisition code. By comparing both the code and carrier range differences between consecutive sampling times, an attempt will be made to remove the higher magnitude noise in the code measurements. The smoothing algorithm will use the initial pseudorange measurement as a starting point and propagate that in time until a cycle slip is encountered, based on the less noisy carrier range. Then, at each cycle slip, the smoothing filter will be reset, such that the value of the code pseudorange immediately after the slip is again used, as its value remains much more stable through the process of signal reacquisition that will restore tracking. This simple smoothing algorithm is described in full detail by [60, sect. 4.7].

In addition to very sizable jumps in the raw carrier measurement for each satellite, cycle slips can also cause a temporary loss of lock in the receiver tracking loop, therefore causing smaller scale errors in the equivalent pseudocode-based range measurements. This introduces the additional need of monitoring for unusual variability in the code measurements, which is a problem that will also be addressed in conjunction with the carrier smoothing process. Any conspicuously erroneous variability will cause the removal from consideration of ranging measurements at those points in time, in order not to introduce unjustifiably large errors in the ensuing user position solution. Based on the high correlation between these large errors in the code measurements and the cycle slips detected in the equivalent carrier measurements, the decision was made to eliminate observations related to a particular satellite for a short amount of time following the detection of a cycle slip in the carrier measurements. This action is also in line with the aviation operational specifications [86, sect. 2.1.4.1.1], and the period of time with higher measurement errors will be proportional to the averaging constant of the smoothing filter that is used.

Larger ranging errors are generally observed in both the L1 and L2 bands as the receiver is trying to recover after each cycle slip and reacquire phase lock. In the

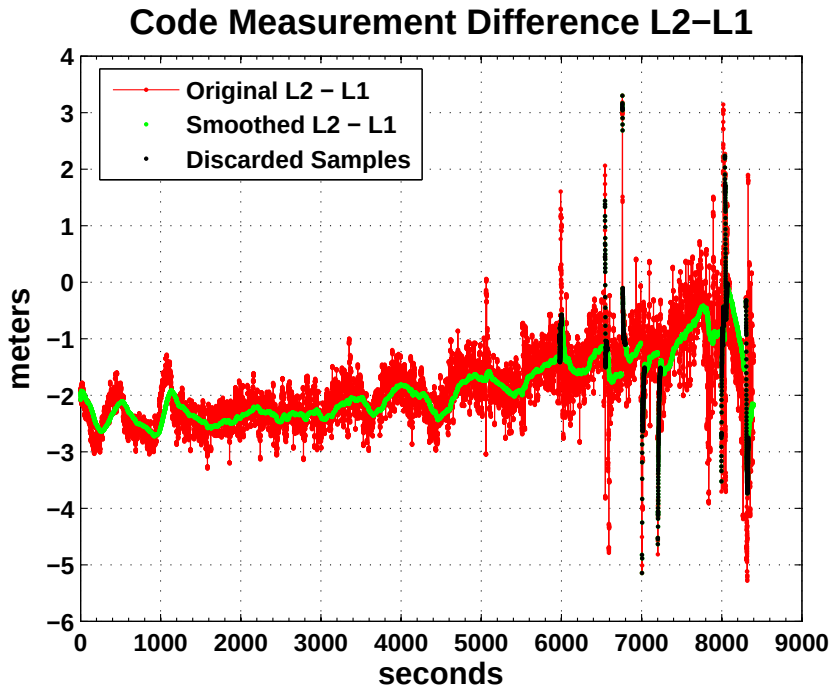

Figure 5.4.: Removal of cycle slip effects from the carrier smoothed L2 - L1 pseudorange difference.

meantime, the smoothing filter will also be in the process of settling to an equilibrium state. In order to avoid introducing additional ranging errors through the carrier smoothing process, the filter with a period of 100 s employed in this work is reset immediately after a detected slip, and the following $10\sqrt{10}$ s (≈30 s) of measurements are discarded. The value of the data blanking interval, close to 30 s, was empirically determined based solely on the currently available data sets. What the WAAS MOPS [85] recommends is an amount closer to 200 s of data being discarded on reacquiring a particular Pseudo-Random Noise (PRN) signal. While that recommendation should be implemented in practice for any automatic cycle slip detection algorithm, in the case of the current data processing effort, since slip detection was partially done by hand, a tradeoff was required to limit the amount of data being discarded from the limited amount of initially-available observations. Based on a statistically-oriented projection of the available results, it was determined that the settling time of the smoothing filter is proportional to the square root of the filter window [63], and such the optimum positioning results were obtained with the discarding interval mentioned

above. The effects of cycle slips on the carrier smoothing process are presented in Figure 5.4 for the PRN 16 satellite during the same set of observations. The difference between the measured pseudoranges at the L2 and L1 frequencies are displayed for ease of scaling.

It is important to mention here that this PhD dissertation is not attempting to establish an optimal way for processing dual-frequency data or for doing slip detection and carrier smoothing. It is recommended that the interested readers implement their own smoothing and cycle slip elimination methods, designed to optimize the performance for their particular application, before applying the MHSS algorithm which makes the object of this thesis work. The purpose of designing a way for processing L1-L2 data as described in this chapter was solely that of validating a theoretical user pseudorange error model and later testing the performance of the RAIM algorithm itself in Chapter 6.

5.1.5. Weighted Least-Squares (WLS) position solution

The process of going between the raw GPS measurements and determining the user position solution starts with importing the information from the RINEX format ephemeris and observation files into MatLab. Cycle slip detection is employed first, and afterwards 100-second carrier smoothing of the code pseudoranges is performed, such that the higher amplitude noise level in the pseudocode measurements is attenuated. The L1 / L2 ionosphere-free pseudorange is then formed from the combination of the two single-frequency smoothed pseudoranges, according to equation (5.1). The processed measurement data is further decimated to match the sampling time of the given reference truth position, available at a 1 Hz rate.

The next step is to compute pseudorange corrections for the measurements according to the GPS Interface Specification document [2]. Ionospheric delays have already been removed through dual-frequency processing and the SV differential group delay ($\boldsymbol{T}_{GD}$) correction does not need to be applied for the case of multiple frequency measurements. Based on the available ephemeris information, values can be computed

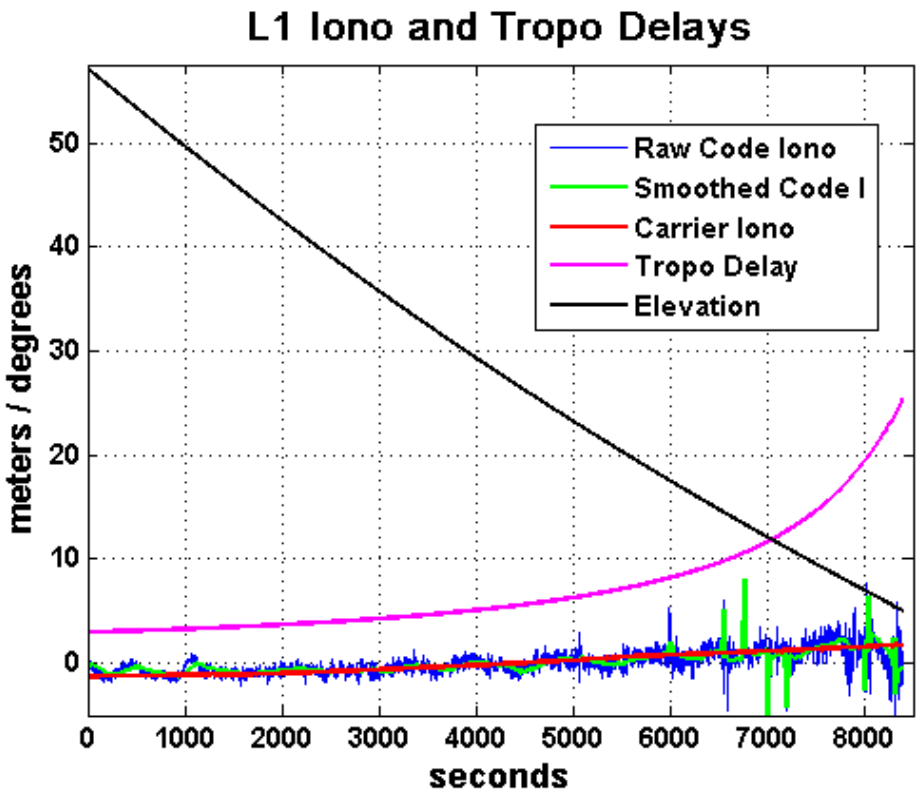

Figure 5.5.: Computed range corrections for atmospheric signal propagation delays.

for the satellite clock bias, as well as the tropospheric corrections, according to [2, sect. 20.3.3.3.3.1] and the GPS / WAAS MOPS [86, appendix A.4.2.4] respectively. Figure 5.5 illustrates the relationship between the elevation (in degrees) of the same PRN 16 and the magnitude of the applied tropo correction, as well as the ionospheric delay computed based on either the code (before or after the smoothing process) or the carrier measurements. Note that the mean of the ionosphere measurements, including unknown bias terms, was explicitly removed in this process, causing the iono delay values to have a zero mean.. Additionally, values of the "true" range between the user and each satellite, and a weighted average estimate of the user clock bias at each time epoch will be computed based on the available "truth" user location. The next section will describe how these latter two values will be used in order to make an accurate determination of the residual User Range Error (URE) due to error sources such as satellite clock and ephemeris, atmospheric propagation and multipath. As an aside, it is important to mention that any current tracking

loss problems with semicodeless L2 signal acquisition generating large range errors are expected to significantly diminish when independent pseudocode acquisition and tracking will be available at each different civilian broadcast frequency (e.g. L1, L2 and L5 for future modernized GPS signals).

Finally, a Weighted Least Squares (WLS) dual-frequency position solution will be computed for the flight inspection airplane, making it possible to estimate both the positioning and the ranging errors to each satellite in view at every instant during the data collection time frame. The only significant differences from the standard single-frequency positioning algorithm come from the use of a iono-free pseudorange estimate and the reduction of $\boldsymbol{T}_{GD}$ in the process. The WLS positioning algorithm is presented in detail in [60, ch. 5], and is based on linearizing the measurement equations to obtained an estimate of the navigation error is a similar manner to that described by equations (3.6) and (3.15) in Chapter 3. The iterative LS algorithm will stop after a few steps, when the difference between the position estimate in the last iteration and the new estimate from the current iteration becomes smaller than a given tolerance. The tolerance threshold was set to a value which is small for all practical purposes, in the current case being on the order of $1\,\mu$m.

5.2. Adjusting the User Pseudorange Error Model

5.2.1. Overview of theoretical error model

Previous literature seems to be much in agreement on a theoretical way to describe errors at the user. For that reason, a standardized error model (also used by [53, 85]), was considered appropriate, with only minor modifications made at the suggestion of the FAA GPS Evolutionary Architecture Study (GEAS) Working Group. The nominal ranging error distribution consists of zero-mean noise, allowing a Gaussian overbound, and a small bias in each channel: $\nu_i = \varepsilon_i + b_i$. In this model, the nominal position error variance for satellite i is described by the equation (3.2).

The different components of ε in the error are modeled as normal distributions characterized by a zero mean and the standard deviations described below. The clock and ephemeris errors are assumed to be independent identically distributed (iid) normal variables (σ_{URA}) under nominal, healthy satellite conditions. Infrequently, clock and ephemeris errors can also affect an entire constellation, but this possibility is separately included in the threat model as constellation failures. The tropospheric errors tend to be much smaller in relative magnitude compared to the other error terms, except for satellites visible at low elevation angles. The troposphere model used here (σ_{tropo}) matches the one in the WAAS MOPS [86, appendix A.4.2.5] and is assumed to be bounded by the same confidence level. Receiver noise and multipath are bounded by the provided $\sigma_{iono-free}$ term, which is the equivalent of σ_{air} in [86, appendix J.2.4]. It should be noted that, like in GBAS and SBAS, receiver failure and excessive multipath terms, which can bring along a significant degree of correlation between ranging errors along multiple LOS, are not explicitly covered by the error model. As the aviation receiver is responsible for the mitigation of such user-specific error terms, RAIM offers some protection against these additional errors right at the user location, where no ground augmentation can.

Ionospheric delays are normally the major term contributing to the single-frequency pseudorange errors. However, the use of a dual-frequency receiver can eliminate these large correlated error terms based on the frequency dependence of ionospheric delays, as explained by Klobuchar [45]. Effectively, the use of dual frequency measurements replaces a dominant source of highly correlated ranging errors with practically independent error sources. In the same article, Klobuchar also discusses second order ionospheric effects and the phenomenon of ionospheric scintillation occurring at low latitudes. The higher order effects have a small enough magnitude, which does not mandate the introduction of an additional error source in the above variance equation. It has been determined that these higher order terms only affect the pseudoranges by an amount which is insignificant [45, pp. 491–493] in the context where the current MHSS algorithm computes the overall VPL itself up to a centimeter

level accuracy. An in-depth study of higher-order ionospheric errors on GPS positioning, both during nominal ionosphere periods and ionospheric storms, can be found in [19], while an analytic model for simulating scintillation errors does not exist at present. This latter type of atmospheric events, mostly at lower geographic latitudes, may cause unpredictable errors and are able to cause GNSS receivers to lose lock on all satellites in a certain solid angle of the sky. A more detailed discussion accompanied by simulation of these ionospheric effects and their role in diluting continuity is currently beyond the scope of this work.

Out of the three sigma terms, the first one depends exclusively on the operational performance of the GNSS space and ground monitoring components, more specifically on the satellite clocks and on how precise the broadcast orbital parameters are. Also, the positioning signal quality can be characterized by the magnitude of the signal deformation, a component of the nominal bias. Therefore, it is expected that these components of the ranging error are independent of the navigation system user, and that a ground system will be in place to monitor the satellite signals and ensure that they comply with the minimum operational specifications guaranteed to all users. As such, the goal of the current model validation effort will be to measure and characterize the remaining components of the error, which are outside of the control of the GNSS operators, and which need to be monitored either by the users themselves or by the operators of the airspace system. In 5.2.2, the $\sigma_{tropo} + \sigma_{iono-free}$ zero-mean noise component of the error ε will be separated and characterized. In conclusion, a RAIM system is good for detecting and possibly correcting independent measurement errors specific to each user, but a monitoring / augmentation system can be useful for broadcasting corrections for correlated errors and fault modes common to multiple users.

5.2.2. Extracting residual errors from pseudorange measurements

In the process of computing the dual-frequency user position, the residual pseudorange errors described by the above model can also be measured directly. Although a very general conclusion cannot be drawn based on several hours of measurement data at a single airport, a sanity check can definitely be completed in the interest of making sure that the error model is on the conservative side. This way, abnormal events that may occur during more extensive testing will be expected to push the errors closer to the envelope, but not radically change the assumptions behind the model, which is already based on an extensive history of single-frequency measurements. The parallel availability of WAAS-processed "truth" measurements for these flight inspection runs is the key factor that allows the comparison between single and double-frequency positioning errors, and also between augmented and autonomous GNSS signals.

The final value for the ranging error to each satellite will be obtained according to:

$$\varepsilon = \rho - r - I - T + B - b \tag{5.3}$$

Here, ρ represents the initial single-frequency carrier-smoothed pseudorange, r is the geometric distance between the "truth" user position and the satellite position according to the ephemeris information, I and T represent the iono and tropospheric delay corrections, while B and b are the estimated satellite and user clock biases respectively. It should be mentioned that while the remainder of the terms in the above expression are frequency-independent, either L1 or L2 values can be used for ρ and I above, since:

$$\rho_{\mathrm{IF}} = \rho_{\mathrm{L1}} - I_{\mathrm{L1}} = \rho_{\mathrm{L2}} - I_{\mathrm{L2}} \tag{5.4}$$

where I is the iono delay based on the code measurements. As such, this approach effectively generates residual errors for the iono-free combination. The residual noise

levels at each frequency will also be examined separately in section 5.3.1, in order to understand their individual contributions and then calibrate the overall dual-frequency error model appropriately.

The WLS weighting matrix will be the inverse of the covariance matrix for the ranging errors, assuming these errors can be approximated as normally distributed and uncorrelated. Consequently, the covariance matrix will be diagonal, with the elements corresponding to the expected variance for the error along each line of sight between the user and a given satellite. The initial model for this variance was agreed upon in FAA GEAS Panel meetings [32], and assumes a User Range Accuracy (URA) standard deviation of 1 m and no ranging biases:

$$\sigma^2 = \sigma^2_{URA} + \sigma^2_{tropo} + \sigma^2_{iono-free} \tag{5.5}$$

In the above equation, σ^2_{URA} represents the variance of the range component of the signal-in-space (SIS) clock and ephemeris error, σ^2_{tropo} is the assumed variance of the tropospheric range error after the corresponding tropospheric correction has been applied, and $\sigma^2_{iono-free}$ is the assumed variance of the ionosphere-free combination of the L1 and L2 measurements, representing a weighted combination of the σ^2_{air} terms at the two frequencies. In turn, σ^2_{air} is the sum of the assumed variances for the multipath error and the rms background Gaussian noise in the receiver. The above error model was adapted based on an earlier model used at the MITRE Corporation [53].

In order to compare the ranging errors observed during the flight test data collection with the magnitude of the errors expected according to the model used in previous simulation studies, a post-processing statistic of the measured errors was assembled. At first, the ranging error time history was analyzed for each different satellite and a first-order fit of the data was performed. Based on this linear fit over the entire observation period for each PRN, the clock and ephemeris errors for the respective satellite were estimated and then removed from the overall range error, ε. The top plot of Figure 5.6 exemplifies the linear fit for approximating the

URA component of the ranging error, related to the satellite clock and ephemeris for PRN 16, this time observed by Receiver 1 during the second data collection session on Sept. 20, 2006. At the same time, the bottom plot depicts the estimated value for the clock bias of Receiver 1 flying onboard the aircraft, which has already been subtracted from the range measurement after the application of the corrections in Fig. 5.5, according to equation (5.3). The results were then combined across all satellites and allocated into bins of the satellite elevation ranging between 0° (horizon) and 90° (zenith). The standard deviation of the remainder of the error and its mean, representing a small residual bias, were subsequently computed and compared to the root-square-sum (rss) of the 2^{nd} and 3^{rd} terms in equation (5.5), which are also dependent on elevation. A mask angle of 5° was employed in this analysis, such that satellites below that elevation did not contribute to the final position solution. The statistics of realized errors in the available data sets exhibited a near-Gaussian

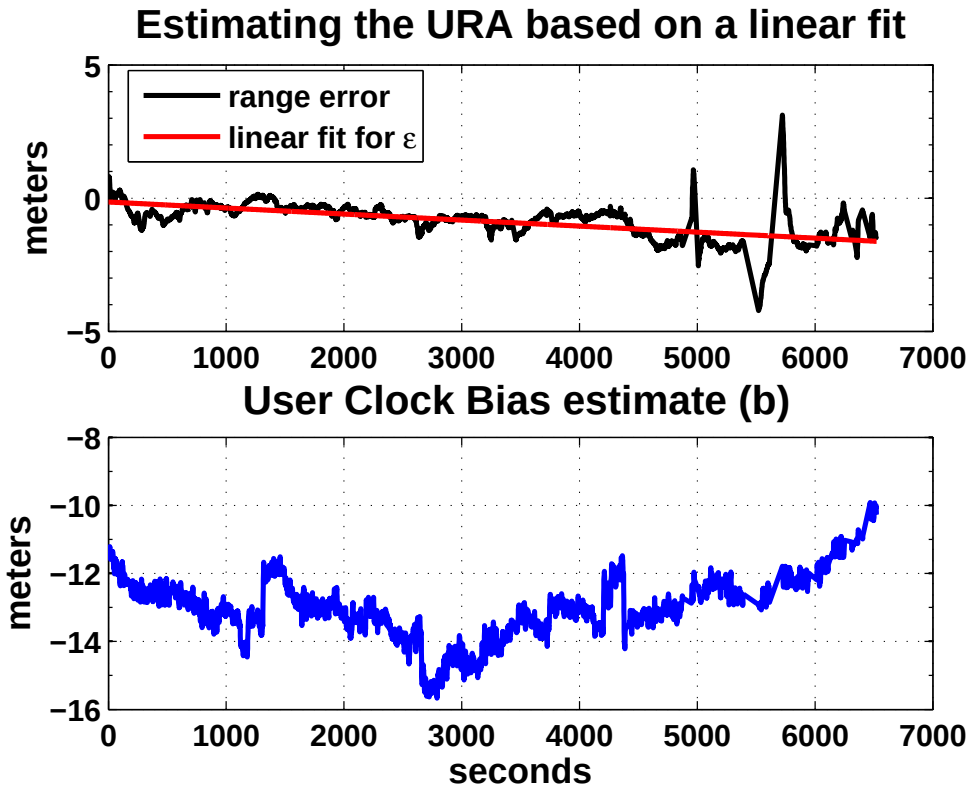

Figure 5.6.: Estimation of URA (ephemeris and satellite clock errors) and user clock drifts.

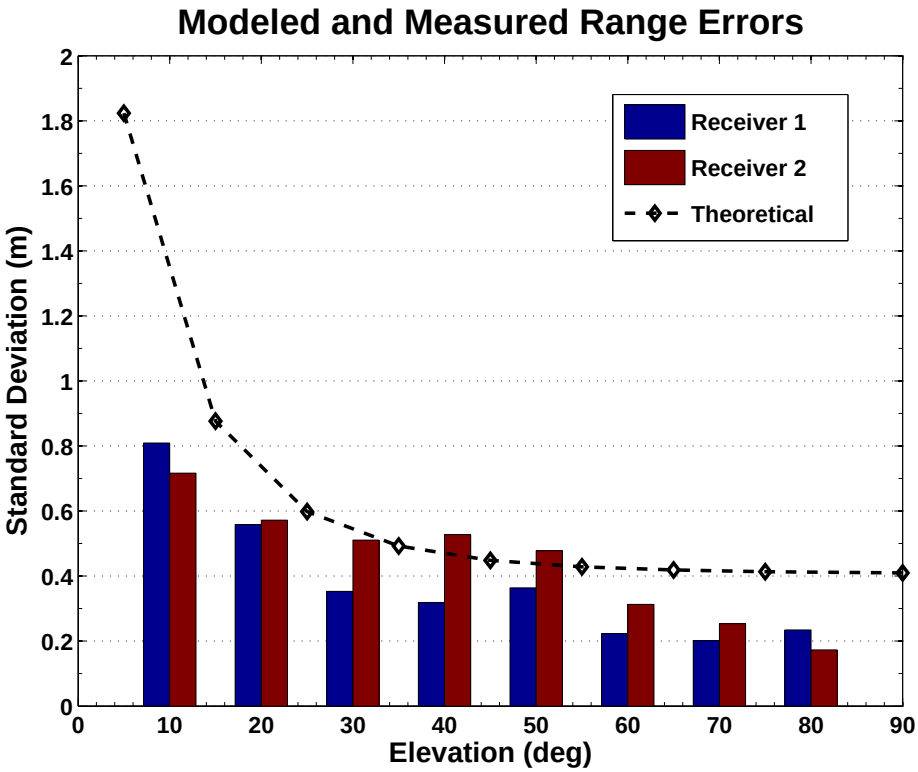

Figure 5.7.: Graphical comparison between the theoretical error model in [32], excluding the URA, and the residual errors measured by the two receivers.

behavior, with a slightly higher amount of probability located in the tails of the distribution and small nominal levels of bias at the centimeter level.

In the end, the WLS error residuals were used to also compute predicted error bounds for the airplane user, according to the MHSS RAIM algorithm developed in Part II. Although it is something not usually required during the course of dual-frequency data processing, a divergence-free difference between the code pseudorange and the carrier range will be taken at each of the two frequencies, L1 and L2 (see section 5.3.1). This is useful for precisely determining the values of the residual noise in each frequency band. Except for the ionospheric propagation of the signal, all other error sources affect the code and carrier measurements identically. However, the goal of the error model validation effort is to compare only the level of remaining noise between the two frequencies, after all the standard corrections have been applied to the measurements. The remainder noise is thus compared with the standard deviation

of the theoretical model for the Gaussian component of the error. If the data is split into bins based on the elevation angle of the ranging sources in the sky, the error distributions in Figure 5.7 are observed, which are not always overbounded by the predictions of the existing L1 error model.

5.3. Calibration of the Error Model

In case the residual errors are computed not for the iono-free pseudorange as described above, but separately for each signal frequency band, it can be observed that there are significant differences in magnitude between L1 and L2 error levels. While the theoretical model initially assumed that the L1 errors will generally be greater or approximately equal to errors at other frequency bands, it proves that for semicodeless acquisition of the L2 signal, the range residual errors can be up to 5 times larger than the corresponding measurement noise at L1. This discovery accounts for the majority of the difference between error prediction and the available real-data measurements. Section 5.3.1 below will describe how the ranging errors can be computed at each frequency, while still using a second frequency for aiding with the elimination of ionospheric propagation errors. Afterwards, a way to re-calibrate the error model and to ensure it is a conservative overbound of the observations will be detailed in section 5.3.2.

5.3.1. Residual noise at the L1 and L2 frequencies

Radiomagnetic waves propagating through dispersive media (such as Earth's ionosphere) will have different group and phase velocities. While the group velocity represents the speed of travel of the energy or information contained in the signal, the carrier envelope will travel at the phase velocity. The particular effect of this physical phenomenon on modulated RF waves is that the data contained in the signal propagates at a different velocity than the carrier waves themselves. The effect of the ionosphere on GNSS signals crossing it is that it delays the positioning codes,

while advancing in time the carrier, relative to the time it would take the signal to arrive at the receiver in the absence of the ionospheric dispersion. The net effect is that a delay correction needs to be made on the code pseudorange, and an equal advance correction needs to be made on the carrier range in order to reduce the user positioning errors. Therefore, the phenomenon is called code-carrier divergence in satellite navigation technical terms. As the residual errors are calculated for the purposes of model validation, the size of this divergence is estimated based on the less noisy ionospheric propagation error affecting the carrier measurements.

The error terms are thus computed at each frequency based on the following equation, expressing ε as the difference between the raw code pseudorange, the carrier range and twice the ionospheric advance measured for the carrier waves:

$$\varepsilon = \rho - (\phi + 2I_{\phi}) \tag{5.6}$$

The amount of residual measurement bias cannot be estimated as well in this process, as the carrier range already contains an unknown level of bias, as discussed above. Instead, the DC bias is eliminated form the measurements of ε at each frequency and subsequently the zero-mean noise levels at the two frequencies are compared to each other, as proposed in [29]. Figure 5.8 illustrates the sigmas for the statistical distributions of ε for each frequency, divided into 5° elevation bins. A slight elevation dependence of the residual noise can be observed, especially for the semicodeless acquisition in the L2 band. Additionally, the data points on the right represent the average standard deviation across all bins.

5.3.2. Adjusting the weights for the L1 and L2 errors in the model

The theoretical error model was designed based on extensive measurements of the GPS signals at the L1 frequency. The calibration suggested here implies leaving the L1 component of the modeled error unchanged, while adjusting the L2 component

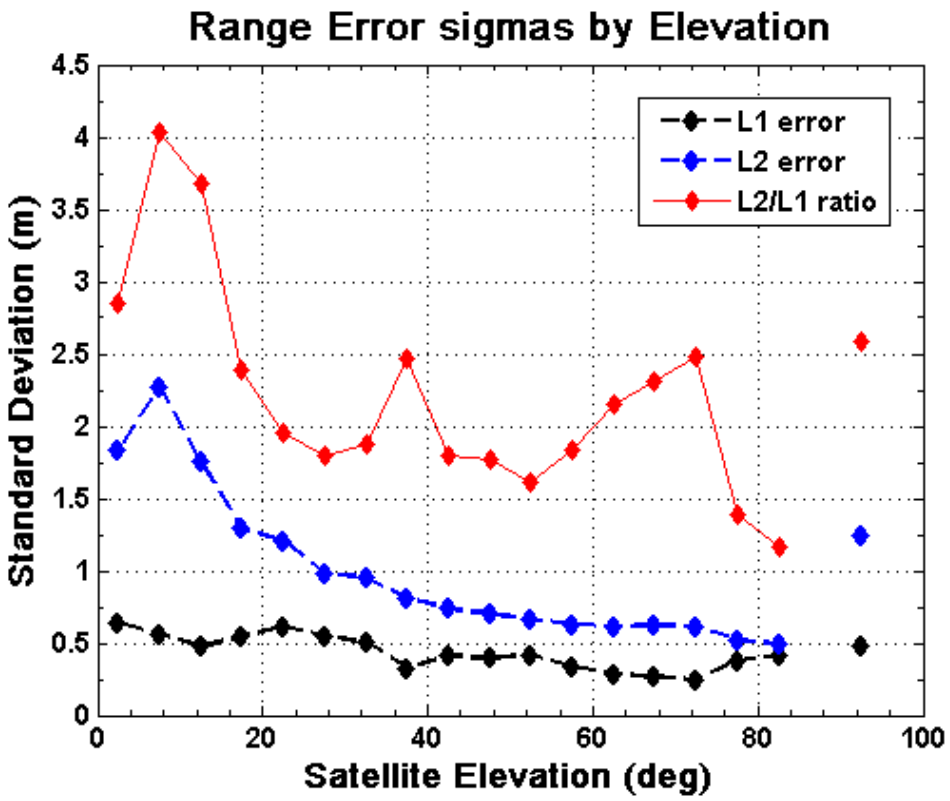

Figure 5.8.: Dependence of standard deviations for residual ranging errors given by equation (5.6) on satellite elevation and signal frequency band.

by a factor which reflects the observed difference between the noise levels for the two signals. As it can be observed from Figure 5.8, the noise ratio at the two frequencies varies based on the satellite elevation, as noise levels tend to be lower and closer to each other at higher elevations.

One way to pick the calibration factor is to choose the average ratio of the noise sigmas (i.e. standard deviations). This procedure is *de facto* equivalent to computing the ratio of the overall sigmas for the L1 and L2 noise, regardless of elevation. In this case, the adjusted error model would bound the overall error on the whole, but not uniformly across elevation bins. Furthermore, by using the average ratio, the insight is lost on the relationship between the noise level and satellite elevation outlined above. Therefore, a second way to determine the calibration factor has been selected. By choosing the maximum sigma ratio among those at each elevation bin, it will be possible to leave a safety margin at all elevations and assure an additional amount

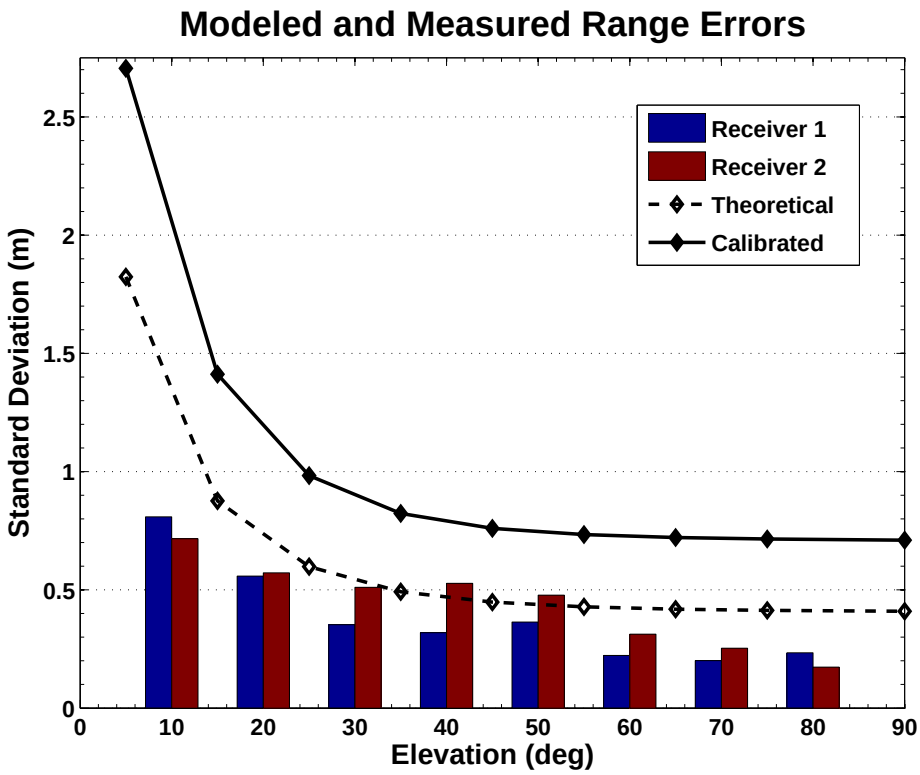

Figure 5.9.: Calibration of error model to compensate for larger L2 residual noise levels.

of conservatism. This better fits the purpose of the calibration process, since the validated model will cover a broad array of situations, from flight at altitude to near landings at any possible airport. Therefore, this model has to be conservative in overbounding errors given the limited amount of real measurements employed in the calibration process. Figure 5.9 illustrates the change in the error standard deviation predicted by the error model as a consequence of the above adjustment for the L2 semicodeless component of the error.

The calibration method proposed here will also be applicable for adapting this error model to future new GNSS signals. One thing that is expected to be different from the case of current GPS signals is that higher chipping rates and increased signal power are expected to make noise levels lower for the new GNSS signals, quite the opposite from the current situation at the L2 frequency. Thus, applying the current calibration method will allow making the error model less conservative under those

circumstances. According to an independent estimation made by van Dierendonck [21], the noise levels for the modernized L2 and L5 signals are expected to be at least 2–3 times lower than is the case for the current L1 signal. However, given the current semicodeless acquisition techniques for the L2 signals, the results presented here are very much in agreement to the aforementioned independent predictions for the residual L2 noise levels.

5.4. Results and Discussion

Due to the fact that more than half of the satellites visible in each data set were either rising or setting and 6 or less of the satellites reach elevations of 45° or higher during each of the approximately 100–150 min flight inspection sessions, the available measurements contain a relatively high number of cycle slips. Data points at which measurements at one of the two frequencies are unavailable have been automatically removed from consideration, as no iono-free position solution could be computed in these cases. Thus, the remaining measurements contain a matching number of cycle slips at both frequencies, to a large extent. A summary of the cycle slips affecting Receiver 1, as well as statistics on the periods of continuous tracking have been provided in Table 5.1. This sample summary is based on the three data collection runs, and represents the cycle slips detected by Receiver 1 in both the L1 and L2 bands simultaneously. The values for the total period that the satellite is in view (Tot Visible), the longest period of continuous tracking (Max Cont Track), and the average length of a continuous track (Avg Track) are also provided in seconds. The 2–3 PRNs with the shortest average track lengths, which are the most affected by cycle slips, correspond to the satellites that never rise above the 5° mask angle during the observation period.

The cycle slips are a consequence of receiver loss of carrier lock, an event especially common at elevations below 15°, when the atmospheric attenuation of the GPS signal is the strongest and signal power is also weak due to the specific

PRN	# Slips	Tot Visible (s)	Max Cont Track (s)	Avg Track (s)
1	75	13380.4	10016	171.5
3	24	21110.6	8311	781.9
6	108	7258.2	651.6	65.4
7	144	21806.4	5955.4	148.3
8	68	10696.6	2935.6	150.7
10	97	1910.8	212.8	19.1
11	195	8723.4	1212.4	44.1
13	24	20152.4	8311	746.4
14	42	6531	2364	145.1
15	39	660.8	71	15.7
16	104	24755	10016	231.4
19	51	17640.8	8311	326.7
20	64	17528	10016	261.6
22	55	1826	1243.4	31.5
23	0	24758.2	9685.2	8252.7
25	44	17958.4	10016	382.1
27	12	16911.2	8311	1127.4
28	55	7386.2	1554.6	127.3
30	43	3441	2019	74.8

Table 5.1.: Statistics of detected cycle slips for Receiver 1 across all data sets.

gain patterns of the antennas installed aboard the aircraft. Increased amounts of multipath reflections also cause cycle slips at low elevation angles. With a single active constellation for measurements, it is difficult to have more high-elevation satellites in sight providing high-quality ranging to the user. Despite this shortcoming, it was possible to remove most of the ranging error relying solely on the GPS Interface Specification document [1] and on available models for error estimation and correction. Even in the absence of precise SBAS corrections, it was possible to obtain 3D position solutions mostly within 10 m of the true user location.

More specifically, the position errors are computed here as the difference between the dual frequency WLS position solution developed in Section 5.1 and the reference position solution provided by the FAA Tech Center alongside with the raw data. This latter "truth" aircraft position was derived by automatic processing of the GPS flight data and the corresponding differential WAAS corrections with the Waypoint GrafNav software package. The resulting relative accuracy of the dual-frequency

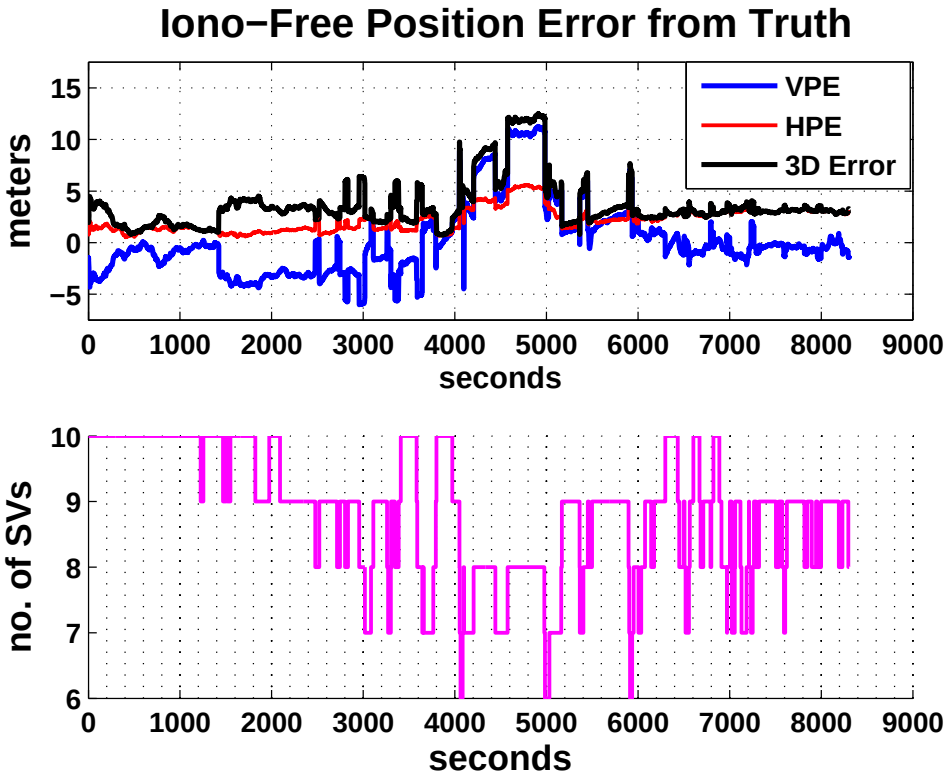

Figure 5.10.: The influence of the number of available satellites on the dual-frequency GPS position error relative to the true user location.

position solution derived as part of the current thesis work is visibly sensitive to the number of satellites used for positioning estimation, such that errors tend to get above 10 m only when the number of ranging sources distributed across the sky drops to 8 SVs or less. The Position Error values in the vertical (VPE) and horizontal (HPE) directions, as well as the overall position errors are displayed in the top plot of Figure 5.10, in correlation to the plot of the total number of satellites included in the position solution on the bottom.

It is expected that the use of more realistic parameters as part of the theoretical error model will allow maintaining the highest possible standards of safety for the user. The error model assumptions that are most likely to explain the observed discrepancy are the URE mean and variance, which are based on previous measurements at L1, and the multipath model which might prove to be very different at near-landing and in the high altitude airborne environment. Significant differences exist between

observations of nominal noise levels in the L1 band for carrier-aided code tracking and the actual noise level for the L2 semicodeless acquisition that was employed in the current data set in order to enable dual frequency measurements. Nevertheless, possible reasons for the differences between the error levels predicted by the original model and the observations could go beyond the fact that a partially encrypted signal at the L2 frequency is employed in this data set. Higher than expected levels of noise could result from the setup and operation of the data collection equipment, or if the theoretical model used was devised based on different assumptions about the aviation receiver, not applicable to the measurement in this flight inspection test.

Once modernized GPS signals (i.e. L1C, L2C and L5) are available on all active satellites, the user error levels are expected to be lower than in L1 today. Thus, it is not desirable to devise an over-conservative theoretical model based solely on the types of errors observed in L1 / L2 positioning in this experiment. The calibration procedure developed in this chapter will yield a theoretical model which will be only moderately conservative with respect to future GPS performance, leading in turn to a minimal degradation of performance (i.e. VPL inflation) due to conservatism in modeling errors.

6. Verification of the Algorithm with Real Data

Once a full-fledged version of the MHSS algorithm is in place, and several dual frequency data sets were used to fine-tune the residual error model, the stage is set for running the first actual tests of this RAIM method under in-flight aircraft conditions. This final step of the algorithm development process comes to validate all the previous steps, as well as to confirm the setup and the expected results of the real-time use of multi-constellation RAIM in the cockpit. The calibrated error model as well as the integrity guarantee of the RAIM algorithm will be put to a test not only by the use of actual flight data, but also under corner cases, such as the insertion of errors that will simulate the use of real data in the presence of faulty satellites.

Section 6.1 will describe how the MHSS algorithm presented earlier was adapted to handle GPS data available in post-processing or real-time (RT), as opposed to the measurement residuals simulated earlier on. Subsequently, both the prediction and fault detection algorithms will be employed in conjunction with the available flight data sets. In Section 6.2, a discussion will ensue on the type of measurement faults which have been observed to infrequently appear in GNSS range measurements. It is extremely unlikely to capture these types of faults during a scheduled flight inspection data collection session, as they are not expected to last more than a total of 1–3 hours on the average per year. However, the safety risk they potentially introduce is far greater than the acceptable limit for civil aviation. Therefore, test cases were devised in order to reproduce a developing range measurement fault and demonstrate

that the present algorithm continues to fulfill its mission even in less than ideal conditions. The performance under fault conditions is described in Section 6.3 for both cases, whether the fault is detectable or not by ARAIM in the airplane cockpit. A summary of what lessons have been learned from the real data analysis will then be presented in Section 6.4.

6.1. Adapting MHSS for Processing Real Data

The MHSS RAIM algorithm used earlier in conjunction with the MatLab Algorithm Availability Simulation Tool (MAAST) in Chapter 4 allowed generating a set of random ranging error residuals for measurements made by virtual users distributed across the globe, based on a normal distribution with the standard deviation predicted by the error model. In the meantime, a real-time user will obtain a different set of information, very similar to what an airport flight inspection run has to offer. This data is collected for a single user who no longer remains at a fixed geographic location. Additionally, the measured residuals are the realized values of the modeled errors under the specific circumstances of the in-flight test aircraft. The slight differences from the information available to RAIM in the previous simulation scenarios have the effect of increasing the influence of the satellite geometry on the outcome of the algorithm in a real data setting. Whether a satellite is present or not in the final position solution makes a difference not only on the position estimate and the size of the error bound, but also on the values of the error residuals. In order to account for that, every time a subset of the visible satellites is considered by MHSS, a separate position estimate has to be computed for that particular set of range measurements. When working with real data, the values of the residuals change when switching between subsets in a deterministic manner, and it can no longer be assumed that they are random or that they remain steady throughout the satellite elimination process. Therefore, a rigorous RAIM algorithm has to be adapted to account for that aspect when it is designed to work with RT data, and it will need to effectively compute multiple WLS position solutions for each measurement time step.

6.1.1. Results with Real-Time and Prediction MHSS

Some differences in performance were observed when applying MHSS to real L1 / L2 GPS data, compared to the results previously recorded in simulation. These differences are due in part to the higher noise level in the actual measurements versus the simulation, and also due to the number of available ranging sources, the variation in the number of satellites used for positioning from one point in time to the other, and due to the distribution of these Space Vehicles (SVs) across the sky. Although the current GPS constellation has more active SVs than the minimum of 24 operational satellites, their orbital configuration is optimized for only 24 SV slots and any additional satellites were deployed as doubles in slots already occupied by an older SV nearing its decommissioning. This aspect will make the real life satellite geometry slightly different from what was assumed in simulation, but the GPS satellites in excess of 24 are not expected to significantly impact RAIM performance. The observed performance is expected to be very close to the single-constellation 24-satellite GPS simulation results, but inferior to an optimized constellation with 27 or 30 SVs, or a multiple constellation. Figure 6.1 shows both the Vertical Position Error (VPE) incurred by the dual-frequency signal user, as well as the VPL computed by the MHSS algorithm as the error bound with the required probability (see equations 3.32, 3.30). The realized vertical is computed as the difference between the dual-frequency position solution based on the raw measurements and the FAA-processed "truth" position, which was obtained by applying WAAS corrections not available to the MHSS RAIM algorithm.

The presented RT VPL is based on measurements with Receiver 1 during the first of the two data collection runs on Sept. 20, 2006. The top plot illustrates how, depending on the available satellite geometry, the vertical error bounds fall either below or above the 35 m VAL considered to be the performance target of the algorithm. The reader shall be reminded here that the research in this dissertation is very forward-looking, and that the observed percentage availability is expected to greatly improve, to the vicinity of 100% worldwide, when both modernized GPS and

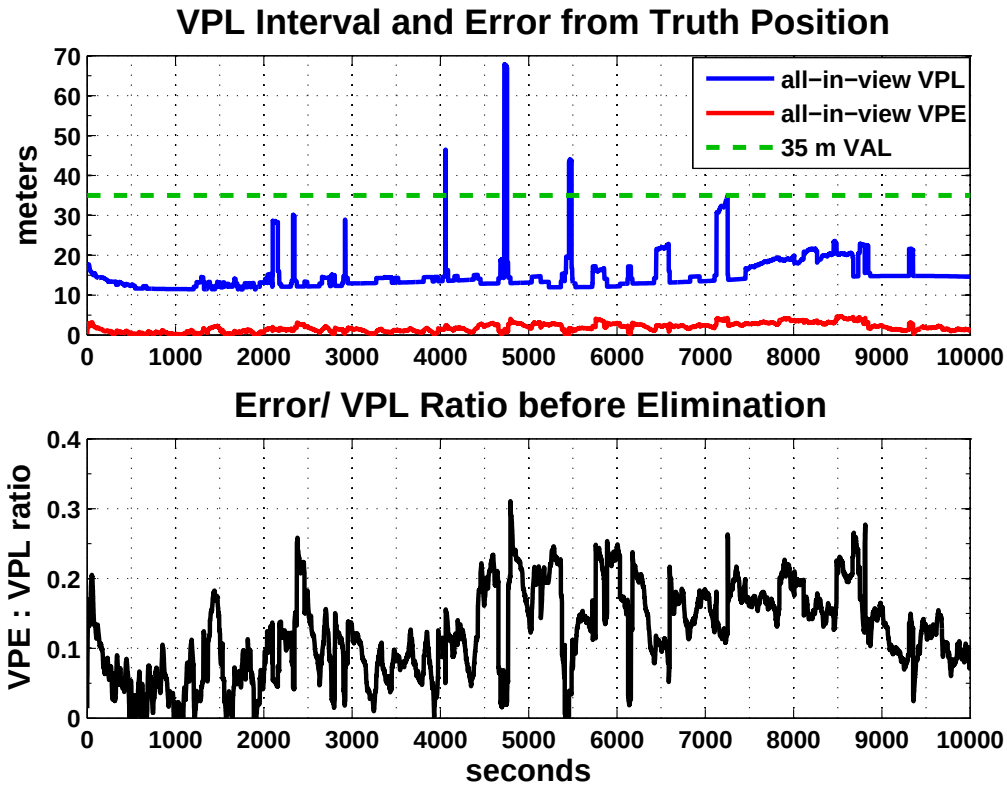

Figure 6.1.: MHSS Real-Time VPL and VPE results.

Galileo constellations will be fully operational with a total of 50–60 SVs broadcasting multiple frequency civilian signals. In the meantime, the current testing of the algorithm with flight data serves the purpose of merely checking the soundness of the underlying theoretical framework for MHSS RAIM. At all times, the blue VPL curve allows for a sizable safety margin of 5–10 m or more from the absolute value of the measured error displayed in red. The bottom plot represents another way to measure this distance between the actual error and the VPL, by taking the ratio of the two. As long as the values of the VPL hover in the $[0, 2{\cdot}\mathrm{VAL}]$ interval (viz. below 70 m), this is an effective way to point out the extent of this safety margin. However, if VPE values were much larger, a similar error bound with a 5–10 m safety margin would cause the VPE / VPL ratio to be much closer to 1, signaling that a potentially dangerous condition exists for the aircraft while the RAIM algorithm would still meet its required integrity. Only a supra-unitary value of the above ratio is indicative of an integrity fault, due to the failure of the RAIM algorithm to properly bound the error.

The performance specifications limit the probability of such Hazardous Misleading Information (HMI) being passed to the airplane pilot to 10^{-7} or less.

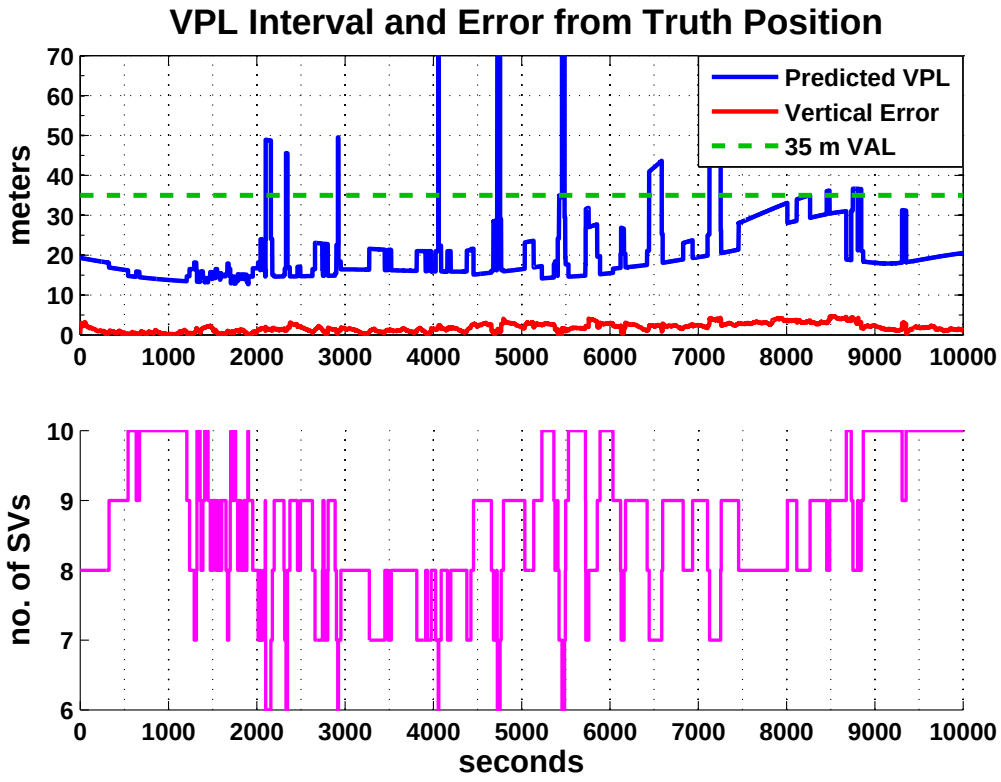

Figure 6.2.: MHSS prediction VPL and VPE results.

The predicted VPL values (see equations 3.32, 3.39) as well as the number of satellites used for positioning for the same data set are exhibited in Figure 6.2. By relating the two plots, it can be confirmed that a very close correlation exists between the number of satellites employed and the quality of the position estimate. Given the already existing relative scarcity of ranging sources due to the use of only a 24-SV optimized GNSS constellation, cases when as little as 6 or 7 satellites are included in the position solution solution can be observed. These circumstances, when not a lot of redundancy is present in the overall SV geometry, correspond to visibly larger and more conservative error bounds, even in the presence of relatively unchanged levels of vertical error. The predicted VPL values are also slightly larger than the ones based on the RT measurements, as they have been slightly inflated in order to insure the probability of loss of continuity for the aviation user is less than the

$4 \cdot 10^{-6}$ specified by the performance requirements. The only measure that made it possible to compensate for the absence of range measurement information is a slight improvement in the prediction VPL obtained by making optimal integrity allocations to fault modes.

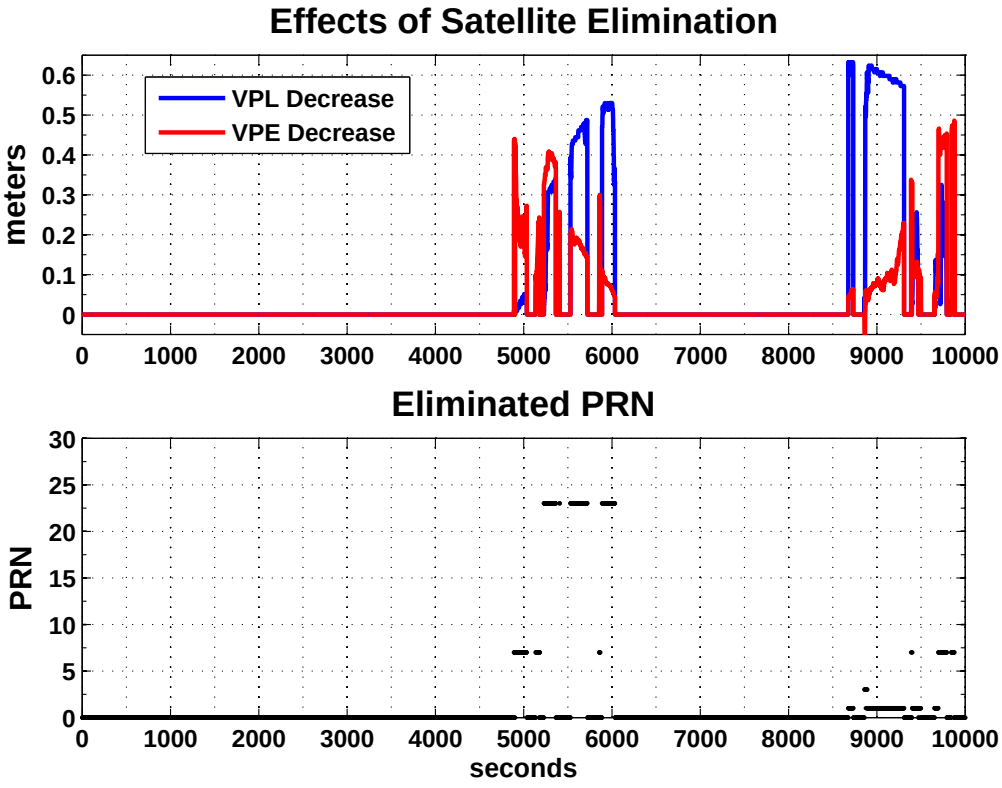

Figure 6.3.: Effects of MHSS FDE on VPL and VPE results.

6.1.2. Effect of employing FDE in the absence of faults

When the fault detection process is employed within the RAIM algorithm (see section 3.3.2), even under nominal measurement conditions, a slight improvement in performance may be available at times to the airplane pilot. Although no dramatic changes are expected to occur in the absence of considerable measurement faults, it can be seen from Figure 6.3 that by selectively eliminating one of the satellites from consideration, up to a half-meter decrease in the positioning error and a decrease in the VPL of over 0.6 m can be achieved during this particular data set. The FDE

algorithm is intently designed to minimize the VPL values, as this is the only performance metric used by the aircraft pilot to determine the forecasted safety for the desired operation regime. The comparison within the cockpit of the VPL value with the appropriate value of the VAL for the intended operation is the process through which a determination is made whether it is safe to proceed or not. The 35 m VAL level pictured in the earlier figures represents the corresponding limit on the VPE for LPV 200 GPS Landing System (GLS) approaches. While the FDE algorithm intentionally minimizes the VPL in order to optimize the performance available for guiding the aircraft, there is not always a direct correspondence between the magnitude of the PE and the size of the PL, as it can also be observed from the Figures 6.1 and 6.2. Although in most cases when a satellite is eliminated in order to decrease the VPL, the VPE also decreases accordingly, this is not a general rule. Different algorithms can be employed in order to guarantee that the PE is minimized and not the PL, but the caveat of this approach would be that the airborne user cannot always take advantage of the reduction in the overall error, if the associated VPL remains steady in the process or even increases during VPE minimization.

6.2. Inserting Faults

In the previous section, the performance of the MHSS algorithm while processing real GPS data has been demonstrated under nominal conditions, both in prediction mode, as well as during RT operation. The question remains however on how to validate the performance of RAIM under detectable satellite fault conditions. Consequently, the current section will be looking into the type of faults that are likely to affect GNSS signals. To better understand what types of faults occur in reality, an overview on the history of GPS faults and outages since the Selective Availability (SA) intentional degradation of civilian signals has been turned off in May 2000 will be provided in 6.2.1. These anomalies have been observed either by the FAA Tech Center in their mission to monitor the navigation signals used by civil

aviation within the National Airspace System (NAS), or on special occasions by independent observers across the globe. Subsequently, 6.2.2 will describe the test cases devised to replicate the effect of such faults within the already available flight data sets, and Section 6.3 will describe how the current MHSS FDE algorithm behaves when such faults are present. As additional redundant RT range measurements are available to ensure protection even against undetected faults, 6.3.1 will illustrate the substantive performance of the RAIM algorithm when presented with these test cases. The closing arguments in 6.3.2 will reflect over the comparison between the expected performance in the presence of faults and the actual behavior of the algorithm. Furthermore, Section 6.4 will contain a summary of the lessons learned here as well as thoughts for the future, when MHSS FDE will be used to monitor the broadcast of a multi-constellation GNSS.

6.2.1. Summary of historically-observed faults

In order to understand the historical aspect of the occurrence of GPS faults, GPS Performance Analysis (PAN) reports prepared by the FAA William J. Hughes Technical Center (Tech Center) [34] have been consulted. These reports have been issued quarterly since 1993, when the FAA began monitoring and analyzing GPS Standard Positioning Service (SPS) performance data, collected at National Satellite Test Bed (NSTB) sites and later also at WAAS reference station locations. The reports are public information, which comes to complement measurements made by the Navstar GPS Operations Center (OC), which is maintained by the US Department of Defense (DoD). The military operators of GPS do not always have the obligation to share the results of their observations with civilian authorities in the US or abroad, though they will make every effort to remedy any problems related to the health of the GPS constellation. While the GPS SVs and the OC will not compile fault probability information or provide monitoring of the performance of the GPS beyond the ranging accuracy for the benefit of the civilian users in the next 25 years, civilian

authorities who manage systems related to the Safety of Life (SOL) are also preoccupied by additional performance metrics, such as integrity and availability, which were described in Chapter 2. Therefore, once the prospect of using GPS signals for civil aviation navigation became reality, so did the need for additional monitoring of the GPS signals. The task of performing this mission fell on to the aviation oversight authority. The stated goal of documenting observation results in regular PAN reports is that "GPS performance as well as specific causes for service outages be monitored and understood".

Although they provide more information than the Notice Advisory to Navstar Users (NANU) messages from the GPS OC, the PAN reports contain only breviary information on the standard monitoring metrics, usually insufficient for a more detailed investigation on the type of GPS measurement faults that occurred over time and their causes. Although faults of any magnitude are relevant for the integrity calculation under the MHSS RAIM algorithm, only those events for which the ranging error exceeds 30 m are detailed as a Problem Report in Appendix C of each PAN document [34]. As no other known comprehensive and regular reports of problems with the GPS performance have been compiled to date, it is not possible at this time to conduct a parallel and independent review of the history of past GPS faults. Thus, the official statistics provided by the FAA Tech Center will be considered as the only reliable source of historical information used for the purposes of this work.

There are two types of relevant events affecting the GPS constellation which are documented in the PAN reports: outages and failures. A satellite *outage* is an event during which a specific SV is either temporarily turned off or set to broadcast a signal identifiable by the user receiver as a "DO NOT USE" signal. Such a signal is considered as unreliable and will be excluded by certified aviation receivers from the computation of a position estimate. The reported outages are of two types: scheduled and unscheduled. The *scheduled* outages refer generally to maintenance and other SV maneuvers during which the GPS OC needs to temporarily set a satellite unusable. These events are announced to GPS users 72 hours in advance by the means of NANU

messages, while *unscheduled* outages refer to all other instances when the OC has to set a SV to unusable while only issuing a related NANU after the fact. In contrast, a satellite *failure* refers to the situation when a SV continues to broadcast an apparently healthy signal which, nevertheless, causes users to experience abnormal range measurement biases or errors [46]. When a failure is detected and announced to the OC, steps will be taken to correct the problem and the corresponding SV will likely be set to "DO NOT USE". However, no NANU message will be issued regarding the period of time when the faulty signal was being broadcast as healthy, and only a summary description of the incident will be provided at the end of the corresponding PAN report when the range error caused by the failure was measured to exceed 30 m by one of the monitoring stations employed by the Tech Center. When a SV reaches the end of its useful life, it is then permanently turned off and marked as decommissioned. The Pseudo-Random Noise (PRN) code formerly broadcast by decommissioned satellites will be made available for re-allocation to a newer, healthy satellite, since each SV is capable of broadcasting any of the PRN Gold codes described in the system specifications [2]. Albeit every satellite tends to broadcast a single PRN code during its entire lifetime, which was allocated to it when it was first placed on orbit. As such, the correspondence between SV and PRN numbers does not change over time except for decommissioning and new launch events.

The Standard Positioning Service (SPS) described by the PAN reports [34] compares the GPS performance with a metric based on 3 service failures per year, lasting no more than 6 hours each. However, after discussion with the FAA and after debate on the GPS Evolutionary Architecture Study (GEAS) panel, it was established that a RAIM algorithm could claim credit for a historical fault rate of 10^{-4}/ user / approach [58, 53]. This figure was arrived upon by considering the frequency and duration of past SV failures, and means that a given navigation user of the GPS has a chance of 1:10,000 of experiencing a satellite fault during any period of time equivalent to that of an aviation approach, defined to be 150 s in length. The terms *failure* and *fault* are used interchangeably throughout this document.

In order to have a clearer understanding on how the failure probability number relates to the aviation requirements and the test cases designed to validate the performance of the MHSS algorithm, the following considerations are made. Given the approximately $3 \cdot 10^7$ seconds in a year, one can look at the failure rate as the average number of seconds a satellite fault is present during a given year. Therefore, an important consideration in determining the overall fault likelihood is the amount of time ground control needs to detect and remove such a fault, by flagging the satellite as "unhealthy". If the number of distinct faults over the course of a year remained constant on the average, the failure probability would then be directly proportional with the interval between the fault onset and its removal by the ground monitoring center. It is thus evident that, with expected improvements due to a more automated system called the Operational Control Segment (OCX) and scheduled to arrive along with the modernized GPS III, the standard performance guarantee will improve. It is anticipated [32] that an average failure will probably last an order of magnitude less than the current 6 hours mentioned in the PAN reports, although no such assurance is being written into the Performance Specification [3].

Finally, in estimating a realistic value for present and future GNSS measurement fault rates, one has to keep in mind that while an average of 10–12 unscheduled outages per year have been mentioned between the PAN reports and other independent observations over the past 8 years, only on 24 different occasions corresponding range measurements indicated User Range Error (URE) values of tens of meters or greater that can be associated with a failure event [36]. Hence, it is important to make the distinction between a fault, defined here as an event causing range error values to significantly deviate from a Gaussian distribution, and a scheduled or unscheduled outage, when a satellite merely becomes unavailable. In the latter instance, the measurement geometry and the corresponding Dilution of Precision (DOP) values will be affected, but the potential measurement errors for the range to the satellite in question will not be passed onto the user.

In agreement with the GEAS Panel, it was considered that, for both current GPS and future modernized GNSS constellations, the failure rate is not likely to exceed a value of $1.4{\cdot}10^{-5}$ / SV / hr [32]. As a satellite failure is conservatively expected to persist for an average of 1 hour after its initial onset, the value of the corresponding fault rate would be identical on a *per approach* basis and a *per hour* basis. Also, if a user with simultaneous access to signals from 10 different SVs is considered, and the satellites are assumed to fail independently from one another, the previous *per SV* fault rate would become equivalent to a $1.4{\cdot}10^{-4}$ / *user* / 150 s rate. Based on the stated assumptions, this rate is only slightly more conservative than the historical rate quoted above. While the MHSS algorithm uses a base failure rate per satellite per approach for all its probabilistic calculations, one of the parametric studies in Chapter 4 examines dependence of the performance of this RAIM algorithm on this particular assumption. Unless specifically mentioned, no failures were introduced in the test measurements employed in this thesis. Nonetheless, the MHSS algorithm always assumes failures could be present and computes position solutions based on partial subsets of the SVs in view, in order to guarantee that a fault-free solution is always included in the VPL.

The most common type of historical GPS SV failures were faults recorded in conjunction with unscheduled outages caused by satellite clock runoffs, according to a study of the errors reported by the FAA Tech Center over the past 10 years. These events occur naturally when the atomic clock onboard a given satellite is getting close to the end of its operational life. The faults manifest themselves in the time domain as ramp errors in the pseudoranges for the affected satellites. Additionally, the most severe SV faults were observed due to operational errors, e.g. when a satellite was not set to unhealthy during a routine orbit maneuver. This type of error similarly manifests itself as a ramp-like anomaly, increasing in time after the initial onset. Figure 6.4 displays a report of observations made during one such incident. On April 10, 2007, the PRN18 signal was not set unhealthy during an orbit adjustment, resulting in a ramp-type range error with a slope overbound of 10 cm/s for about two hours. The plot of the URE for the corresponding satellite is shown here by courtesy of

Figure credit: Prof. B. Pervan, IIT

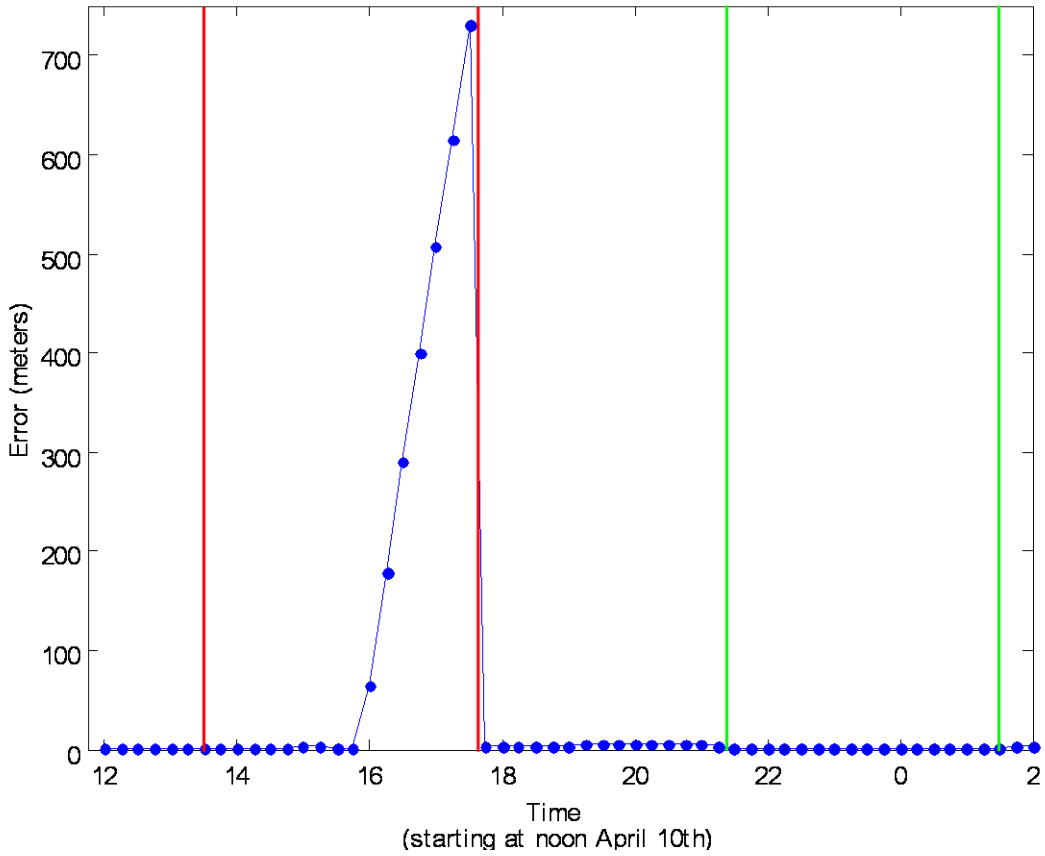

Figure 6.4.: Observations of Apr 10, 2007 fault on PRN 18.

Prof. Boris Pervan from the Illinois Institute of Technology, who reported the findings to the FAA. The first red vertical bar represents the beginning of the maintenance outage as announced by NANU 2007053 on April 6, 2007, and the red vertical bar on the right marks the time point when the satellite was actually set to unhealthy. The green vertical line on the left represents the time when the same satellite signal was again set as healthy, compared to the initially planned time for the termination of the maintenance window, marked by the second green line. Maintenance orbit maneuvers started and the boosters were fired on the satellite shortly before 1600 ZULU on Apr. 10, 2007, causing the actual SV position to diverge significantly from the broadcast ephemeris position. This induced ranging errors that ended up exceeding 700 m for the observer collecting the data presented in the figure. As a result of this incident, the GPS OC took corrective action to prevent future recurrence.

6.2.2. Description of artificially inserted faults

In order to test the capabilities of the MHSS FDE RAIM algorithm, ramp ranging errors were inserted into the recorded flight inspection data. Successive tests were performed, with the slope of the introduced error gradually increasing from $\pm 1\,\mathrm{cm/s}$ to $\pm 1\,\mathrm{m/s}$. These values were chosen to be an order of magnitude on either side of the ramp slope for the real error presented in Figure 6.4. The challenge for the MHSS FDE algorithm actually presented itself for the cases of smaller magnitude errors, which are more difficult to distinguish from the nominal measurement noise defined by the previously described error models. The intention of the current work was to study both the onset and the further development of such a fault. As such, the first few hundred seconds in the original data sets were preserved as initially recorded, and gradually increasing errors were inserted in the later parts of the data. In this manner an entire family of observation sets containing faults of varying severity was generated based on the three original data sets provided by the Tech Center. As a consequence of the fact that larger errors are more rapidly identified by the FDE algorithm, the onset for the ramp-like errors with a higher slope was established later in the data set. While $1\,\mathrm{cm/s}$ ramp errors were initiated $500\,\mathrm{s}$ into the data, the outset of $1\,\mathrm{m/s}$ failure ramps was scheduled as late as $1500\,\mathrm{s}$ after the initial sample.

Figures 6.5 and 6.6 represent an example of the range errors for PRN 16 before and after the fault insertion. Figure 6.5 displays the values of the ranging error residuals as measured by Receiver 1 for the September 19, 2006 data set. These residuals represent the remaining amount of error obtained after the code-carrier smoothing process and after corrections were applied for the satellite clock bias and the atmospheric propagation of the signals, as described in Chapter 5, but before correcting for the user clock bias as well. This bias will be automatically estimated and removed from the position measurement by the recursive WLS algorithm. In Figure 6.6, the same residual error is pictured after the insertion of a ramp with slope of $5\,\mathrm{cm/s}$ starting with time $\mathrm{t} = 500\,\mathrm{s}$. For consistency purposes, all the simulated failure results presented below were generated by inserting the fault on the same

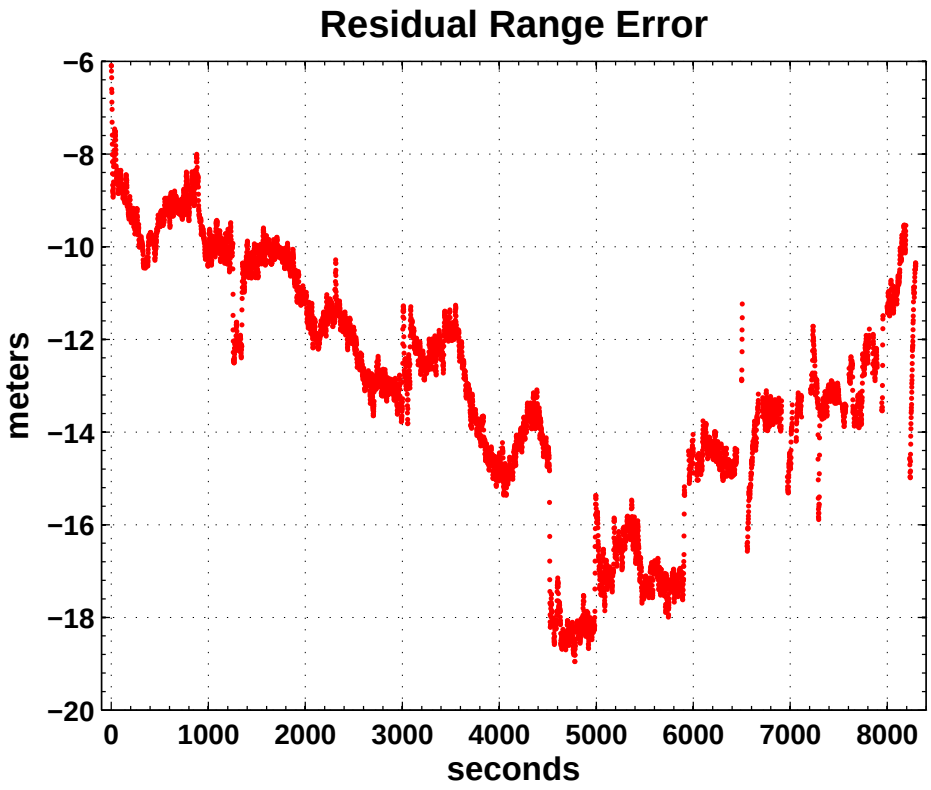

Figure 6.5.: Residual range error for PRN 16 on Sept. 19, 2006.

PRN 16, which was present in all of the collected flight data sets. Since the SV broadcasting the PRN 16 signal is visible at medium elevations and is above the mask angle for almost the entire duration of the three data sets, it can be assessed that it is a critical ranging source for navigation during all three airport inspection flights, and thus its failure would generate a severe scenario for the GNSS aviation user. The role and importance of the FDE algorithm in mitigating such situations can therefore be well understood from the study of the approximately 1.3 million sets of snapshot measurements generated in this error insertion process. Overall, a satellite geometry with 6 or less SVs visible above the 5° mask angle occurred only in about 1% of the cases.

The next selected example, presented in Figure 6.7, represents the effect of a −10 cm/s ramp error introduced in the measurements made by Receiver 1 during the first data collection session on Sept. 20, 2006. This particular example based on an intermediate ramp error slope will be followed through the rest of the current chapter

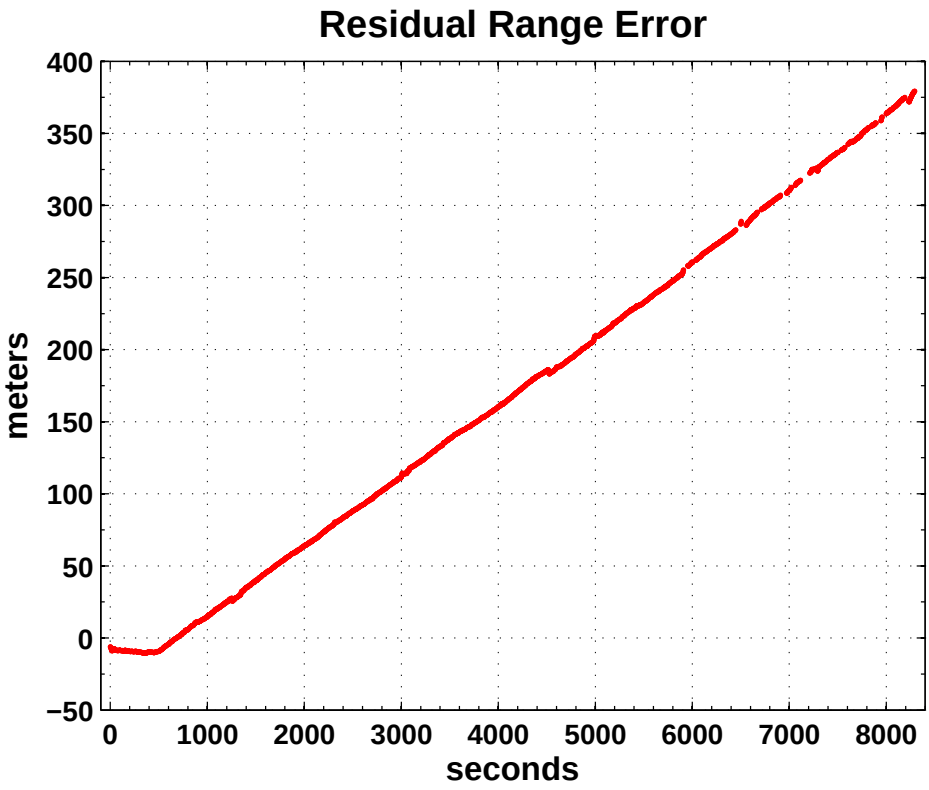

Figure 6.6.: Error on PRN 16 after insertion of 5 cm/s ramp.

in order to illustrate the results derived from employing the MHSS FDE method for an aviation receiver. Since a snapshot RAIM algorithm has been employed, error detection is performed solely based on the snapshot of current measurements at each time point. Therefore the response of the FDE algorithm for each time step to either pulse, step or ramp errors will be identical, and testing its performance against ramp errors will also be reflective of the performance in the presence of potential step or pulse errors of various magnitudes.

Figure 6.7, however, only reflects how a MHSS algorithm without the FDE capabilities enabled would behave in the presence of such errors. In the top part, the plots of the VPE and VPL are superposed onto each other, while in the bottom plot their ratio is pictured. In addition to the visible variations of the VPL also observed in Figure 6.1 caused by the changes in the number of satellites used in the position solution, an additional trend can be observed as the VPL values follow the increasing VPE, which they are supposed to overbound. While a safety margin of at least 4–5 m

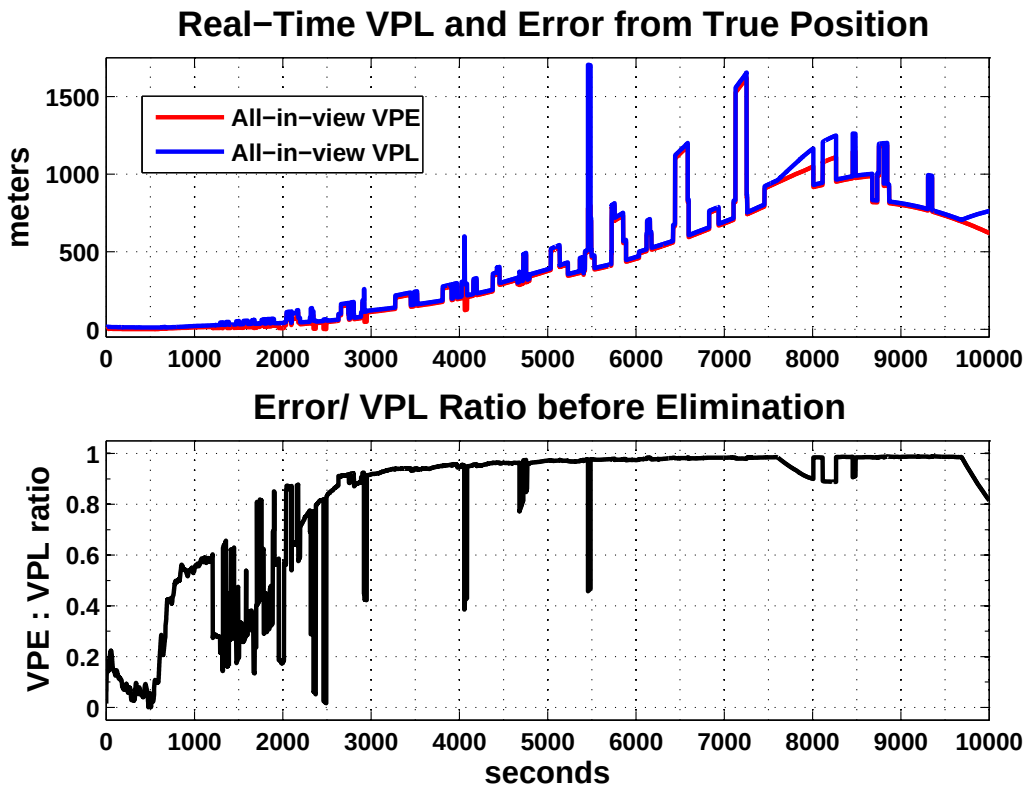

Figure 6.7.: Effect of inserted range error on the Vertical Position Error and Protection Level.

is continuously present between the VPL and the magnitude of the observed error, the VPL values grow in order to bound the error which gets to exceed 1,000 m. Hence, the ratio between the two reaches a value very close to 1, though it never exceeds that value. In conclusion, it can be said that even in the unlikely presence of 1 km of unannounced range error and in the absence of fault detection capabilities, the use of the MHSS algorithm does not result in HMI potentially being passed to the airborne user over the course of this data set. Nevertheless, the presence of such large VPL values would cause an availability loss for the GNSS-guided approaches, as these large error bounds make it unsafe for an aviator to proceed with landing at an airport. This is where the FDE method employed in conjunction with the RT MHSS algorithm becomes essential for allowing continuous operation of civil aviation applications, even during periods of time when failures affect the navigation signals.

6.3. Results with the FDE Algorithm

As mentioned in Chapter 2, there is a stringent FAA integrity requirement associated with LPV 200 type approaches, which a certified RAIM algorithm will need to satisfy:

$$\mathcal{P}\{\, HMI \,|\, geometry,\, error\, model \,\} \;\leq\; 10^{-7}/approach \tag{6.1}$$

Given an *a priori* $\mathcal{P}\{1\, SV\, failure\} = 1.4 \cdot 10^{-5}$ per approach for a single satellite failure, the $\mathcal{P}\{HMI \,|\, geometry,\, error\, model,\, 1\, failure\}$ for the simulated failure scenario described above should be at most around $0.7 \cdot 10^{-2}/\,150\,\mathrm{s}$. This equals the equivalent of no more than one instance of HMI for every test data set analyzed (of about 10^4 sec in length), and in which a satellite fault has been inserted for algorithm testing purposes. To verify that this is indeed the case, section 6.3.1 will examine the results obtained after the application of the FDE method. Subsequently, in 6.3.2 it will be discussed what conclusions can be logically inferred by examining the ratio of the PE to the PL, and where these results can actually be misleading about the performance level of MHSS FDE.

6.3.1. Validation results

Position solution and VPL values were computed at each snapshot in time for all the data sets created by the insertion of faults with various slopes on PRN 16. Statistics were subsequently compiled for both the case where all available satellites are considered in the position estimate (*all-in-view*) and where detection and elimination were performed as necessary to obtain an optimal partial subset (*healthy subset*). As it was mentioned in Section 6.1 above, no HMI event occurred during the processing of the flight data with no additional faults inserted in it. Although the navigation integrity requirement was satisfied 100% of the time, the availability percentage given by comparing the VPL with the VAL at each instant in time was only of 85.4% in Real-Time and 81.5% for the VPL Prediction mode. This outcome is largely due

to the fact that with only the current GPS constellation with 24 orbital SV slots available for measurements, only 5–10 satellites are available for ranging and thus the Vertical Dilution of Precision (VDOP), and implicitly σ_v values do not get small enough to always allow vertical error bounds tighter than 35 m. These results were expected, as they agree with the conclusions of earlier RAIM algorithms, that the existing GPS alone cannot provide sufficient integrity for vertically-guided approaches. For the same reasons, the observed navigation availability for the prediction VPL is even lower, since the prediction error bounds tend to be larger in order to accommodate improbable scenarios that nevertheless are likely enough to impact the continuity requirement. A single ranging fault is an example of a worst-case scenario that is according to the algorithm assumptions probable enough to affect both continuity and integrity beyond what is permissible by the aviation requirements, therefore the VPL values always have to consider the possible existence of an undetected failure.

Upon failure insertion, on top of the natural measurement noise existing in the data, the range errors contain an inserted fault about 90% of the time, whose magnitude is gradually increasing. As the test data was processed with the FDE method, the values for the VPL, VPE and the number of satellites used for positioning were recorded and were used for putting together graphs similar to those in Figures 6.8 and 6.9 for each data set. In Figure 6.8, the VPL and VPE values are once again compared after FDE was employed, by plotting the two values against each other and also by taking their ratio. With respect to Figure 6.7, both VPE and VPL values have decreased significantly by an amount specifically shown in the top plot of Figure 6.9. This fact reconfirms that after the correct removal of the faulted signal, the VPL returns to values closer to nominal conditions, which are under 35 m most of the time, allowing for an availability increase in the navigation system.

The second plot in Figure 6.9 also indicates visually which PRNs have been identified and removed by the FDE algorithm. After the onset of the failure, once the fault magnitude has increased sufficiently to emerge from the noise floor and influence the error bounds, the solid black line corresponding to PRN 16 marks the continuous

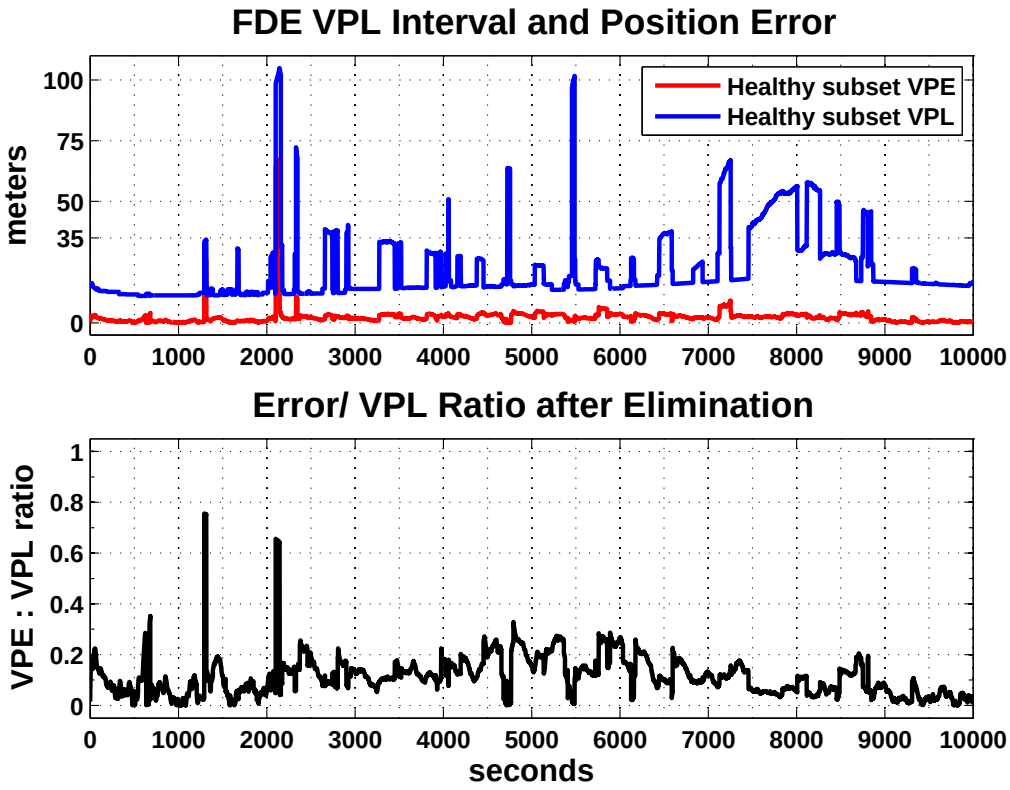

Figure 6.8.: Detection and elimination of the inserted fault.

removal of this satellite signal from the position estimate, with only two minor exceptions. These exceptions correspond to the two spikes in the plot of the VPE / VPL ratio at approximately 1500 and 2000 s into the data set. By further matching these features with the total number of used satellites pictured in Figure 6.2, it can be observed that even before the FDE processing, a low number of range measurements were available to the RAIM algorithm. Thus, should PRN 16 also be identified as faulty at these time points, only 5–6 additional satellites with a particularly poor geometry would remain available for positioning. As little to no measurement redundancy would remain for the integrity calculations, even after removing the affected PRN 16 the VPL values would remain quite high despite the relatively lower amount of URE associated with the remaining ranges. This example allows a first-hand observation from the real data of the counterbalancing effects of the range errors and losses in satellite geometry.

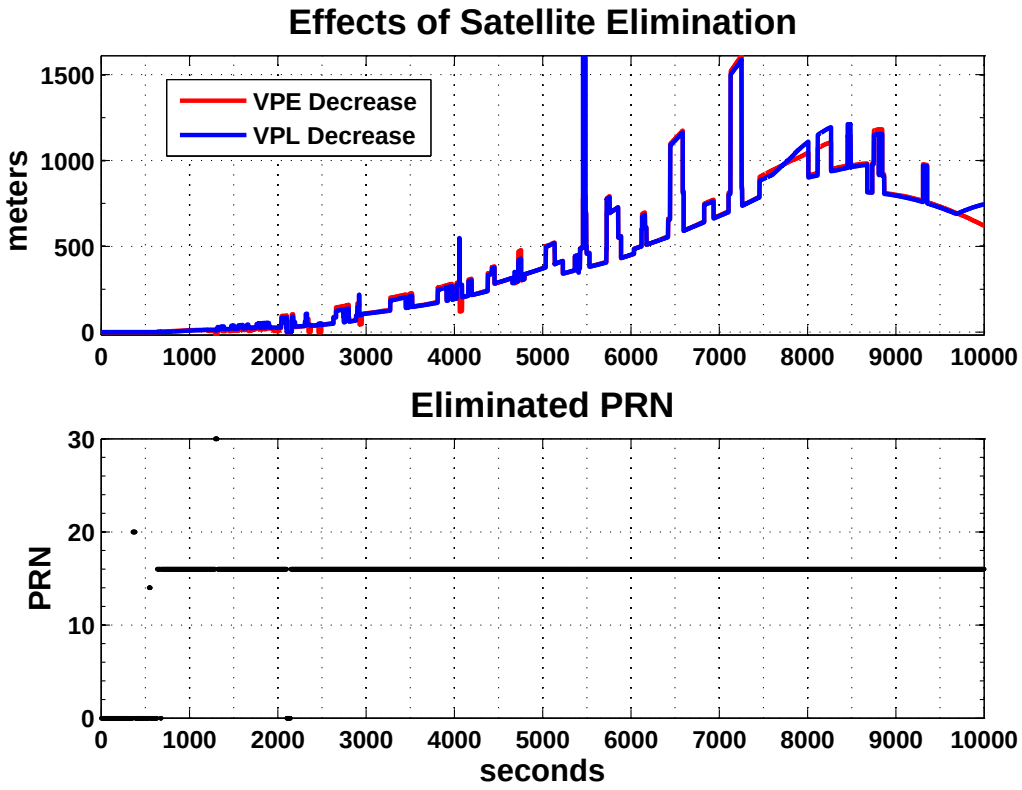

Figure 6.9.: Ramp error detection and the outcome of using the FDE method.

In particular, situations can exist when removing a faulty satellite with some 50–100 m worth of range error might still cause the overall VPL to deteriorate instead of decreasing. Although counter-intuitive, this is an expected behavior of the algorithm, in agreement with what was stated in section 3.3.2. It was stated earlier that particular cases can exist when the removal of large ranging error may not fully counterbalance the ensuing loss in measurement geometry, thus leading to an actual deterioration in performance. In the top plot of Figure 6.8 it can be seen that, at the corresponding time points, the MHSS FDE VPL values are of 70 or 100 m and they are minimal when PRN 16 is actually included in the position solution. It must be noted here that since the satellite geometry across the sky is an important factor influencing the GNSS positioning accuracy, there is not always a one-to-one relationship between the values of the range error and overall position error. For example, the VPL for the measurement set containing a fault might still be lower than the subset VPL not including that fault, but consequently having a much larger VDOP.

Thus, there are circumstances in which there is not a direct correspondence between the minimal error bound and the minimum error. Since an airplane pilot always has to be mindful of the potentially unannounced faults in the system, it is not possible to take advantage of a lower realized value of the VPE when the contingent VPL value is not also lower. In order to make a safety assessment, the navigation system will compare the VPL against the fixed VAL which is relevant for the desired operation. Therefore, the MHSS FDE algorithm presented here chooses to minimize the VPL in order to derive an optimum performance from each set of available snapshot measurements.

An *integrity fault* or HMI event is said to occur whenever the measured error exceeds the computed error bound (viz. VPE $>$ VPL). While a certified system is mandated by the FAA to guarantee a very low probability for the occurrence of this type of events, integrity faults are theoretically more likely to arise under severe fault conditions. However, none of the test data sets obtained through the insertion of a failure produced such an HMI event, despite the wide range of fault biases inserted in the measurements, with time gradients between 1 cm/s and 1 m/s. Both the MHSS RT algorithm computing a VPL for the all-in-view case and the MHSS FDE algorithm yielded protection levels that bound the VPE 100% of the time. While it is certain that larger amounts of real data are necessary in order to certify that this RAIM algorithm protects the user up to a P(HMI) of 10^{-7}, these initial tests subjected the algorithm to a varied array of test and failure cases which served to validate the robustness of the algorithm and rule out any problems with the concepts behind it. While the average operational availability (viz. VPL $\leq$ 35 m) with the RAIM algorithm decreased to around 22% when faults where added on top of the original measurement data, after FDE was applied this availability increased back to around 81.5%. It can further be observed that the availability levels after the removal of the fault are very similar to the availability corresponding to the prediction VPL, which serves to also confirm what was claimed above, that the prediction VPL is a high confidence upper bound on the RT VPL.

6.3.2. Examining the VPE / VPL ratio

The VPE / VPL ratio has been used in the past in order to assess the performance of RAIM algorithms in GNSS augmentation systems [30, 81]. However, these algorithms were generally similar to LS RAIM, which does not use the knowledge of the RAIM measurements directly in determining the VPL. As such, the size of the VPL depended to a large extent on the satellite geometry, while only the VPE was directly related to the measurement noise. If the measurement errors were then assumed to be near-Gaussian as long as they were below a certain error threshold, as is the case with classical RAIM algorithms, then it could also be assumed that the values of the VPE / VPL ratio should be normally distributed. While not attempting to qualify this latter assumption, it can be said that it implies to a large extent that a statement can be made about the long-term performance of a RAIM algorithm based solely on the specific distribution of the VPL / VPE ratio for a relatively small data sample. The question here is whether this approach would also be useful in helping generalize the results of the current study of the performance of MHSS RAIM with real GPS data, such that a wider-reaching conclusion could be drawn.

In particular, is VPE / VPL a good measure for the performance of the MHSS FDE RAIM algorithm? Actually, from the above results it can be deduced that the VPE / VPL ratio is also higher for poor geometries and low failure biases as well as in the case of extremely large ranging errors. In fact, the ratio is not statistically described by a well-known distribution (e.g. a Gaussian) for the case of the MHSS FDE algorithm. In Figure 6.10, the distribution of the values of this ratio as measured from the data sets with inserted ramp errors is given on both a linear scale (a) and a logarithmic scale (b). While the top plot shows how the most realized values of this ratio lie below 0.5, at the lower end of the scale, the bottom plot evidences the distribution of the tails, which flattens out to 0.01–0.03% of the samples in the 8 bins between 0.55 and 0.95 before finally cutting off. Although in a few cases the VPE / VPL ratio nears 1, this exclusively happens for VPL values of several hundred meters and significantly above the VAL value, such that the margin between the

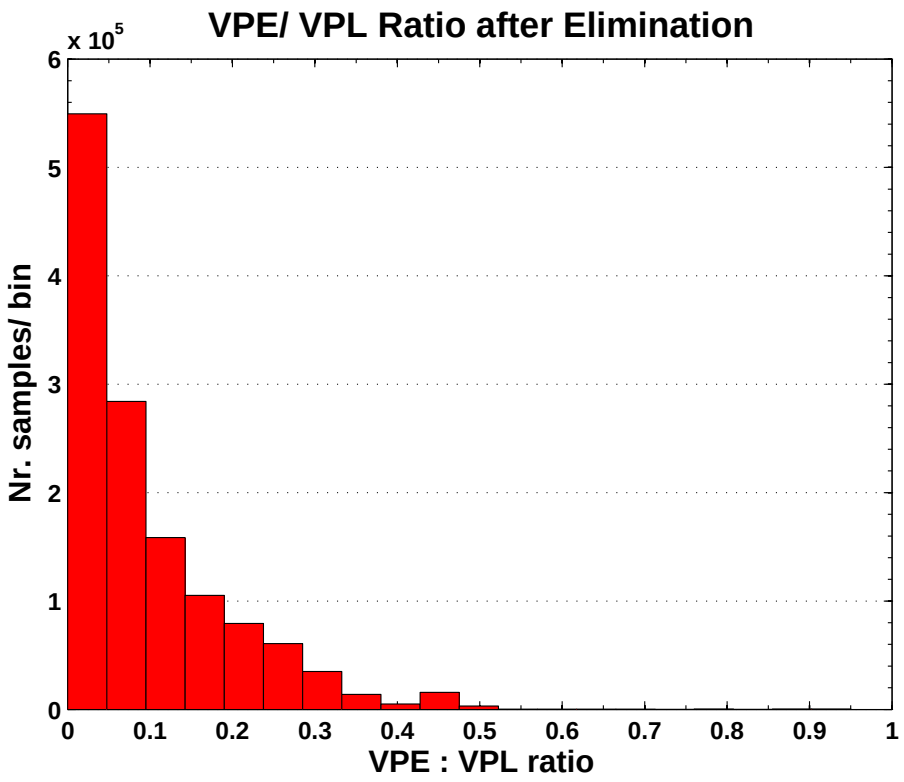

(a) Linear histogram of the distribution of the VPE / VPL ratio.

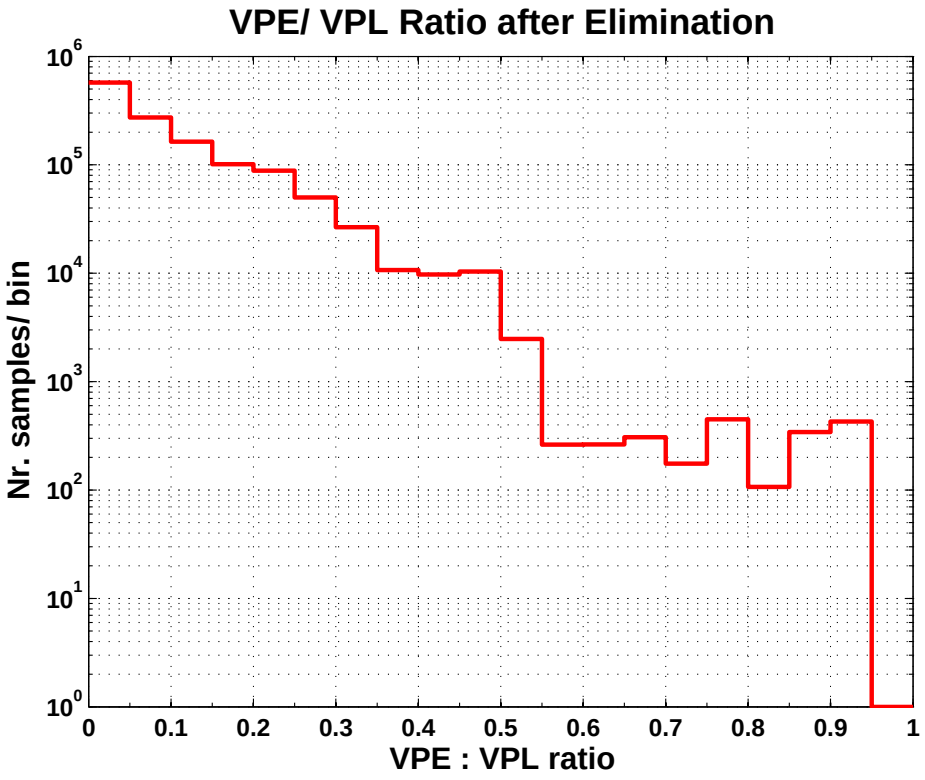

(b) Logarithmic histogram of the distribution of the VPE / VPL ratio.

Figure 6.10.: Comparison of VPE and VPL in the presence of ramp-like errors.

error and the protection level never gets smaller than several meters. As the current algorithm seeks to minimize the VPL values, which appear in the denominator of the ratio, it appears that optimizing performance can actually end up increasing the value of this fraction in a minority of the cases.

If the ultimate goal were to minimize the VPE / VPL only, then a solution to the integrity problem would be to simply make VPL values extremely large in all cases. However, the performance goals of the current work on MHSS RAIM are quite different. They are measured by four different metrics derived directly from the aviation navigation requirements mandated by the FAA: integrity, availability, continuity, and accuracy. As such, the only way in which the VPE / VPL ratio is relevant to navigation performance is that a supra-unitary value of this ratio would signal an integrity fault. A more appropriate question would be to what extent is the VPE / VPL ratio a measure of the MHSS integrity performance. In the context of the MHSS-type algorithms using RT measurements for determining the VPL, the distribution of the VPE / VPL values is irrelevant to navigation performance as long as these values remain below 1. During further considerations on this algorithm, only the set of the four performance metrics mentioned above will be used to measure the performance of MHSS.

6.4. Discussion and Conclusions

Ideally the VPE $\leq$ VPL $\leq 35\,\mathrm{m}$ conditions would all be met simultaneously at all times, in order to satisfy the aviation requirements. Nevertheless, in order for that to happen, a larger number of redundant measurements have to be performed at each snapshot of time. The number of measurement sources can be increased either by increasing the number of active orbital slots in the future GPS constellation or, more likely, by using signals from multiple GNSS constellations simultaneously. Augmentation systems can also add additional sources broadcasting navigation signals, but the purpose of this work is only to study worldwide unaugmented systems, whose size

does not scale with the geographical area covered, the number of airports or the total number of users. A discussion will be made here on how many satellites are needed in optimized orbits to provide the desired performance. An optimized constellation is one that seeks to maximize the average VDOP for all users, by placing its satellites in equally spaced orbital slots across the sky.

Given the assumed SV failure prior of $1.4{\cdot}10^{-5}$ per approach, in order to meet the integrity requirement, the all-in-view subset as well as all subsets with one potential satellite fault removed need to produce a finite VPL. The largest of these VPLs will then be compared to the appropriate VAL in order to determine availability. When more than 10 SVs are in view, all subsets with either 1 or 2 potential faults will be analyzed, as the probability of two simultaneous faults starts to exceed the 10^{-8} probability threshold used by MHSS algorithm to determine which fault modes require a significant share of the overall integrity budget. This information is reflected by Table 6.1, which is meant to show what minimum number of satellites is required to ensure a high enough availability for a VAL of 35 m, in order to meet the operational requirements of civil aviation. The reader is reminded here that all other assumptions stated in section 3.1.1 are assumed to hold here, including the fact that satellite orbits are expected to be optimized for the best average user geometry.

Number of Satellites	Position Solution	VPL All-in-View	VPL – 1 Fault	VPL – 2 Faults
$N \leq 3$	✘	✘	✘	✘
$N = 4$	✓	∞	✘	✘
$N = 5$	✓	HIGH	∞	✘
$N = 6$	✓	≈ 100 m	HIGH	∞
$N = 7$	✓	≈ 50 m	≈ 100 m	**N/A**
$N = 8$	✓	≈ 35 m	≈ 50 m	**N/A**
$N = 9, 10$	✓	≈ 25 m	15 - 50 m	**N/A**
$N \geq 11$	✓	5 - 15 m	10 - 35 m	15 - 50 m

Table 6.1.: VPL Performance dependence on number of visible satellites.

The first column of the table goes through the possible numbers of satellites available for integrity monitoring in increasing order. The second column tells

whether a position solution is available to the user given the number of available measurements, assuming there are only 1 temporal and 3 spatial unknowns to solve for. The following three columns state whether it is possible to compute a PL based on the corresponding number of satellites, considering the no-fault, single-fault and double-fault scenarios. In case a VPL can be calculated, a rough conservative estimate of its value is also offered. The rows of the table are color-coded with nuances varying from red to green, which relate to how the RAIM performance evolves when the number of satellites in view is taken as a variable parameter. Colors symbolize how likely it is to achieve high levels of availability of 99.5% and above given the number of SVs in view, a VAL of 35 m along with the usual assumptions made by the MHSS FDE algorithm. The highlighted table cells mark the number of possible unannounced faults that the current RAIM algorithm must consider at all times, given the $1.4{\cdot}10^{-5}$/ satellite / approach probability prior enounced earlier. The Not Applicable (N/A) notation in the last column signifies the fact that with 10 or less ranging sources, the chance of multiple simultaneous failures is so low that it does not pose an integrity threat and thus it does not significantly affect the VPL. This table serves as a visual way to estimate what is the worst possible effect of the satellite geometry on the VPL, and can be further adapted to serve the same purposes for a wide range of failure priors. Under the current fault probability assumptions, however, even having 7–8 satellites contribute range measurements to the position solution is not sufficient to provide availability under all geometries in the presence of faulted measurements.

It was important to conduct an evaluation of the MHSS RAIM algorithm with real GNSS data and under realistic operating conditions, as the results presented above added greatly to the current understanding on the prospects of MHSS RAIM. This final part of the work served to validate all remaining assumptions under the real setting of an aircraft that can operate under complex conditions, something which is not always possible to render with fidelity in simulation. Finally, the real data validation process allowed a realistic estimate of the capabilities of current GPS and future GNSS in terms of RAIM performance, with an algorithm that focuses directly

on satisfying the aviation operational requirements while avoiding additional overly conservative assumptions.

Part IV.

Final Remarks

7. Conclusions

In the near foreseeable future, GNSS will provide the means for seamless airplane navigation from takeoff to touchdown in the same way that GPS and its augmentations are able to do today. While the goal of enabling vertically guided approaches with RAIM has been highly motivating in the past, significant technical challenges have existed. The most difficult of these has been associated with ensuring navigation integrity even in the presence of multiple unannounced faults. This dissertation has directly addressed the issue of navigation integrity along with its close connections to navigation system accuracy, continuity and availability within the framework of an autonomous navigation architecture, relying on ground-monitored but unaugmented GNSS.

7.1. Summary of Accomplishments

The principal accomplishments of this dissertation were grouped around two research directions. The first part of the thesis research involved the algorithm and threat model development for the MHSS RAIM method. The theoretical development was accompanied by computer simulation studies of the performance of this RAIM algorithm and the external parameters to which these performance results are the most sensitive. The second part of the thesis research represents the validation of the developed MHSS algorithm through the use of real in-flight GNSS measurements, based on the currently operational GPS constellation. A summary of the contributions in this work and the corresponding results will be detailed below.

7.1.1. RAIM algorithm development

An advanced RAIM algorithm was developed to take advantage of the increased number of ranging sources expected with future multiple GNSS constellations. The current research explored the new issues and opportunities that will come with a combined constellation relative to the current single-constellation GPS. The improved Multiple Hypothesis Solution Separation (MHSS) algorithm can handle multiple simultaneous range measurement faults in a flexible manner and was completed with additional Fault Detection and Elimination (FDE) and Vertical Protection Level (VPL) Prediction methods. The integrity calculation for these algorithms allows for a straightforward mathematical proof that the computed protection levels meet the Probability of Hazardous Misleading Information (PHMI) requirements. The Fault Detection and Elimination (FDE) method designed on top of the RT MHSS algorithm takes advantage of the probabilistic failure definition in order to minimize the overall VPL for any snapshot in time. Very pragmatically, this FDE method explores whether unusually large ranging biases need to be removed or not, in order to obtain the smallest possible confidence interval for the position error.

The overall algorithm is well-equipped to handle multiple simultaneous faults and a comprehensive threat model. While no definite decision can be made on the presence of a measurement fault based on the limited amount of information available to a GNSS user, the MHSS FDE algorithm is optimally adapted to make a statistical determination on the likelihood of a fault. The proposed method was proven to optimize the integrity performance while overbounding the user position error and making the conservative assumption that undetected failures can be present at any time in the measurements with a reasonable probability. The current approach was shown to have significant performance advantages over classical snapshot RAIM algorithms.

7.1.2. Determination of parameter space over which desired RAIM performance is achievable

An analysis of the simulated performance of unaided RAIM for users worldwide was conducted. The performance capabilities of future GNSS under multiple possible scenarios were assessed, in terms of the overall number of operational satellites and constellations. Parametric studies were conducted in order to identify on which external factors is the VPL the most sensitive, and for which assumptions performance is not significantly affected over a large range of possible values. These studies identified the parameter space width over which the results with the current MHSS RAIM algorithm are applicable and the assumptions that need to be met.

The algorithm was determined to be the most sensitive on the externally provided values for the user range error, in terms of both the error mean and variance. At the same time, the MHSS RAIM algorithm is capable of providing the required aerial navigation performance for a wide range of assumed satellite and constellation prior fault probabilities, covering all possible realistic values based on the currently available historical data on GNSS signal health. It was discovered that significant variations in the assumed prior failure probabilities leave VPL values relatively unaffected. In terms of the number of GNSS satellites necessary to meet the Required Navigation Performance (RNP) specifications, it was determined that the signals from a minimum of 30 active SVs evenly distributed in orbital positions across the sky, or a higher number of spacecraft in non-optimized orbits should be available to the civilian user. On the average, one third of the number of active satellites would be visible to a GNSS user, therefore the above recommendations translate into having an average 10 or more visible SVs to a user with an unobstructed view of the sky.

7.1.3. Validation of the pseudorange error model

Based on the real flight test data made available by the FAA Tech Center, the subsequent effort served to ensure that the model used by the algorithm for satellite

range measurement errors accurately provides an upper limit for the actually measured errors. Error models across different signal frequencies were properly calibrated. A realistic model for the actual ranging errors was obtained based on GPS L1-L2 dual frequency ground station and flight inspection data. The statistics of realized errors in the available data sets exhibited a near-Gaussian behavior, with a slightly higher amount of probability located in the tails of the distribution and small nominal levels of bias at the centimeter level.

7.1.4. Verification of the MHSS algorithm with real data

As the final step, the performance of the Real Time, Prediction and Fault Detection and Elimination capabilities of the MHSS RAIM algorithm was evaluated while employing an appropriately calibrated user range error model. Testing was conducted under a variety of scenarios that include both nominal measurement data and a wide range of inserted satellite failures. The ability of the developed RAIM method to detect and eliminate faulty measurements as they propagate and increase over time was verified, and no instances HMI were observed while using either the original flight data or subsequent to the artificial fault insertion. It was determined that the developed algorithm is able to meet the aviation specifications for standard LPV 200' approaches with a Vertical Alert Limit (VAL) of 35 m within the operational parameter space delimited earlier through simulation.

8. Future Work

8.1. Algorithm Implementation

This thesis showed the benefits of ARAIM in conjunction with modernized GNSS. It is hoped that the very promising results of the present work will stimulate further investigation in this field. Further research will amount to certifying, building and flying navigation instruments using this technology. At the current point in time, it is foreseeable that GNSS will gradually become the certified primary-means aircraft navigation system all the way from taxi to takeoff and landing at airports around the world. The current research was one of the necessary steps to making this vision a reality in the next 25–30 years. Absolute RAIM allows aviation users to operate autonomously for a longer time in the presence of multiple frequency GNSS signals, with the same high availability they would receive from WAAS with the current single civilian frequency GPS.

Any additional capabilities of the ground stations, such as a LAAS-like system, in conjunction with RAIM could push aviation performance from satisfying the requirements for LPV 200' DH to autoland. A more progressive idea would be establishing communication channels between airplanes to provide information about common navigation system faults. This method would allow employing each user certified to share this information to serve as a monitoring checkpoint within the NAS. An improved RAIM system would be able to change the assumed failure prior for a satellite that was detected as faulted. For faster computational times, implementing

prior probability tables is also possible, and it would allow providing a fixed probability for each type of fault mode (i.e. simultaneous ranging failures or failures common to an entire constellation). Potentially correlated fault probabilities would generally sum up to a total greater than 1, as they would account for the degree of correlation between different possible events.

An operational algorithm should also have some form of memory. The *a priori* probability for a specific satellite would be increased for a minimum period of time into the future as soon as the FDE algorithm made the decision to remove its corresponding range measurement as faulty. Therefore, future studies will be needed to observe what influence on the performance is caused by an increase in the prior for only one partial fault mode. It will also need to be determined under what conditions a previously removed satellite can be included again in the measurement set, and its *a priori* probability be reset to its nominal value.

Finally, a standard version of the MHSS RAIM method should be integrated directly with the WLS receiver and position fix software algorithm, such that the resulting enhanced GNSS aviation receivers would come with a built-in integrity monitor. The receiver prototypes should represent a test bed for validating the MHSS FDE algorithm in conjunction with an actual multiple constellation GNSS receiver, while processing either simulated RF signals or actual satellite multi-frequency data when modernized GNSS constellations become operational. In terms of the range error model to be employed in the presence of modernized GNSS signals, the calibration method proposed in this work can be employed, along with the use of additional flight test data to further refine the model for residual errors and biases. A detailed analysis should be employed to determine the elevation dependence of the errors during the different phases of flight, based on the ground altitude, and also in order to study the receiver and antenna dependence of the observed errors.

In order to address both the performance requirements laid out in the opening arguments of this work, and also ensure that large errors of the VPE are altogether

avoided, the GEAS Panel discussed adding an additional constraint to the performance requirements. The Effective Monitoring Threshold (EMT) would ensure not only that the 10^{-7} tails of the error distribution do not exceed the VPL, but also that the realized value of the error is below 15 m at least half of the time when faults are present. This would help address a potential drawback of a RAIM FDE algorithm which minimizes the VPL, as described in Chapter 6, but does not also bias its selection process towards geometries with a low VPE. This additional constraint can then be combined with the calculated RT and Dispatch VPLs to determine the availability of a measurement geometry that not only guarantees vertical errors of less than 35 m, but also that these errors are distributed with a higher probability in the 0-15 m interval.

A good understanding of the interaction between these different performance metrics will then help establish how to better implement the MHSS algorithm in the aircraft. The Dispatch VPL is essential for guaranteeing the continuity of operation, and as such it needs to be evaluated in advance of performing the approach operation. When an airplane reaches the Final Approach Fix (FAF) point in its descent towards an airport, it needs to compare the Predicted VPL value with the VAL before proceeding. If this comparison is successful (viz. Dispatch VPL $\leq$VAL), the onboard navigation system could continue to use the RT VPL for the remainder of the approach in order to be able to observe any potential measurement faults with the aid of the FDE capabilities of the MHSS algorithm. A second alternative would be for the aviation user to continuously monitor the values of both the Dispatch and RT VPL throughout the approach sequence, and assume that it is safe to navigate relying on satellite signals only if both values are below the VAL. The third option is for the pilot to use the EMT in conjunction with the Dispatch VPL, such that predicted VPLs below 35 m would assure the operational integrity while comparing the EMT with the 15 m limit would help also insure that the instantaneous VPE values are low as the aircraft approaches the runway. Further investigation with RT flight data will be necessary to determine which of these three approaches is the most

appropriate for balancing both the highest safety standards and the highest possible navigation availability in the cockpit.

8.2. Epilogue

Superior performance will become possible once the Galileo system or additional ranging sources from other GNSS systems currently under development become operational in the near future. Even if the European Galileo or the Chinese Beidou systems incur delays in becoming globally operational, MHSS RAIM could also provide additional performance by using signals from the partly operational Russian GloNaSS or from GPS satellites in excess of the minimum of 24. The flexibility of the algorithm allows employing non-GPS satellites for measurement redundancy even if they are not part of a fully operational constellation, that could be used independently for positioning. Each additional satellite beyond the currently guaranteed 24 GPS SVs can provide another range measurement to increase the confidence about the estimated user location and help decrease the overall error bounds. The only advantage of having at least one orbit-optimized 30 SV constellation as opposed to multiple smaller constellations is that the measurement geometry improves considerably when all the satellite orbits are coordinated to provide an even coverage across the sky at all times, and not solely based on fortuitous alignments of the different constellations. A robust GNSS would therefore optimize navigation availability by providing a strong geometry on a consistent basis.

List of References

[1] Aeronautical Radio, Inc. (ARINC) Engineering Services, LLC, *Interface Control Document – Navstar GPS Space Segment / Navigation User Interfaces*, ICD-GPS-200C, Navstar GPS Joint Program Office, El Segundo, CA, 14 January 2003.

[2] ARINC Engineering Services, LLC, *Interface Specification – Navstar GPS Space Segment / Navigation User Interfaces*, IS-GPS-200D, Navstar GPS Joint Program Office, El Segundo, CA, 7 December 2004.

[3] ARINC Engineering Services, LLC, *Navstar GPS Space Segment / User Segment L5 Interfaces*, IS-GPS-705, Navstar GPS Joint Program Office, El Segundo, CA, 22 September 2005.

[4] Akos D.M., Ene A., Thor J., *A Prototyping Platform for Multi-Frequency GNSS Receivers*, in Proceedings of the ION GNSS 16^{th} International Technical Meeting of the Satellite Division, Portland, OR, 9-12 September 2003.

[5] Angus J., *RAIM with Multiple Faults*, NAVIGATION, Journal of the Institute of Navigation, vol. 53, no. 4, ION, 2006.

[6] Blanch J., Walter T., and Enge P., *Understanding PHMI for Safety of life applications in GNSS*, in Proceedings of the ION National Technical Meeting, San Diego, CA, 22-24 January 2007.

[7] Blanch J., Ene A., Walter T., and Enge P., *An Optimized Multiple Hypothesis RAIM Algorithm for Vertical Guidance*, in Proceedings of the ION GNSS 20^{th} International Technical Meeting of the Satellite Division, Ft. Worth, TX, 25-28 September 2007.

[8] Blanch J., Walter T., Enge P., *A Simple Algorithm for Dual Frequency Ground Monitoring Compatible with ARAIM*, in Proceedings of the ION GNSS 21^{st} International Technical Meeting of the Satellite Division, Savannah, GA, 16-19 September 2008.

[9] Blanch J., Walter T., Enge P., *RAIM with Optimal Integrity and Continuity Allocations under Multiple Satellite Failures*, submitted to IEEE Transactions

on Aerospace and Electronic Systems, IEEE, 6 March 2008.

[10] Brenner M., *Implementation of a RAIM Monitor in a GPS Receiver and an Integrated GPS/IRS*, in Proceedings of the ION GPS 3^{rd} International Technical Meeting of the Satellite Division, pp. 397-414, Colorado Springs, CO, 19-21 September 1990.

[11] Breeuwer E., Farnworth R., and Humphreys P., McGregor A., Michel Ph., Secretan H., Leighton S.J., and Ashton K.J., *Flying EGNOS: The GNSS-1 Testbed*, GALILEO'S WORLD, pp. 10-21, Questex Media Group, Winter 2000.

[12] Brown A.K., *Receiver Autonomous Integrity Monitoring Using a 24-Satellite GPS Constellation*, in Proceedings of the ION GPS 1^{st} Technical Meeting of the Satellite Division, pp. 256-262, Colorado Springs, CO, 21-25 September 1987.

[13] Brown R.G., and Hwang P., *GPS Failure Detection by Autonomous Means Within the Cockpit*, in Proceedings of the 42^{nd} Annual Meeting of the ION, pp. 5-12, Seattle, WA, 24-26 June 1986.

[14] Brown R.G., and McBurney P., *Self-Contained GPS Integrity Check Using Maximum Solution Separation*, NAVIGATION, Journal of the Institute of Navigation, vol. 35, no.1, ION, 1988.

[15] Brown R.G., Chin G.Y., and Kraemer J.H., *RAIM: Will It Meet The RTCA GPS Minimum Operational Performance Standards?*, in Proceedings of the ION National Technical Meeting, pp. 103-111, Phoenix, AZ, 22-24 January 1991.

[16] Brown R.G., *A Baseline GPS RAIM Scheme and a Note on the Equivalence of Three RAIM Methods*, NAVIGATION, Journal of the Institute of Navigation, vol. 39, no. 3, ION, 1992.

[17] Brown R.G., *Receiver Autonomous Integrity Monitoring*, in Global Positioning System: Theory and Application, Volume II, pp. 143-165, Eds. Parkinson B.W., Spilker J.J., Axelrad P., Enge P., AIAA, Washington, DC, 1996.

[18] Cabler H., and DeCleene B., *LPV: New, Improved WAAS Instrument Approach*, in Proceedings of the ION GPS 15^{th} International Technical Meeting of the Satellite Division, Portland, OR, 24-27 September 2002.

[19] Datta-Barua S., Walter T., Blanch J., and Enge P., *Bounding higher-order ionosphere errors for the dual-frequency GPS user*, DOI:10.1029/2007RS003772, RS5010, Radio Science, vol. 43, AGU, 2008.

[20] DeCleene B., *Defining Pseudorange Integrity – Overbounding*, in Proceedings of the ION GPS 13^{th} International Technical Meeting of the Satellite Division, Salt Lake City, UT, 19-22 September 2000.

[21] van Dierendonck A.J., *Scaling Measurements to Simulate L1 / L5 Dual-Frequency Pseudoranges*, private notes, 30 April 2008.

[22] Dieter G.L., Hatten G.E., and Taylor J., *MCS Zero Age Of Data Measurement Techniques*, in Proceedings of the 35^{th} Annual Precise Time and Time Interval Systems and Applications Meeting, San Diego, CA, December 2 - 4, 2003.

[23] El-Arini B., and Lee Y.C., *Performance of ARAIM Using Flight Test Data at Memphis, TN on September 19, 2006*, Presented at GEAS Panel Workgroup Meeting, Arlington, VA, 12 June 2008.

[24] Ene A., Qiu D., Luo M., Pullen S., and Enge P., *A Comprehensive Ionosphere Storm Data Analysis Method to Support LAAS Threat Model Development*, in Proceedings of the Institute of Navigation National Technical Meeting, San Diego, CA, 24-26 January 2005.

[25] Ene A., Blanch J., and Walter T., *Galileo-GPS RAIM for Vertical Guidance*, in Proceedings of the Institute of Navigation National Technical Meeting, Monterey, CA, 18-20 January 2006.

[26] Ene A., *Further Development of Galileo-GPS RAIM for Vertical Guidance*, in Proceedings of the ION GNSS 19^{th} International Technical Meeting of the Satellite Division, Fort Worth, TX, 26-29 September 2006.

[27] Ene A., Blanch J., and Powell J.D., *Fault Detection and Elimination for Galileo-GPS Vertical Guidance*, in Proceedings of the Institute of Navigation National Technical Meeting, San Diego, CA, 22-24 January 2007.

[28] Ene A., *Multiple Hypothesis RAIM with Real-Time FDE and Forecasted Availability for Combined Galileo-GPS Vertical Guidance*, in Proceedings of the European Navigation Conference - GNSS / TimeNav, Geneva, Switzerland, 28-31 May 2007.

[29] Ene A., Blanch J., Walter T., and Powell J.D., *Validation of Multiple Hypothesis RAIM Algorithm Using Dual-Frequency GNSS Signals*, in Proceedings of the European Navigation Conference - GNSS / Toulouse Space Show, Toulouse, France, 22-25 April 2008.

[30] Eurocontrol, *EGNOS SIS analysis: PRN 126*, `http://stargate.fgt.bme.hu`, Budapest University of Technology and Economics, Budapest, Hungary, 11 September 2006.

[31] European Space Agency / European GNSS Supervisory Authority, *Galileo Open Service Signal In Space Interface Control Document (OS SIS ICD)*, Draft 1, 14 February 2008.

[32] FAA GEAS Panel, *GNSS Evolutionary Architecture Study: Phase I - Panel Report*, `http://www.faa.gov/about/office_org/headquarters_offices/ato/service_units/techops/navservices/gnss/library/documents/media/GEAS_PhaseI_report_FINAL_15Feb08.pdf`, February 2008.

[33] FAA Technical Center, Navigation / LAAS T&E Team, *Local Area Augmentation System Performance Analysis / Activities Report #11: July 1 to September 30, 2006*, `http://www.gps.tc.faa.gov/REPORTS/Performance/LPAR_11.pdf`, Atlantic City, NJ, 31 October 2006.

[34] FAA Technical Center, NSTB / WAAS T&E Team, *Archived PAN Reports*, `http://www.nstb.tc.faa.gov/DisplayArchive.htm`, Atlantic City, NJ, 1999-2008.

[35] Giremus A., Escher A.-C., *A GLR Algorithm to Detect and Exclude up to Two Simultaneous Range Failures in a GPS / Galileo / IRS Case*, in Proceedings of the ION GNSS 20^{th} International Technical Meeting of the Satellite Division, Ft. Worth, TX, 25-28 September 2007.

[36] Gratton L., Pramanik R., Tang H., and Pervan B., *Ephemeris Failure Rate Analysis and its Impact on Category I LAAS Integrity*, in Proceedings of the ION GNSS 20^{th} International Technical Meeting of the Satellite Division, Ft. Worth, TX, 25-28 September 2007.

[37] Groves P.D., and Harding S.J., *Ionosphere Propagation Error Correction for Galileo*, DOI: 10.1017/S0373463302002084, THE JOURNAL OF NAVIGATION, vol. 56, pp. 45–50, The Royal Institute of Navigation, UK, 2003.

[38] Hein G.W., Godet J., Issler J.-L., Martin J.-C., Erhard P., Lucas-Rodriguez R., and Pratt T., *Status of Galileo Frequency and Signal Design*, in Proceedings of the ION GPS 15^{th} International Technical Meeting of the Satellite Division, Portland, OR, 24-27 September 2002.

[39] Hwang P., and Brown R.G., *RAIM FDE Revisited: A New Breakthrough in Availability Performance with* NIO*RAIM (Novel Integrity-Optimized RAIM)*, in Proceedings of the ION National Technical Meeting, San Diego, CA, 24-26 January 2005.

[40] Hwang P., and Brown R.G., *From RAIM to* NIO*RAIM: A New Integrity Approach to Integrated Multi-GNSS Systems*, INSIDEGNSS, vol. 3, no. 4, Gibbons Media & Research, May-June 2008.

[41] International Civil Aviation Organization (ICAO), *Aeronautical Telecommunications*, in Annex 10 to the Convention on International Civil Aviation International Standards and Recommended Practices (SARPs), Volume I (Radio Navigation Aids), Montreal, Canada, 16 July 2007.

[42] Jan S., Chan W., Walter T., and Enge P., *Matlab Simulation Toolset for SBAS Availability Analysis*, in Proceedings of the ION GPS 14^{th} International Technical Meeting of the Satellite Division, Salt Lake City, UT, 11-14 September

2001.

[43] Kaplan E.D., and Hegarty C.J. (eds.), *Understanding GPS: Principles and Applications*, 2^{nd} ed., Artech House, Norwood, MA, 2006.

[44] Kelly R.J., *The Linear Model, RNP, and the Near-Optimum Fault Detection and Exclusion Algorithm*, in Global Positioning System, Volume V, pp. 227-259, Eds. Kalafus, R.M., and van Dyke, K.L., ION, Alexandria, VA, 1998.

[45] Klobuchar J.A., *Ionospheric Effects on GPS*, in Global Positioning System: Theory and Application, Volume I, pp. 485-515, Eds. Parkinson B.W., Spilker J.J., Axelrad P., Enge P., AIAA, Washington, DC, 1996.

[46] Kovach K., Berg J., Lin V., *Investigation of Upload Anomalies Affecting IIR Satellites in October 2007*, in Proceedings of the ION GNSS 21^{st} International Technical Meeting of the Satellite Division, Savannah, GA, 16-19 September 2008.

[47] Kovach K., Dobyne J., Crews M., Miles C., *GPS III Integrity Concept*, in Proceedings of the ION GNSS 21^{st} International Technical Meeting of the Satellite Division, Savannah, GA, 16-19 September 2008.

[48] Kubo Y., Sone K., and Sugimoto S., *Cycle Slip Detection and Correction for Kinematic GPS Based on Statistical Tests of Innovation Processes*, in Proceedings of the ION GNSS 17^{th} International Technical Meeting of the Satellite Division, Long Beach, CA, 21-24 September 2004.

[49] Lawrence D., and Bunce D., Mathur N.G., Sigler C.E., *Wide Area Augmentation System (WAAS) - Program Status*, in Proceedings of the ION GNSS 20^{th} International Technical Meeting of the Satellite Division, Ft. Worth, TX, 25-28 September 2007.

[50] Lee Y.C., *Analysis of the Range and Position Comparison Methods as a Means to Provide GPS Integrity in the User Receiver*, in Proceedings of the 42^{nd} Annual Meeting of the ION, pp. 1-4, Seattle, WA, 24-26 June 1986.

[51] Lee Y.C., Van Dyke K., DeCleene B., Studenny J., Beckmann M., *Summary of RTCA SC-159 GPS Integrity Working Group Activities*, NAVIGATION, Journal of the Institute of Navigation, vol. 43, no. 3, ION, 1996.

[52] Lee Y.C., *Investigation of Extending Receiver Autonomous Integrity Monitoring (RAIM) to Combined Use of Galileo and Modernized GPS*, in Proceedings of the ION GNSS 17^{th} International Technical Meeting of the Satellite Division, Long Beach, CA, 21-24 September 2004.

[53] Lee Y.C., Braff R., Fernow J.P., Hashemi D., McLaughlin M.P., and O'Laughlin D., *GPS and Galileo with RAIM or WAAS for Vertically Guided Approaches*, in Proceedings of the ION GNSS 18^{th} International Technical Meeting of the Satellite Division, Long Beach, CA, 13-16 September 2005.

[54] Lee Y.C., Braff R., Fernow J.P., Hashemi D., McLaughlin M.P., and O'Laughlin D., *Application of GPS and Galileo with RAIM or SBAS for Vertically Guided Approaches*, in Proceedings of the European Navigation Conference, Manchester, UK, 7-10 May 2006.

[55] Lee Y.C., McLaughlin M.P., *Feasibility Analysis of RAIM to Provide LPV-200 Approaches with Future GPS*, in Proceedings of the ION GNSS 20^{th} International Technical Meeting of the Satellite Division, Ft. Worth, TX, 25-28 September 2007.

[56] Martineau A., *Performance of Receiver Autonomous Integrity Monitoring (RAIM) for Vertically Guided Approaches*, Ph.D. Thesis, National Civil Aviation School of the Polytechnic Institute of Toulouse, France, 14 November 2008.

[57] Madden D.W., *GPS Wing Program Update*, in Proceedings of the ION GNSS 21^{st} International Technical Meeting of the Satellite Division, Savannah, GA, 16-19 September 2008.

[58] McGraw G., Murphy T., *Safety of Life Considerations for GPS Modernization Architectures*, in Proceedings of the ION GPS 14^{th} International Technical Meeting of the Satellite Division, Salt Lake City, UT, 11-14 September 2001.

[59] Miret E.A., *Galileo Signal-in-Space Design*, http://www.galileoic.org/la/files/SignalPresentation_MasterPolito_9thMay2005.pdf, Galileo Information Centre for Latin America, 9 May 2005.

[60] Misra P., Enge P., *Global Positioning System: Signals, Measurements, and Performance*, 1^{st} ed., Ganga-Jamuna Press, Lincoln, MA, 2001.

[61] Misra P., Enge P., *Global Positioning System: Signals, Measurements, and Performance*, 2^{nd} ed., Ganga-Jamuna Press, Lincoln, MA, 2006.

[62] Murphy T., Miller D., Heine D., Howell Ch., Both A., Wright M., Pierce C., Semler J., *The Boeing / Industry GPS Landing System Flight Test Experiments*, in Proceedings of the ION National Technical Meeting, pp.155 – 166, Santa Monica, CA, 22 – 24 January 1996.

[63] Murphy T., Harris M., Booth J., Geren P., Pankaskie T., Clark B., Burns J., Urda T., *Results from the Program for the Investigation of Airborne Multipath Errors*, in Proceedings of the ION National Technical Meeting, San Diego, CA, 24-26 January 2005.

[64] Murphy T., Geren P., Pankaskie T., *GPS Antenna Group Delay Variation Induced Errors in a GNSS Based Precision Approach and Landing Systems*, in Proceedings of the ION GNSS 20^{th} International Technical Meeting of the Satellite Division, Ft. Worth, TX, 25-28 September 2007.

[65] Murphy T., Harris M., *RAIM Performance in the Post SA Era*, in Proceedings of the ION GNSS 21^{st} International Technical Meeting of the Satellite Division, Savannah, GA, 16-19 September 2008.

[66] Nieto J., Cosmen J., García I., Ventura-Traveset J., Neto I., Tiemeyer B., Bondarenco N., Hoshinoo K., *Interoperability Test Analysis between EGNOS and MSAS SBAS Systems*, in Proceedings of the ION GPS 12^{th} International Technical Meeting of the Satellite Division, Nashville, TN, 14-17 September 1999.

[67] Nikiforov I., *New Optimal Approach to Global Positioning System / Differential Global Positioning System Integrity Monitoring*, Journal of Guidance,

CONTROL, AND DYNAMICS, vol. 19, no. 5, AIAA, 1996.

[68] Nikiforov I., Roturier B., *Advanced RAIM Algorithms: First Results*, in Proceedings of the ION GNSS 18^{th} International Technical Meeting of the Satellite Division, Long Beach, CA, 13-16 September 2005.

[69] Ober P.B., *New, Generally Applicable Metrics for RAIM / AAIM Integrity Monitoring*, in Proceedings of the ION GPS 9^{th} International Technical Meeting of the Satellite Division, pp. 1677-1686, Kansas City, MO, 17-20 September 1996.

[70] Ober P.B., *Integrity Prediction and Monitoring of Navigation Systems*, Integricom Publishers, Leiden, The Netherlands, 2003.

[71] Oehler V., Trautenberg H.L., Luongo F., Boyero J.-P., Lobert B., *User Integrity Risk Calculation at the Alert Limit without Fixed Allocations*, in Proceedings of the ION GNSS 17^{th} International Technical Meeting of the Satellite Division, Long Beach, CA, 21-24 September 2004.

[72] Ouzeau C., Macabiau C., Escher A.-C., Roturier B., *Compliance of Single Frequency Ionospheric Delay Estimation and Cycle Slip Detection with Civil Aviation Requirements*, in Proceedings of the ION National Technical Meeting, San Diego, CA, 22-24 January 2007.

[73] Palmqvist J., *Integrity Monitoring of Integrated Satellite / Inertial Navigation Systems Using the Likelihood Ratio*, in Proceedings of the ION GPS 9^{th} International Technical Meeting of the Satellite Division, pp. 1686-1696, Kansas City, MO, 17-20 September 1996.

[74] Park K., and Crassidis J., *A Robust GPS Receiver Self Survey Algorithm*, NAVIGATION, Journal of the Institute of Navigation, vol. 53, no. 4, ION, 2006.

[75] Parkinson B.W., and Axelrad P., *Autonomous GPS Integrity Monitoring Using the Pseudorange Residual*, NAVIGATION, Journal of the Institute of Navigation, vol. 35, no. 2, ION, 1988.

[76] Pervan B., *Navigation Integrity for Aircraft Precision Landing Using the Global Position System*, Ph.D. Thesis, Stanford University, USA, March 1996.

[77] Pervan B., Pullen S., and Christie J., *A Multiple Hypothesis Approach to Satellite Navigation Integrity*, NAVIGATION, Journal of the Institute of Navigation, vol. 45, no. 1, ION, 1998.

[78] Rife J., Pullen S., Pervan B., and Enge P., *Paired Overbounding and Application to GPS Augmentation*, in Proceedings of the IEEE Position, Location and Navigation Symposium, pp. 439-446, Monterey, CA, 26-29 April 2004.

[79] Rife J., Walter T., and Blanch J., *Overbounding SBAS and GBAS Error Distributions with Excess-Mass Functions*, in Proceedings of the International Symposium on GPS / GNSS, Sydney, Australia, 6-8 December 2004.

[80] Rife J., and Pullen S., *The Impact of Measurement Biases on Availability for CAT III LAAS*, in Proceedings of the ION 61^{st} Annual Meeting, Cambridge, MA, 27-29 June 2005.

[81] Rosen N., Nelthropp D., McDonnell B., *WAAS Technical Report*, FAA Technical Center, `http://www.nstb.tc.faa.gov/`, Pomona, NJ, 2 May 2007.

[82] Radio Technical Commission for Aeronautics (RTCA), Inc., SC-159, *Report of Special Committee 159 on Minimum Aviation System Performance Standards (MASPS) for Global Positioning System (GPS)*, RTCA / DO-202, Washington, DC, 28 November 1988.

[83] RTCA, Inc., SC-159, *Minimum Aviation System Performance Standards DGNSS Instrument Approach System: Special Category I (SCAT-I)*, RTCA / DO-217, Washington, DC, 15 April 1995.

[84] RTCA, Inc., SC-159, *The Role of the Global Navigation Satellite System (GNSS) in Supporting Airport Surface Operations*, RTCA / DO-247, Washington, DC, 7 January 1999.

[85] RTCA, Inc., SC-159, *Minimum Operational Performance Standards for Global Positioning System / Wide Area Augmentation System Airborne Equipment*, RTCA / DO-229C, Washington, DC, 28 November 2001.

[86] RTCA, Inc., SC-159, *Minimum Operational Performance Standards for Global Positioning System / Wide Area Augmentation System Airborne Equipment*, RTCA / DO-229D, Washington, DC, 13 December 2006.

[87] RTCA, Inc., SC-159, *Minimum Aviation System Performance Standards for the Local Area Augmentation System (LAAS)*, RTCA / DO-245A, Washington, DC, 9 December 2004.

[88] Russell S.J., Norvig P., *Artificial Intelligence: A Modern Approach*, 2^{nd} ed., Prentice Hall, Upper Saddle River, NJ, 2003.

[89] Russian Space Agency, GLONASS, Глобальная Навигационная Спутниковая Система (ГЛОНАСС), *Interface Control Document*, version 5.0, published by the Coordination Scientific Information Center under the authority of the Russian Federation Ministry of Defence, Moscow, Russian Federation, 30 September 2002.

[90] Sturza M.A., *Navigation System Integrity Monitoring Using Redundant Measurements*, NAVIGATION, Journal of the Institute of Navigation, vol. 45, no. 4, ION, 1988.

[91] Taylor J., Barnes E., *GPS Current Signal-in-Space Navigation Performance*, in Proceedings of the ION National Technical Meeting, San Diego, CA, 24-26 January 2005.

[92] Thuringer D., McGraw G., *Cycle Slip Detection in Carrier Tracking Loops*, in Proceedings of the ION GPS 14^{th} International Technical Meeting of the Satellite Division, Salt Lake City, UT, 11-14 September 2001.

[93] US DOD, *Global Positioning System Standard Positioning Service Performance Standard*, published by the Office of the Assistant Secretary of Defense for Command, Control, Communications, and Intelligence (OASD-C3I), Washington, DC, 4 October 2001.

[94] Walter T., and Enge P., *Weighted RAIM for Precision Approach*, in Proceedings of the ION GPS 8^{th} International Technical Meeting of the Satellite Division,

Palm Springs, CA, 12-15 September 1995.

[95] Walter T., Blanch J., Rife J., *Treatment of Biased Error Distributions in SBAS*, in Proceedings of the International Symposium on GPS / GNSS, Sydney, Australia, 6-8 December 2004.

[96] Walter T., Blanch J., Enge P., *L5 Satellite Based Augmentation Systems Protection Level Equations*, in Proceedings of the International Symposium on GNSS, Sydney, Australia, 4-6 December 2007.

[97] Walter T., Blanch J., Enge P., Pervan B., and Gratton L., *Future Architectures to Provide Aviation Integrity*, in Proceedings of the ION National Technical Meeting, San Diego, CA, 28-30 January 2008.

[98] Walter T., Blanch J., Enge P., Pervan B., and Gratton L., *Shaping Aviation Integrity: Two RAIMs for Safety*, GPS World, vol. 19, no. 4, Questex Media Group, April 2008.

[99] Walter T., Enge P., Blanch J., Pervan B., *Worldwide Vertical Guidance of Aircraft Based on Modernized GPS and New Integrity Augmentations*, in Proceedings of the IEEE, vol. 96, no. 12, December 2008.

[100] Zandbergen R., Dinwiddy S., Hahn J., Breeuwer E., Blonski D., *Galileo Orbit Selection*, in Proceedings of the ION GNSS 17^{th} International Technical Meeting of the Satellite Division, Long Beach, CA, 21-24 September 2004.